Influence of Phosphine and Halide Ligands on the Properties of Undecagold Nanoclusters

by

Bo Hyung Ryoo

Bachelor in Chemistry, University of Pittsburgh, 2016

Submitted to the Graduate Faculty of the

Dietrich School of Arts and Sciences in partial fulfillment

of the requirements for the degree of

Master of Science

University of Pittsburgh

2019

UNIVERSITY OF PITTSBURGH

DIETRICH SCHOOL OF ARTS AND SCIENCES

This thesis was presented

by

Bo Hyung Ryoo

It was defended on

November 29, 2018

and approved by

Tara Meyer, Professor, Department of Chemistry

Peng Liu, Assistant Professor, Department of Chemistry

Jill E Millstone: Associate Professor, Department of Chemistry

Influence of Phosphine and Halide Ligands on the Properties of Undecagold Nanoclusters

Bo Hyung Ryoo, M.S.
University of Pittsburgh, 2019

Surface ligands are essential components of nanomaterial identity, as they passivate the surfaces of many nanomaterials. Traditionally, ligands were considered for their size- and shape-directing properties in nanoparticles. Besides their usage in syntheses to control the morphologies of the nanomaterials, various ligands were used in tuning the surface functionality of nanomaterials for many applications, ranging from drug targeting to nanosensors. Recently, identities of the surface ligands were found to influence nanomaterial chemical and physical properties, including enhancement of stability, catalytic behaviors, and photoluminescence. These old and new ligand-controllable properties (achieved by various ligand modification through synthetic organic chemistry routes) necessitate a fundamental understanding of the ligand effect on the nanomaterials. In order to take another stride towards having a fundamental understanding of the ligands on nanomaterials, we study influences of and halide ligands on undecagold nanoclusters (Au_{11}NCs). With the small size, the suite of atomically precise Au_{11}NCs is easily accessible synthetically and theoretically. In addition, the ligand influences are intensified due to having majority of the gold atoms oriented on the surface of Au_{11}NCs interacting with surface molecules. Systematically altering the type and composition of the surface ligands, which are subsequently characterized and compared with the local and overall electronic structures of computationally modelled Au_{11}NCs, provides critical information about the ligand's role in nanomaterials. Further, several overarching theories are suggested to elucidate the influence of the ligand identities on the enhancement of photoluminescence properties in Au_{11}NCs. From this work, the mechanisms underlying ligand influence on Au_{11}NCs can be translated to commonly used, larger nanoparticles and in the design of next-generation applications of nanomaterials.

Table of Contents

1.0 Introduction 1

1.1 Motivation 1

1.2 Research Objectives 7

2.0 Experimental 10

2.1 Materials 10

2.2 Nanoparticle Synthesis and Post-Synthetic Modification 11

2.2.1 Synthesis of Mononuclear Precursors 11

2.2.1.1 Chloro(dimethylsulfide) Gold(I) 11

2.2.1.2 Chloro(triphenylphosphine) Gold(I) 11

2.2.1.3 Bromo(triphenylphosphine) Gold(I) 12

2.2.1.4 Iodo(triphenylphosphine) Gold(I) 12

2.2.1.5 Bis(chlorogold(I)) 1, 3-bis(diphenylphosphino)propane 12

2.2.1.6 Chloro(triphenylarsine) Gold(I) 13

2.2.1.7 Chloro(triphenylstibine) Gold(I) 13

2.2.2 Synthesis of Gold Nanoparticles 13

2.2.2.1 $Au_{11}(PPh_3)_8Cl_2^+$ 13

2.2.2.2 $Au_{11}(PPh_3)_8Br_2^+$ 14

2.2.2.3 $Au_{11}(PPh_3)_8I_2^+$ 14

2.2.2.4 $Au_{11}(PPh_3)_7Cl_3$ 15

2.2.2.5 $Au_{11}(PPh_3)_7Br_3$ 15

2.2.2.6 $Au_{11}(PPh_3)_7I_3$ 16

2.2.2.7 Au_{11}NCs with Cyanide Group 16

2.2.2.8 $Au_{11}(dppp)_5^{3+}$ 16

2.2.2.9 $Au_{13}(dppp)_4Cl_4^+$ 17

2.2.2.10 $Au_{13}(AsPh_3)_8Cl_4^+$ 17

2.2.2.11 $Au_{13}(SbPh_3)_8Cl_4^+$ 18

2.3 Extinction Spectroscopy 19

2.4 Electrospray Ionization Mass Spectroscopy 19

2.5 Single Crystal X-Ray Diffraction 19

2.6 Photoluminescence Spectroscopy 20

2.7 Fourier Transform Infrared Spectroscopy (FTIR) 20

2.8 Raman Spectroscopy 21

3.0 Computational Details 22

4.0 Results 24

4.1 Experimental Characterization of Gold Precursors and Nanoclusters 24

4.1.1 Crystal Structures 24

4.1.2 Absorption Spectrum 28

4.1.3 Photoluminescence Spectrum 29

4.2 Computational Characterization of Gold(I) Precursors and Nanoclusters 32

4.2.1 Validation of Theory 32

4.2.2 Relaxed Geometry and Bond Lengths 35

4.2.3 Bader Charge 38

4.2.4 Projected Density of States 41

4.2.5 Orbital Diagram 44

4.2.6 Computed Extinction Spectrum 49
5.0 Discussion 52
5.1 Structures and Symmetries of Phosphine Gold Products 52
5.2 Stabilities and Charges on Undecagold Clusters 54
5.3 Molecular Orbitals and Energy States 57
5.4 Absorption 65
5.5 Emission 66
5.5.1 Triplet States of the Undecagold Nanoclusters 68
5.5.2 Ligand Factors in the Relaxation Pathways 70
6.0 Conclusion 73
7.0 Future Work: Influence of Pnictogen Ligands on AuNCs 74
Appendix A 80
References 236

List of Tables

Table A1 (continued). Crystallographic data for Au(I) precursor and AuNCs. **80**

Table A2 (continued). Summary of Au-Au and Au-ligand bond distances (Å) of AuNCs compared to the computational models. **83**

Table A3 (continued). Summary of Bader charges of AuNCs. **87**

Table A4. Life time (τ) of emissions of AuNCs. **97**

List of Figures

Figure 1. Picture of President John F. Kennedy (left) and Richard Feynman (right)............ 1

Figure 2. Aerobic oxidation of organic molecules catalyzed by gold nanoclusters 2

Figure 3. Structure of $Au_{11}(PPh_3)_8Br_2^+$, which is one of many phosphine-halide-protected undecagold nanoclusters 4

Figure 4. Molecular orbital diagrams of Green's covalent bond classification....................... 6

Figure 5. Crystal structure of Au(I) precursors and $Au_{11}NCs$ 25

Figure 6. Distribution plots of bonding distance in mononuclear gold precursors and nanoclusters measured from their crystal structures 26

Figure 7. Normalized absorption spectra of $Au_{11}(PPh_3)X_2^+$ and $Au_{11}(PPh_3)X_3$ (X = Cl, Br, and I) with different quantity and types of halides. 28

Figure 8. Emission spectra of $Au_{11}NCs$ excited at 3.44 eV 30

Figure 9. Photoluminescence maps of undecagold nanoclusters A) $Au_{11}(PPh_3)_8Cl_2^+$, B) $Au_{11}(PPh_3)_8Br_2^+$, C) $Au_{11}(PPh_3)_8I_2^+$, D) $Au_{11}(PPh_3)_7Cl_3$, E) $Au_{11}(PPh_3)_7Br_3$, and F) $Au_{11}(PPh_3)_7I_3$ 31

Figure 10. Single point calculation on $Au_{11}(PPh_3)_8Cl_2^+$ with various calculation parameters 33

Figure 11. Converging potential energy of $Au_{11}(PPh_3)_8Br_2^+$ and constant quantity from the MD simulation of $Au_{11}(PPh_3)_8Br_2^+$ over simulated time 34

Figure 12. Geometries of the $Au_{11}(PMe_3)_8Br_2^+$ and $Au_{11}(PPh_3)_8Br_2^+$ after completing geometry optimization 35

Figure 13. Relaxed geometries of mononuclear gold precursor (A) $AuPPh_3Cl$, (B) $AuPPh_3Br$, (C) $AuPPh_3I$ and undecagold nanoclusters (D) $Au_{11}(PPh_3)_8Cl_2^+$, (E) $Au_{11}(PPh_3)_8Br_2^+$, (F) $Au_{11}(PPh_3)_8I_2^+$, (G) $Au_{11}(PPh_3)_7Cl_3$, (H) $Au_{11}(PPh_3)_7Br_3$, and (I) $Au_{11}(PPh_3)_7I_3$. 36

Figure 14. Distribution plots of bonding distance in mononuclear gold precursors and nanoclusters 37

Figure 15. Electron charge distribution plots of atoms in the Au(I) precursors and Au_{11}NCs 38

Figure 16. Relaxed structures of phosphine-halide-protected Au_{11}NCs with Bader charges projected on gold atoms 40

Figure 17. PDOS of $Au(PPh_3)Br$, $Au_{11}(PPh_3)_8Br_2^+$, and $Au_{11}(PPh_3)_7Br_3$ 41

Figure 18. PDOS of undecagold clusters A) $Au_{11}(PPh_3)_8Cl_2^+$, B) $Au_{11}(PPh_3)_7Cl_3$, C) $Au_{11}(PPh_3)_8Br_2^+$, D) $Au_{11}(PPh_3)_7Br_3$, E) $Au_{11}(PPh_3)_8I_2^+$, and F) $Au_{11}(PPh_3)_7I_3$ near HOMO-LUMO regions........ 43

Figure 19. Orbital diagrams of $Au(PPh_3)Br$ near the frontier orbitals. HOMO and LUMO states are doubly degenerates........ 44

Figure 20. One of three degenerate Highest-Occupied-Molecular-Orbital representations of a) $Au_{11}(PPh_3)_8Cl_2^+$, b) $Au_{11}(PPh_3)_8Br_2^+$, and c) $Au_{11}(PPh_3)_8I_2^+$ 45

Figure 21. Kohn-Sham orbital representations of $Au_{11}(PPh_3)_8Br_2^+$ and $Au_{11}(PPh_3)_7Br_3$ at different energies near HOMO 47

Figure 22. Kohn-Sham orbital representations of $Au_{11}(PPh_3)_8Br_2^+$ and $Au_{11}(PPh_3)_7Br_3$ at different energies near LUMO........ 48

Figure 23. Direct comparison of experimentally collected absorptions and simulated absorptions of $Au_{11}(PPh_3)_8X_2^+$........ 49

Figure 24. The major electronic transition of $Au_{11}(PPh_3)_8Br_2$ and $Au_{11}(PPh_3)_7Br_3$ at the various excitation energies 51
Figure 25. Crystal structures based on the computational models of $Au_{11}(PPh_3)_8Cl_2^+$ and $Au_{11}(PPh_3)_7Cl_3$ 53
Figure 26. PDOS of gold's orbital angular momentum in A) AuBr and B) $Au(I)PPh_3^+$ and C) $Au(PPh_3)Br$ 58
Figure 27. PDOS of orbital angular momentum of A) gold in Au_{11}^{3+}, B) gold, C) Br, D) organic elements of PPh_3 in $Au_{11}(PPh_3)_8Br_2^+$ 60
Figure 28. The HOMO of the gold core with or without ligands for $Au_{11}(PPh_3)_8Br_2^+$ and $Au_{11}(PPh_3)_7Br_3$ 61
Figure 29. PDOS of all X-type ligands ($Au_{11}Cl_{10}^{7-}$, left) and all L-type ligands ($Au_{11}(dppp)_4Cl_2^+$, right) with computationally optimized structures depicted in the insets 63
Figure 30. Experimental absorption spectrum with KS orbital energy level diagram for model $Au_{11}(PPh_3)_8Br_2^+$ 65
Figure 31. Jablonski diagram describing excitation and emission pathways 67
Figure 32. The direct comparison of PDOS and two-dimensional emission contour map of $Au_{11}(PPh_3)_8Br_2^+$ 69
Figure 33. Emission spectrum of cyanide substituted Au_{11}NCs (Left) and PDOS calculation of geometrically optimized $Au_{11}(PPh_3)_8(CN)_2^+$ similar to $Au_{11}(PPh_3)_8Cl_2^+$ (Middle) 71
Figure 34. Computationally relaxed model based on the crystal structure of A) $Au_{13}(dppp)_4Cl_4^+$, B) $Au_{13}(AsPh_3)_8Cl_4^+$, and C) $Au_{13}(SbPh_3)_8Cl_4^+$ 75
Figure 35. Absorption (top) and emission (bottom) spectra of Au_{13}NCs 77

Figure 36. Bader charge (top) and PDOS (bottom) of Au_{13}NCs with different ligand structures..78

Figure A1. ESI spectrum showing the existence of A) $Au_{11}(PPh_3)_8Cl_2^+$, B) $Au_{11}(PPh_3)_8Br_2^+$, and C) $Au_{11}(PPh_3)_8I_2^+$, and D) $Au_{13}(AsPh_3)_8Cl_4^+$...99

Figure A2. The crystal and computation structure of dppp. 100

Figure A3. Crystal structure of decomposed product Au_{25}NC from Au11$(PPh_3)_7Cl_3$........100

Figure A4. Absorption spectrum of $Au_{11}(dppp)_5^+$ and Au_{11}NC with CN^-...........................101

Figure A5. Absorption spectrum of Au_{11}NCs with addition of other ligands 101

Figure A6. Emission maps of Au_{11}NCs in DCM..102

Figure A7. FTIR spectrum comparing the features in KBr pallet containing $Au(PPh_3)Cl$ and $Au(PPh_3)I$. 102

Figure A8. FTIR spectrum comparing the features in KBr pallet containing $Au(PPh_3)Cl$ and $Au_{11}(PPh_3)_8Cl_2^+$...103

Figure A9. FTIR spectrum comparing the features in KBr pallet containing $Au(PPh_3)I$, $Au_{11}(PPh_3)_8I_2^+$, and $Au_{11}(PPh_3)_7I_3$...103

Figure A10. FTIR spectrum comparing the features in KBr pallet containing $Au_{11}(PPh_3)_8Cl_2^+$, $Au_{11}(PPh_3)_8Br_2^+$, and $Au_{11}(PPh_3)_8I_2^+$. 104

Figure A11. FTIR spectrum comparing the features in DCM solution containing $Au(PPh_3)I$, $Au_{11}(PPh_3)_8I_2^+$, and $Au_{11}(PPh_3)_7I_3$...104

Figure A12. FTIR spectrum comparing the features in DCM solution containing $Au(PPh_3)Cl$ and $Au(PPh_3)I$..105

Figure A13. FTIR spectrum comparing the features in DCM solution containing $Au(PPh_3)Cl$ and $Au_{11}(PPh_3)_8Cl_2^+$. 105

Figure A14. FTIR spectrum comparing the features in DCM solution containing $Au_{11}(PPh_3)_8Cl_2^+$, $Au_{11}(PPh_3)_8Br_2^+$, and $Au_{11}(PPh_3)_8I_2^+$. 106

Figure A15. Raman spectra of PPh_3 and $Au(PPh_3)X$ (X = Cl, Br, I) at low Raman shifts. 107

Figure A16. Raman spectra of PPh_3, $Au(PPh_3)Cl$, $Au_{11}(PPh_3)_8Cl_2^+$, and $Au_{11}(PPh_3)_7Cl_3$ at low Raman shifts. 107

Figure A17. Raman spectra of PPh_3, $Au(PPh_3)Br$, $Au_{11}(PPh_3)_8Br_2^+$, and $Au_{11}(PPh_3)_7Br_3$ at low Raman shifts. 108

Figure A18. Raman spectra of PPh_3, $Au(PPh_3)I$, $Au_{11}(PPh_3)_8I_2^+$, and $Au_{11}(PPh_3)_7I_3$ at low Raman shifts. 108

Figure A19. Raman spectra directly comparing the features of $Au_{11}(PPh_3)_8X_2^+$ (X = Cl, Br, I) in low Raman shifts. 109

Figure A20. Raman spectra directly comparing the features of $Au_{11}(PPh_3)_7X_3$ (X = Cl, Br, I) in low Raman shifts. 109

Figure A21. Raman spectra directly comparing the features between $Au_{11}(PPh_3)_8I_2^+$ and $Au_{11}(PPh_3)_8Cl_2^+$ with KCN in low Raman shifts. 110

Figure A22. Fully optimized geometries of $PtAu_{10}(dppp)_5^{2+}$ 110

Figure A23. Fully optimized geometries of Au_{11}^{3+} 111

Figure A24. Orbital angular momentum PDOS of A) gold in Au_{11}^{3+}, B) gold, C) Br, and D) organic elements of PPh_3 in $Au_{11}(PPh_3)_7Br_3$ 112

Figure A25. PDOS of theoretical compound $Au_{11}Cl_{10}^{7-}$ by substituting phosphine ligands with chlorine on the geometrically optimized $Au_{11}(PPh_3)_8Cl_2^+$ (left) and $Au_{11}(PPh_3)_7Cl_3$ (right) 113

Figure A26. KS orbitals of $Au_{11}(PPh_3)_8X_2^+$ near the frontier orbitals. 117

Figure A27. KS orbitals of $Au_{11}(PPh_3)_8X_2^+$ near the frontier orbitals. 127

Figure A28. KS orbitals of $Au_{11}(PPh_3)_7X_3$ near the frontier orbitals. 137

Figure A29. KS orbitals of Au_{11}^{3+} with $Au_{11}(PPh_3)_8Br_2^+$ core (left) and $Au(PPh_3)_7Br_3$ core (right) near the frontier orbitals. 143

Figure A30. KS orbitals of $Au_{11}Cl_{10}^{7-}$ and $Au_{11}(dppp)_5^{3+}$ near their frontier orbitals. 153

Figure A31. KS orbitals of Au_{13}NCs with different pnictide ligands. *$Au_{13}(AsPh_3)_8Cl_4^+$ represents the $Au_{13}(AsPh_3)_8Cl_4^+$ with similar halide orientation with $Au_{13}(SbPh_3)_8Cl_4^+$. 163

Figure A32. Optimized coordinates of PPh_3. 164

Figure A33. Optimized coordinates of AuCl. 165

Figure A34. Optimized coordinates of Au-PPh_3. 165

Figure A35. Optimized coordinates of $Au(PPh_3)Cl$. 166

Figure A36. Optimized coordinates of $Au(PPh_3)Br$. 167

Figure A37. Optimized coordinates of $Au(PPh_3)I$. 168

Figure A38. Optimized coordinates of $Au_2(dppp)Cl_2$. 169

Figure A39. Optimized coordinates of $Au_2(dppp)Cl_2$ in different orientation. 170

Figure A40. Coordinates for optimized structure of $Au(AsPh_3)Cl$. 171

Figure A41. Coordinates for optimized structure of $Au(SbPh_3)Cl$. 172

Figure A42. Optimized coordinates of $Au(BiPh_3)Cl$. 173

Figure A43. Coordinates for optimized structure of Au_{11}^{3+}. 173

Figure A44. Coordinates for optimized structure of $Au_{11}(PPh_3)_8Cl_2^+$. 178

Figure A45. Optimized coordinates of $Au_{11}(PPh_3)_8Br_2^+$. 184

Figure A46. Optimized coordinates of $Au_{11}(PPh_3)_8I_2^+$. 189

Figure A47. Optimized coordinates of $Au_{11}(PPh_3)_7Cl_3$. **194**

Figure A48. Optimized coordinates of $Au_{11}(PPh_3)_7Br_3^+$. **198**

Figure A49. Optimized coordinates of $Au_{11}(PPh_3)_7I_3^+$. **203**

Figure A50. Optimized coordinates of $Au_{11}(PPh_3)_8(CN)_2^+$. **208**

Figure A51. Optimized coordinates of $Au_{11}(dppp)_5^{3+}$. **214**

Figure A52. Initial coordinates of $Au_{11}Cl_{10}^{7-}$. **214**

Figure A53. Optimized coordinates of $Au_{11}Cl_{10}^{7-}$. **215**

Figure A54. Optimized coordinates of $Au_{13}(dppp)_4Cl_4^+$. **219**

Figure A55. Optimized coordinates of $Au_{13}(AsPh_3)_8Cl_4^+$. **224**

Figure A56. Optimized coordinates of $Au_{13}(AsPh_3)_8Cl_4^+$ with different ligand orientation. **230**

Figure A57. Optimized coordinates of $Au_{13}(SbPh_3)_8Cl_4^+$. **235**

List of Equations

Equation 1. Quantum yields (Φ) calculations 29

1.0 Introduction

1.1 Motivation

On September 12, 1962, President John F. Kennedy (**Figure 1**) delivered his iconic "We Choose to Go to the Moon" speech in which he expressed his vision to have a man land on the moon and return safely back to earth.[1] On July 20, 1969, President Kennedy's vision would be realized when Neil Armstrong and Buzz Aldrin successfully stepped onto the lunar surface. Even after Apollo 11's moon landing mission fulfilled President Kennedy's vision, the speech "We Choose to Go to the Moon" inspires scientists and engineers all over the world to expand the boundaries of the human universe and knowledge.

Figure 1. Picture of President John F. Kennedy (left) and Richard Feynman (right). President Kennedy was known for his inspirational speech that led to exploding growth in the space program, and Feynman for his lecture resulting in flourishing research in nanotechnology. The inset pictures show the success in the Apollo program in 1962 and the manipulation of atoms by IBM in 1989, respectively.[1, 2]

Approximately three years before President Kennedy's speech in Texas, a near-legendary physicist by the name of Richard Feynman (**Figure 1**) delivers his "There's Plenty of Room at the Bottom" lecture at the American Physical Society in which he envisions technology developed to manipulate matter on an atomic scale.[3] Similar to President Kennedy's speech, Feynman's lecture is credited with starting the era of nanotechnology. In his talk, Feynman emphasizes the incredible economic potential in miniaturizing the large complicated machines and devices to a system several hundred atoms large. Furthermore, he recognized the enormous potential of new nanotechnology devices resulting from the laws of quantum mechanics in infinitesimal systems. The following decades of explosive growth in nanoscience and nanotechnology demonstrates the accuracy of visionary Richard Feynman. Beginning about a half century after Feynman's speech, nanotechnology has since been incorporated into many commercial products ranging from cosmetics and solar cells to clothing and medications – and the potential is only getting larger (**Figure 2**).[4-6]

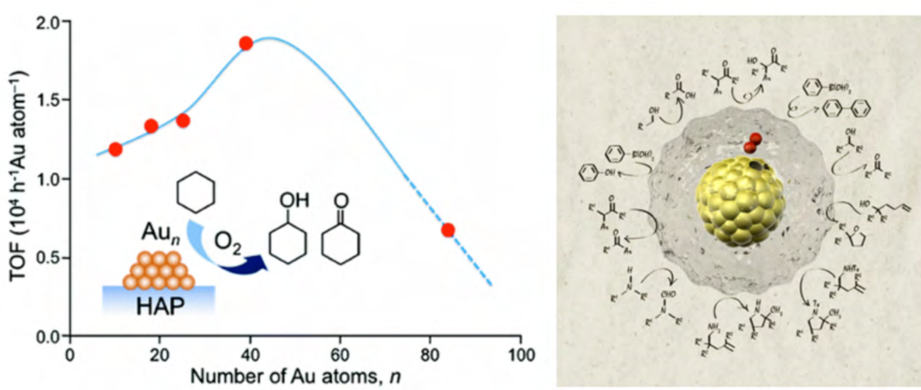

Figure 2. Aerobic oxidation of organic molecules catalyzed by gold nanoclusters. The efficiencies of these nanomaterials can be tuned for the suited applications. On the left, the turnover frequency (TOF) of cyclohexane to cyclohexanone is highly dependent on the size of the gold cluster on the surface of hydroxyapatite.[7] On the right, the catalytic application of these new nanomaterials can be applied in broad species of organic molecules.[8] Both figures are from the reference 4 and 5, respectively.

Among the many nanomaterials that can be comprised of nearly every element on the periodic table, gold nanoclusters (AuNCs) and nanoparticles (AuNPs) are particularly interesting because they display a rich array of chemical, catalytic, electronic, and optical properties that can be tailored for a range of applications in nanotechnology (e.g., nanomedicine, catalysis, nanoelectronics, biological imaging and sensing).[9-11] Detailed investigation into structure-property relationships of these materials has been made possible by recent advances in syntheses and characterization technologies.[12-15] Additionally, advances in theoretical chemistry have allowed us to understand the unique chemistry of gold nanoclusters and nanoparticles that is not observed in bulk gold.[16, 17] Bulk gold is a simple monovalent 6s-metal with high electric and thermal conductivity. Confining the electrons in the delocalized conduction band of bulk gold into nanometer scales causes discretization of the electron states. With the enhanced relativistic effect of elemental gold, gold atoms have contracted 6s orbitals with expanded 5d orbitals. This becomes an active component in gold's unique coordination chemistry (e.g. aurophilicity) often observed in gold complexes and gold nanoparticles.[18, 19] Just as Feynman had anticipated, the emergence of the law of quantum mechanics becomes more apparent as the energy states of AuNPs become more quantized. The finite energy levels, which are sensitive to size, shape and symmetry point group of the AuNCs, are important in defining many physical and chemical properties of the AuNCs.[20]

Unlike the shape and size of the gold core, the importance of surface ligands on the properties of AuNPs have only recently begun to be studied, even though most solvated noble metal NPs are passivated by at least a monolayer of organic ligands.[21, 22] Ligands are traditionally considered morphology-directing agents, used to synthesize NP cores of various sizes and shapes.[23-25] More recent work has noted the significant impact of the ligand on the electronic structure of NPs as well as their catalytic and emission properties.[26-30] With limitless tunability of various ligands, it is important to understand the influence of surface ligands on NPs. However, the complicated nature of surface ligands makes it harder to separate ligand-only influences from other NP parameters, such as size and shape. In this work, we control the variations on the surface while holding the gold core constant using experimental techniques combined with theoretical predictions. From the acquisition of data, we will be able to elucidate the influence of ligands and detail how the ligand influences the overall properties of NPs.

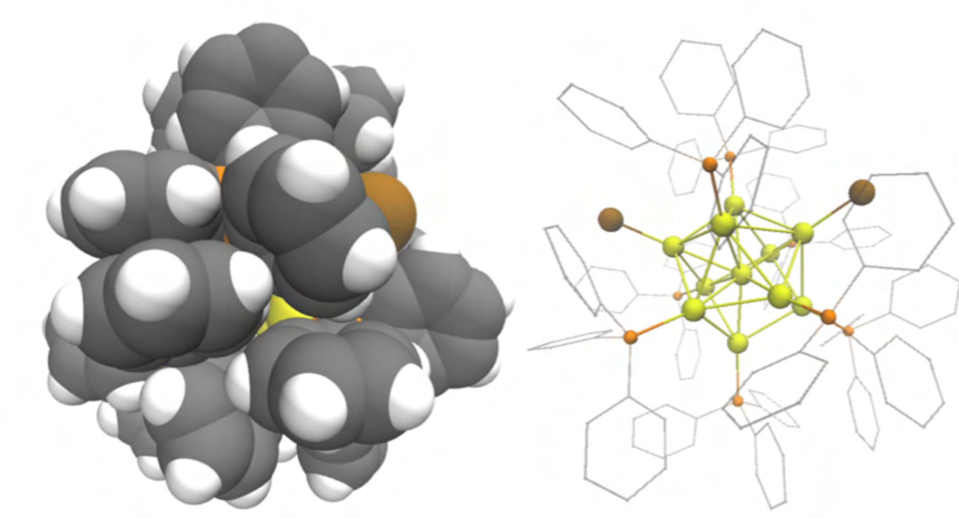

Figure 3. Structure of $Au_{11}(PPh_3)_8Br_2^+$, which is one of many phosphine-halide-protected undecagold nanoclusters. The gold core is passivated by the surface ligands described with the Van der Waals model (left). With emphasis on the geometry of the gold core and the binding moieties of the ligands, the same gold cluster was shown using the ball-and-stick model (right). The colors represent elements: Au (yellow), Br (brown), P (orange), C (grey), H (white).

Here, various phosphine-halide-protected undecagold nanoclusters (Au_{11}NCs) were synthesized and characterized as well as computationally modelled using density functional theory (DFT). This particular suite of nanoclusters was studied for several reasons. First, Au_{11}NCs passivated by phosphine and halide are one of the smallest gold clusters having at least one gold atom surrounded by a neighboring metal atom.[31] This small size, coupled with the number of transition metal atoms in the core, allows $Au_{11}NCs$ to be easily accessed both experimentally and theoretically. This small size also makes the gold nanoparticles comparatively more sensitive to small variations in structure than larger nanomaterials. These differences allow for easier separation using column chromatography as well as crystallization, which is useful for determining their crystal structures. With a minimal number of gold atoms and precisely known atomic coordination, relatively inexpensive computational models can be used to calculate the electronic structures of the $Au_{11}NCs$. Secondly, the phosphine-halide-protected $Au_{11}NCs$ can be synthesized with different numbers and types of surface ligands without greatly altering the core geometry. The halogens on $Au_{11}NCs$ can be chlorine, which has a comparably high electronegativity compared to gold atoms (Cl: 3.16 to Au: 2.54), or bromine and iodine, which have electronegativities near that of gold (Br: 2.96 and I: 2.66). The systemic differences in electronegativity among halide ligands can direct local electronic densities, providing crucial information of subtle ligand identity on the properties of gold nanoclusters. Furthermore, the phosphine:halide ligand ratio on the surface can be controlled to elucidate the effect of different bonding types between ligands and the gold surface defined in Green's covalent bond classification (**Figure 4**).[32, 33] The assembly of a monolayer with different bonding types on the surface of the nanomaterials will interfere with the electronic structures of the bare metal clusters.

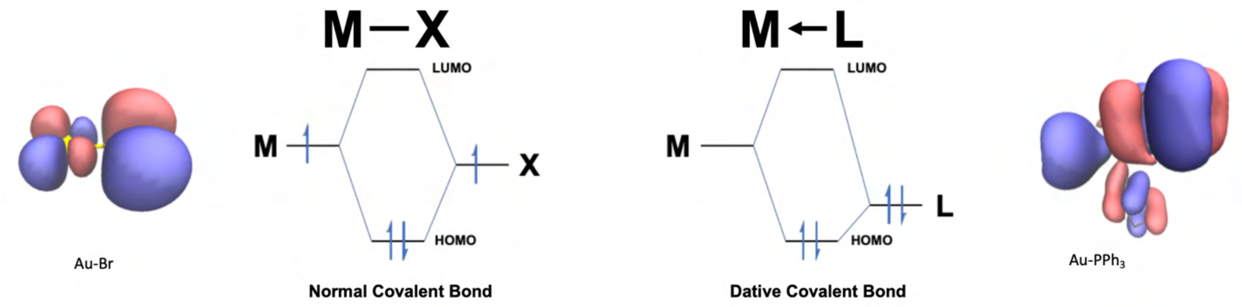

Figure 4. Molecular orbital diagrams of Green's covalent bond classification.[32, 33] Halogens are known as X-type ligands (X), which donate one electron and accept one electron from the metal (M), contrary to L-type phosphine ligands (L), which donate a lone pair to the metal center, producing a dative bond. Kohn-sham orbitals depict the electron density of gold complexes bound to either bromine or triphenylphosphine (PPh_3) at the highest occupied molecular orbital states.

Previously synthesized and studied diphenylphosphinopropane (dppp) capped clusters, $Au_{11}(dppp)_5^{3+}$, are included in this work to correlate properties of Au_{11}NCs without X-type ligands to other Au_{11}NCs.[34] Additionally, unlike the gold clusters capped with thiolated ligands, the gold clusters passivated with phosphine or halides have a simple on-top gold-ligand binding motif. The presence of an identical gold-ligand binding motif in various reported phosphine-halide capped clusters suggests that the ligand-gold interaction in Au_{11}NCs can be translated to other gold clusters with different core geometries or size.[31, 35] By experimentally observing the optoelectronic properties of Au_{11}NCs using various ligands and correlating them to theoretically established electronic structures of the Au_{11}NCs, we are able to gain an understanding of the mechanisms underlying the ligand-gold cluster binding interaction.

Through this work, the fundamental and mechanistic understanding of ligand-nanocluster interaction and ligand-based nanomaterial properties can be applied to designing new noble metal nanomaterials. As the more recent body of work in nanoscience has demonstrated, improving the surface properties of nanomaterials can lead to sophisticated nanomaterials with many applications, ranging from bioimaging dyes to catalysts. As Feynman had envisioned seven decades ago, many possibilities for nanotechnology exist in a very small world, stemming from its large surface area. It is our hope that this work can provide humanity with "a small step for nanomaterial surface modification, and one giant step for new customizable nanomaterials having different ligands to suit their application purposes."

1.2 Research Objectives

A key goal in the development of nanomaterials is to understand the influence of surface ligands on the nanomaterial structure and their resulting optoelectronic properties. The synthesis and characterization of atomically precise nanoclusters can be significantly less challenging than larger nanoparticles, in part due to knowing the precise location of individual atoms as well as having the ability to computationally model them. Therefore, successful nanoparticle technologies can be enhanced by incorporating well-studied characterization of the analogous nanoclusters. Importantly, in order to correlate ligand influences to nanoparticle behavior, one must be able to measure the differentiating parameter without altering multiple variables.

Here, I chose to study the optoelectronic properties of phosphine-halide-protected Au_{11}NCs. Identities and structures of some phosphine-halide-protected Au_{11}NCs have been reported previously, and a few of the reported Au_{11}NCs has been rigorously studied more recently.[12, 17, 36-39] With their small size, stability, and non-toxicity, modified $Au_{11}(PPh_3)_8Cl_2^+$ were demonstrated as highly useful labeling agents in various biochemical molecules.[40-43] With less stability, $Au_{11}(PPh_3)_7Cl_3$ has been shown to be very useful in catalysts as well as a template for various nanoclusters.[44, 45] Along with many potential applications, the suite of phosphine-halide-protected Au_{11}NCs is desirable starting point to study ligand-nanocluster interaction and the resulting chemical properties of the AuNCs. The extensive studies on the mononuclear gold(I) precursors of these Au_{11}NCs provides basic and direct interaction between singular gold atom and ligands, which can be compared to the interactions between gold atoms and ligands.[46-50] Also, phosphine-halide-protected Au_{11}NCs are one of the smallest gold nanoclusters with a center gold atom that is only bound by neighboring gold atoms, which makes them an easy system on which to perform computational calculations. In addition to these Au_{11}NCs, there are libraries of analogous phosphine-halide-protected gold nanoclusters reported, where both halides and phosphines are bound in an on-top position to the surface gold atoms.[12, 31, 38] These different sizes and shapes of phosphine-halide-protected gold nanoclusters can be used in the future to compare with this study to translate some ligand-dependent properties to slightly different systems. Further, the easily distinguishable differences between halide and phosphine, as well as smaller differences between three halides without changing much of the nanocluster system can provide in-depth information regarding the magnitude of ligand influence on the properties of nanoclusters. My overarching research goals are twofold: i) assigning the emergent electronic structures in phosphine-halide-protected Au_{11}NCs as a function of different surface ligands and ii) correlating the electronic structures to empirically determined nanocluster properties to aid understanding of ligand-based properties in gold nanomaterials.

To accomplish these objectives, we established reproducible and well-controlled conditions to synthesize phosphine-halide-protected Au_{11}NCs with different amounts and types of halide ligands. In order to systematically understand the influence of surface ligands on the electronic structures of phosphine-halide-protected Au_{11}NCs, each cluster was purified and analyzed using X-ray diffractometry (XRD) before computationally modelling the nanocluster structure. With the use of the CP2K software package, each nanocluster was translated and calculated using density functional theory (DFT).[51] As a result, these calculations allowed for the correlation of nanocluster electronic structures to changes in surface ligands.

By establishing a theoretical portrayal of phosphine-halide-protected Au_{11}NCs, we can further understand and modify the optoelectronic properties of the clusters by altering the identity of the surface ligands. Further, by systematically comparing the theoretical understanding of the clusters and their observed optoelectrical properties, we can confirm the degree of surface ligand influence on nanomaterials. Our initial studies show that we can decouple the influences of individual ligand components and correlate such changes to the differences in nanocluster behaviors including their optoelectronic properties. The ability to understand ligand-based properties on overall nanomaterial properties will allow us to develop design rules to systematically tune the optoelectric properties of noble metal nanomaterials.

2.0 Experimental

2.1 Materials

Gold (III) chloride trihydrate ($HAuCl_4 \cdot 3H_2O$, 99.9%), triphenylphosphine (PPh_3, 99%), 1, 3-Bis(diphenylphosphino)propane (dppp, 97%), triphenylarsine ($AsPh_3$, 97%), triphenylantimony ($SbPh_3$, 99%), triphenylbismuth ($BiPh_3$, 98%), chloro(dimethylsulfide) gold(I) ($Au(Me_2S)Cl$, 99%), and octane (>99.0%) were purchased from Sigma Aldrich (St. Louis, MO). Dichloromethane (DCM, >99.8%), pentane (99.0%), hexane (99.0%), dimethyl sulfide (Me_2S, >99%), diethyl ether (Et_2O, 99.5%), potassium bromide (KBr, >99.0%), potassium cyanide (KCN, >= 98%), absolute ethanol (EtOH), and silica gel of various mesh sizes (SiO_2, mesh = 60, 100-200) were purchased from Thermo Fisher Scientific (Pittsburgh, PA). Chloro(triphenylphosphine) gold(I) ($Au(PPh_3)Cl$, 99.9%), bromo(triphenylphosphine) gold(I) ($Au(PPh_3)Br$, 99.99%), potassium iodide (KI, >99,0%), and sodium borohydride ($NaBH_4$, 99.99%) were purchased from Alfa Aesar (Haverhill, MA). Styrene divinylbenzene beads with 40-80µm, also known as Bio-Beads S-X1, were purchased from Bio-Rad (Hercules, CA).

All chemicals were used as received. Prior to use, all glassware and Teflon-coated stir bars were washed with aqua regia (3:1 ratio of concentrated HCl to HNO_3) and rinsed with copious amounts of water prior to drying. *Caution: aqua regia is highly toxic and corrosive and should only be used with proper personal protective equipment and training. Aqua regia should be handled only inside a fume hood.*

2.2 Nanoparticle Synthesis and Post-Synthetic Modification

2.2.1 Synthesis of Mononuclear Precursors

2.2.1.1 Chloro(dimethylsulfide) Gold(I)

$Au(Me_2S)Cl$ was prepared according to a literature procedure.[52] 0.500 g (1.3 mmol) of $HAuCl_4 \cdot 3H_2O$ was fully dissolved in 10 mL of degassed EtOH. Rapid addition of 5 mL of degassed EtOH containing 295 μL (4.0 mmol) of Me_2S in the stirring the gold solution produced white precipitate. After allowing the reaction to stir for two hours, the solution was cooled down to near 0°C. The precipitate was washed with excess EtOH and dissolved in small amount of DCM. The $Au(Me_2S)Cl$ crystals were collected using solvent-solvent diffusion of EtOH in DCM at cold temperature.

2.2.1.2 Chloro(triphenylphosphine) Gold(I)

$Au(PPh_3)Cl$ was prepared according to a literature procedure.[50] 0.380 g (1 mmol) of $HAuCl_4 \cdot 3H_2O$ was fully dissolved in acetone and EtOH mixture (1:1 v/v). Rapid addition of 3 mL of purified DCM containing 0.525 g (2 mmol) of PPh_3 in the stirring the gold solution produced white precipitate. After allowing the reaction to stir for several hours, the precipitate was collected and washed with excess EtOH. The $Au(PPh_3)Cl$ crystals were collected by dissolving the white precipitate in DCM and using both solvent-solvent diffusion of EtOH in DCM and slow evaporation.

2.2.1.3 Bromo(triphenylphosphine) Gold(I)

$Au(PPh_3)Br$ was synthesized by KBr halide anion exchange on $Au(PPh_3)Cl$. An organic layer of 2 mL DCM containing 100 mg of $Au(PPh_3)Cl$ (0.2 mmol) was mixed with 2 mL of aqueous layer containing 238 mg KBr (2 mmol). Prior to extracting out the organic layer, the mixture was stirred violently for several hours. The $Au(PPh_3)Br$ crystals were collected by solvent-solvent diffusion of EtOH in DCM and slow evaporation.

2.2.1.4 Iodo(triphenylphosphine) Gold(I)

$Au(PPh_3)I$ was synthesized similar to the preparation of $Au(PPh_3)Br$. An organic layer of 2 mL DCM containing 100 mg of $Au(PPh_3)Cl$ (0.2 mmol) was mixed with 2 mL of aqueous layer containing 332 mg KI (2 mmol). Prior to extracting out the organic layer, the mixture was stirred violently for several hours. The $Au(PPh_3)I$ crystals were collected by solvent-solvent diffusion of EtOH in DCM and slow evaporation.

2.2.1.5 Bis(chlorogold(I)) 1, 3-bis(diphenylphosphino)propane

$Au_2(dppp)Cl_2$ was prepared according to a literature procedure.[53] 0.500 g (1.3 mmol) of $HAuCl_4{\cdot}3H_2O$ was fully dissolved in 8 mL of EtOH. Rapid addition of 2 mL of EtOH containing 0.530 mg (1.3 mmol) of dppp in the stirring the gold solution produced white precipitate. After allowing the reaction to stir for several hours, the precipitate was collected and washed with excess EtOH. The $Au_2(dppp)Cl_2$ crystals were collected by dissolving the white precipitate in DCM before using both solvent-solvent diffusion of EtOH in DCM and slow evaporation for the crystallization.

2.2.1.6 Chloro(triphenylarsine) Gold(I)

$Au(AsPh_3)Cl$ was synthesized similar to the preparation of $Au(PPh_3)Cl$.[50] 0.250 g (0.635 mmol) of $HAuCl_4 \cdot 3H_2O$ was fully dissolved in acetone and EtOH mixture (1:1 v/v). Rapid addition of 3 mL of purified DCM containing 0.200 mg (0.635 mmol) of $AsPh_3$ in the stirring the gold solution produced white precipitate. After allowing the reaction to stir for several hours, the precipitate was collected and washed with excess EtOH. The crude $Au(AsPh_3)Cl$ was dissolved in DCM and crystallized using both solvent-solvent diffusion of EtOH in DCM and slow evaporation

2.2.1.7 Chloro(triphenylstibine) Gold(I)

$Au(SbPh_3)Cl$ was prepared according to a literature procedure.[54] 5 mL of DCM containing 50 mg (0.17 mmol) of $Au(Me_2S)Cl$ and 60 mg (0.17 mmol) of $SbPh_3$ was prepared in an amber vial. The solution was left to stir under dark for 80 minutes before completely drying under vacuum to remove Me_2S. The precipitate containing crude $Au(SbPh_3)Cl$ was solvated in DCM and repeated washed with excess EtOH. The $Au(SbPh_3)Cl$ crystals were collected using both solvent-solvent diffusion of EtOH in DCM and slow evaporation.

2.2.2 Synthesis of Gold Nanoparticles

2.2.2.1 $Au_{11}(PPh_3)_8Cl_2^+$

$Au_{11}(PPh_3)_8Cl_2^+$ was prepared according to a literature procedure.[45] 50 mg (0.1 mmol) of $Au(PPh_3)Cl$ was fully dissolved in 2 mL of DCM to produce clear solution. Rapid addition of 0.3 mL EtOH containing 1.05 mg (0.07 mmol) of $NaBH_4$ in the stirring $Au(PPh_3)Cl$ solution produced a dark brownish-red solution. After allowing the reaction to stir overnight, the crude sample was precipitated from 50 mL pentane. The supernatant was removed, and the orange pellet was resuspended in minimum amount of DCM. This precipitation was repeated and further purified by column chromatography that was prepared with silica gel and solvent mixture of 20:1 DCM:EtOH. The dark orange band containing $Au_{11}(PPh_3)_8Cl_2^+$ was collected and monitored using UV-Vis. More pure sample of $Au_{11}(PPh_3)_8Cl_2^+$ was attained via evaporative crystallization using 5:1 DCM:octane.

2.2.2.2 $Au_{11}(PPh_3)_8Br_2^+$

$Au_{11}(PPh_3)_8Br_2^+$ was prepared similar to the $Au_{11}(PPh_3)_8Cl_2^+$ procedure. 55 mg (0.1 mmol) of $Au(PPh_3)Br$ was fully dissolved in 2 mL of DCM to produce a clear solution. Rapid addition of 0.3 mL EtOH containing 1.05 mg (0.07 mmol) of $NaBH_4$ in the stirring $Au(PPh_3)Br$ solution produced a dark brownish-red solution. After allowing the reaction to stir overnight, the crude sample was precipitated from 50 mL pentane. The supernatant was removed, and the orange pellet was resuspended in minimum amount of DCM. This precipitation was repeated and further purified by column chromatography that was prepared with silica gel and solvent mixture of 20:1 DCM:EtOH. The dark orange band containing $Au_{11}(PPh_3)_8Br_2^+$ was collected and monitored using UV-Vis. More pure sample of $Au_{11}(PPh_3)_8Br_2^+$ was attained via evaporative crystallization using 5:1 DCM:octane.

2.2.2.3 $Au_{11}(PPh_3)_8I_2^+$

$Au_{11}(PPh_3)_8I_2^+$ was prepared by KI halide anion exchange on $Au_{11}(PPh_3)_8Cl_2^+$. Crude product of $Au_{11}(PPh_3)_8Cl_2^+$ was synthesized using 50 mg of $Au(PPh_3)Cl$ (0.1 mol) prior to removal of excess triphenylphosphine and chlorine ions. The dried $Au_{11}(PPh_3)_8Cl_2^+$ product was then resuspended with 2 mL of DCM and 2 mL of nanopure water containing 166 mg (1 mmol) of KI was added. This solution was mixed vigorously for 2 hours before the aqueous layer was removed, and $Au_{11}(PPh_3)_8I_2^+$ was purified by column chromatography that was prepared with silica gel and solvent mixture of 20:1 DCM:EtOH.

2.2.2.4 $Au_{11}(PPh_3)_7Cl_3$

$Au_{11}(PPh_3)_8Cl_3$ was prepared according to a literature procedure.[45] 50 mg (0.1 mmol) of $Au(PPh_3)Cl$ was added to 2.8 mL of EtOH. 0.3 mL EtOH containing 1.05 mg (0.07 mmol) of $NaBH_4$ was slowly dripped in the stirring cloudy white solution produced a dark brownish-red solution. After allowing the reaction to stir for two hours, the crude sample was precipitated from 50 mL hexane overnight. The supernatant was removed, and the orange pellet was resuspended in minimum amount of DCM. After running through a simple vacuum filtration, further purification of the crude $Au_{11}(PPh_3)_7Cl_3$ was performed by multiple precipitation and resuspension using hexane and DCM, respectively. The $Au_{11}(PPh_3)_7Cl_3$ crystals were collected using solvent-solvent diffusion of hexane in DCM under -20℃.

2.2.2.5 $Au_{11}(PPh_3)_7Br_3$

$Au_{11}(PPh_3)_7Br_3$ was prepared by KBr halide anion exchange on $Au_{11}(PPh_3)_7Cl_3$. Crude product of $Au_{11}(PPh_3)_7Cl_3$ was synthesized using 50 mg of $Au(PPh_3)Cl$ (0.1 mol) prior to removal of excess triphenylphosphine and chlorine ions. The dried $Au_{11}(PPh_3)_7Cl_3$ product was then resuspended with 2 mL of DCM and 2 mL of nanopure water containing 119 mg (1 mmol) of KBr was added. This solution was mixed vigorously for 2 hours before the aqueous layer was removed, and $Au_{11}(PPh_3)_7I_3$ was purified by column chromatography that was prepared with silica gel and solvent mixture of 20:1 DCM:EtOH.

2.2.2.6 $Au_{11}(PPh_3)_7I_3$

$Au_{11}(PPh_3)_8I_3$ was prepared similar to $Au_{11}(PPh_3)_8Cl_2^+$. 59 mg (0.1 mmol) of $Au(PPh_3)I$ was fully dissolved in 2 mL of DCM to produce a clear solution. Rapid addition of 0.3 mL EtOH containing 1.05 mg (0.07 mmol) of $NaBH_4$ in the stirring $Au(PPh_3)I$ solution produced a dark red-brownish solution. After allowing the reaction to stir for 90 minutes, the crude sample was precipitated from 50 mL pentane. The supernatant was removed, and the orange pellet was resuspended in a minimum amount of DCM. This precipitation was repeated and further purified by column chromatography that was prepared with silica gel and solvent mixture of 20:1 DCM:EtOH. The dark orange band containing $Au_{11}(PPh_3)_8I_2^+$ was collected and monitored using UV-Vis. More pure sample of $Au_{11}(PPh_3)_8I_2^+$ was attained via evaporative crystallization using 5:1 DCM:octane.

2.2.2.7 Au_{11}NCs with Cyanide Group

Au_{11}NCs with a cyanide group were prepared by KCN cyanide anion exchange on $Au_{11}(PPh_3)_8Cl_2^+$. Crude product of $Au_{11}(PPh_3)_8Cl_2^+$ was synthesized using 50 mg of $Au(PPh_3)Cl$ (0.1 mmol) prior to removal of excess triphenylphosphine and chlorine ions. The dried $Au_{11}(PPh_3)_8Cl_2^+$ product was then resuspended with 2 mL of DCM and 2 mL of nanopure water containing 65 mg (1 mmol) of KCN was added. This solution was mixed vigorously for 2 hours before the aqueous layer was removed, and Au_{11}NCs with cyanide were purified by column chromatography that was prepared with silica gel and solvent mixture of 20:1 DCM:EtOH.

2.2.2.8 $Au_{11}(dppp)_5^{3+}$

$Au_{11}(dppp)_5^{3+}$ was prepared according to a literature procedure.[31] 35 mg (0.048 mmol) of $Au_2(dppp)Cl_2$ was added to 7.5 mL of EtOH. The white cloudy solution containing $Au_2(dppp)Cl_2$

was stirred 15 minutes prior to the addition of 2.5 mg $NaBH_4$ (0.066 mmol) in 2.5 mL of EtOH, which produced a dark brown solution. After heating up the solution to 70 ℃ overnight, the crude $Au_{11}(dppp)_5^{3+}$ sample was washed with hexane multiple times. The sample was further purified by column chromatography prepared with biobeads S-X1 and DCM. The brown band containing $Au_{11}(dppp)_5^{3+}$ was collected and monitored using UV-Vis. More pure sample of $Au_{11}(dppp)_5^{3+}$ was attained via evaporative crystallization using 5:1 DCM:octane.

2.2.2.9 $Au_{13}(dppp)_4Cl_4^+$

$Au_{13}(dppp)_4Cl_4^+$ was prepared with two step synthesis according to a literature procedure.[55] 40 mg (0.055 mmol) of $Au_2(dppp)Cl_2$ was added to 35 mL of EtOH and mixed with 8.74 mg of $NaBH_4$ (0.23 mmol) in 5 mL EtOH. The dark brown solution was stirred for 2 hours, followed by the removal of insoluble precipitates. The remaining solution was dried and redissolved in 10 mL of EtOH containing 0.25 mL of 37.7% w/w HCl (~ 3 mmol) solution. After 68 hours of stirring, the crude $Au_{13}(dppp)_4Cl_4^+$ solution was dried and resuspended in minimal amount of DCM for column chromatography that was prepared with biobead S-X1 and DCM. The dark red band containing $Au_{13}(dppp)_4Cl_4^+$ was collected and monitored using UV-Vis. More pure sample of $Au_{13}(dppp)_4Cl_4^+$ was attained via evaporative crystallization using 5:1 DCM:octane.

2.2.2.10 $Au_{13}(AsPh_3)_8Cl_4^+$

$Au_{13}(AsPh_3)_8Cl_4^+$ was prepared in a similar manner to $Au_{11}(PPh_3)_8Cl_2^+$. 54 mg (0.1 mmol) of chloro(triphenylarsine) gold (I) was fully dissolved in 2 mL of DCM to produce a clear solution. Rapid addition of 0.3 mL EtOH containing 1.14 mg (0.07 mmol) of $NaBH_4$ in the stirring chloro(triphenylarsine) gold (I) solution produced a dark brownish solution. After allowing the reaction to stir for 90 minutes, the crude sample was precipitated from 50 mL of pentane. The supernatant was removed, and the brown pellet was resuspended in minimum amount of DCM. This precipitation was repeated and further purified by column chromatography that was prepared with biobead S-X1 and DCM. The dark red band containing $Au_{13}(AsPh_3)_8Cl_4^+$ was collected and monitored using UV-Vis. More pure sample of $Au_{13}(AsPh_3)_8Cl_4^+$ was attained via evaporative crystallization using 5:1 DCM:octane.

2.2.2.11 $Au_{13}(SbPh_3)_8Cl_4^+$

$Au_{13}(SbPh_3)_8Cl_4^+$ was prepared according to a literature procedure.[54] 50 mg (0.17 mmol) of $Au(Me_2S)Cl$ was fully dissolved in 2 mL of DCM to produce a clear solution which was then mixed with 60 mg (0.17 mmol) of $SbPh_3$ in 3 mL of DCM. After stirring 80 minutes in the dark, the solution was fully dried to remove any remaining Me_2S. In the fully dried $Au(SbPh_3)Cl$, additional 16.66 mg of $SbPh_3$ (0.05 mmol) was added with 5 mL of DCM. Dropwise addition of 0.83 mL EtOH solution containing 1.58 mg of $NaBH_4$ (0.04 mmol) in the stirring $Au(SbPh_3)Cl$ solution produced a dark brown solution. After allowing the reaction to stir for 6 hours, the crude sample was washed with hexane multiple times. The sample was further purified by column chromatography prepared with Bio-Beads S-X1 and DCM. The brown band containing $Au_{13}(SbPh_3)_8Cl_4^+$ was collected and monitored using UV-Vis. More pure sample of $Au_{13}(SbPh_3)_8Cl_4^+$ was attained via evaporative crystallization using 5:1 DCM:octane.

2.3 Extinction Spectroscopy

Purified Au(I) precursors and AuNCs were suspended in DCM or EtOH and characterized by UV-vis-NIR extinction spectroscopy using a Cary 5000 spectrophotometer (Agilent, Inc.) in quartz cuvettes (Starna Cells, Inc.) with a 1 cm path length. All spectra were baseline corrected with respect to the spectrum of the solvent (DCM or EtOH).

2.4 Electrospray Ionization Mass Spectroscopy

A small amount of purified and dried AuNCs was suspended in 15 μL of MeOH and characterized by electrospray ionization mass spectroscopy (ESI-MS) through direct injection on Shimadzu instrument LCMS-2020. The spray voltage was 3.2-4.0 kV, supplied with a flow rate of 3.00 μL min^{-1}. All the ions were detected in negative mode from 500 to 5000 m/z

2.5 Single Crystal X-Ray Diffraction

The X-ray diffraction intensity data were collected on a Bruker Apex II diffractometer equipped with CCD detector, using Cu IMuS micro-focus radiation (λ = 1.54178 Å). The frames were integrated with the Bruker SAINT software package using a narrow-frame algorithm. Data were corrected for absorption effects using the multi-scan method (SADABS). All the structural solutions and refinements were performed with the SHELXTL suite of programs. Crystal data, data collection parameters, and refinement data are summarized in **Table A1**.

2.6 Photoluminescence Spectroscopy

Purified Au(I) precursors and AuNCs were suspended in DCM or EtOH and characterized by photoluminescence spectroscopy using a Horiba Jobin-Yvon NanoLog spectrometer with 450 W xenon source and a Symphony II InGaAs array detector. Excitation gratings were blazed at 330 nm with 1200 grooves/mm and emission gratings blazed at 780 nm with 100 grooves/mm. All spectra were corrected for gratings, lamp, and detector response. A dark off-set was used for all measurements. A 780 nm NIR cut-on filter (Oriel Instruments) was used in all measurements to block the excitation source. Quartz cuvettes with 1.0 cm × 0.4 cm dimensions (Hellma, Inc.) were used for these analyses.

Particles and standards were excited at 360 nm using an excitation slit width of 5 nm and an emission slit width of 10 nm. Emission was measured from 750 to 1500 nm, using a 30 s integration time with the InGaAs array operating in high dynamic range. For emission/excitation contour maps, the excitation measurements ranged from 300 to 600 nm with 3 nm slits, and the emission measurement ranged from 750 to 1500 nm with 3 nm slits. A 10 s integration time was used with the InGaAs array operating in high sensitivity mode.

2.7 Fourier Transform Infrared Spectroscopy (FTIR)

Infrared vibrational data for Au(I) precursors and AuNCs were collected using Bruker VERTEX-70LS FTIR microscope. Pressed KBr pellets containing each sample were prepared for the IR measurement within the range of 4000-400 cm^{-1}. Additionally, a drop of DCM containing the sample was sandwiched between two NaCl salt plates for liquid phase FTIR measurement. The raw spectra were correct with a background correction.

2.8 Raman Spectroscopy

Raman samples were prepared prior to the experiment by dropping and drying Au(I) precursors and AuNCs in DCM on microscope glass slides. Raman shifts for Au(I) precursor and AuNCs were measured using Renishaw inVia Raman microscope. Dried samples were radiated with 633 nm laser operating at 50 mW CW and measured using 1800 1/mm grating and Renishaw CCD Camera. Different timescale (~ 10-15 seconds) and laser power output (10-50%) was used for various samples.

3.0 Computational Details

All density functional theory (DFT) calculations were performed using CP2K package.[51] The exchange-correlation energy was described by the generalized-gradient approximation with Perdew-Burke-Ernzerh (PBE) exchange-correlation energy functional.[56] The wavefunctions were expended in an optimized double-ζ valence potential molecularly optimized basis sets in their shirt range variant (DZVP-MOLOPT-SR-GTH) with the complementary planewave cut-off of 320 rydberg (Ry) for electron density.[51] Core electrons for Au and halogen atoms have been modelled by norm-conserving scalar relativistic Godeker-Theta-Hutter (GTH) pseudopotentials.[57] Additionally, dispersion interactions were corrected using third order density functional tight binding (DFTB3) methods. [58] The Au(I) precursors were placed in a cubic simulation box of 20 Å while AuNCs were placed in a box size ranging from 40 to 50 Å, which is large enough to separate periodic replica of Au(I) precursors and AuNCs. Structure optimizations were performed using the original crystal structure of each Au(I) precursors and AuNCs with a convergence criterion of 0.023 eV/Å for a residual force and without a symmetry constraint. To further validate the relaxed structure from the DFT optimization, molecular dynamics (MD) simulations were performed on the previously relaxed structure in a canonical (NVT) ensemble with temperature at 300 K. MD simulations were performed for 125 fs scale with 0.5 fs timesteps, which lead to convergence of potential energy and constant quantity of the system. Fully relaxed geometries of each Au(I) precursors and AuNCs were then used to calculate single point energy, projected density of states (PDOS), Kohn-Sham (KS) orbitals, and total electron density. Calculated discrete PDOS were broaden with Gaussian functions having width of 0.07 eV. The Bader charge analyses of individual atoms on the molecules was evaluated by assigning the calculated electron density captured in the zero flux surfaces onto the atom's electron charge density. The optical absorption calculations were performed from the relaxed structure using time dependent density functional theory (TDDFT) implemented in CP2K.[59] Same parameters were used to calculate optical transitions, which were then broadened with Gaussian functions having width of 0.02 eV. Visualization of computational results were done with use of maplotlib package and Visual Molecular Dynamics (VMD) software.[60, 61]

4.0 Results

4.1 Experimental Characterization of Gold Precursors and Nanoclusters

Both gold(I) precursors and phosphine capped AuNCs were synthesized and purified (see **Section 2.2** for experimental details). Using single crystal X-ray diffractometry (SC-XRD), geometry and type of AuNCs were confirmed and analyzed. Experimental optoelectrical measurements, such as absorption, photoluminescence, and vibrational spectroscopy, were used to elucidate the influence of different ligands on overall nanoparticle properties.

4.1.1 Crystal Structures

After the syntheses and purification, the atomic coordination of Au_{11}NCs were identified using SC-XRD (**Figure 5**). Due to low-quality crystals, the X-ray diffraction patterns had large errors for the coordination of $Au_{11}(PPh_3)_7Cl_3$ and $Au_{11}(PPh_3)_8I_2^+$, especially for the lighter elements like carbon and hydrogen. Even with the low resolution of $Au_{11}(PPh_3)_7Cl_3$ and $Au_{11}(PPh_3)_8I_2^+$, X-ray diffraction patterns provided the coordinates for the heavier atoms: gold, halogen, and phosphorous. For $Au_{11}(PPh_3)_7Br_3$, many crystallization attempts yielded no representable crystal to be measured using SC-XRD to produce a reasonable data set. Some crystals structures of previously solved crystal, including $Au_{11}(dppp)_5^{3+}$ and Au(I) precursors, were referenced and used here when they had matching unit cell data from the X-ray diffraction.[34, 50]

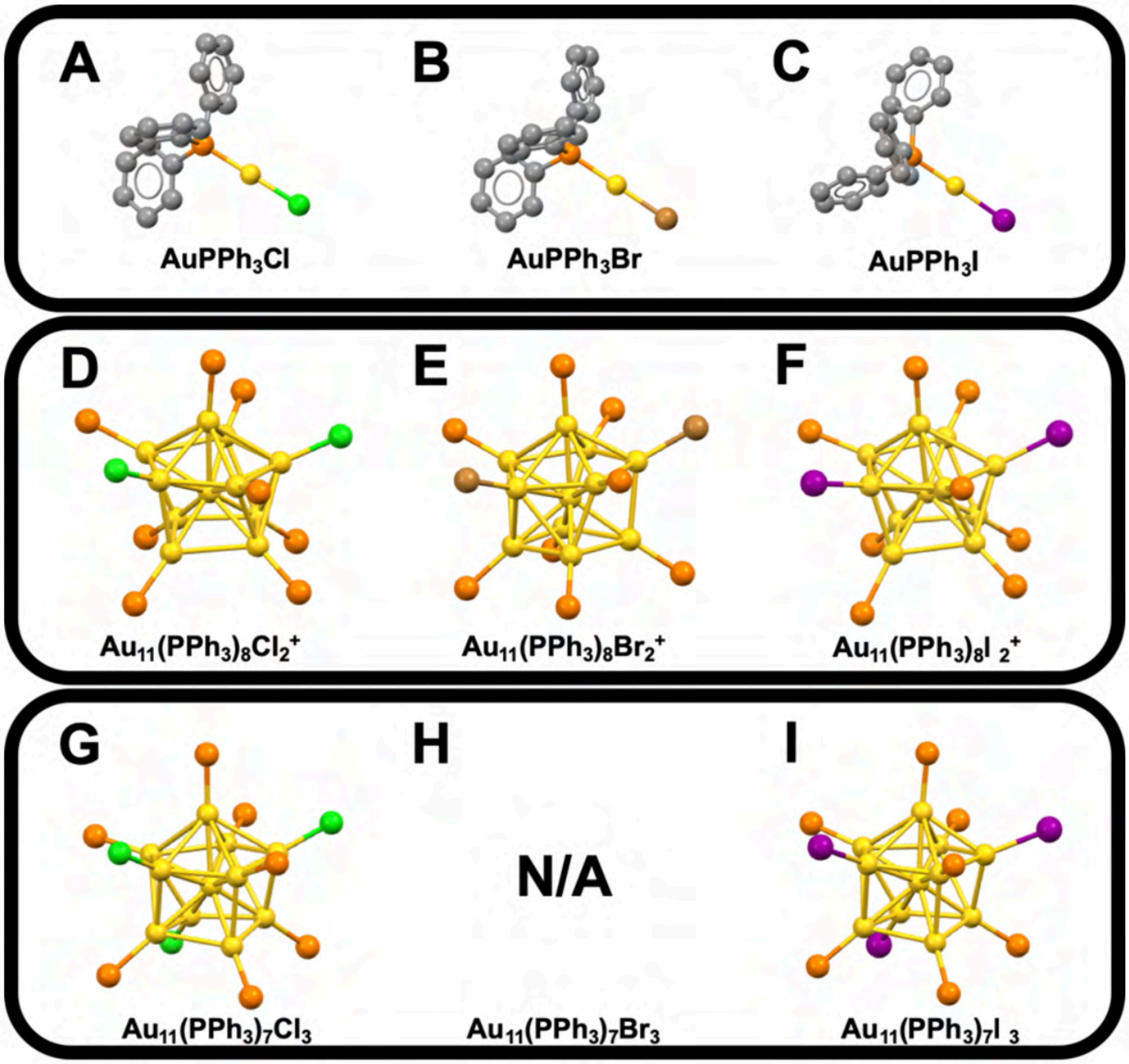

Figure 5. Crystal structure of Au(I) precursors and Au_{11}NCs. The previously reported crystal structures of A) $Au(PPh_3)Cl$, B) $Au(PPh_3)Br$, and C) $Au(PPh_3)I$ were used to match the unit cell of Au(I) precursor crystals. The crystal structure of D) $Au_{11}(PPh_3)_8Cl_2^+$, E) $Au_{11}(PPh_3)_8Br_2^+$, F) $Au_{11}(PPh_3)_8I_2^+$, G) $Au_{11}(PPh_3)_8Cl_3$, and I) $Au_{11}(PPh_3)_8I_3$ were collected using SC-XRD. H) $Au_{11}(PPh_3)_7Br_3$ is left blank due to lack of quality crystal structure.

The crystal structures of the Au(I) precursors and Au_{11}NCs show that the coordination of the ligands on the adjacent gold atom does not change much among different species. The P-Au-

X angle are very close to 180° as well as center Au – surface Au – ligands in the clusters are approximately 180°. Among the Au_{11}NCs, the geometries of the gold core remain very similar: one center gold atom surrounded by the neighboring ten gold atoms, keeping the cluster of the gold core in a pseudospherical shape. The ten surface gold atoms are bound to either halide or phosphine ligands. Among the three $Au_{11}(PPh_3)_8X_2^+$ (X = Cl, Br, I), the overall structures do not change at all. Similarly, with the identical structures among $Au_{11}(PPh_3)_7X_3$ (X = Cl and I), it is safe to assume a similar $Au_{11}(PPh_3)_7Br_3$ structure. In addition to having a different coordination of ligands, the gold core geometries of the $Au_{11}(PPh_3)_8X_2^+$ and $Au_{11}(PPh_3)_7X_3$ are slightly different by having symmetry of C_1 and C_3, respectively.[45]

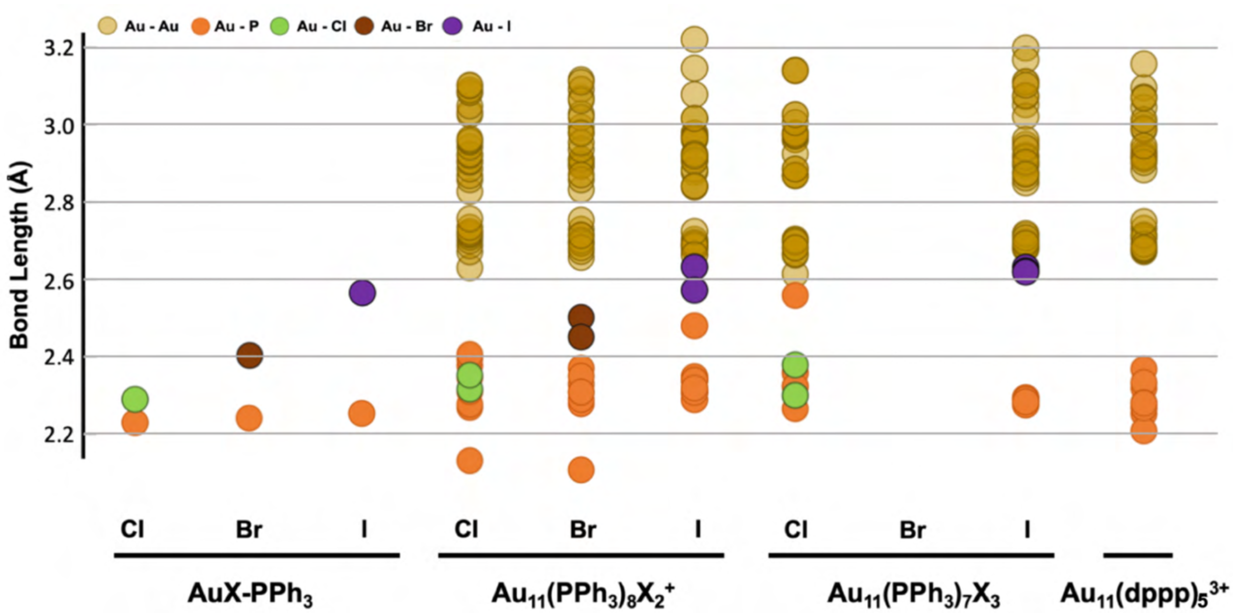

Figure 6. Distribution plots of bonding distance in mononuclear gold precursors and nanoclusters measured from their crystal structures. Color indicates bonds between two elements: gold-gold (yellow), gold-phosphorous (orange), gold-chlorine (green), gold-bromine (brown), and gold-iodine (purple). From left to right: $Au(PPh_3)Cl$, $Au(PPh_3)Br$, $Au(PPh_3)I$, $Au_{11}(PPh_3)_8Cl_2^+$, $Au_{11}(PPh_3)_8Br_2^+$, $Au_{11}(PPh_3)_8I_2^+$, $Au_{11}(PPh_3)_7Cl_3$, $Au_{11}(PPh_3)_7Br_3$, $Au_{11}(PPh_3)_7I_3$, and $Au_{11}(dppp)_5^{3+}$. The bonding distance plot of $Au_{11}(PPh_3)_7Br_3$ was left blank due to lack of its crystal structure.

From the crystal structure of each Au(I) precursor and Au_{11}NC, the bonding lengths between atoms can be plotted to give further insight into the nature of the bonding. For all the compounds, including both Au(I) precursors and Au_{11}NCs, the lengths of the Au-X bonds increase as the atomic radius of the halogen expands. Interestingly, the distance between the Au-P bonds remain uninfluenced by the type of halogen in the system. The average Au-P bonds are slightly larger in the Au_{11}NCs compared to when they are present in mononuclear gold precursors. Similarly, the slight increases in bond length are observed for the gold-phosphorous bonds across the precursors and nanoclusters, but the degree of expansion is rather obscure. Unlike the previously mentioned gold-halogen and gold-phosphorous bonds, the bond lengths among gold atoms in the core have a wide range of lengths, varying from 2.6 to 3.2 Å. For all the Au_{11}NCs, shorter bonds exist between the center gold atom to the neighboring gold atoms while longer bonds form between surface gold atoms to its neighboring surface atoms. The distribution of bonds between gold atoms indicates that each gold atom is in a slightly different environment.

4.1.2 Absorption Spectrum

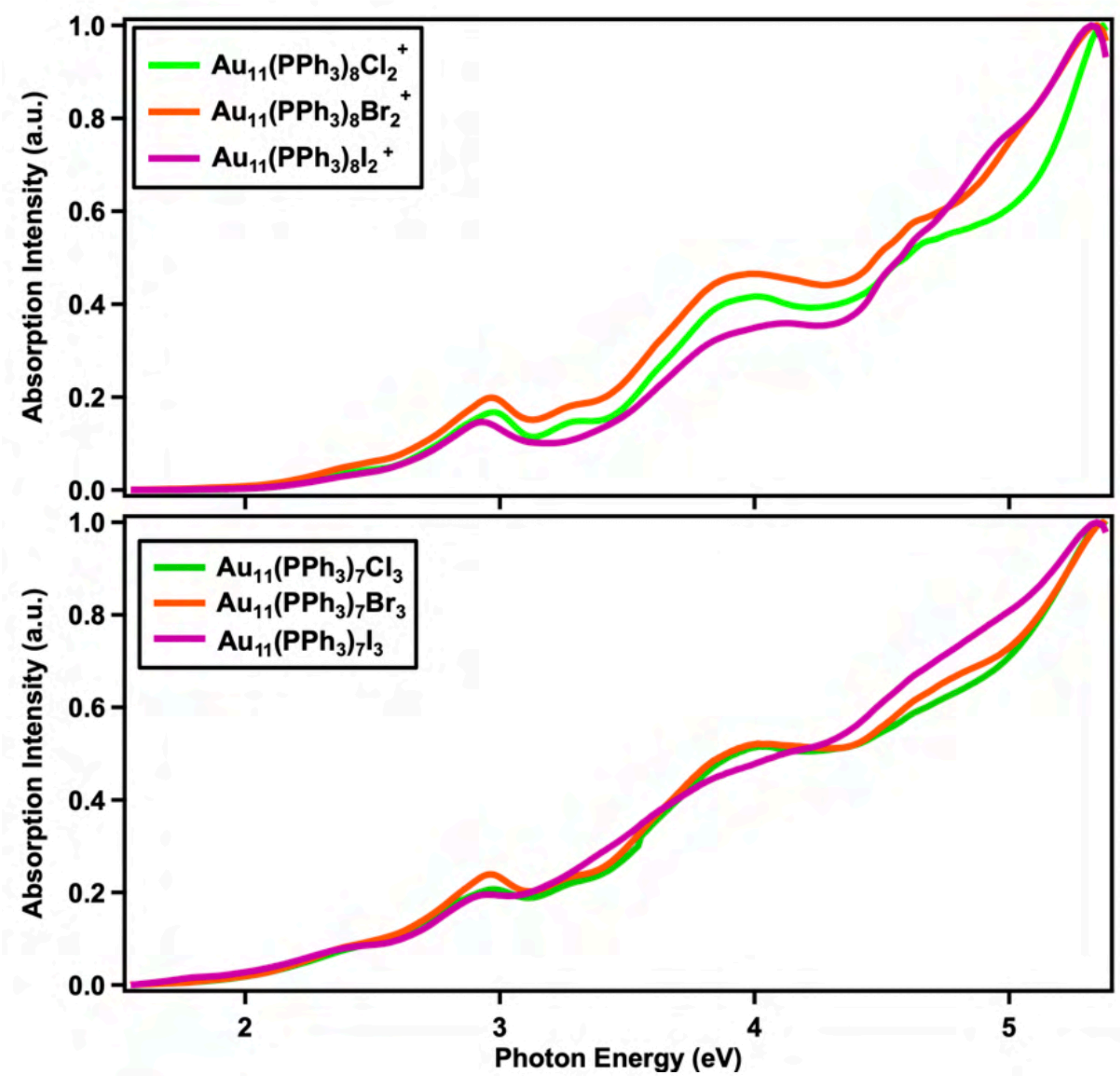

Figure 7. Normalized absorption spectra of $Au_{11}(PPh_3)X_2^+$ and $Au_{11}(PPh_3)X_3$ (X = Cl, Br, and I) with different quantity and types of halides.

All the Au_{11}NCs solvated in DCM have a similar reddish orange color that is indistinguishable with the naked eye. Using the extinction spectroscopy, the absorption features of Au_{11}NCs in the visible to UV regions were measured. The absorption spectrum of $Au_{11}(PPh_3)_8Cl_2^+$

appears to absorb light slightly before 2 eV and shows characteristic absorptions near 2.98, 3.30, 3.85 and 4.70 eV. This pattern, consistent with previous reports, can be assigned to the distorted icosahedral geometry in the gold core (**Figure 7**).[17, 45] As the halogen on gold core becomes heavier, the absorption peak at 2.98 nm redshifts slightly to 2.90 nm. Other features like quenching of small bump at 3.30 nm and broadening of peak at 3.85 nm is also noticeable. The difference between absorption features of $Au_{11}(PPh_3)_8Cl_2^+$ to $Au_{11}(PPh_3)_7Cl_3$ is much harder to detect. For Au_{11}NCs capped with chlorine, there is a minor red shift in the peak at 2.98 for $Au_{11}(PPh_3)_7Cl_3$ compounds followed by a peak shoulder feature near 3.85. Similarly, $Au_{11}(PPh_3)_7Br_3$'s absorption spectrum is virtually indistinguishable from $Au_{11}(PPh_3)_8Br_2^+$, as it only has subtle differences after the 4 eV region. Unlike $Au_{11}(PPh_3)_7Cl_3$ and $Au_{11}(PPh_3)_7Br_3$, absorption features of $Au_{11}(PPh_3)_7I_3$ is more distinguishable from the rest of the Au_{11}NCs. Taken together, these observations confirm that the excitation pathways of nanoclusters are almost identical to each other except for very minor changes in features caused by the differences in their geometry and surface ligand orientations.

4.1.3 Photoluminescence Spectrum

In addition to the observation of excitation pathways in the absorption spectrum, the photoluminescence spectrum can be used to evaluate the relaxation pathways of gold nanoclusters. By exciting the nanoclusters at 3.44 eV, the quantum yield (Φ) in the NIR regions of each nanocluster was calculated based on the two-dimensional emission profiles relative to a $[Yb(tropolone)_4]^-$ standard in optically dilute conditions, shown in the following equation:

$$\frac{\Phi_x}{\Phi_r} = \frac{A_r(\lambda_r)}{A_x(\lambda_x)} \times \frac{I(\lambda_r)}{I(\lambda_x)} \times \frac{n_x^2}{n_r^2} \times \frac{D_x}{D_r} \tag{1}$$

where A and I refer to the absorbance and intensity of the excitation light at the wavelength λ, n is the refractive index, and D is the luminescence intensity integrated from 750 nm (1.65 eV) to 1500 nm (0.827 eV). The subscript x denotes the sample while r is the reference (i.e., $[Yb(tropolone)_4]^-$). The $[Yb(tropolone)_4]^-$ standard was synthesized using a dry dimethyl sulfoxide solution as previously reported in Zhang et al., producing Φ_r = 0.019. A minimum of five data sets using fresh standards of different concentrations were measured prior to making a calibration curve of extinction area versus emission area.[62] The slope of the calibration is forced to go through the origin, representing A_r/D_r in equation 1. With refractive index values of n_x = 1.3617 (ethanol) and n_r = 1.4793 (DMSO), the Φ of each nanocluster was calculated and is listed in the inset table of **Figure 8**.

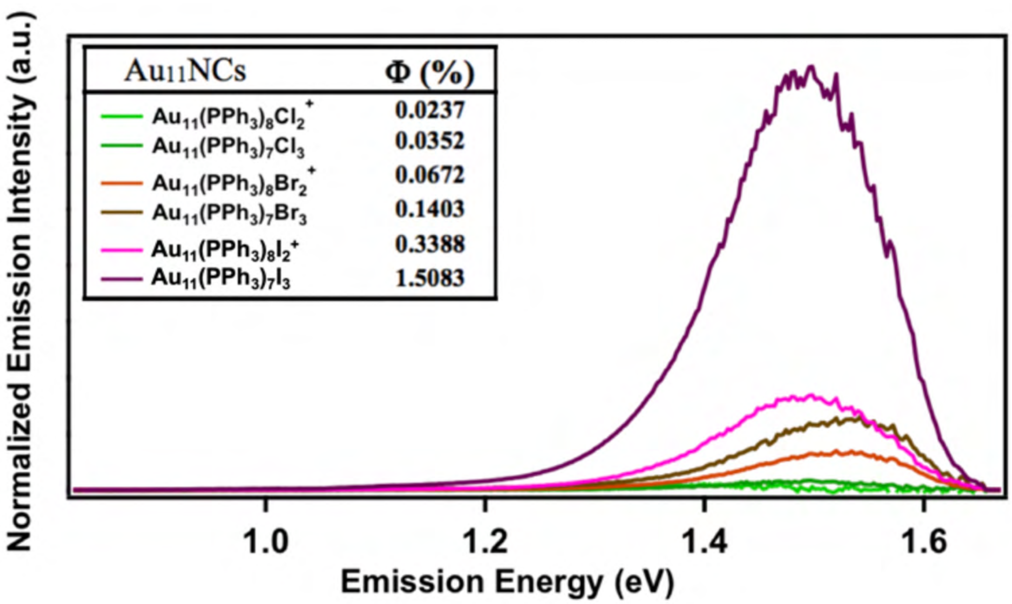

Figure 8. Emission spectra of Au_{11}NCs excited at 3.44 eV. The emission spectra are normalized to their quantum yield (**Φ**) and plotted afterwards to compare their emission profile. The inset table shows each nanocluster and their quantum yield data.

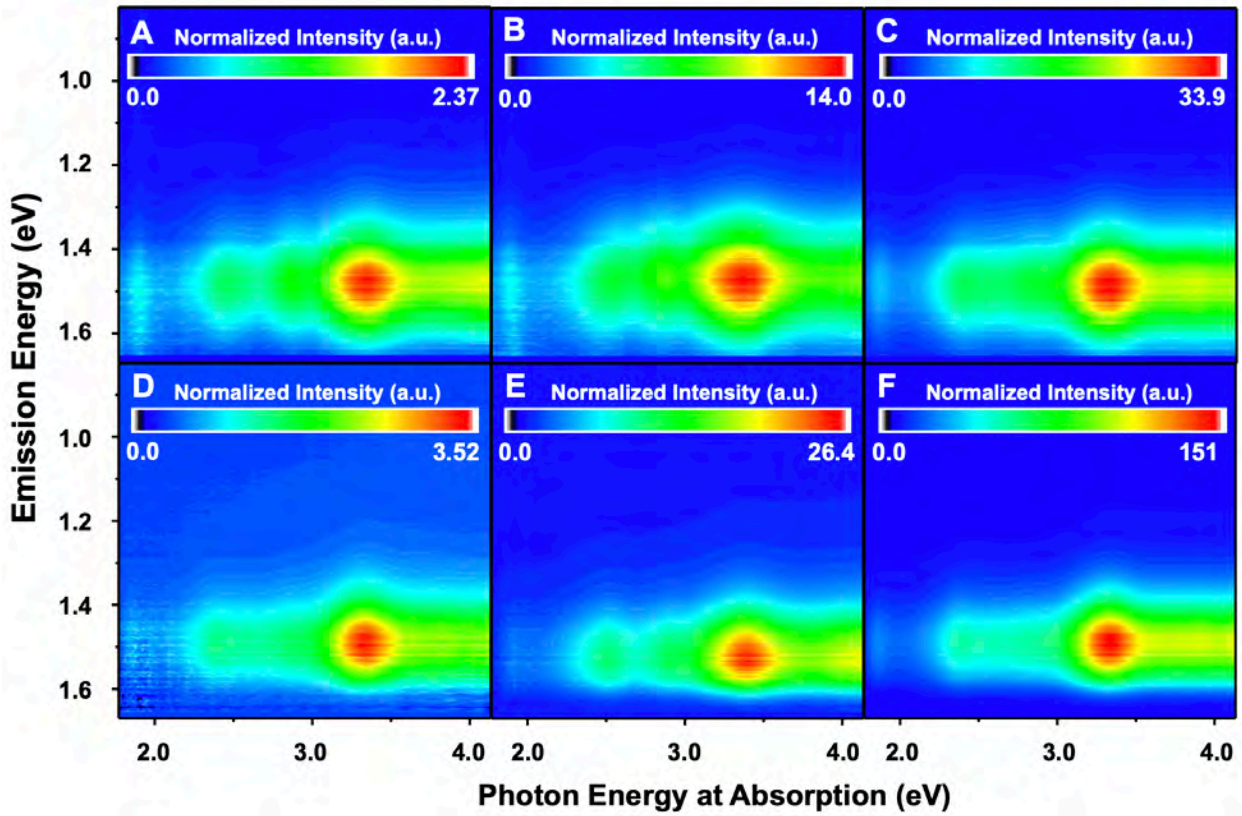

Figure 9. Photoluminescence maps of undecagold nanoclusters A) $Au_{11}(PPh_3)_8Cl_2^+$, B) $Au_{11}(PPh_3)_8Br_2^+$, C) $Au_{11}(PPh_3)_8I_2^+$, D) $Au_{11}(PPh_3)_7Cl_3$, E) $Au_{11}(PPh_3)_7Br_3$, and F) $Au_{11}(PPh_3)_7I_3$. The X-axis shows the photon energy applied to the nanoclusters ranging from 1.8 to 4.1 eV, and the Y-axis shows the photon energy collected from emissions ranging from 0.82 to 1.7 eV. The intensities of each sample are normalized to its own quantum yield. Intense emissions are shown with a red color, while low to no emissions are marked with blue.

After normalizing each emission profile to their own Φ, the same emission spectra are plotted in **Figure 8**. Each gold cluster has a unique Φ, increasing from $Au_{11}(PPh_3)_8Cl_2^+$ to $Au_{11}(PPh_3)_7I_3$. For all the Au_{11}NCs, the emission peak appears close to 1.5 eV. This similarity in the emission peak across all Au_{11}NCs as well as their features are obvious in **Figure 9**, which shows contour maps of emission with varying excitation for each Au_{11}NCs. The first small peak arises short of the excitation photon energy at 2.0 eV, followed by three larger island-like peaks appearing at 2.5, 2.9, and 3.4 eV. Since the maximum emission peak of all the Au_{11}NCs occurs at

3.4 eV, an increase in excitation energy does not increase the intensities of the emissions occurring at higher photon energy in the system. These similar emission features indicate that the relaxation pathways for these nanoclusters are identical, and the difference in the surface ligands is contributing to the increase in Φ.

4.2 Computational Characterization of Gold(I) Precursors and Nanoclusters

Based on the Au(I) precursors and Au_{11}NCs structures collected from SC-XRD (see **Section 4.1.1** for experimental details), computational models were geometrically optimized. The relaxed structures were used to elucidate more information about the electronic structures of the systems. Computationally analyzed electronic behaviors were provided as an addition to experimental observables to correlate the influence of ligands on Au_{11}NCs properties.

4.2.1 Validation of Theory

CP2K executes the first principle molecular dynamics calculation using a mix of Gaussian and plane wave approaches.[51] The Gaussian approach is to describe the wave-function with combination of Gaussian, while the electron density is calculated on a grid using plane wave approach. Having the mixture of two approaches together, CP2K has efficient algorithm that requires smaller memory.[17] With known crystal structures, the computational model is optimized using DFT, which maps out the electron density and product Gaussian functions onto the real-space integration grids. Further, CP2K implements multi-grid system to represent the product Gaussians, which allows plotting smoother Gaussian functions on a grid. The parameters of multi-grid are important in convergence of the calculation which is shown in **Figure 10**. The finer grid requires higher planewave cutoff and results in the overall accuracy of the calculation. Additionally, to ensure not to truncate the planewaves by the edge of the box, the size of the simulation box was always at least two times larger than the Au_{11}NCs including the ligand shell, providing more than 2 nm size from the edge of the Au_{11} NCs in all three dimensions.

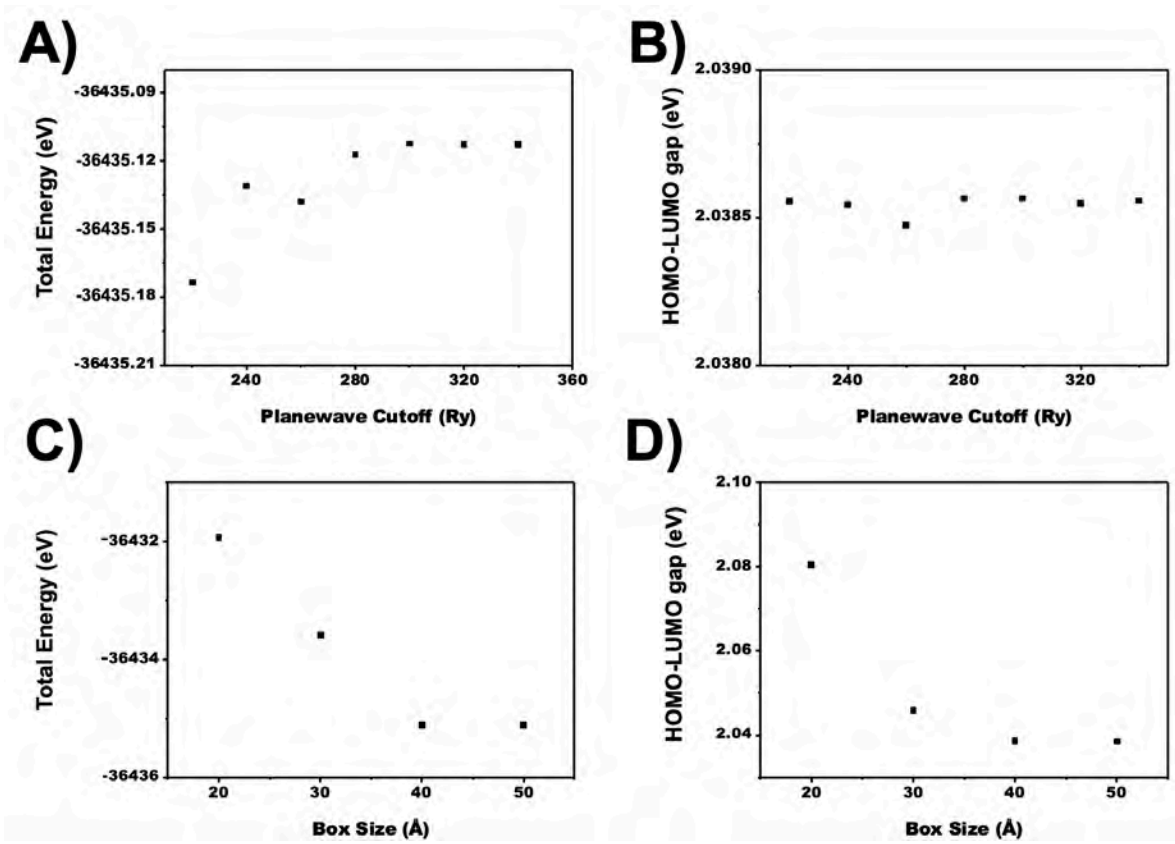

Figure 10. Single point calculation on $Au_{11}(PPh_3)_8Cl_2^+$ with various calculation parameters. A) total energy and B) energy of HOMO-LUMO gap resulting from change in the planewave cutoffs in addition to C) Total energy and D) energy of HOMO-LUMO gap as a function of simulation box size.

After optimizing the geometries of the Au_{11}NCs in the established size of the simulation box with the planewave cutoffs, MD calculations of canonical ensemble were completed to validate the globally optimized structure. In the canonical (NVT) ensemble, the system containing Au_{11}NCs is in contact with a heat bath at 300 K. With both the number of the particles and volume of the system box held constant, the energies can transfer from in and out of the system to the heat bath, meaning that the potential energy of the Au_{11}NCs is no longer conserved. The sum of the energies stored in the Au_{11}NCs and the heat bath, labeled as constant quantity, should be in or close to equilibrium if the geometry of the Au_{11}NC is in the global minimum energy. After 125 fs of MD simulation, the constant quantity converges with less than 0.1 eV differences, indicating that the initial $Au_{11}(PPh_3)_8Br_2^+$ is fully optimize to the global minimum energy (**Figure 11**). The potential energy of $Au_{11}(PPh_3)_8Br_2^+$ converges quickly with slight increase in its value, likely due to the transfer of heat from the heat bath. The geometries of $Au_{11}(PPh_3)_8Br_2^+$ throughout the 125 fs MD simulation show almost no changes, except for small movements of phenyl rings on the PPh_3.

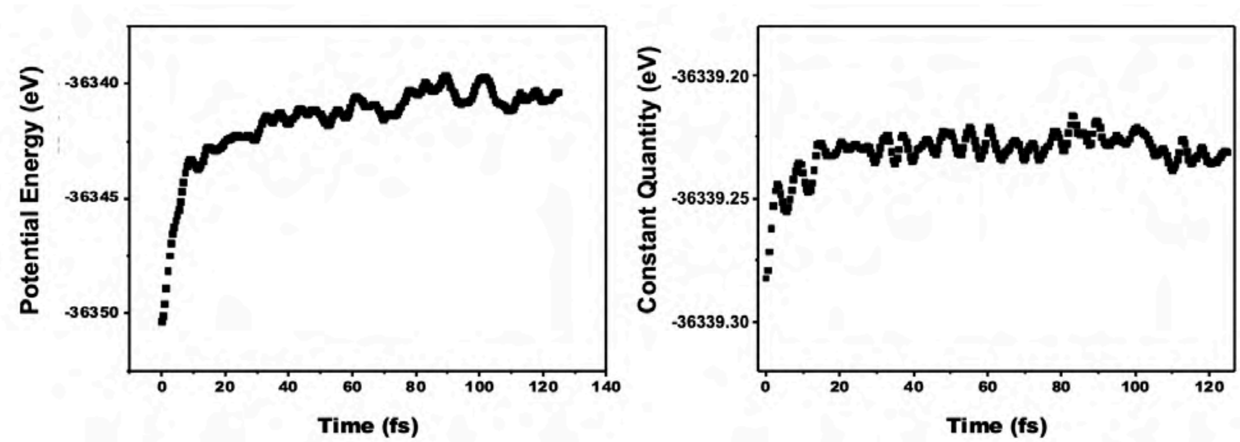

Figure 11. Converging potential energy of $Au_{11}(PPh_3)_8Br_2^+$ and constant quantity from the MD simulation of $Au_{11}(PPh_3)_8Br_2^+$ over simulated time. The MD simulation in canonical ensemble at 300 K was simulated for 125 fs with 0.5 fs timesteps.

Previous theoretical studies on noble metal nanostructures often focus heavily on the binding moieties of the ligands while neglecting the rest of the ligands' geometries for inexpensive calculation time.[17, 55, 63] In this study, the PPh_3 ligands were initially replaced with trimethylphosphine (PMe_3) for computationally relaxed structure (**Figure 12**). While the fully optimized geometries for trimethyl phosphine capped nanoclusters show similar gold cores as the original crystal structure, the angle at which ligands are aligned with the gold on the surface show several distortions. The optimization of the Au_{11}NCs with full ligand shells, including the phenyl rings on the phosphorous, provide much closer geometries to what is observed experimentally. To acknowledge the ligand-ligand interaction among phenyl rings, all the computational models used in this study contain full phenyl rings in PPh_3.

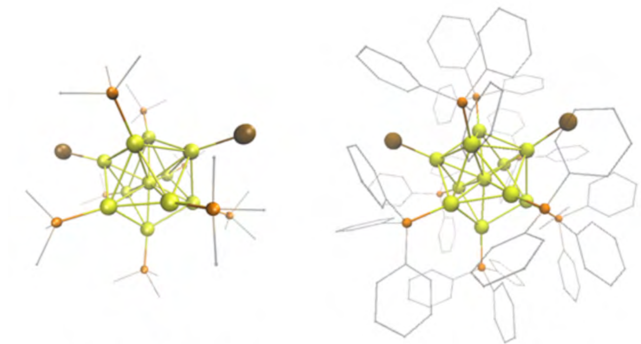

Figure 12. Geometries of the $Au_{11}(PMe_3)_8Br_2^+$ and $Au_{11}(PPh_3)_8Br_2^+$ after completing geometry optimization. The symmetry and geometry of the gold core in the optimized geometry of Au_{11}NCs are highly indistinguishable, but the ligands on the gold surface shows major distortion in $Au_{11}(PMe_3)_8Br_2^+$.

4.2.2 Relaxed Geometry and Bond Lengths

The relaxed geometries and symmetries of mononuclear Au(I) precursors and P-Au_{11}NCs do not deviate much from the original crystal structure of each chemical (**Figure 5**). In general, all bonds expanded 1-5% compared to their crystal structure after the optimization. This expansion is expected from PBE functional, which overestimates bonding energy due to self-interactions.

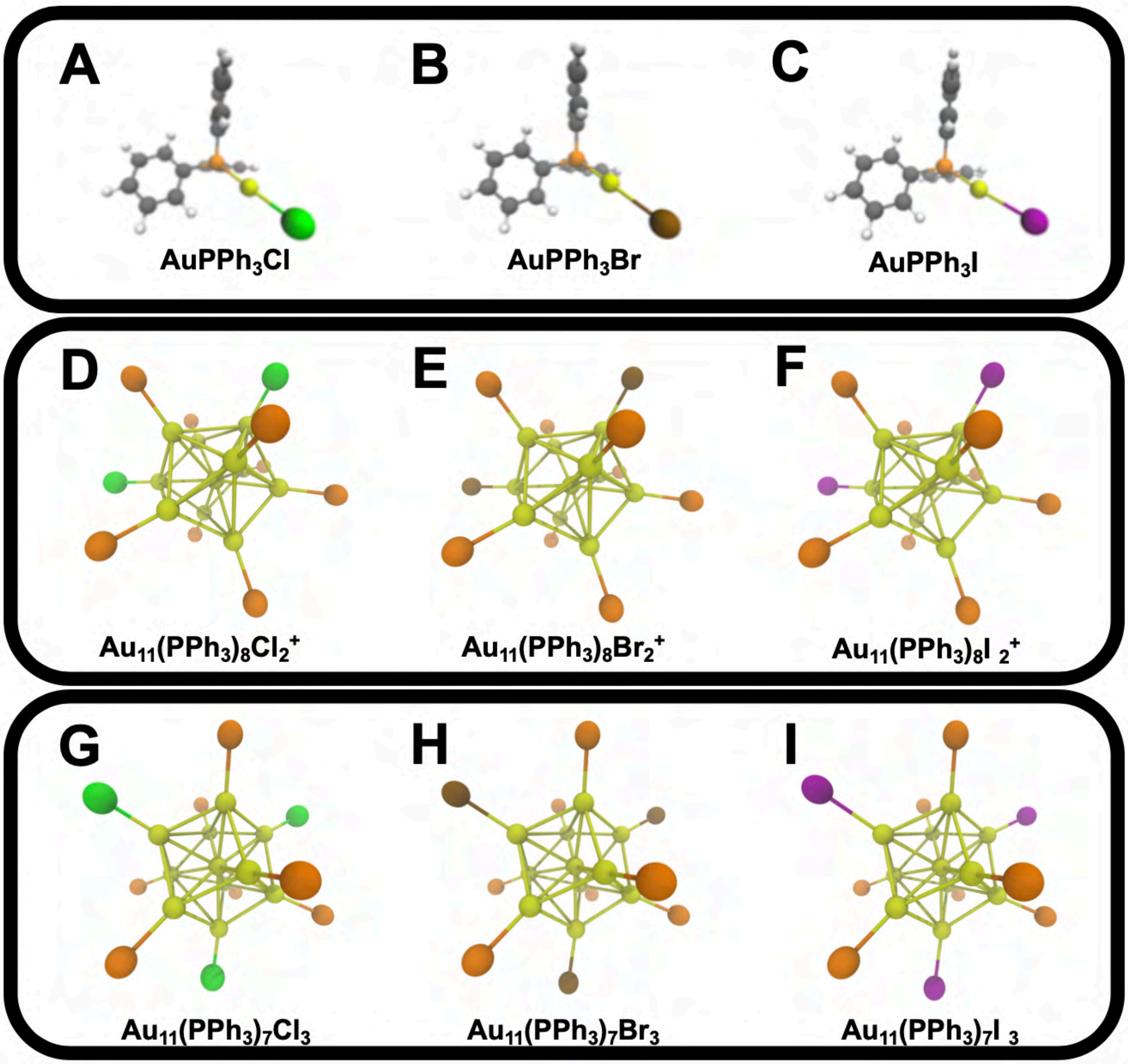

Figure 13. Relaxed geometries of mononuclear gold precursor (A) $AuPPh_3Cl$, (B) $AuPPh_3Br$, (C) $AuPPh_3I$ and undecagold nanoclusters (D) $Au_{11}(PPh_3)_8Cl_2^+$, (E) $Au_{11}(PPh_3)_8Br_2^+$, (F) $Au_{11}(PPh_3)_8I_2^+$, (G) $Au_{11}(PPh_3)_7Cl_3$, (H) $Au_{11}(PPh_3)_7Br_3$, and (I) $Au_{11}(PPh_3)_7I_3$. Phenyl rings of triphenylphosphine (PPh_3) in nanoclusters are omitted from the figure for clarity. Au, yellow; P, orange; Cl, green; Br, brown; I, purple.

The fully relaxed geometries of mononuclear gold precursors and gold nanoclusters can be analyzed further by plotting the individual bonding between two atoms (**Figure 13**). Besides the slight expansion of the bond lengths for all the bonds, the general trends of bond distances are identical to their crystal structures (see **section 4.1.1**). Even the wide range of the bond lengths in Au-Au bonding and the visible separation in the length distributions from center to neighboring gold atoms and surface to other surface gold atoms are present in the computational model of Au_{11}NCs. The major difference between the crystal structure and the computational model is the heterogeneity of the Au-P bond in crystal data. This range of Au-P ligands is likely due to the thermal vibration, whereas the computationally optimized structure does not consider the thermal vibration in calculating the minimum energy point. This correlation between the optimized geometry of the computational model and the crystal structure, combined with the MD simulation, indicates the strong agreement between the theory and the experiment.

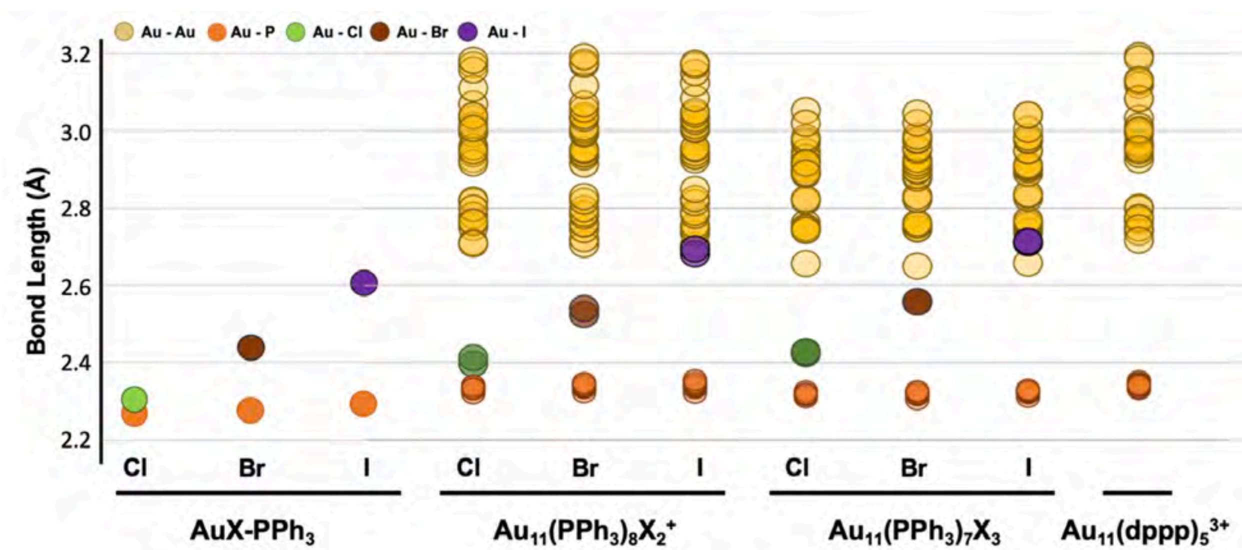

Figure 14. Distribution plots of bonding distance in mononuclear gold precursors and nanoclusters. Color indicates the bonds between two elements: gold-gold (yellow), gold-phosphorous (orange), gold-chlorine (green), gold-bromine (brown), and gold-iodine (purple). From left to right: $Au(PPh_3)Cl$, $Au(PPh_3)Br$, $Au(PPh_3)I$, $Au_{11}(PPh_3)_8Cl_2^+$, $Au_{11}(PPh_3)_8Br_2^+$, $Au_{11}(PPh_3)_8I_2^+$, $Au_{11}(PPh_3)_7Cl_3$, $Au_{11}(PPh_3)_7Br_3$, $Au_{11}(PPh_3)_7I_3$, and $Au_{11}(dppp)_5^{3+}$.

4.2.3 Bader Charge

Having elucidated fully relaxed geometries of each molecule, the electron densities can be calculated for each grid point. Using Bader analyses, the electron densities are captured by zero flux surface and can be assigned to the nearby atom. The sum of the collected electron densities for each atom becomes the Bader charge of individual atoms. The Bader charges of individual atoms, especially those near the metal core, are evaluated to correlate effects of surface ligands on charge densities (**Figure 15**).

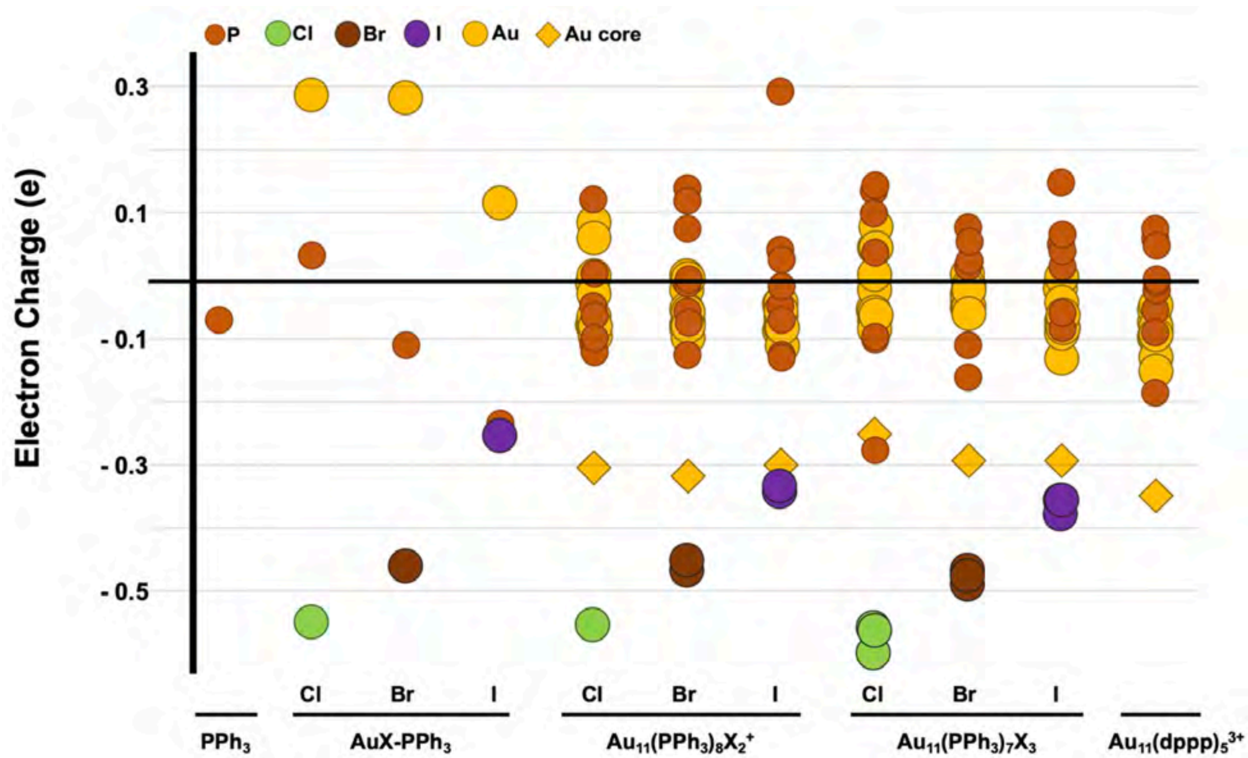

Figure 15. Electron charge distribution plots of atoms in the Au(I) precursors and Au_{11}NCs. Each element is denoted by a color: phosphorous (orange), chlorine (green), bromine (brown), iodine (purple), and gold (yellow). The center gold atom is distinguished with a diamond shape. From left to right: PPh_3, $Au(PPh_3)Cl$, $Au(PPh_3)Br$, $Au(PPh_3)I$, $Au_{11}(PPh_3)_8Cl_2^+$, $Au_{11}(PPh_3)_8Br_2^+$, $Au_{11}(PPh_3)_8I_2^+$, $Au_{11}(PPh_3)_7Cl_3$, $Au_{11}(PPh_3)_7Br_3$, $Au_{11}(PPh_3)_7I_3$, and $Au_{11}(dppp)_5^{3+}$.

Similar to the trend observed for bond length, the charge of the halogen atom is directly related to the size and electronegativity of the halogen atom. As the electronegativity of the halogen increases, the charge on the halogen shows a gradually increasing trend. While there are almost no differences among the charges of chlorine or bromine in the precursors and nanoclusters, the negative charge on iodine atoms, shown as a purple dot in **Figure 15**, seems to increase as the number of iodine atoms increases in the system of $Au(PPh_3)I$, $Au_{11}(PPh_3)_8I_2^+$, and $Au_{11}(PPh_3)_7I_3$. Due to less electronegativity, phosphorous and gold atoms are more susceptible to their surroundings, especially in the mononuclear gold precursor. In comparison to the slightly negative charge on the phosphorous atom in PPh_3, the charge on phosphorous in PPh_3 bound on gold halide transitions from positive to negative as the halide moves from chlorine to iodine. This halide-dependent phosphorous charge trend is not apparent in nanocluster cases where the charge of phosphorous on PPh_3 normally falls somewhere near neutral. The influence of halogens on the charge of the gold core is much more obvious, notably on the gold atoms that are adjacent to the halogen atoms (**Figure 16**). Unlike most of the gold atoms in the core possessing neutral or slightly negative charges, the gold atoms neighboring the chloride ligands show electron deficiency, which is due to the direct influence of the highly electronegative chlorine atoms. Once the chloride ligands are replaced with bromide and iodide ligands, gold bound to the halogen atom shows neutral and negative charges, respectively. The gold atoms that are not directly bound to the halogen atom display very subtle changes in their charges as a function of halogens. Plotted as yellow diamonds in **Figure 15**, the charges on the gold atom in the center of the nanocluster core are relatively independent from various ligands and have the most negative values compared to all the other gold atoms in the metal core.

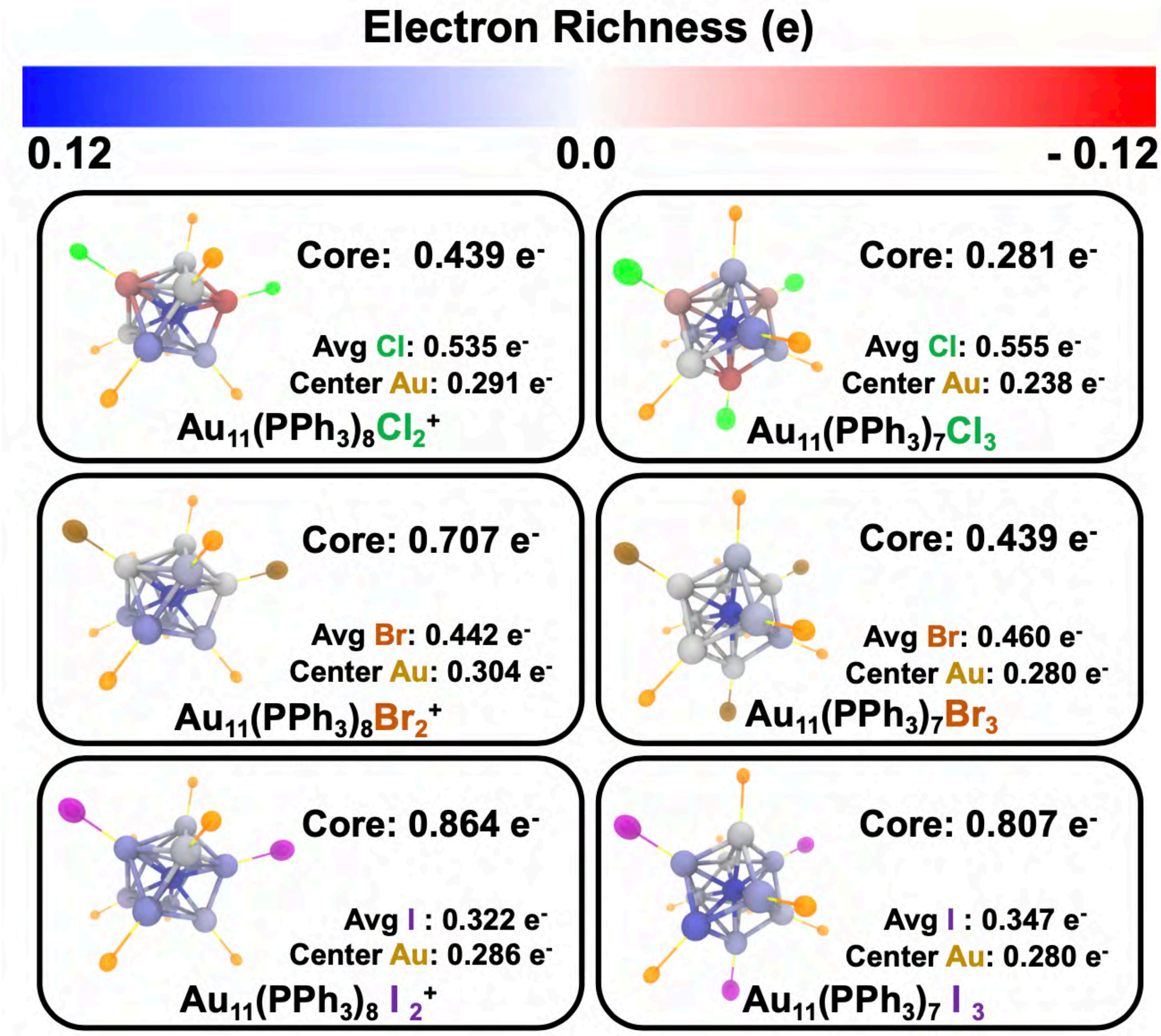

Figure 16. Relaxed structures of phosphine-halide-protected Au_{11}NCs with Bader charges projected on gold atoms. The blue color indicates an electron rich atom whereas the red color indicates an electron poor atom. The core charges of each cluster were calculated by adding up the Bader charges of each gold atom. The electron richness of the center gold atom and an average electron richness for the halide atoms are also denoted below.

4.2.4 Projected Density of States

Projected density of state (PDOS) calculation is a useful way of describing the electronic structure by the electron energy states and the possible states that electrons can occupy at specific energy. In a simple and small molecule like $Au(PPh_3)Br$, the PDOS shows highly quantized energy levels even after some degree of Gaussian broadening has been considered (**Figure 17**). Each discrete energy level is visualized with a different color to illustrate the contributions of atomic orbitals (AO) at each energy state. For instance, the electron density at the HOMO state of $Au(PPh_3)Br$ is mostly located on the gold and bromine, as the majority of the HOMO peak consists of yellow and brown colors. The HOMO state of $Au(PPh_3)Br$ also contains more states per energy compared to neighboring states, which is an indicator that the HOMO state has two degenerate states.

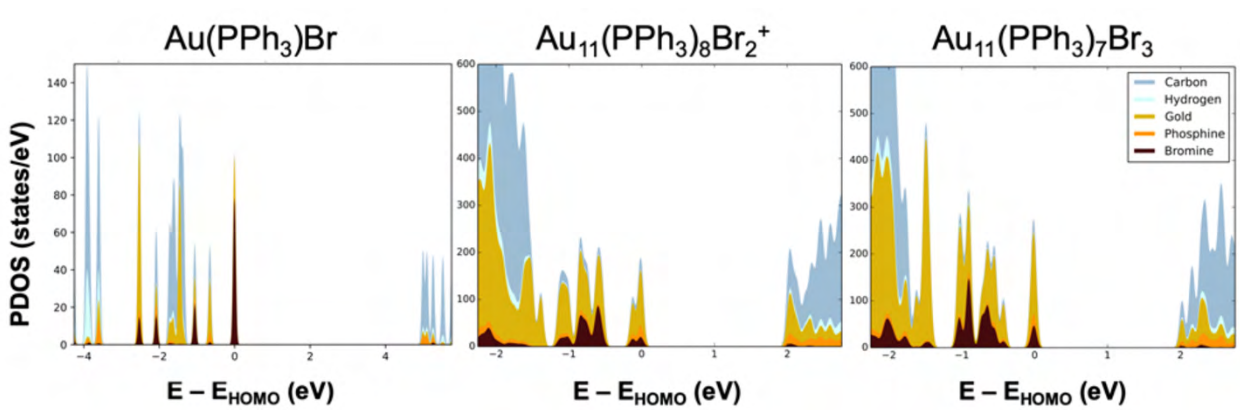

Figure 17. PDOS of $Au(PPh_3)Br$, $Au_{11}(PPh_3)_8Br_2^+$, and $Au_{11}(PPh_3)_7Br_3$. The x-axis denotes energy states with reference to HOMO level. The y-axis shows possible electronic occupancy for the specific energy states. Different colors were used to describe the elemental contributions: carbon (dark blue), hydrogen (light blue), gold (yellow), phosphorous (orange), and bromide (brown). Each state in PDOS was broadened with 0.05 eV.

Having more atoms incorporated to the system, PDOS of $Au_{11}(PPh_3)_8Br_2^+$ and $Au_{11}(PPh_3)_7Br_3$ both display increased states per energy and more continuous states compared to

Au(I) precursors. While having more continuous lower occupied energy states, due to their small sizes, $Au_{11}NCs$ still contain molecule-like discrete energy levels, especially near the HOMO region. There is a major decrease in the energy of HOMO-LUMO gap in $Au_{11}NCs$ (1.94 eV for $Au_{11}(PPh_3)_8Br_2^+$) compared to Au(I) precursors (4.46 eV for $Au(PPh_3)Cl$), which is also evidenced by appearance of absorption features of $Au_{11}NCs$ in the visible spectrum (see **section 4.1.2**). Interestingly, the HOMO-LUMO gap between the two $Au_{11}NCs$ are virtually indistinguishable, as well as the other general trends observed in the PDOS of two $Au_{11}NCs$.

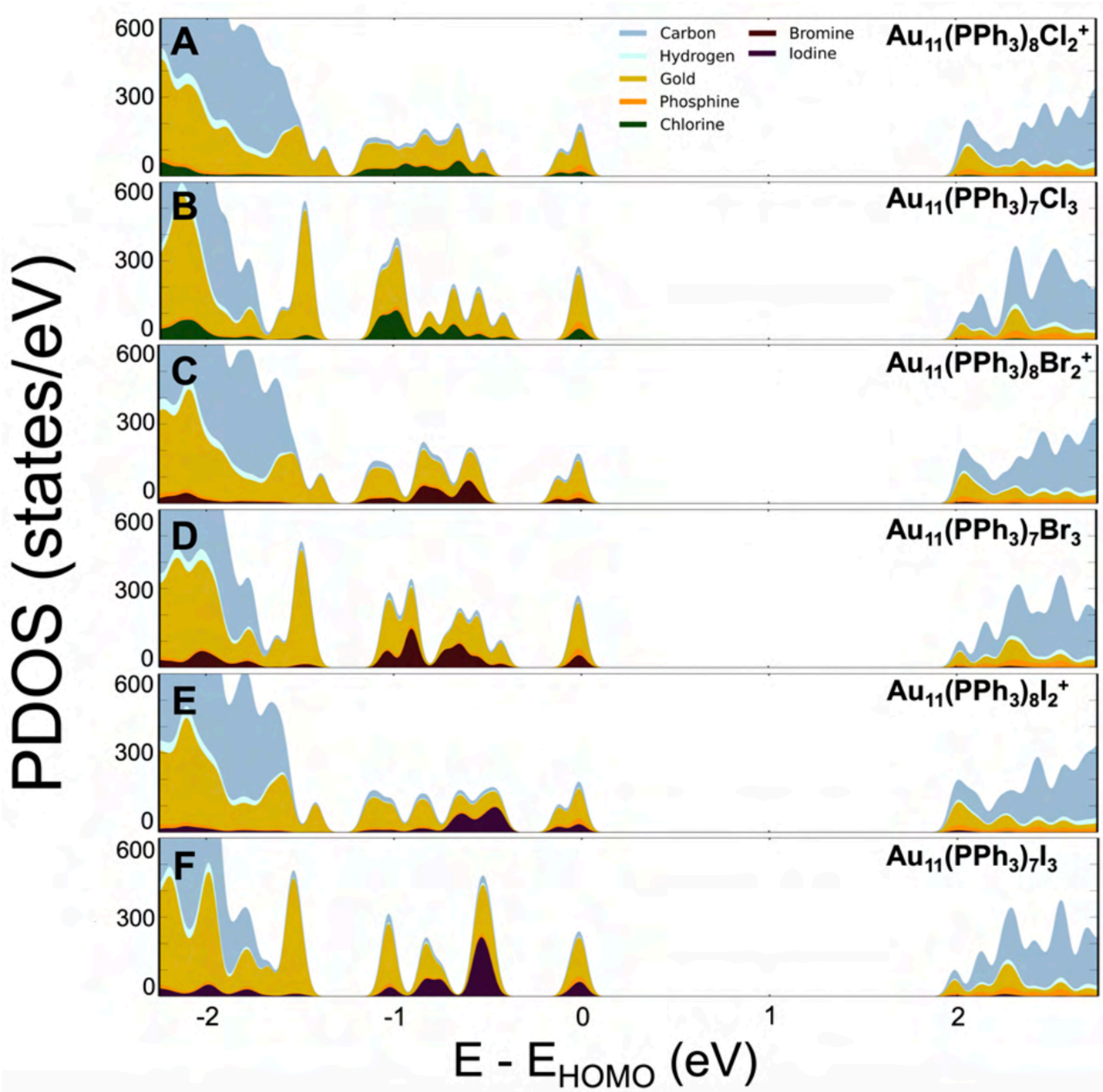

Figure 18. PDOS of undecagold clusters A) $Au_{11}(PPh_3)_8Cl_2^+$, B) $Au_{11}(PPh_3)_7Cl_3$, C) $Au_{11}(PPh_3)_8Br_2^+$, D) $Au_{11}(PPh_3)_7Br_3$, E) $Au_{11}(PPh_3)_8I_2^+$, and F) $Au_{11}(PPh_3)_7I_3$ near HOMO-LUMO regions. Energies are represented respect to the energies at HOMO. Colors represent different elemental contribution to the orbital energy level.

Comparing across the nanoclusters, general features are very alike, including the HOMO-LUMO gaps among all the nanoclusters, which are approximately 2 eV. There are a few degenerate orbitals at the HOMO state, which are composed of AOs of gold and halogen. After a small separation in energy, the HOMO state is followed by the islands of energy states near HOMO – 0.75 eV, also composed mainly of gold and halogen AOs. Further down in the occupied MO, more continuous states constitute large portions of orbital contributions from gold and PPh_3, whereas unoccupied MO states are mostly consisting of MOs from PPh_3. Among these general features of Au_{11}NC's electronic structures, there are minor differences observed between the PDOS of Au_{11}NCs. The differences will be discussed further (see **Section 5.3** for more discussion of PDOS).

4.2.5 Orbital Diagram

Apart from the observation of AO contributions in different energy levels, electron density calculations can be used to display Kohn-Sham (KS) orbitals in three dimensions. Represented as red and blue, the two phases in the molecular orbitals provide information on localization of electrons and the type of the bonding at specific energy levels, especially near the frontier orbitals.

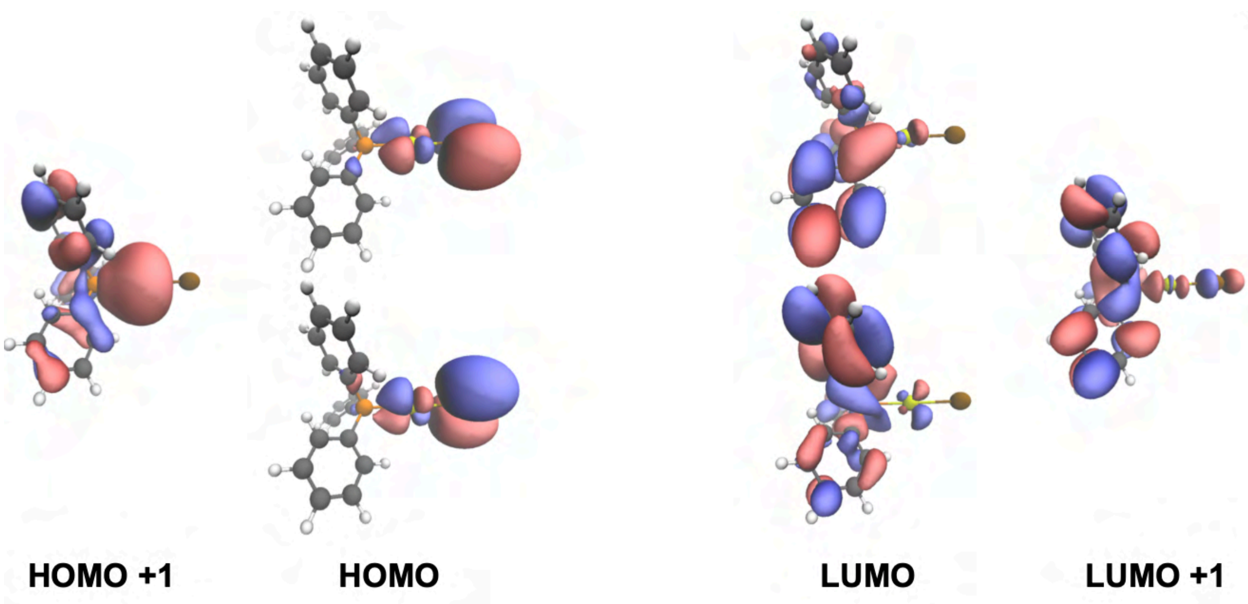

Figure 19. Orbital diagrams of $Au(PPh_3)Br$ near the frontier orbitals. HOMO and LUMO states are doubly degenerates. The orbitals were displayed with isosurface value of 0.02. The blue and red colors indicate differences in their phase.

Just as it was in PDOS, the additional gold atoms in Au_{11}NCs add more complication to the orbital diagrams of Au_{11}NCs compared to what is observed with Au(I) precursors. The HOMO of the Au_{11}NCs shows partially distorted superatomic p-orbital, which is propagated through the core of nanoclusters and interacts with the p-orbitals of bromide and phosphorous on the same plain that bromide is on (**Figure 20**).[17] This HOMO diagram is one of the three degenerate orbitals for $Au_{11}(PPh_3)_8X_2^+$. As seen in **Figure 19**, even with changes in their halogen moieties, the orbital structures are virtually indistinguishable besides the slight enlargement of p-orbitals on the halogens. These orbital similarities among the set of 2-halogen nanoclusters also exist for all the energy levels calculated.

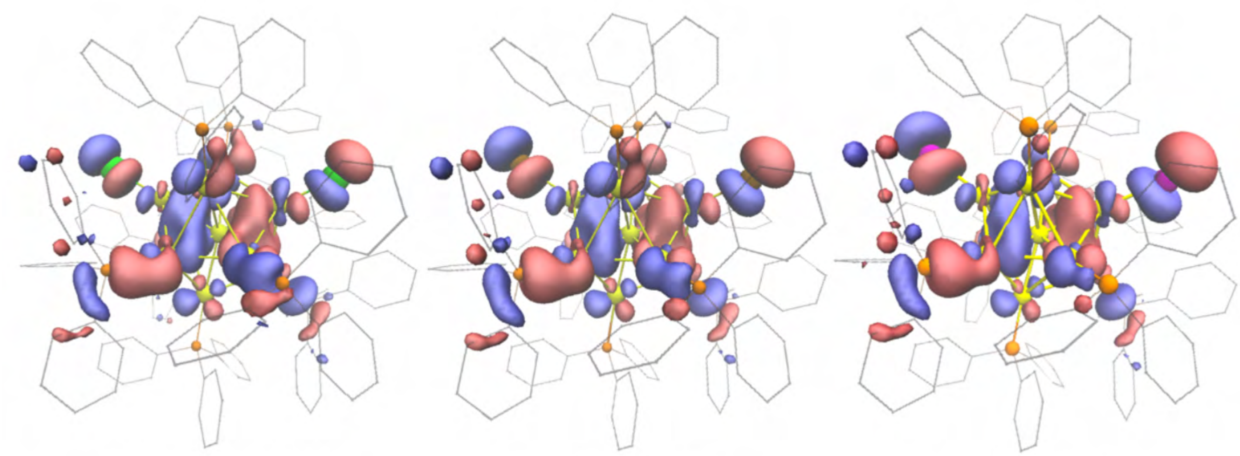

Figure 20. One of three degenerate Highest-Occupied-Molecular-Orbital representations of a) $Au_{11}(PPh_3)_8Cl_2^+$, b) $Au_{11}(PPh_3)_8Br_2^+$, and c) $Au_{11}(PPh_3)_8I_2^+$. The orbitals were displayed with an isosurface value of 0.02. The blue and red colors indicate differences in their phase.

With increasing symmetry, $Au_{11}(PPh_3)_7X_3$ compounds show more degenerate molecular orbitals compared to $Au_{11}(PPh_3)_8X_2^+$. However, as previously observed with similar elemental contribution on PDOS (**Figure 18**), the overall trends orbital diagrams for both $Au_{11}(PPh_3)_8X_2^+$ and $Au_{11}(PPh_3)_7X_3$ near the frontier orbitals are comparable to each other (**Figure 21**). First, in the low-energy occupied orbital near the – 2eV corresponding to the energy of HOMO, major orbital contributions originate from π-conjugated bonds in phenyl rings, which have almost no direct interaction with the d orbitals of gold that are responsible for the d-band. There are minor contributions from π-bonding between gold's d-orbitals and the halogen's p-orbitals. At the edge of this d-band, electron density is mostly localized in the gold core and has almost no participation from the orbitals of ligands. As the molecular orbital gets energetically closer to the HOMO, π^* orbitals from gold and π-donating halide ligands start to fill up. Even with only a few halogen atoms, especially compared to the number of gold atoms in Au_{11}NCs, the electron density of the halide dominates the energy states as seen in both PDOS and KS orbital. Another interesting behavior of this molecular orbital is that the weak π^* bond starting from the halides to the adjacent gold atom propagates through the d-orbitals in the gold core to the p orbitals in other halides. Some of the d-orbital propagation in the gold core reaches the phosphorous atoms and form a σ^* interaction. In the HOMO of the phosphine-halide-capped Au_{11}NCs, the overall orbital interaction behaves similarly, except that the gold core has now occupied the super atomic p-orbital, which is visualized in the center gold.

Unlike the localized electron densities near the HOMO, electron density of the LUMO spreads out on the surfaces of the gold core as well as on the PPh_3 (**Figure 22**). The d and p-orbitals of surface gold atoms donate their electron density to the empty d-orbitals of the phosphorous, which produces π-back-bonding as displayed by the KS orbital and the appearance of d-orbitals in phosphorous. As electrons are promoted further into unoccupied orbitals, more electron densities from gold transfer to unoccupied s and d orbitals of phosphine and π^* orbitals of phenyl rings.

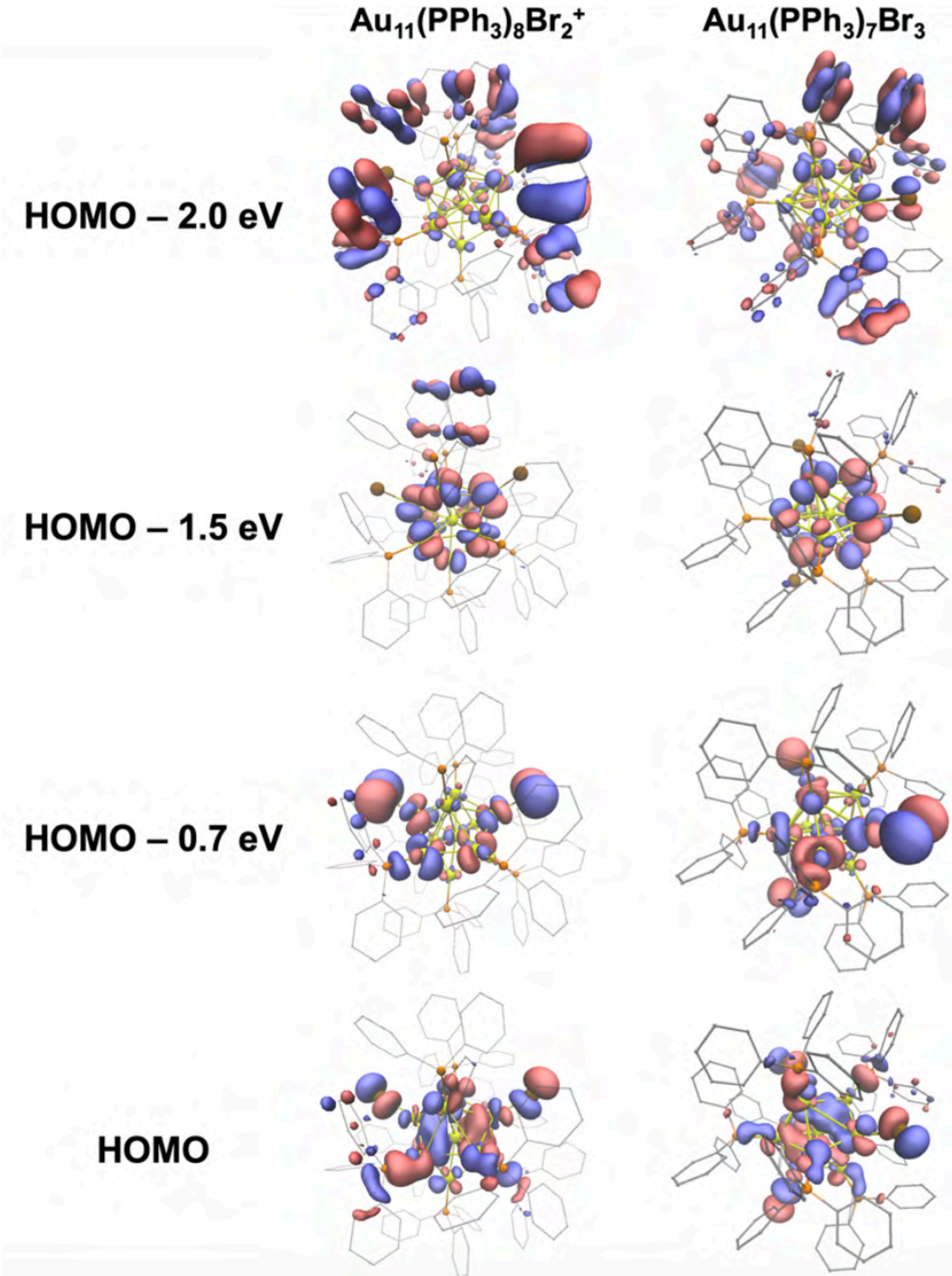

Figure 21. Kohn-Sham orbital representations of $Au_{11}(PPh_3)_8Br_2^+$ and $Au_{11}(PPh_3)_7Br_3$ at different energies near HOMO. The labels on the left indicates approximate energies of represented orbitals respect to HOMO energy.

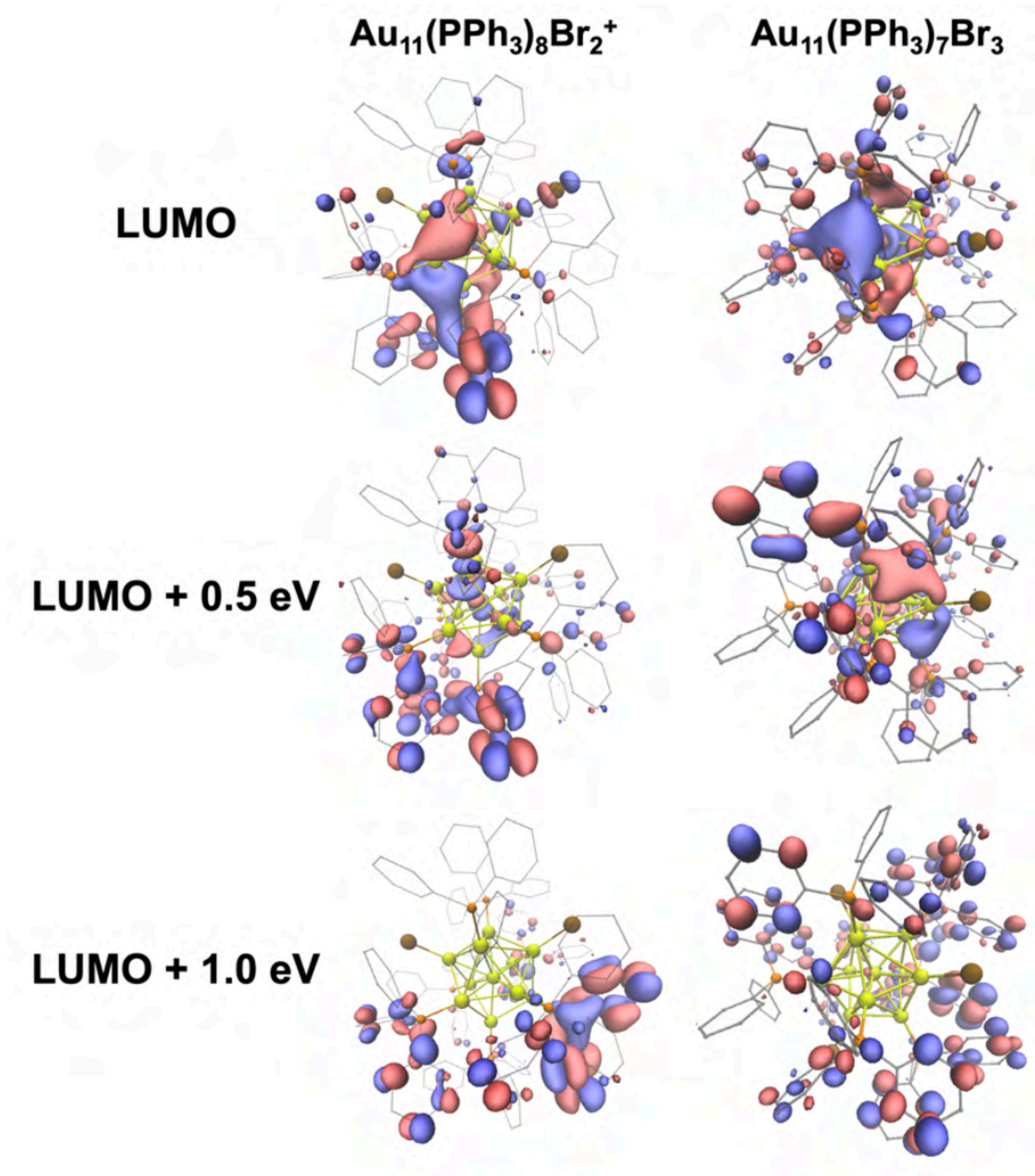

Figure 22. Kohn-Sham orbital representations of $Au_{11}(PPh_3)_8Br_2^+$ and $Au_{11}(PPh_3)_7Br_3$ at different energies near LUMO. The labels on the left indicates approximate energies of represented orbitals respect to LUMO energy.

4.2.6 Computed Extinction Spectrum

With TDDFT, transitions from occupied energy states to unoccupied energy states and their oscillator strength is calculated, which was used to simulate the absorption spectrum (**Figure 23**). The noticeable shifts in the absorption energy between simulated and experimental spectra is due to the overestimation of the transition energy in TDDFT, which has been reported previously, including the systems containing gold nanoclusters of similar sizes.[34] However, the general features in the experimentally collected spectra exist in the simulated spectra, which is a good indicator that the simulated spectra of Au_{11}NCs can be used to described the electronic structure of the nanoclusters as a function of incoming energies.

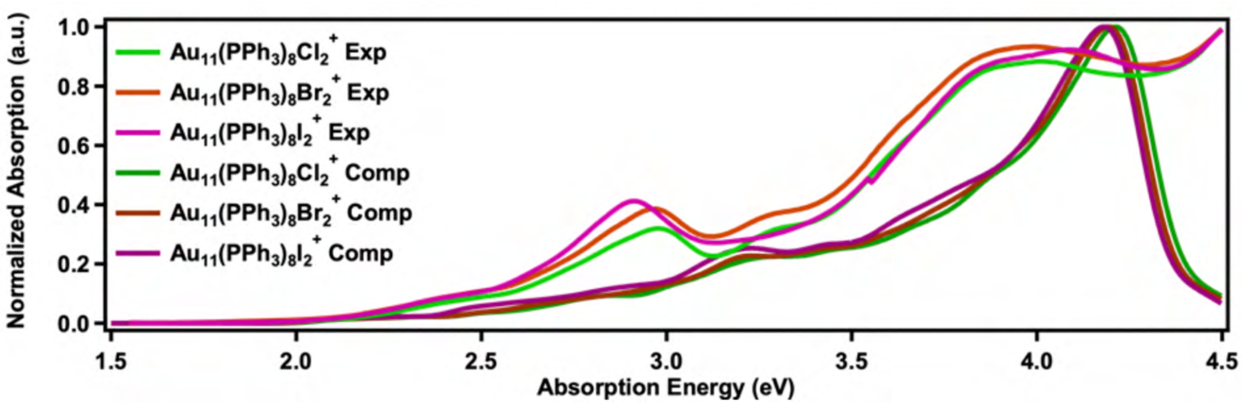

Figure 23. Direct comparison of experimentally collected absorptions and simulated absorptions of $Au_{11}(PPh_3)_8X_2^+$. The chlorine, bromine, and iodine capped Au_{11}NCs are indicated by color green, brown, and purple, respectively. The experimentally collected spectrum is lightly colored compared to the simulated collected spectrum of similar shade of color. The simulated spectrum of nanoclusters was broadened with 0.02 eV to closely match the features seen in the experimental result.

While the HOMO-LUMO gap of the Au_{11}NCs are near the 2 eV regions, the visible absorption of the nanoclusters in the simulated spectrum starts to appear around 2.4 eV. The major contributor of this initial absorptions is still occurring near the frontier orbitals, which shows the superatomic p-orbitals to the superatomic d-orbital transitions (**Figure 24**).[64] This superatomic p-orbitals to the superatomic d-orbital transitions continue to play a major role in the increasing absorption intensity following the first frontier orbital transitions near 2.4 eV. Near the 3.0 eV, the electrons from the HOMO states reaches higher unoccupied states where the majority of the electron density is localized in the phenyl rings of the PPh_3. Additionally, the orbitals with energy levels below the HOMO states begin to participate in the excitation to the LUMO states. The simulated absorption spectrum shows that the combination of these two different electronic transitions leads up to the peak near 3.2 eV, which is much more pronounced in the experimental absorption spectra slightly before 3.0 eV. The halide ligands' induced peak shift observed in the experimental absorption spectra is also present in the simulated spectrum but to a much smaller degree as seen in **Figure 23**. The halide ligands play no role in the peaks near the 4.2 eV because the transitions are mostly composed of the d-band near the HOMO -1.5 eV to higher energy unoccupied orbitals (**Figure 24**).

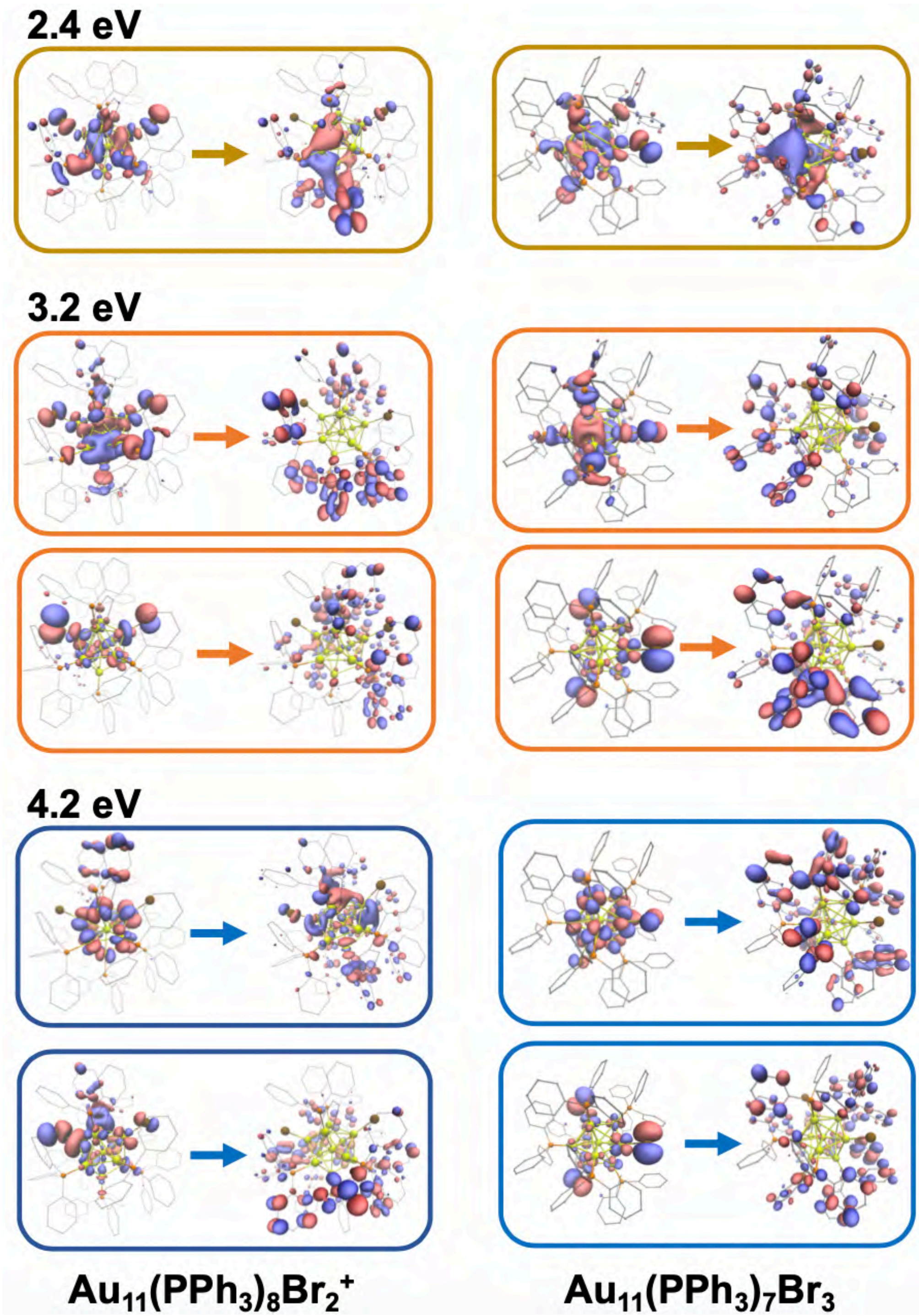

Figure 24. The major electronic transition of $Au_{11}(PPh_3)_8Br_2$ and $Au_{11}(PPh_3)_7Br_3$ at the various excitation energies. The electronic transitions from occupied to unoccupied orbitals with most contributing oscillator strength at A) 2.4 eV, B) 3.2 eV, and C) 4.2 eV were described. The excitation energies are labeled on the top of each transitions.

5.0 Discussion

5.1 Structures and Symmetries of Phosphine Gold Products

Upon reduction with strong reductant like $NaBH_4$, mononuclear gold precursors undergo nucleation and form AuNCs. The composition of the AuNCs is influenced by the identity of the initial precursors as well as reduction procedures. We synthesized $Au_{11}(PPh_3)_8Cl_2^+$ and $Au_{11}(PPh_3)_7Cl_3$ using previously reported procedures that use $Au(PPh_3)Cl$ as the initial precursor and vary the solvent and the amount of reducing agent to produce clusters of different compositions (see **Section 2.2.2.1** and **Section 2.2.2.4** for experimental details). The resulting $Au_{11}(PPh_3)_8Cl_2^+$ and $Au_{11}(PPh_3)_7Cl_3$ clusters are very similar in structure. They each have a gold core (a single gold atom in the center surrounded by ten gold atoms) and PPh_3 and chlorine surface ligands (coordinated to the ten outer gold atoms in an on-top position). The clusters have the same number of total ligands, but the ratio of halide to phosphine ligands is different. With an additional halide atom on the surface of the cluster, $Au_{11}(PPh_3)_7Cl_3$ has higher symmetry of C_{3v} compared to C_1 symmetry for $Au11(PPh_3)_8Cl_2^+$ (**Figure 25**).

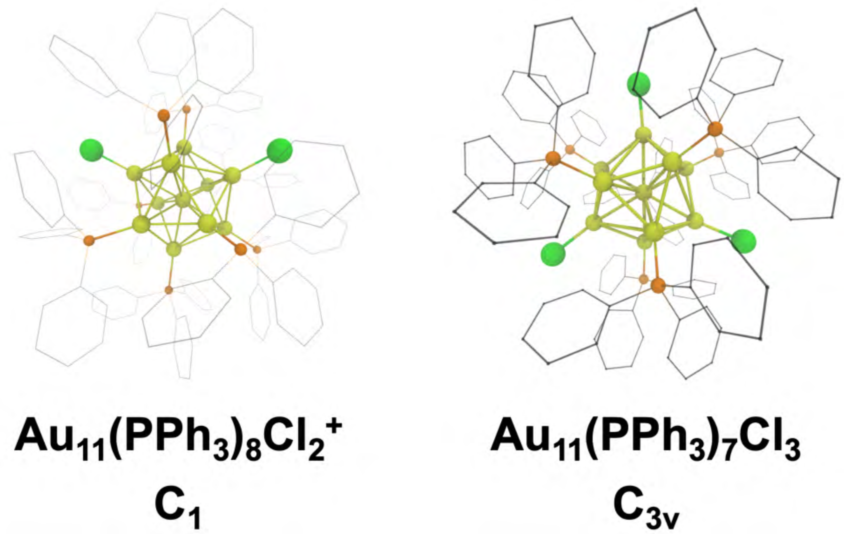

Figure 25. Computational models based on the crystal structures of $Au_{11}(PPh_3)_8Cl_2^+$ and $Au_{11}(PPh_3)_7Cl_3$. Both the crystal structures and computationally relaxed models have the same symmetry for each nanocluster. With the primal axis going through the plane of the page, $Au_{11}(PPh_3)_8Cl_2^+$ has C_1 while $Au_{11}(PPh_3)_7Cl_3$ has C_{3v} symmetry.

We next varied the identity of the halide ligands on the cluster surface with halogens such as bromide and iodide to create other $Au_{11}(PPh_3)_8X_2^+$ and $Au_{11}(PPh_3)_7X_3$ clusters, which exhibit the same symmetry as $Au_{11}(PPh_3)_8Cl_2^+$ and $Au_{11}(PPh_3)_7Cl_3$, respectively. For these Au_{11}NCs, the cluster symmetry and ligand orientations seem to play a larger role than the identity of the halide ligands in the overall core geometry, including the bond lengths shown in both **Figure 6** and **Figure 13**. Although the average bond length between the gold atoms in $Au_{11}(PPh_3)_8X_2^+$ and $Au_{11}(PPh_3)_7X_3$ is roughly 2.880 Å, which is about equal to the gold-gold bond lengths in a bulk FCC structure, the trends in variability of the gold-gold bond lengths are different in $Au_{11}(PPh_3)_8X_2^+$ and $Au_{11}(PPh_3)_7X_3$. The bond distributions of $Au_{11}(PPh_3)_8X_2^+$ are much more variable compared to $Au_{11}(PPh_3)_7X_3$ due to the lower symmetry of $Au_{11}(PPh_3)_8X_2^+$ compared to $Au_{11}(PPh_3)_7X_3$. In addition, $Au_{11}(PPh_3)_8X_2^+$ exhibits shorter bond lengths between the center gold atom and neighboring gold atoms and longer bond lengths between surface gold atoms to other surface gold atoms. This difference still exists in the $Au_{11}(PPh_3)_7X_3$ system but is harder to distinguish.

Outside the gold core, the lengths of the gold-halide bonds seem to be mostly dependent on the atomic radii. However, the bond lengths of the phosphine-gold bonds are almost independent of the identity and number of halogens bound to the surface of the gold nanoclusters. Interestingly, all the gold-ligand bonds are longer in the Au_{11}NCs compared to the Au(I) precursors. This trend is expected because unlike the +1 oxidation state of gold in the mononuclear gold precursor, the collective gold atoms in the Au_{11}NCs nanoclusters are more neutral. Thus, the surface of the Au_{11}NCs is more electron rich, promoting more electron-electron repulsion between the gold and the ligands.

5.2 Stabilities and Charges on Undecagold Clusters

While the Au_{11}NCs were observed to have the same symmetry and geometry for each of the different halides (i.e., all of the $Au_{11}(PPh_3)_8X_2^+$ clusters have the same symmetry and geometry, and all of the $Au_{11}(PPh_3)_7X_3$ clusters have the same symmetry and geometry), the synthetic approach for each of these nanoclusters varied. The $Au_{11}(PPh_3)_8Cl_2^+$ synthesis involves reduction of $Au(PPh_3)Cl$ by $NaBH_4$ in DCM and is similar to the synthesis to $Au_{11}(PPh_3)_8Br_2^+$, which involves reduction of $Au(PPh_3)Br$ in DCM (see **Section 2.2.2.1** and **Section 2.2.2.2** for the synthetic detail). On the other hand, the reduction of $Au(PPh_3)I$ produces a mixture of $Au_{11}(PPh_3)_8I_2^+$ and $Au_{11}(PPh_3)_7I_3$, and during the filtration process, $Au_{11}(PPh_3)_8I_2^+$ becomes $Au_{11}(PPh_3)_7I_3$ (**Section 2.2.2.6**). Therefore, $Au_{11}(PPh_3)_8I_2^+$ was synthesized by anion exchange of

$Au_{11}(PPh_3)_8Cl_2^+$ with use of KI (**Section 2.2.2.3**). $Au_{11}(PPh_3)_7Cl_3$ was synthesized in a similar way to $Au_{11}(PPh_3)_8Cl_2^+$, but the reduction of $Au(PPh_3)Cl$ occurred in ethanol with a higher concentration of reducing agent $NaBH_4$ (**Section 2.2.2.4**). Finally, anion exchange of $Au_{11}(PPh_3)_7Cl_3$ with KBr produced $Au_{11}(PPh_3)_7Br_3$ (**Section 2.2.2.5**).

Previous works on chlorinated Au_{11}NCs observed different stability and reactivity of $Au_{11}(PPh_3)_8Cl_2^+$ and $Au_{11}(PPh_3)_7Cl_3$.[38, 45, 65] $Au_{11}(PPh_3)_8Cl_2^+$ was shown to be stable for months at room temperature, whereas $Au_{11}(PPh_3)_7Cl_3$ rapidly decomposes within hours in room temperature, even though the only difference between these two clusters is one ligand. After several months of decomposition, the X-ray diffraction data of $Au_{11}(PPh_3)_7Cl_3$ suggests that the major decomposition product consists of a biicosahedral cluster with 25 gold atoms, as two 13 gold atom icosahedral clusters share one gold atom (**Figure A3**). Konishi *et al.* observed similar structures for rod-like Au_{25}NC when Au_{11}NCs was treated with alkane thiols.[66] Interestingly, near the edges of the cluster, the suggested structure has PPh_3 and chlorine bound to the gold on-top, while chlorine near the center of the cluster is bound in a staple motif. The properties of this new structure and its stability compared to $Au_{11}(PPh_3)_7Cl_3$ may be of future interest, but since both the cluster size and ligand structures change, this new decomposed product was not considered further in this study. The stability of the iodinated Au_{11}NCs contrasts with the stability of the chlorinated clusters, where the $Au_{11}(PPh_3)_8I_2^+$ product degrades to $Au_{11}(PPh_3)_7I_3$, while the $Au_{11}(PPh_3)_7I_3$ product is stable for a longer period of time.

Previous work hypothesizes two major possibilities for the stability of the Au_{11}NCs: steric stabilization or core charge induced by the ligands.[38] With three phenyl groups on a phosphorous, PPh_3 is considered a sterically bulky ligand. In addition, the phenyl rings can interact with other phenyl rings on the surface through π-stacking, which makes it much more difficult for other species to adsorb to the gold surface as seen in **Figure 3**. Thus, the bulky PPh_3 ligands are important for the stability of the clusters, and most similarly-sized clusters synthesized using phosphine-based ligands are made with PPh_3-like bulky ligands. Computationally, the importance of π-stacking among PPh_3 ligands is observed in how the ligands are bound to the surface of the nanoclusters. When the phenyl rings and their interactions are not considered on the gold nanocluster surfaces, the bonding angle between gold and the ligands becomes highly distorted (**Figure 12**). Having the phenyl rings on Au_{11}NCs, the Tolman cone angle of PPh_3 is larger and all the ligands on the surface are coordinated in an on-top position, showing an almost 180^o angle between the two bonds connecting the center gold atom to surface gold to the ligand moieties. Further, the π-stacking and steric hinderances among the phenyl rings also induced the halogen ligands to coordinate in an on-top position as well. However, considering the enhanced stability of $Au_{11}(PPh_3)_7I_3$ compared to that of $Au_{11}(PPh_3)_8I_2^+$ (which has one less phenyl ring), the steric stability of PPh_3 does not seem to play as much of a role in the cluster stability compared to the charge of the gold core.

As seen in **Figure 15**, electron charges on the halogen ligands are highly dependent on the identity of the halogen atoms. Strongly electronegative chlorine atoms are more charged than less electronegative iodine atoms, as they withdraw more electron density from the gold core. The increase in the number of halogens on the surface does not appreciably change the individual halogen charges, but an increased number of halogens on the surface pulls more electron density away from the gold core. The direct influence of the halides on the gold core is shown in **Figure 16**, where the gold atoms adjacent to chlorine atoms are electron poor, gold atoms bound to bromine have roughly neutral charge, and the gold atoms bound to iodine are electron rich. The changes in electron density of the gold atoms adjacent to halide ligands are propagated to nearby gold atoms and influence the overall charge of the gold core. However, the charge propagation is much less noticeable on the center gold atom, which has a consistent value for its charge, even with the various surface ligands. The consistency of the charge of the center gold atom compared with the changes of the charges of the surface gold atoms indicates that the halide ligands more easily influence charges on the surface layer of the gold nanoclusters. By changing the charges propagated throughout the surface of the gold, and that there is a range of surfaces charges specific to the nanomaterial, the ligands can alter the stability and reactivity of the nanoparticles. Another possibility is that the ionic and dative bonds of the halide and phosphine ligands, respectively, lead to an electron richness of the surface that is directly related to the lability of the coordinating ligands. In the case of Au_{11}NCs, surface gold charges seem to be more important for determining the cluster stability than the sterics of the ligands.

5.3 Molecular Orbitals and Energy States

The electron behaviors in the phosphine-halide-protected Au_{11}NCs at various energy levels can be elucidated using the electronic structure described by PDOS and MO. PDOS depicts the possible energy states electrons can occupy at each energy level. The orbital contributions at different energy states can be labeled differentially, such as elemental AO contribution shown in **Figure 17** and orbital angular momentum shown in **Figure 26**. Complimentary to the PDOS depictions, MO illustrates the electronic structure at specific energies in three dimensions, describing the location of the electron density related to the location of atoms. Having both PDOS and MO, each Au_{11}NC and their electronic structures, in both local and general energies, are described as a function of ligands.

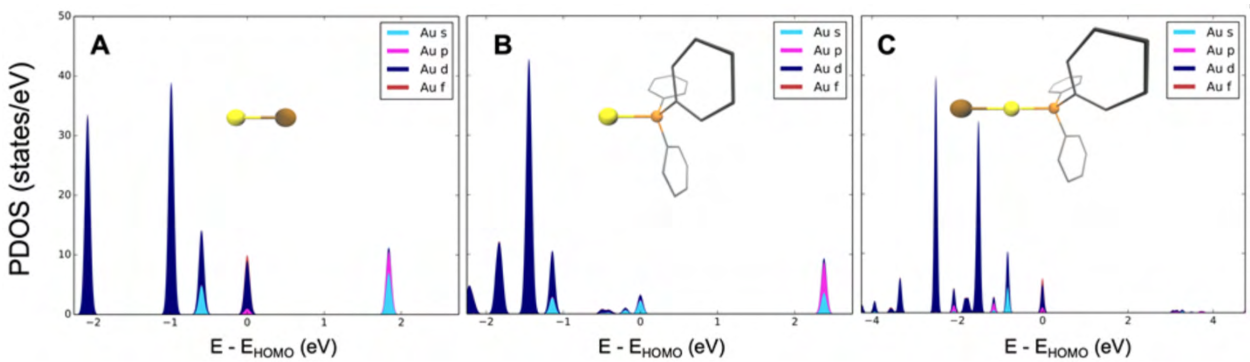

Figure 26. PDOS of gold's orbital angular momentum in A) AuBr and B) Au(I)PPh_3^+ and C) Au(PPh_3)Br. Pictured as insets are all the geometries of the molecules were optimized before the calculation of PDOS. The energies in PDOS are represented with respect to their energies at the HOMO.

First, the electronic structure of mononuclear gold precursor is considered. Mononuclear gold precursors, such as Au(PPh_3)Cl, have been rigorously studied both experimentally and computationally to observe the strong relativistic behaviors of gold atoms bound to electron withdrawing chloride and electron donating phosphorous.[67] Without any interactions, gold cations have empty 6s orbitals and fully occupied 5d orbitals. The introduction of an X-type halogen ligand induces major interaction between its p-orbitals and the d-orbitals corresponding to gold (**Figure 4**). In addition to gold's d-orbitals, a small s-orbital characteristic appears at the HOMO as well as a considerable amount of p-orbital characteristics in the occupied regions slightly below HOMO (~ HOMO – 0.7eV), indicating gold's strong s-p-d hybridization (**Figure 26A**).[18] On the other hand, regions near the HOMO of gold cations bound by L-type PPh_3 display a significant amount of s-orbital character (**Figure 26B**). This is due to the presence of dative bonding with electron donating PPh_3, which partially fills up the empty 6s orbitals in gold cations. While some of the electron densities are constantly showing the π-bonds of conjugated phenyl rings near the HOMO regions of Au(I)PPh_3^+, the electron densities on phosphorous are either absent or shifted more towards the gold atom (**Figure 26**). The excited states of the L-type ligand also exhibit nearly opposite influences on electron densities compared to the excited states of the X-type ligands. The immediate LUMO of X-type ligands with gold cations has most of the electron density localized at both gold and the ligand, creating a π*-bonding structure between the two atom centers. The increase in excitation energy drives the majority of electron density to move from the more electronegative X-type ligand to the metal center. In the excited states of $Au(I)PPh_3^+$, the gold atom retains some portion of the electron density, but the majority of the electron density is now localized in phosphorous and in the π* orbitals of the conjugated phenyl rings. The electron density near gold and phosphorous atoms shows σ*-bonding in the LUMO state, and a further increase in energy states reduces the size of the localized orbital on the metal center.

The combination of both X-type and L-type ligands on a single gold atom appears to have the features of each ligand on the electronic structure of the metal center, especially in the ground state where the electron density of gold is partially taken by the L-type and partially donated by the X-type (**Figure A26**). The HOMO and HOMO + 1 of gold's angular orbital momentum in $Au(PPh_3)Br$ resembles what is observed with the HOMO and HOMO + 1 of AuBr. The features shown in the lower energy states of gold PDOS appear to be closer to that of $Au(I)PPh_3^+$. However, the PDOS of $Au(PPh_3)Br$ shows a much larger HOMO-LUMO gap, indicating that the coexistence of electron density donating and accepting ligands on the gold atom synergistically enhances the stability of gold complexes. Additionally, the contribution of gold's AO in the LUMO is very low compared to that of AuBr and $Au(I)PPh_3^+$. Even when the general behavior of the excited MO, featuring both X and L-type ligand influences, is observed in $Au(PPh_3)Br$, the shift of the electron densities from X-type to gold to L-type ligands happens much more rapidly, resulting in gold's low electron density contribution in the LUMO (**Figure 19**).

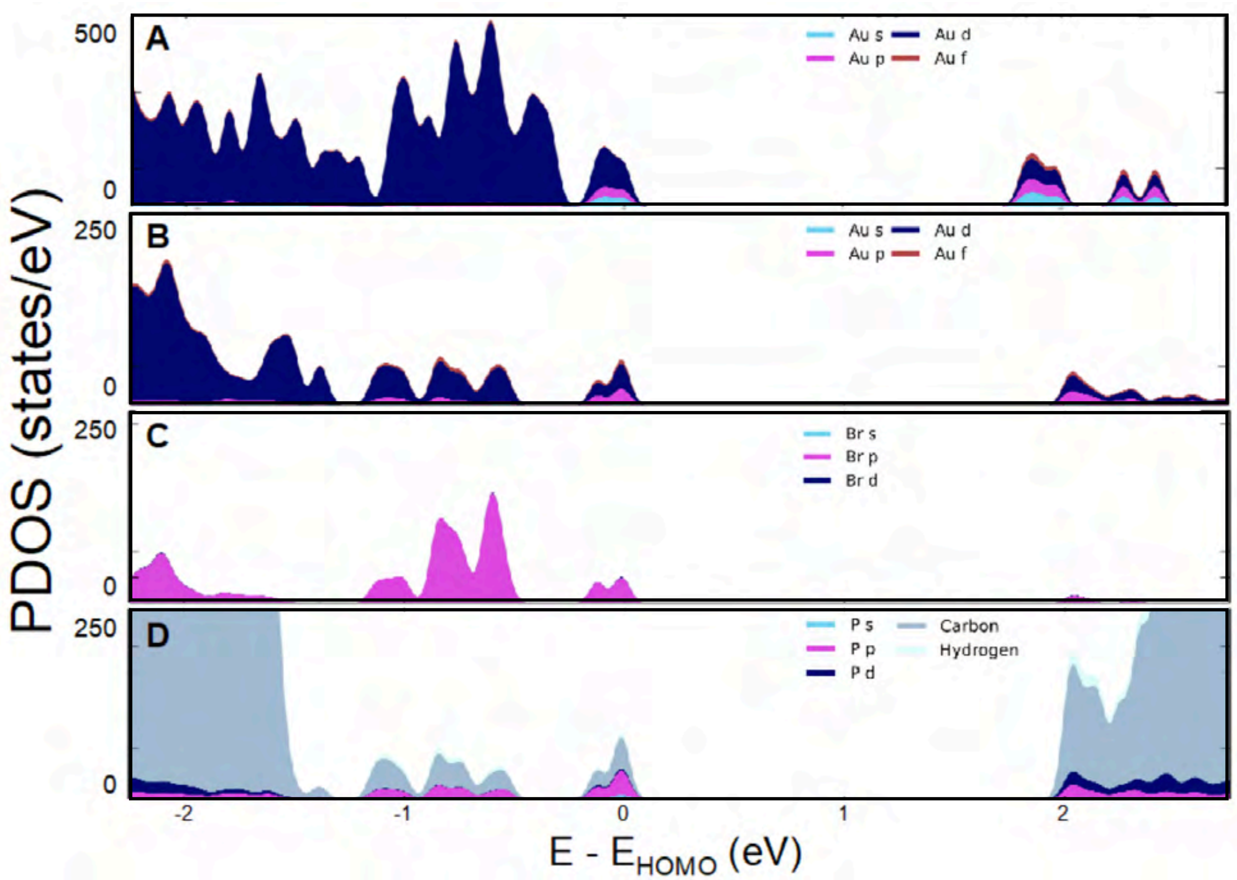

Figure 27. PDOS of orbital angular momentum of A) gold in Au_{11}^{3+}, B) gold, C) Br, D) organic elements of PPh_3 in $Au_{11}(PPh_3)_8Br_2^+$. The PDOS of bare Au_{11}NCs with the same core geometry as $Au_{11}(PPh_3)_8Br_2^+$ is modelled in A) for comparison. Unlike the rest of the elements, the orbital angular momentums of carbon and hydrogen were combined.

When looking at the bare gold nanocluster without any ligands on the surface, the collection of gold orbitals forms super atomic orbitals (**Figure A29**). To make a reasonable comparison between the pure gold cluster and ligated gold clusters, the initial geometries of $Au_{11}(PPh_3)_8X_2^+$ or $Au_{11}(PPh_3)_7X_3$ were considered with +3 charges on the clusters to fulfill the super atomic electron counts.[20] As the AO of gold in the bare Au_{11}NCs (Au_{11}^{3+}s) mixes with other AO of gold atoms in the clusters, the PDOS of Au_{11}^{3+}s show increase in the occupancies per each energy states as well as more continuous energy states that can be occupied. The PDOS of the

Au_{11}^{3+} shows a considerable amount of contribution from gold's s- and p- orbitals in addition to the d-orbital characters appearing in the frontier orbitals, signifying the s-p-d hybridization of gold atoms as they interact with neighboring gold atoms. Through the hybridization of multiple AOs in the NC, the Au_{11}NC shows fully filled super atomic p-orbitals in the HOMO and unoccupied super atomic d-orbitals in the LUMO. With the lack of symmetry in the structure of the Au_{11}^{3+}, the super atomic orbitals of the bare Au_{11}NCs display some degree of distortion. However, still having pseudospherical geometries, the Au_{11}^{3+} has electronic densities that are well-propagated in all directions.

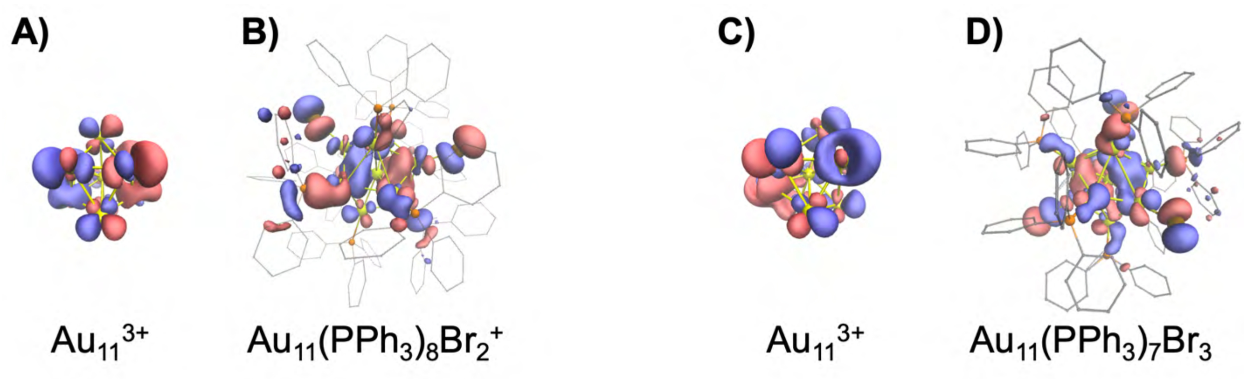

Figure 28. The HOMO of the gold core with or without ligands for $Au_{11}(PPh_3)_8Br_2^+$ and $Au_{11}(PPh_3)_7Br_3$. A) Au_{11} in $Au_{11}(PPh)_8Br_2^+$, B) $Au_{11}(PPh)_8Br_2^+$, C) Au_{11} in $Au_{11}(PPh_3)_7Br_3$, and D) $Au_{11}(PPh_3)_7Br_3$.

The electronic densities of the Au_{11}^{3+} are modified when bromine and phosphine ligands are added on the surface. On the local scale, the X and L-type ligands are interacting with the adjacent gold AO similar to the ligand interactions in mononuclear gold complexes: the X-type ligands are sharing electron density with the gold's s-p-d hybridized orbital, whereas L-type ligands are providing electron density to the gold's s-p-d hybridized orbital. These profound influences on local electronic structure have been demonstrated by the Bader charges of the gold atoms (see **Section 4.2.3**). The uneven distribution of the electron densities on the gold core of Au_{11}NCs leads to a change in the electronic structure as further evidenced by the direct comparison of PDOS of bare 11 gold atoms (**Figure 28**). Color-coded according to the orbital angular momentum contributions of the gold atoms, PDOS of gold in $Au_{11}(PPh_3)_8Br_2^+$ shows a slight increase in the HOMO-LUMO energy gap compared to that of Au_{11}^{3+} (**Figure 27**). Furthermore, the decrease in the occupiable states per energy and increase in the distribution of gold's s- and p-orbital angular momentum in $Au_{11}(PPh_3)_8Br_2^+$ indicates that the HOMO states observed in Au_{11}^{3+} are spread out to lower energy in the presence of the surface ligands. The addition of these ligands also promotes further hybridization of s- and p-orbitals with the d-band in Au_{11}^{3+}, while shifting the d-band to even lower energies. Similar changes in the electronic structure are observed with $Au_{11}(PPh_3)_7X_3$ compared to bare Au_{11}^{3+}, highlighting the ligand's ability to manipulate and stabilize the electronic structure of noble metal nanoparticles (**Figure A24**).

While the replacement of the halide for a single PPh_3 ligand in $Au_{11}(PPh_3)_7X_3$, regardless of the halogen, resulted in a comparable electronic structure to $Au_{11}(PPh_3)_8X_2^+$, the stability between the analogous Au_{11}NCs is highly dependent on the type of halide ligands (see **Section 5.2** for stability of Au_{11}NCs). As discussed previously, the local charges induced by the adjacent halogen ligands are likely to be responsible for the different trends in the stability of Au_{11}NCs, especially because there are almost no differences in the size of the HOMO-LUMO gaps. General trends of the PDOS among Au_{11}NCs are also very similar, but with some minor noticeable features among the Au_{11}NCs (**Figure 18**). The narrow peaks in the PDOS $Au_{11}(PPh_3)_7X_3$ compared to $Au_{11}(PPh_3)_8X_2^+$ indicate the increase in degeneracies in various energy states due to $Au_{11}(PPh_3)_7X_3$ having more symmetry. In addition, the extra halide ligand in $Au_{11}(PPh_3)_7X_3$ not only prompts more halogen AO contribution in the HOMO regions but also draws more electron densities toward adjacent gold atoms (**Figure 21**). While additional L- type ligand in $Au_{11}(PPh_3)_8X_2^+$ results in lower electron densities in the HOMO regions, more electron density appears in the LUMO region where the majority of the MO contribution is from the PPh_3 and the neighboring gold atoms.

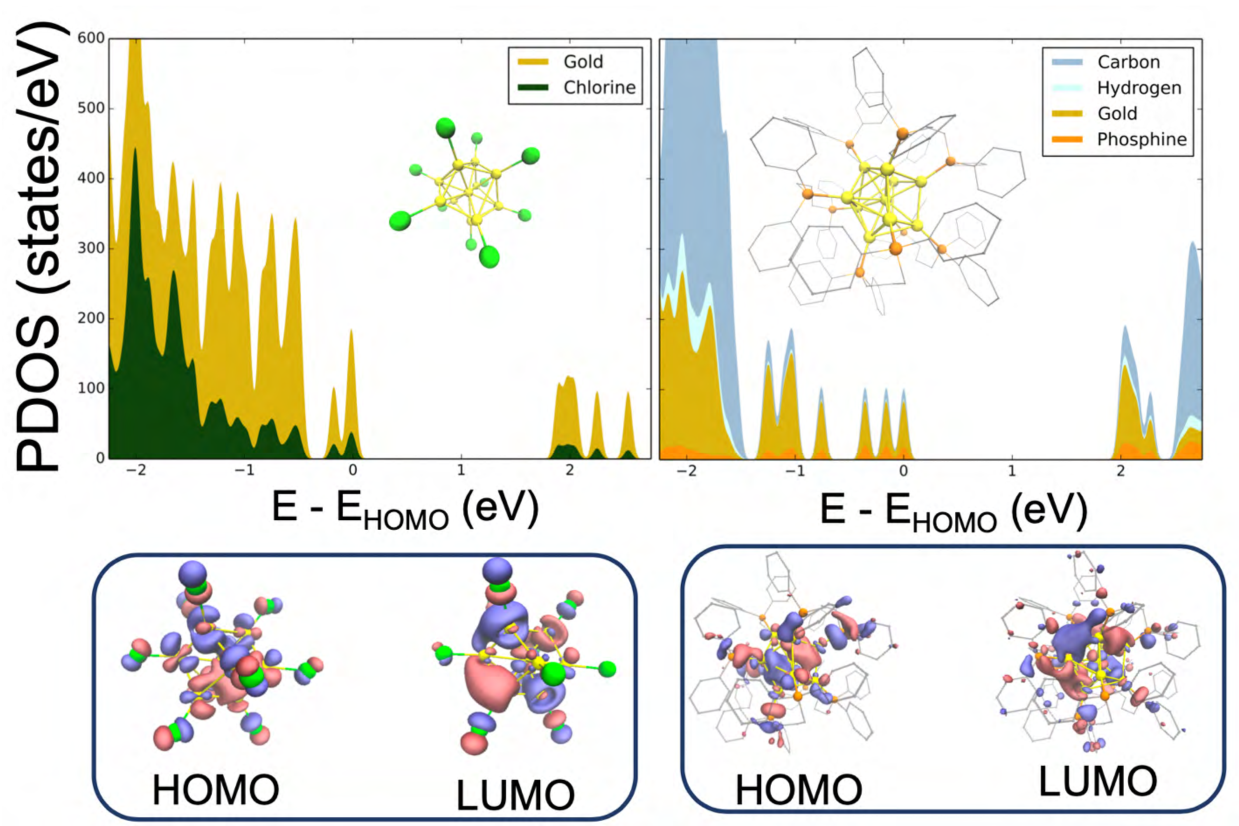

Figure 29. PDOS of all X-type ligands ($Au_{11}Cl_{10}^{7-}$, left) and all L-type ligands ($Au_{11}(dppp)_4Cl_2^+$, right) with computationally optimized structures depicted in the insets. Figures below represent the electron density of the frontier orbitals for each Au_{11}NC.

The influences of the X- and L- type ligands are much more apparent in Au_{11}NCs passivated with either all X-type ligands ($Au_{11}Cl_{10}^{7-}$) or all L-type ligands ($Au_{11}(dppp)_5^{3+}$) (**Figure 29**). $Au_{11}Cl_{10}^{7-}$ is a geometrically optimized computational model of hypothetical Au_{11}NC, where the PPh_3 on $Au_{11}(PPh_3)_8Cl_2^+$ is replaced with chloride ligands containing negative charges. $Au_{11}(dppp)_5^{3+}$ is a Au_{11}NC synthesized with bidentate phosphine ligands dppp, where phosphines are separated by propane (**Figure A2**). With correct electron counts, both of the Au_{11}NCs display super atomic orbitals in their frontier orbitals. Only capped with X-type ligands, $Au_{11}Cl_{10}^{7-}$ has massive gold and chlorine AO contributions in the HOMO regions while $Au_{11}(dppp)_5^{3+}$ obtains much of the electronic contributions from the dppp at the LUMO. However, unlike the electron density localized on X-type ligands in the HOMO and L-type ligands in the LUMO during the frontier orbitals of $Au_{11}(PPh_3)_8X_2^+$ or $Au_{11}(PPh_3)_7X_3$, the electron densities of $Au_{11}Cl_{10}^{7-}$ and $Au_{11}(dppp)_5^{3+}$ exist on X- and L- type ligands, respectively, for both the HOMO and LUMO states. Therefore, $Au_{11}Cl_{10}^{7-}$ and $Au_{11}(dppp)_5^{3+}$ lack the charge transfer between the metal core and the surrounding ligands during the change in energy levels.

Compared to the discernable changes caused by the ratio of X- type and L- type ligands, the difference in the electronic structures of Au_{11}NCs as a function of change in X-type ligands, from chloride to iodide, is much less noticeable. With the same number of valance electrons in their p-orbital, the only difference among the halogen ligands lies in their principal quantum numbers, which contributes to different energy levels when interacting with gold's atomic orbitals. Having the valance electrons in 5p orbitals, iodine's interaction with the gold core occurs much closer to the HOMO of the Au_{11}NCs at HOMO – 0.5 eV, whereas bromine's 4p and chlorine's 3p orbitals contributes most near the HOMO – 0.75 eV and HOMO – 1.0 eV, respectively (**Figure 18**). Even with the same number of electrons participating in the gold-halogen interaction, the 5p orbitals in iodine have larger radial distribution functions compared to the 4p and 3p orbitals of the other halogens. This results in larger electron distributions near the halogens in $Au_{11}(PPh_3)_8I_2^+$ as opposed to $Au_{11}(PPh_3)_8Br_2^+$ or $Au_{11}(PPh_3)_8Cl_2^+$ (**Figure 20**).

5.4 Absorption

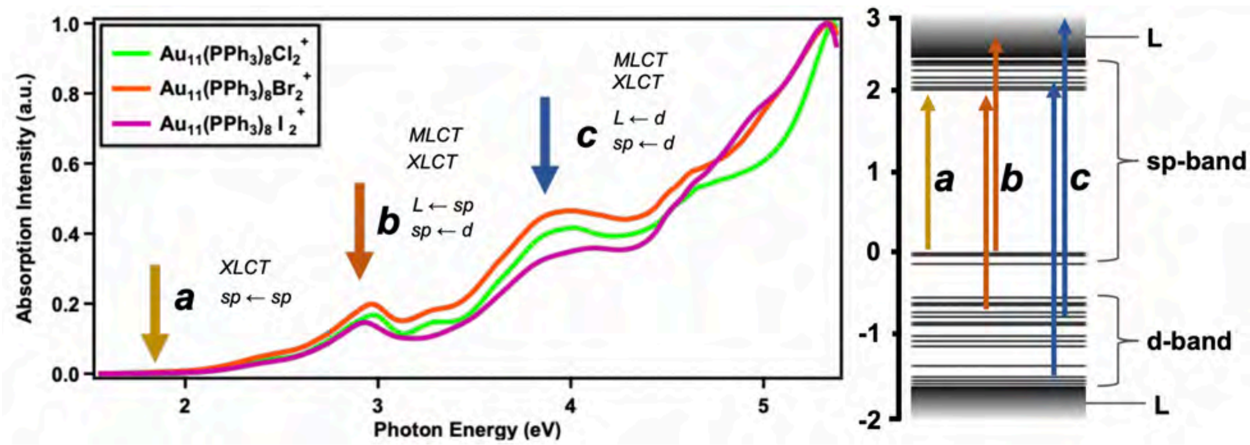

Figure 30. Experimental absorption spectrum with KS orbital energy level diagram for model $Au_{11}(PPh_3)_8Br_2^+$. The arrows in the absorption spectrum correspond to the major contributing transitions in KS orbital energy level diagram. The type of charge transfers and the major orbitals involved in the transitions are also provided in the spectrum: halogen-to-ligand charge transfer (XLCT), metal-to-ligand charge transfer (MLCT), gold's sp-bands (sp), d-band (d), and PPh_3 (L).

With more molecular-like electronic structure, the Au_{11}NCs have very distinct absorption spectra in the visible range. The electron transitions in the energy levels of Au_{11}NCs are responsible for the translucent red brown color (see **Section 4.1.2**). Having small sizes with defined atomic coordination, the transitions of the electronic levels can be simulated using TDDFT (see **Section 4.2.6**).[59] Besides the ~0.5 eV blueshift in the simulated absorption spectra, both absorption spectra contain the same electronic transition features: appearance of a peak with frontier orbital transitions at 2 eV (**Figure 30a**), metal to ligand charge transfer (MLCT) and halogen to ligand charge transfer (XLCT) around 2.9 eV (**Figure 30b**), MLCT of D-band around 3.8 eV (**Figure 30c**), and ligand to ligand charge transfer (L'LCT) for even higher energy levels. The minor red shift (~0.02 eV) of the peak at 2.9 eV among the three $Au_{11}(PPh_3)_8X_2^+$ clusters also matches with the energy levels in PDOS.[68] However, almost the indistinguishable spectral features of both

$Au_{11}(PPh_3)_8X_2^+$ and $Au_{11}(PPh_3)_7X_3$ implies that the electron transitions are heavily dependent on the geometry of the gold core.[17, 69] This result is also due to the fact that the electron density contribution near the HOMO region is coming from the gold core.[64]

5.5 Emission

Once Au_{11}NCs are excited with electromagnetic radiation ranging near the visible regions (1.8 – 4.3 eV), the nanoclusters were shown to emit light at NIR region (1.2 – 1.6 eV) (**Figure 8**). This enhanced NIR emission from gold nanoclusters have been repeatedly reported in previous literature, which includes gold nanoclusters capped with halogen-phosphine ligands.[31] Many previous studies of luminescent gold nanoclusters indicate that the mechanism of PL is influenced by a variety of nanocluster properties like size, shape, composition, and surfaces.[30] To the extent to which these variables affect the PL mechanism is not fully elucidated, due to the complexity of the system and the mechanism.

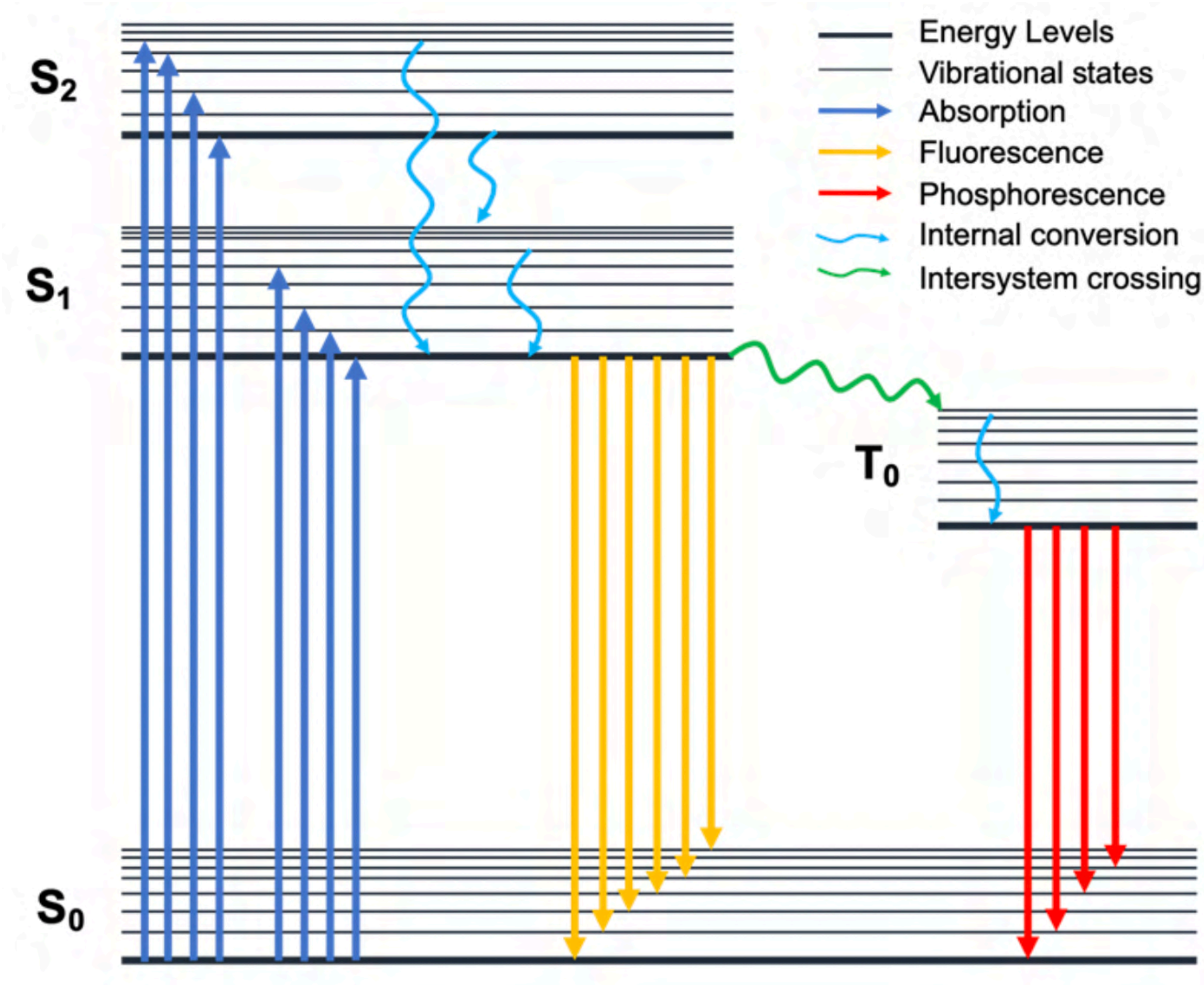

Figure 31. Jablonski diagram describing excitation and emission pathways. S_n and T_n denote the singlet and triplet states, respectively, where n denotes the excited energy levels with n = 0 being the ground state. Smaller energy levels between S_n indicates possible vibrational levels for internal conversion (IC) to occur.

Unlike the promotion of the ground state electrons to unoccupied excited states ($S_n \leftarrow S_0$) observed in the absorption properties, emission properties initially begin with the excited states of the electron that ends with the ground state electron ($S_n \rightarrow S_0$). As seen in the Jablonski diagram, there are many mechanisms to which the excited electron can pursue.[70] Depending on the size of the gaps between the energies of excited states, the excited electron can enter different excited states via non-radiative processes called internal conversion (IC). Kasha's rule states that the excited electron must relax down to the lowest unoccupied energy state as long as the energy gaps between the excited states are relatively close ($S_n \rightarrow S_1$).[71] Once the excitation reaches the energy minima allowed by the internal conversion, the electron can be either relax down to the ground state via fluorescence or phosphorescence producing a photon as a consequence. Fluorescence is simply an excited electron returning back to the ground state ($S_1 \rightarrow S_0$), whereas phosphorescence requires intersystem crossing (ISC), which is a non-radiative process of an excited electron in singlet states transfer to triplet state ($S_1 \rightarrow T_n$). After IC in the excited triplet states ($T_n \rightarrow T_1$), the electron emits a photon as phosphorescence ($T_1 \rightarrow S_0$). Because of these additional pathways that the electron takes during ISC, phosphorescence tends to have an increased lifetime of the excited state electron and decreased energy of the emitted photon.

Unlike the previously reported identical gold core $Au_{11}(dppp)_5^{3+}$ having no emission properties, phosphine-halide-capped Au_{11}NCs emit photons with an emission peak near 1.5 eV when excited with UV and visible light.[31] As shown in **Figure 8**, the quantum yield (Φ) of this emission varies from 0.0237% for $Au_{11}(PPh_3)_8Cl_2^+$ to 1.51% for $Au_{11}(PPh_3)_7I_3$ (**Figure 9**). This drastic difference in Φ as a function of different ligands in Au_{11}NCs suggests that emission of Au_{11}NCs is highly influenced by the identity of the ligands.

5.5.1 Triplet States of the Undecagold Nanoclusters

With photon emission on the microsecond timescale as well as energy of photon energy being much lesser than the HOMO-LUMO gap, we can reasonably assume that the emission pathway is phosphorescence (**Table A4**). In addition to having similar molecular orbitals as well as excitation pathways, the similarity of the features described in two-dimensional emission contour maps of Au_{11}NCs indicate that the difference in the Φ of emission depends on certain Au_{11}NCs having different probabilities of ISC (**Figure 9**). According to Kasha's rule, the excited electrons in any unoccupied molecular orbital relaxes down to LUMO state non-radiatively if there are no major energy gaps in unoccupied molecular orbitals.[71] Since there are no discrete transitions in LUMO of ligated Au_{11}NCs, excited electrons will have vibrational relaxation down to the LUMO before going through the ISC process (**Figure 31**). Additionally, we observe an extremely strong correlation between energy transition described by a computational approach in PDOS to features shown in the two-dimensional emission contour maps (**Figure 32**). In the emission map of $Au_{11}(PPh_3)_8Br_2^+$, first weak peak appears right before 2.0 eV, which matches with the energies of the HOMO-LUMO gap. Emission appears again but strongly at 2.3 eV, 2.6 eV, and 3.0 eV, each corresponding to the three peaks located near -0.7 eV in PDOS.

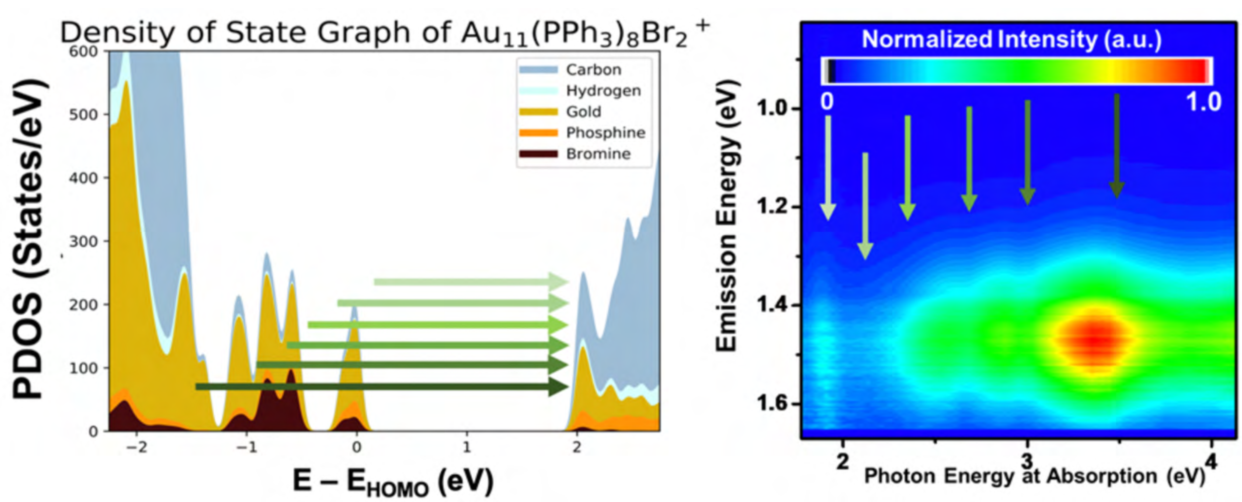

Figure 32. The direct comparison of PDOS and two-dimensional emission contour map of $Au_{11}(PPh_3)_8Br_2^+$. The energy gap between ground state to LUMO in PDOS and the features observed in the emission map show high correlation, indicating the importance of LUMO in triplet state emission of Au_{11}NCs.

5.5.2 Ligand Factors in the Relaxation Pathways

From the electronic behaviors observed from the DFT calculation and experimental data, we can propose three hypotheses of ligand properties that influence the promotion of triplet states in gold clusters: 1) heaviness of the ligand, 2) softness of the ligand, and 3) ligand's type, categorized by Green's covalent bond classification. These classifications are not mutually exclusive but are rather more likely to be related to each other.

The effect of the heavy (halogen) atom substitution is shown previously with many organic molecules. El-Sayed *et al*. observed the increase in phosphorescence in various organic systems by substituting a lighter halogen with a heavier halogen.[72, 73] Many of his works indicate that the increase in phosphorescence with the presence of a heavy atom in a molecular system is due to the enhanced spin-orbit coupling, which is called the heavy atom effect. The spin-orbit coupling leads to an increase in the rate of spin-forbidden process and ISC, which allows an excited electron to experience change in the multiplicity and generates phosphorescence. While most of the electron density is removed from the halides in the LUMO, a small amount of π-orbitals are observed on the halide atom (**Figure 22**). This small amount of contribution from the halides is sufficient to promote an increase in phosphorescence.

To understand the extent of the heavy atom effect from the ligand on the increased phosphorescence, we tested phosphorescence of Au_{11}NCs with lighter pseudo halogen cyanide. While there is no crystal structure to confirm the exact coordination of atoms in halogen cyanide, C=N stretch in IR and Raman suggests the presence of CN on the Au_{11}NCs, which is evidenced by the similar absorption spectrum to other already defined $Au_{11}NCs$ (**Figure A4**). If the heavy atom effect of the ligand is the only contributor in the ISC process, the $Au_{11}NCs$ capped with the cyanide ligand should have almost no emission. However, $Au_{11}NCs$ with presence of cyanide show phosphorescence with Φ of 0.067%, which falls between the Φ of $Au_{11}(PPh_3)_8Cl_2^+$ (0.024%) and $Au_{11}(PPh_3)_7Cl_3$ (0.140%) (**Figure 33**).

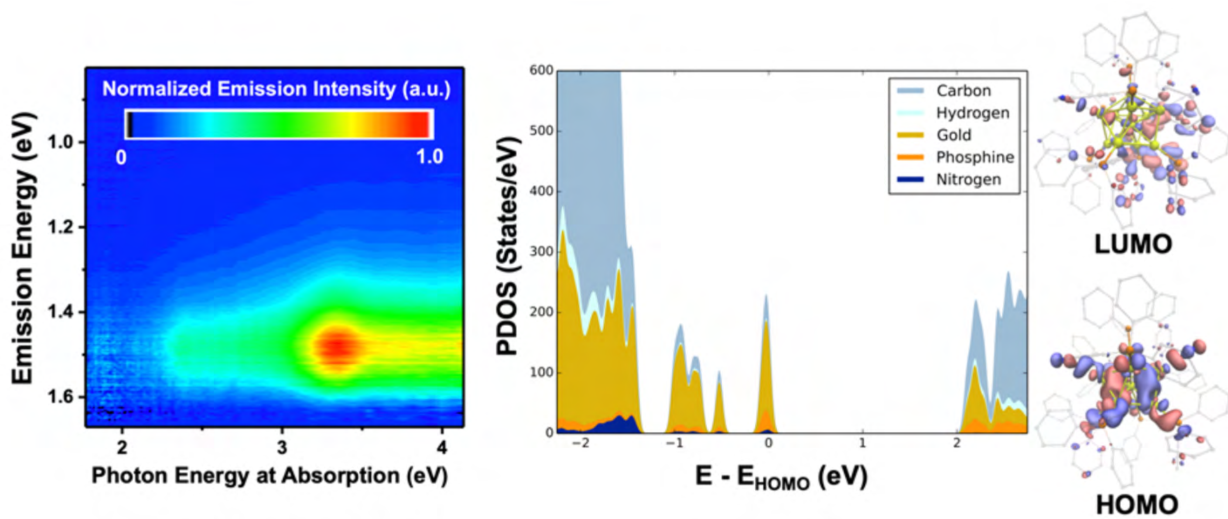

Figure 33. Emission spectrum of cyanide substituted $Au_{11}NCs$ (Left) and PDOS calculation of geometrically optimized $Au_{11}(PPh_3)_8(CN)_2^+$ similar to $Au_{11}(PPh_3)_8Cl_2^+$ (Middle). KS orbital at HOMO and LUMO states of $Au_{11}(PPh_3)_8(CN)_2^+$ are described (Right). The emission shows highly similar features to the other halogen base $Au_{11}NCs$ with **Φ** of 0.067%.

This difference in these emissions is where hard soft acid base theory (HASAB) comes into play.[74] Although cyanide is lighter than chlorine or bromine, cyanide is considered a soft base, meaning that cyanide has a large ionic radius and is easily polarizable. The polarizability is an important parameter for the mixing of the orbitals. Having soft (pseudo) halide ligands bound to gold clusters with PPh_3, which is also considered a soft ligand, the overall $Au_{11}NCs$ polarizability amplifies. This polarizability allows efficient charge transfer in the clusters when illuminated by light.[75] When the electron density in the $Au_{11}NCs$ is more polarized, it will take a longer time to relax, providing more time for the rate of ISC to increase.[73, 76] While Φ of Au_{11}NCs with the presence of cyanide is in between chlorinated and brominated $Au(PPh_3)_8X_2^+$, and with cyanide being softer than chlorine and bromine, we conclude that both the heavy atom effect and softness of the ligand atoms are contributing to the phosphorescence intensity. Thus iodine, being both the softest base and the heaviest atom, has an extremely intense phosphorescence compared to any other clusters.

Finally, the type of ligands under covalent bond classification is an important factor in phosphorescence.[32] Konishi *et al*. reports that there is no photoluminescence from $Au_{11}(dppp)_5^{3+}$.[31] Although $Au_{11}(dppp)_5^{3+}$ has the same gold core as studied in this work, the PDOS of the Au_{11}NCs shows a drastic difference with the lack of X-type ligands. X-type ligands, especially the σ-acceptor and π-donor ligands, govern the HOMO regions of Au_{11}NCs, allowing efficient charge transfer ability. X-type dominates the HOMO region while L-type becomes a major electron density contributor in the LUMO. As previous works on transition metal complex have observed, this MLCT/XLCT from the HOMO to the LUMO plays an important role in phosphorescence.[77, 78] Many researchers have published observations on ^{1}MLCT behaviors from HOMO to LUMO followed by ^{3}MLCT in singlet excited states to triplet excited states, leading to an increase in phosphorescence.[79, 80] This finding implies that phosphine ligands are not just a protective ligand with dative bonding on the gold surface but are actively contributing to the properties of AuNCs.

6.0 Conclusion

In conclusion, we synthesized a suite of phosphine-halide-protected Au_{11}NCs with varying surface ligands. By systematically changing the surface ligands while holding the geometry of the nanoclusters' gold core constant, the ligand-based influence on the properties of nanoclusters were studied with the use of two complementary methods, i.e., calculation of the electronic structures using DFT and measurement of optoelectrical properties using absorption and emission spectroscopy. Using both methods, we demonstrate that by changing the amounts and types of the ligands, the electronic structures of Au_{11}NCs as well as their optical properties change. Specifically, we analyzed the relaxation pathways of excited electrons in Au_{11}NCs using their emission properties to hypothesize the origin of phosphorescence in nanoclusters and the influence of ligands on those origins.

Ultimately, surface ligands are anticipated to be a valuable tool to control the chemical and physical properties of nanomaterials. From this work, we have demonstrated that the identities of the ligands determine not only the charge of the adjacent metal atoms and their neighboring surface metal atoms to induce chemical changes such as stability and reactivity of the nanoclusters but also the overall electronic structure of the nanocluster and resulting physical properties. Through further studies, the mechanistic knowledge gained from halide and phosphine ligands on the gold core can be applied to other metals as well as other larger nanoparticles, leading to a more generalizable theory for designing and tuning nanomaterial properties for different applications. We anticipate that complete understanding of ligand-based properties on nanomaterials will be pivotal in the development and implementation of next-generation nanomaterials

7.0 Future Work: Influence of Pnictogen Ligands on AuNCs

With the evidence provided from both experimental data and computational models, we conclude that the L-type of ligands in Au_{11}NCs are not just passive bystanders when it comes to nanocluster properties. To elucidate further on the nanocluster properties that are affected by the L-type of the ligands, similar studies with AuNCs passivated with some systematical changes in the L-types of ligands can be conducted. Although there are many methods to add systematic variation to the L-type ligands, the modification of pnictogen binding moieties, phosphorous to bismuth, are chosen for the future study with regards to understand the influence of the L-type ligands. The pnictogen series is comprised of non-metal (N, P), metalloid (As, Sb), and metal (Bi) elements going vertically down the periodic table which contain the same pentavalent electrons in their outermost p-orbital and are therefore chemically similar. Since there are only a small number of noble metal nanoparticles synthesized with ligands containing metalloid or metal binding groups, the new nanoclusters with new chemical and physical properties can be of much interest in next-generation nanomaterials.

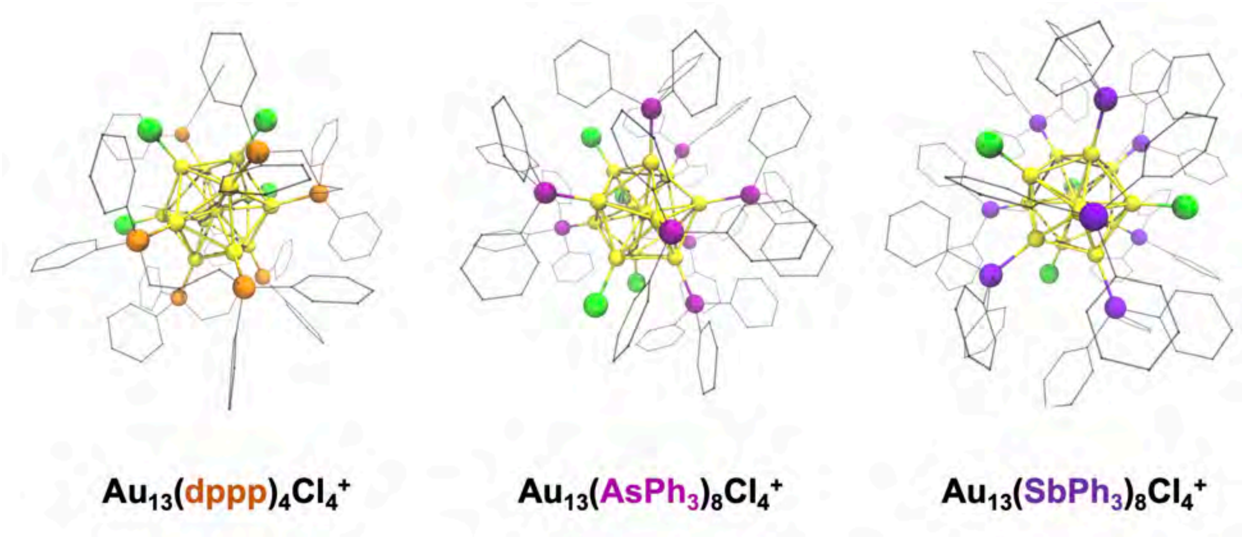

Figure 34. Computationally relaxed model based on the crystal structure of A) $Au_{13}(dppp)_4Cl_4^+$, B) $Au_{13}(AsPh_3)_8Cl_4^+$, and C) $Au_{13}(SbPh_3)_8Cl_4^+$. All three Au_{13}NCs contain same number of gold, pnictogen, and chlorine atoms.

Since many AuNCs capped with pnictide ligands are synthesized by reducing the Au(I) precursors already containing Au-pnictogen bonding, three different Au(I) precursors, $Au(LPh_3)Cl$ (L = P, As, and Sb), were synthesized according to the previous reports and reduced to produce AuNCs.[54, 55] While the reduction of $Au(AsPh_3)Cl$ and $Au(SbPh_3)Cl$ created $Au_{13}(AsPh_3)_8Cl_4^+$ and $Au_{13}(SbPh_3)_8Cl_4^+$, respectively, the reduction of $Au(PPh_3)Cl$ produced the Au_{11}NCs. In order to make reasonable comparisons between the ligand binding moiety influence on the same icosahedral Au_{13}NCs, $Au(PPh_3)Cl$ was replaced with $Au_2(dppp)Cl_2$ to produce $Au_{13}(dppp)_4Cl_4^+$. Shown in **Figure 34**, the three Au_{13}NCs have the same icosahedral gold geometry in the core and the same number of pnictogen and chlorine atoms on the surface. However, the orientation of the pnictide and chloride ligands on the surface vary with respect to the identity of the pnictogen, but the different orientation does not alter the absorption spectrum of the Au_{13}NCs.

In the absorption spectrum of Au_{11}NCs, the ligand identities seem to play a minor role in the absorption properties, rather the transitions of MLCT are heavily influenced by the metal core.

In the Au_{13}NCs, the major features in absorption spectrum originate from the icosahedral geometry of the core with minor shifts in the peaks that are derived from the ligands on the surface. The difference in absorption features is more apparent after 4.5 eV, where most of the transitions are related to LLCT. Emission spectra also indicate similar relaxation pathways with very similar emission features. Unfortunately, the Φ of the phosphorescence has not been studied rigorously, which will be very useful in elucidating the influence of L-type ligands on the emission properties.

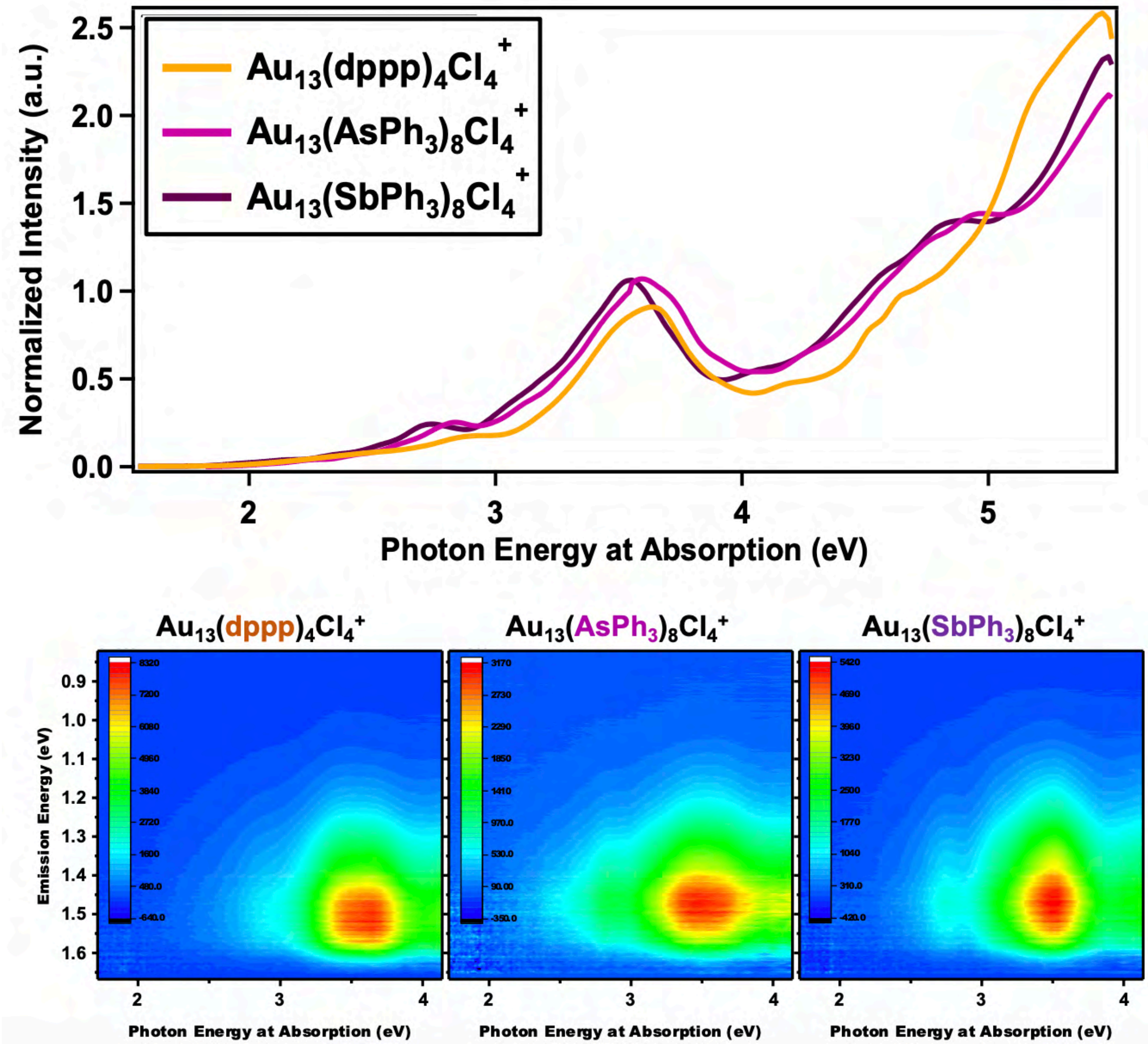

Figure 35. Absorption (top) and emission (bottom) spectra of Au_{13}NCs. The characteristic features of absorption and emission spectrum does not see affected by the ligand's identities or the orientation of the ligands on the surface. Unlike the emission spectra from Au_{11}NCs, the emission spectrum of Au_{13}NCs was not normalized by their **Φ**.

While the experimental data seems to be very close to what was observed in Au_{11}NC systems, where change in the halide ligands only leads to minor changes in the electronic structure of Au_{11}NCs, the computational data of Au_{13}NCs indicates that the L-type ligand identity and the orientation of these L-type ligands play a huge role in the new electronic structure of Au_{13}NCs

(**Figure A31**). The Bader charge analysis show similar ligand induced local charges on gold atoms adjacent to halogen atoms as well as ligand-independent center gold atom observed in Au_{11}NCs (**Figure 36**). However, the charge trend of the gold core differs drastically among three Au_{13}NCs, making the extent of the influence with respect to the identities of pnictogen ligands comparably hard to interpret. Additionally, the vast differences in electronic structures shown in PDOS suggest that the separation of the influences based on the ligand orientations and the influences originating from the ligand identities is the initial step in the understanding the ligand-based properties.

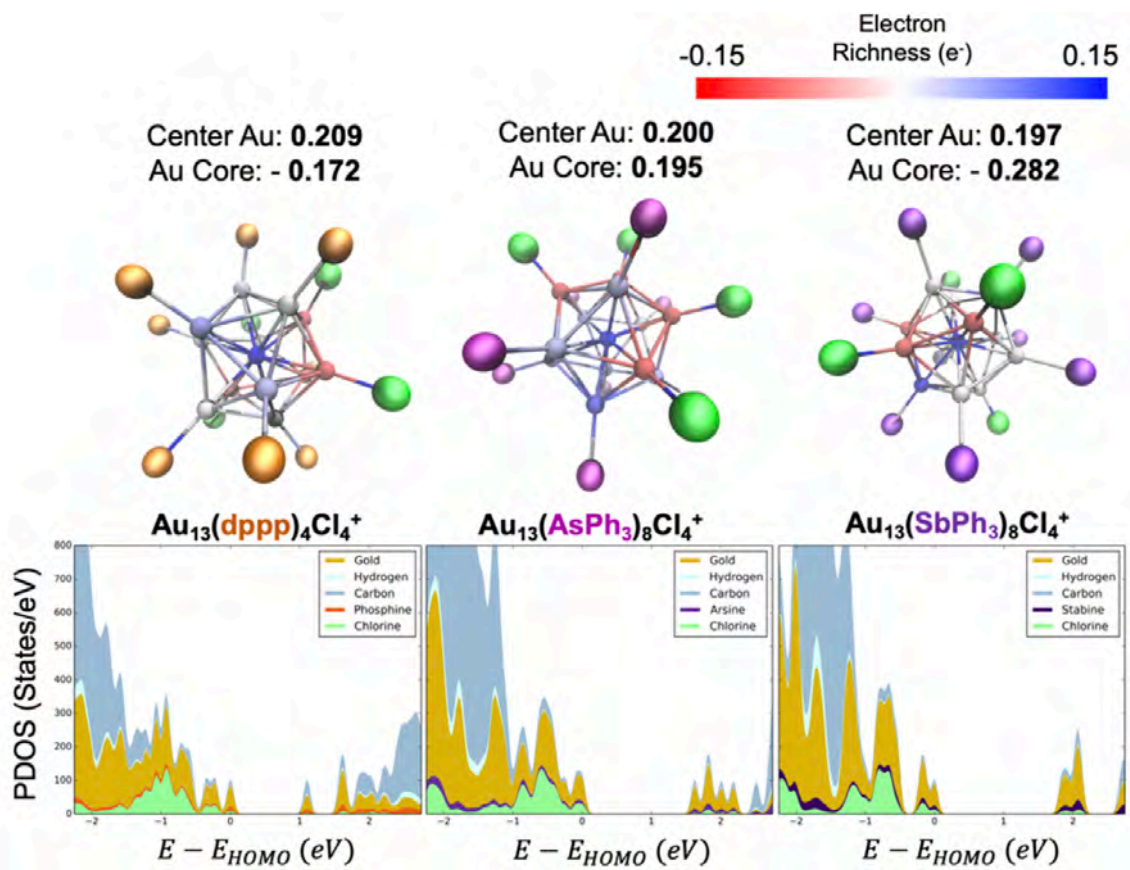

Figure 36. Bader charge (top) and PDOS (bottom) of Au_{13}NCs with different ligand structures. Bader charges were projected on the gold atoms inside the icosahedral core. Binding moieties of the ligands adjacent to the gold atoms were marks with color: P (orange), As (light purple), Sb (dark purple), and Cl (green). PDOS of Au_{13}NCs depict the electronic structures near the frontier orbitals. Different elemental AOs were indicated with colors.

To fully elucidate the complicated nature of ligands on AuNCs observed in the current sets of Au_{13}NCs, some additional studies, including syntheses and analyses of other pnictide capped Au_{13}NPs with comparable ligand orientations (P, As to Sb-like orientation, or vice versa) as well as new $Au_{13}(BiPh_3)_8Cl_4^+$, are highly desirable. The studies consisting of Au_{13}NP with different ligand orientation will provide a robust understanding of both binding-moiety-dependent and orientation-dependent influences of the L-type ligands on the properties of metallic nanoclusters. The new $Au_{13}(BiPh_3)_8Cl_4^+$ can provide further information in the different classification of matter (organic, metalloid, and metal) with regards to their interaction with metallic nanoclusters. Furthermore, these new suites of nanoclusters may turn out to be highly applicable. While Au-Sb bond in $Au(SbPh_3)Cl$ is sensitive to light, the same bond in $Au_{11}(SbPh_3)_8Cl_4^+$ is stable in natural light, yet the strength of the Au-Sb bonds in $Au_{11}(SbPh_3)_8Cl_4^+$ are still weak compared to Au-P bonds, making stibine capped AuNCs useful for initiators for different reactions or the base for new nanostructures.[54] We expect that the bismuth capped AuNCs will likely expose the bare gold surface even better, which can possibly lead to new gold-driven chemistry. With previous knowledge of halogen ligands and new knowledge from the pnictogen ligands in hand, various architecture and properties of nanomaterials can be designed for their appropriate use, hopefully taking more steps to fulfill what Richard Feynman had envisioned seven decades ago.

Appendix A

Table A1 (continued)**.** Crystallographic data for Au(I) precursor and AuNCs.

Compound	$Au(PPh_3)Cl$	$Au(PPh_3)Br$	$Au(PPh_3)I$
Empirical formula	$C_{18}H_{15}AuPCl$	$C_{18}H_{15}AuPBr$	$C_{18}H_{15}AuPI$
Formula weight	494.72	539.17	586.16
Temperature (K)	230	230	230
Crystal system	Orthorhombic	Orthorhombic	Orthorhombic
Space group	$P2_12_12_1$	$P2_12_12_1$	$P2_12_12_1$
a (Å)	10.17	10.10	10.18
b (Å)	12.38	12.50	12.53
c (Å)	13.08	13.47	13.87
α (deg)	90	90	90
β (deg)	90	90	90
γ (deg)	90	90	90
V (Å^3)	1646.8	1700.6	1769.2

Compound	$Au(SMe_2)Cl$	$Au(AsPh_3)Cl$	$Au(SbPh_3)Cl$
Empirical formula	C_2H_6AuSCl	$C_{18}H_{15}AuAsCl$	$C_{18}H_{15}AuSbCl$
Formula weight	294.56	538.66	585.49
Temperature (K)	230	230	230
Crystal system	Orthorhombic	Orthorhombic	Orthorhombic
Space group	$P2_1/c$	$P2_12_12_1$	$P2_12_12_1$
a (Å)	6.141	10.25	10.92
b (Å)	14.88	12.26	12.01
c (Å)	6.455	13.31	12.68
α (deg)	90	90	90
β (deg)	95.71	90	90
γ (deg)	90	90	90
V (Å^3)	586.9	1672.6	1663.0

Compound	$Au_{11}(PPh_3)_8Cl_2^+$	$Au_{11}(PPh_3)_8Br_2^+$	$Au_{11}(PPh_3)_8I_2^+$
Empirical formula	$C_{144}H_{120}Au_{11}P_8Cl_2$	$C_{144}H_{120}Au_{11}P_8Br_2$	$C_{144}H_{120}Au_{11}P_8I_2$
Formula weight	4335.91	4424.81	4518.81
Temperature (K)	298	230	150
Crystal system	Monoclinic	Monoclinic	Triclinic
Space group	$P2_1/c$	$P2_1/c$	P-1
a (Å)	22.641(4)	22.6474(17)	18.5494(10)
b (Å)	18.395(2)	18.4886(12)	25.986(2)

c (Å)	34.574(4)	34.547(2)	33.8120(19)
α (deg)	90	90	82.798(5)
β (deg)	95.959(10)	95.971(5)	90
γ (deg)	90	90	90
V (Å^3)	14321(3)	14386.9(17)	16169.8(18)
Z value	4	4	4
ρ_{calc} (g/cm^3)	2.011	2.084	1.856
μ(Cu K$_\alpha$) (mm^{-1})	22.133	22.713	22.297
Radiation (λ, Å)	CuKα (λ = 1.54178)	CuKα (λ = 1.54178)	CuKα (λ = 1.54178)
F(000)	8028.0	8329.0	8316.0
Crystal size, mm^3	0.320 × 0.280 × 0.031	0.202 × 0.182 × 0.033	0.374 × 0.242 × 0.064
Θ_{max} (°)	104.252	65.542	108.764
Reflections collected	43966	26968	119137
Independent reflections	14312	5129	38385
Data/parameters	14312/85	5129/640	38385/354
Goodness of fit F^2	1.639	0.991	1.169
Final R indices [I>2sigma(I)]	R_1 = 0.2806 wR_2 = 0.5926	R_1 = 0.0665 wR_2 = 0.1771	R_1 = 0.2496 wR_2 = 0.4849
R indices (data)	R_1 = 0.4384 wR_2 = 0.6429	R_1 = 0.0904 wR_2 = 0.2012	R_1 = 0.4181 wR_2 = 0.6090
Largest diff. peak and hole (e· Å^{-3})	8.27 and -5.00	1.66 and – 1.18	4.76 and – 2.79

Compound	$Au_{11}(PPh_3)_7Cl_3$	$Au_{25}(PPh_3)_{10}Cl_7$	$Au_{11}(PPh_3)_7I_3$
Empirical formula	$C_{126}H_{105}Au_{11}P_7Cl_3$	$C_{180}H_{150}Au_{25}P_{10}Cl_7$	$C_{126}H_{105}Au_{11}P_7I_3$
Formula weight	4109.07	7795.34	4383.41
Temperature (K)	293	149.99	230
Crystal system	P2$_1$/c	P2$_1$/n	P2$_1$/c
Space group	Monoclinic	Monoclinic	Monoclinic
a (Å)	16.011(5)	26.450(3)	18.2154(8)
b (Å)	26.339(8)	29.702(2)	26.2280(10)
c (Å)	16.467(5)	26.801(3)	27.0521(11)
α (deg)	90	90	90
β (deg)	112.685(10)	99.626(7)	91.758(3)
γ (deg)	90	90	90
V (Å^3)	6407.(3)	20758(3)	12918.2(9)
Z value	2	50	4
ρ_{calc} (g/cm^3)	2.130	1.754	2.254
μ(Cu K$_\alpha$) (mm^{-1})	24.760	33.817	29.619
Radiation (λ, Å)	CuKα (λ = 1.54178)	CuKα (λ = 1.54178)	CuKα (λ = 1.54178)
F(000)	3772	8976.0	7976.0
Crystal size, mm^3	0.254 × 0.341 × 0.024	0.262 × 0.282 × 0.034	0.368 × 0.470× 0.053

Θ_{max} (°)	50.45	109.39	108.798
Reflections collected	37787	61249	72535
Independent reflections	6829	24373	15799
Data/parameters	6829/112	24373/379	15799/1084
Goodness of fit F^2	1.216	2.097	1.447
Final R indices [I>2sigma(I)]	R_1 = 0.1405 wR_2 = 0.3083	R_1 = 0.2036 wR_2 = 0.4817	R_1 = 0.0889 wR_2 = 0.2295
R indices (data)	R_1 = 0.3898 wR_2 = 0.3849	R_1 = 0.3391 wR_2 = 0.5348	R_1 = 0.1191 wR_2 = 0.2484
Largest diff. peak and hole (e· $Å^{-3}$)	3.348 and – 2.457	11.02 and – 4.91	7.11 and -4.05

Compound	$Au_2(dppp)Cl_2$	$Au_{11}(dppp)_5^{3+}$	$Au_{13}(AsPh_3)_8Cl_4^+$
Empirical formula	$C_{27}H_{26}Au_2P_2Cl_2$	$C_{135}H_{130}Au_{11}P_{10}$	$C_{144}H_{120}Au_{13}As_8Cl_4$
Formula weight	877.3	4228.93	5152.34
Temperature (K)	149.99	232.58	230
Crystal system	Orthorhombic	Triclinic	Monoclinic
Space group	Pbcn	P-1	$P2_1/n$
a (Å)	19.3978(7)	16.2727(11)	16.8208(8)
b (Å)	14.2120(6)	16.4346(13)	29.8849(16)
c (Å)	19.6453(7)	32.134(3)	26.4313(18)
α (deg)	90	90	90
β (deg)	90	90	91.833(5)
γ (deg)	90	118.437(6)	90
V ($Å^3$)	5415.8(4)	7556.8(11)	13279.9(13)
Z value	8	2	4
ρ_{calc} (g/cm^3)	2.152	1.858	2.577
μ(Cu K_α) (mm^{-1})	23.115	20.827	29.579
Radiation (λ, Å)	CuKα (λ = 1.54178)	CuKα (λ = 1.54178)	CuKα (λ = 1.54178)
F(000)	3280.0	3918.0	9372.0
Crystal size, mm^3	1.224 × 0.558 × 0.543	0.328 × 0.273× 0.041	0.222 × 0.22 × 0.047
Θ_{max} (°)	117.852	117.97	130.136
Reflections collected	15143	62399	101464
Independent reflections	3859	21179	16220
Data/parameters	3859/298	21179/190	16220/226
Goodness of fit F^2	1.049	1.121	1.387
Final R indices [I>2sigma(I)]	R_1 = 0.0407 wR_2 = 0.1229	R_1 = 0.2294 wR_2 = 0.4510	R_1 = 0.1852 wR_2 = 0.4669
R indices (data)	R_1 = 0.0434 wR_2 = 0.1262	R_1 = 0.4965 wR_2 = 0.5773	R_1 = 0.3266 wR_2 = 0.5123
Largest diff. peak and hole (e· $Å^{-3}$)	1.96 and -1.68	3.36 and -2.35	4.07 and – 2.57

Table A2 (continued)**.** Summary of Au-Au and Au-ligand bond distances (Å) of AuNCs compared to the computational models.

Au(PPh$_3$)Cl Crystal (Å)		**Au(PPh$_3$)Br** Crystal (Å)		**Au(PPh$_3$)I** Crystal (Å)	
Au-P	Au-X	Au-P	Au-X	Au-P	Au-X
2.2903	2.2314	2.4031	2.2407	2.5633	2.2534

Au(PPh$_3$)Cl Computational (Å)		**Au(PPh$_3$)Br** Computational (Å)		**Au(PPh$_3$)I** Computational (Å)	
Au-P	Au-X	Au-P	Au-X	Au-P	Au-X
2.3058	2.2695	2.4403	2.2769	2.6076	2.2932

$Au_{11}(PPh_3)_8Cl_2^+$ Crystal (Å)			**$Au_{11}(PPh_3)_8Br_2^+$** Crystal (Å)			**$Au_{11}(PPh_3)_8I_2^+$** Crystal (Å)		
Au-Au	Au-P	Au-X	Au-Au	Au-P	Au-X	Au-Au	Au-P	Au-X
2.626	2.32	2.13	2.654	2.50	2.28	2.689	2.63	2.31
2.668	2.35	2.27	2.896	2.45	2.29	2.972	2.57	2.29
2.684		2.28	3.062		2.37	2.873		2.35
2.696		2.31	2.669		2.33	2.685		2.34
2.705		2.35	3.108		2.35	2.682		2.31
2.711		2.38	2.904		2.31	2.965		2.34
2.714		2.39	2.974		2.31	2.676		2.32
2.720		2.40	2.725		2.11	2.912		2.48
2.730			2.711			2.701		
2.753			2.889			2.962		
2.822			2.749			2.837		
2.852			2.827			2.688		
2.863			2.886			3.010		
2.880			2.692			2.693		
2.898			2.987			2.955		
2.901			2.689			3.211		
2.914			3.084			2.960		
2.918			2.698			2.906		
2.937			2.906			2.881		
2.949			3.021			2.685		
2.953			3.012			3.071		
2.957			2.678			2.901		
3.020			2.852			2.721		
3.026			2.864			2.920		
3.042			2.710			2.835		
3.075			3.056			2.914		
3.076			2.930			3.138		
3.080			2.947			3.010		

3.093	2.971	2.662
3.094	3.102	2.838

$Au_{11}(PPh_3)_8Cl_2^+$ Computational (Å)			**$Au_{11}(PPh_3)_8Br_2^+$** Computational (Å)			**$Au_{11}(PPh_3)_8I_2^+$** Computational (Å)		
Au-Au	Au-P	Au-X	Au-Au	Au-P	Au-X	Au-Au	Au-P	Au-X
2.8159	2.3965	2.3302	2.7058	2.5244	2.3231	2.7037	2.6814	2.3223
2.7607	2.4123	2.3361	2.7206	2.5397	2.3337	2.7349	2.6944	2.3332
2.7486		2.3359	2.7439		2.3368	2.7366		2.3371
2.8201		2.3199	2.758		2.3373	2.7469		2.3391
2.7814		2.3384	2.7596		2.3373	2.7563		2.3403
2.7654		2.3401	2.7791		2.3412	2.7802		2.3434
2.7994		2.3396	2.7855		2.3462	2.7891		2.3487
2.7116		2.332	2.7974		2.3463	2.8134		2.3545
2.7623			2.817			2.8247		
2.7078			2.8297			2.8485		
3.031			2.9134			2.9248		
2.9569			2.932			2.9336		
2.925			2.9388			2.9343		
3.069			2.9394			2.9422		
3.1702			2.9475			2.9529		
3.004			2.952			2.9553		
3.0011			2.9909			3.0021		
2.9405			2.9949			3.0027		
2.9929			3.0013			3.005		
3.1096			3.009			3.0117		
3.1571			3.0315			3.0235		
2.9169			3.0325			3.0308		
2.9581			3.0382			3.0429		
3.0138			3.0554			3.0495		
3.0391			3.0688			3.0833		
3.0382			3.1157			3.123		
2.9477			3.1718			3.1504		
3.1816			3.177			3.1685		
3.0058			3.1917			3.1736		

$Au_{11}(PPh_3)_7Cl_3$ Crystal (Å)			**$Au_{11}(PPh_3)_7Br_3$** Crystal (Å)			**$Au_{11}(PPh_3)_7I_3$** Crystal (Å)		
Au-Au	Au-P	Au-X	Au-Au	Au-P	Au-X	Au-Au	Au-P	Au-X
2.611	2.378	2.358	N/A	N/A	N/A	2.682	2.628	2.294
2.955	2.3	2.324				2.676	2.619	2.280
2.955	2.3	2.324				3.065	2.616	2.277
2.92		2.358				2.683		2.290
2.663		2.265				3.190		2.296
2.881		2.324				2.618		2.290
2.863		2.557				2.943		2.285

3.132		2.710
2.659		2.888
2.864		2.915
3.134		2.677
2.864		3.044
2.663		3.014
2.863		3.103
3.132		2.694
2.881		2.955
2.701		2.845
2.964		3.160
2.972		2.715
2.701		2.895
2.964		3.104
2.972		2.856
2.693		2.704
2.969		3.068
2.969		2.869
2.678		2.910
3.02		2.690
2.999		3.095
2.695		2.934
3.02		2.898
2.678		2.866

$Au_{11}(PPh_3)_7Cl_3$ Computational (Å)			**$Au_{11}(PPh_3)_7Br_3$** Computational(Å)			**$Au_{11}(PPh_3)_7I_3$** Computational (Å)		
Au-Au	Au-P	Au-X	Au-Au	Au-P	Au-X	Au-Au	Au-P	Au-X
2.76	2.4235	2.3183	2.6492	2.5568	2.3044	2.6578	2.71	2.3116
2.7485	2.4249	2.3194	2.7447	2.557	2.3154	2.7393	2.7113	2.3202
2.7493	2.4281	2.3158	2.7464	2.5576	2.3182	2.741	2.7133	2.3225
2.6554		2.3101	2.747		2.3192	2.7532		2.3244
2.8176		2.3154	2.7555		2.3193	2.7557		2.3245
2.7452		2.3261	2.7555		2.3242	2.763		2.3261
2.7492		2.3187	2.761		2.3251	2.7689		2.3302
2.8227			2.8216			2.826		
2.823			2.8233			2.8331		
2.7415			2.8314			2.8358		
2.9691			2.8773			2.8896		
2.945			2.8837			2.8898		
2.9081			2.8946			2.8995		
2.9313			2.8961			2.9044		
2.9746			2.8985			2.9069		
2.9819			2.9079			2.9116		
2.899			2.9168			2.9476		
2.886			2.9252			2.9493		

3.0513	2.9495	2.974
3.0185	2.9542	2.9766
2.8931	2.9748	2.9828
2.9178	2.9773	2.9835
2.9146	2.9865	3.0027
2.916	3.0198	3.0402
2.8906	3.0446	3.0409

$Au_{11}(dppp)_5^{3+}$			
Crystal (Å)		Computational(Å)	
Au-Au	Au-P	Au-Au	Au-P
2.7287	2.3198	2.7977	2.3388
2.9189	2.2539	2.7668	2.3374
2.8785	2.3684	2.7715	2.3424
3.0877	2.2693	2.7752	2.3516
2.7101	2.2109	2.7377	2.3304
2.9125	2.2717	2.7715	2.3463
3.1495	2.2703	2.8023	2.3346
2.9187	2.3343	2.7745	2.3438
3.0384	2.2826	2.7474	2.3402
3.064	2.2817	2.7165	2.3418
2.6693		3.1177	
2.7033		3.1941	
2.9114		2.9239	
2.672		2.9387	
2.9286		2.9627	
2.6751		3.1853	
2.9963		3.1268	
2.7119		3.0815	
2.9073		2.9603	
2.9808		3.0315	
2.6876		3.0104	
2.9064		2.9675	
2.9117		2.9921	
2.7463		3.0837	
2.8968		2.9477	
2.9856		2.9989	
2.6789		3.0019	
3.0074		2.9536	
3.0615		3.1319	

Table A3 (continued)**.** Summary of Bader charges of AuNCs.

Atom	PPh_3 Charge (e^-)	$Au(PPh_3)Cl$ Charge (e^-)	$Au(PPh_3)Br$ Charge (e^-)	$Au(PPh_3)I$ Charge (e^-)
Au	-	-0.298012	-0.294313	-0.12804
X	-	0.531875	0.443641	0.220838
P	0.055884	-0.043966	0.09566	0.238725
C	0.191171	0.109852	0.099114	-0.278621
C	0.151428	0.056849	0.055023	0.099295
C	-0.09222	-0.141079	0.045944	0.149755
C	-0.007161	0.114507	-0.374576	0
C	0.098004	-0.044669	0.16685	0.045403
C	-0.218734	0.275164	0	0
C	-0.199413	-0.079388	-0.024388	-0.359532
C	0.058501	0	0	0.006067
C	-0.2696	-0.049525	0.335173	0
C	-0.240061	0.151442	-0.003747	0.116209
C	-0.313977	0	0	0
C	0.125987	-0.086884	0.065634	0.225042
C	-0.186961	-0.599168	-0.000936	0.032998
C	0.039596	0.407343	0.216262	0
C	0	-0.032914	-0.316814	0.00293
C	0	-0.377345	0.044805	-0.18643
C	0.081154	0.344353	0.041564	0.109299
C	0.069725	0.016339	-0.064008	-0.374384
H	0.02398	-0.215894	-0.249907	-0.183672
H	0.15234	-0.047631	-0.000472	0.011012
H	0.096644	-0.165733	0.008529	-0.186947
H	-0.058365	0.050264	0.048549	-0.018721
H	-0.091807	-0.185167	-0.00425	0.078425
H	-0.083662	-0.055356	-0.147614	0.013593
H	-0.182617	-0.052051	-0.187282	0.018609
H	-0.044476	-0.164408	-0.158593	-0.047019
H	0.010367	-0.06002	-0.091754	-0.139058
H	0.050887	0.003365	-0.143595	-0.166463
H	0.111978	-0.112759	-0.20844	-0.168954
H	0.218078	-0.020278	0.150327	-0.112607
H	0.270768	0.012671	-0.031623	0.068788
H	-0.296507	-0.162271	-0.130602	-0.049011
H	-0.156599	0.177454	-0.143156	0.190028

Atom	$Au_{11}(PPh_3)_8Cl_2^+$ Charge (e^-)	$Au_{11}(PPh_3)_8Br_2^+$ Charge (e^-)	$Au_{11}(PPh_3)_8I_2^+$ Charge (e^-)
Au	0.290513	0.304496	0.285632
Au	-0.002959	0.008335	0.030025
Au	0.062741	0.067526	0.071797
Au	0.062919	0.063098	0.06063

Au	-0.09782	-0.01286	0.067039
Au	-0.014481	0.039093	0.027537
Au	0.015646	0.057608	0.049497
Au	-0.0728	-0.010299	0.06734
Au	0.04929	0.042982	0.041202
Au	0.080151	0.082421	0.095819
Au	0.065338	0.064805	0.067066
P	0.034484	-0.087389	-0.303553
P	0.094568	-0.000692	-0.053349
P	-0.134088	-0.151727	0.035328
P	0.050015	0.044585	0.002963
P	0.085862	0.112596	0.056199
P	-0.016887	-0.130411	-0.038472
P	0.108615	-0.007832	0.110989
P	0.086127	0.060988	0.116232
X	0.5353	0.448897	0.32716
X	0.535399	0.435251	0.316332
C	0	0.129493	0
C	0.162977	0	-0.250335
C	0.091919	0.165995	0
C	-0.108703	0.027763	0.017663
C	0.040945	-0.203224	0
C	-0.188904	0.215913	0.30989
C	0.210335	-0.063366	0
C	-0.323905	-0.018923	-0.065496
C	0.016097	-0.208245	0.214143
C	0.030445	0.041859	-0.087137
C	-0.156927	0	0
C	-0.14276	0.19665	0.214612
C	-0.085675	-0.207024	-0.115096
C	0	0.123385	0
C	-0.051036	-0.1608	0.240717
C	0.259277	0	-0.192548
C	0.164916	0.046896	0.178725
C	-0.072824	-0.079933	-0.048759
C	0.170244	-0.203019	-0.326796
C	0.130372	-0.01003	0.319685
C	0	0	0.106849
C	-0.184754	0.142961	0.068825
C	0	-0.027354	0
C	0.007265	-0.132444	0.25671
C	-0.023802	-0.042287	-0.020047
C	0.155804	0.135623	0.10562
C	0.223322	0	0
C	-0.322387	0.14152	0.097209
C	0	-0.022422	0.124062
C	0.212117	0.126331	-0.182901
C	-0.057001	-0.368729	-0.1253
C	0.135756	0.100732	0.360779
C	0	0	0.122123
C	0.165056	-0.001776	-0.002657
C	0	0	0.296281
C	-0.110873	0.028285	-0.210947
C	-0.005155	0.111175	-0.22951
C	0.278243	-0.243729	0.174948
C	0.10295	0.114727	0

C	-0.16692	-0.194326	0.26343
C	0	0	-0.208345
C	0.000404	0.013096	0.04704
C	-0.252279	-0.314311	-0.232662
C	-0.301573	-0.185021	-0.234064
C	0.377721	0.256302	0.048543
C	-0.46351	-0.460919	-0.322347
C	0.176988	-0.034298	0
C	-0.018748	0.186667	0.224846
C	0	0	0.12752
C	0.089931	-0.071805	-0.139594
C	0.287829	0.378787	0
C	-0.015462	0.033593	0.215771
C	0.1278	0	0.004901
C	-0.037385	0.228819	-0.181336
C	-0.130935	-0.252047	-0.021173
C	-0.018157	0.317341	0
C	-0.249821	-0.208634	0.044604
C	0.226882	-0.049404	0.184724
C	0	0	0
C	0.247712	0.172229	-0.381133
C	-0.076451	-0.540535	-0.067613
C	0.058426	0	0
C	0	0.005483	-0.329444
C	0.056608	-0.135845	0
C	0.170373	0.007393	0.308967
C	0.117662	0.185401	0.147874
C	-0.269809	-0.185344	-0.227191
C	0	0	0
C	0.180392	0.157729	0.163681
C	-0.204808	-0.0204	0.050022
C	0	0.355013	0.336644
C	0.172046	-0.083166	-0.21146
C	-0.211036	0	0.02038
C	-0.199981	-0.111938	0.107221
C	-0.269197	-0.134347	0.164849
C	0.14644	0.205241	0.242248
C	0	-0.335387	-0.285767
C	-0.287441	0.209351	0.408085
C	0	0	0.010432
C	-0.159657	0.074648	-0.0319
C	-0.068284	0	0
C	0	-0.218496	-0.044186
C	-0.237161	0.121847	0.215493
C	0.481322	0.256921	-0.278399
C	-0.347871	-0.065856	0.068323
C	0	0	0
C	-0.090052	-0.018875	-0.025871
C	0	0	-0.029163
C	0.237961	0.115862	0.031015
C	-0.082684	-0.352734	0.010629
C	-0.254664	-0.094149	-0.186074
C	0.112473	0.012648	0.059883
C	0.15316	0.331937	0.110679
C	-0.16683	0.03381	0
C	0	0	-0.083016

C	0.111594	-0.018111	-0.11057
C	-0.281731	0	0.368563
C	0	0.090561	0
C	-0.114607	0	-0.158705
C	0.2379	0.056573	-0.058829
C	0	0.06966	0.240324
C	0.041076	-0.097045	-0.218875
C	0.166531	0.052293	-0.013401
C	-0.105224	0	0
C	0	-0.152953	0.04633
C	-0.090498	0.13658	0.19618
C	0.179733	0.240526	0.24297
C	0.327835	0.25097	-0.14044
C	0.148011	0.267953	-0.059828
C	0	0	0
C	-0.186682	-0.018737	0.049058
C	-0.01348	0.095694	-0.324337
C	-0.22951	0	0.105722
C	-0.036589	0.080308	0.165418
C	0.178511	-0.207266	-0.000689
C	-0.102496	0.152284	0.000149
C	-0.133219	0.410656	0
C	0.095839	-0.342059	0.037596
C	-0.002069	0.004026	-0.243896
C	0.229459	-0.141023	-0.2046
C	-0.241709	0.166868	0.03571
C	-0.129625	-0.114186	-0.350883
C	0.120285	0.03609	0
C	-0.205386	0	0.080584
C	0.13243	-0.306052	-0.256167
C	0.110605	-0.321779	-0.217953
C	-0.31187	0.038482	-0.174799
C	0.068331	0.01066	0.207964
C	-0.057548	-0.169503	0
C	-0.101034	-0.153318	-0.165285
C	0.018808	0.230934	0.220445
C	0.000108	-0.162413	-0.192148
C	-0.22975	-0.222361	-0.097878
C	0.144597	-0.142866	-0.000972
C	0.027691	0	0
C	0.032677	0.03455	0.196313
C	-0.017391	0.051741	0.337172
C	-0.13584	0.27057	-0.032418
C	0.205269	-0.271646	0.006852
C	-0.047179	0	-0.371611
C	-0.039277	-0.294648	0
C	-0.094477	-0.208062	0.322774
C	-0.138515	0.151065	0.040437
C	0.198056	0.02732	-0.18719
H	-0.021862	0.04562	0.125139
H	0.038284	-0.073471	-0.165157
H	-0.255198	-0.111805	-0.102607
H	0.026904	-0.136232	-0.014002
H	-0.043876	-0.058613	-0.089648
H	-0.019806	-0.075338	0.023883
H	0.0288	0.15837	-0.190694

H	0.034042	-0.040761	-0.233672
H	0.147126	-0.066668	-0.020186
H	-0.155608	-0.152405	0.042917
H	-0.051803	0.226028	0.025193
H	0.088457	-0.08247	-0.148018
H	-0.223575	-0.086766	-0.062622
H	-0.020071	-0.047425	0.073739
H	-0.144254	-0.085971	-0.049142
H	0.022337	0.229503	0.077707
H	-0.114588	-0.08492	-0.011707
H	-0.161286	-0.133414	-0.321016
H	0.009116	-0.013816	0.043034
H	0.000683	-0.054623	-0.221995
H	-0.167733	-0.203495	-0.203899
H	-0.029678	-0.000432	0.12017
H	-0.099769	-0.138421	-0.095706
H	-0.207185	0.007975	-0.005541
H	0.046488	-0.098765	-0.215176
H	0.082007	0.127404	-0.1165
H	-0.047336	-0.025685	-0.159272
H	-0.150765	-0.112688	-0.120553
H	-0.301459	-0.122971	-0.134874
H	-0.173551	0.064107	-0.249568
H	0.002343	-0.027432	0.143019
H	-0.257404	0.140845	-0.131143
H	-0.068552	-0.074381	-0.171746
H	-0.086169	-0.070306	-0.106601
H	-0.033022	-0.014375	0.038594
H	-0.133095	-0.12835	-0.101474
H	0.140939	0.129131	0.213571
H	-0.00231	-0.026092	-0.004475
H	-0.023984	0.014353	0.141531
H	0.161237	0.200725	0.112155
H	-0.111485	0.057164	-0.238575
H	-0.087026	-0.140967	-0.117863
H	-0.140678	-0.317642	0.128873
H	0.020401	-0.016846	-0.049341
H	-0.297854	-0.276069	-0.087413
H	-0.012269	0.023599	0.05546
H	-0.084588	-0.2058	-0.019288
H	0.047133	-0.047414	-0.188449
H	-0.045089	0.194902	0.102257
H	-0.162284	-0.149606	-0.170132
H	-0.237291	0.146841	-0.013675
H	0.073608	0.156004	0.050854
H	-0.033738	-0.144901	0.192758
H	-0.313089	0.15002	-0.219612
H	0.026178	-0.025251	-0.076681
H	0.026993	0.045255	-0.024866
H	-0.047546	-0.134341	-0.157362
H	-0.053051	-0.202224	-0.061325
H	0.001427	-0.016848	-0.125514
H	-0.026661	-0.112547	-0.106411
H	0.127196	-0.028159	-0.295156
H	0.036235	0.158772	-0.012457
H	0.212255	-0.087887	-0.272612

H	-0.075817	-0.012532	-0.069737
H	0.090584	-0.065974	-0.09698
H	0.001419	0.086369	0.134385
H	0.003622	-0.150095	0.012898
H	-0.038765	0.005082	-0.170557
H	0.174922	-0.013148	-0.009498
H	-0.090734	-0.188327	-0.067012
H	0.057416	0.121861	-0.215032
H	-0.032667	-0.038304	0.022192
H	-0.092126	-0.164354	0.091535
H	0.116262	0.060128	-0.095482
H	-0.022891	0.031374	-0.134532
H	0.004619	-0.05047	0.087532
H	-0.079813	0.04102	-0.106311
H	-0.182641	-0.293111	-0.140615
H	0.183598	-0.227945	-0.065461
H	-0.174319	-0.141312	0.081213
H	-0.053641	0.095111	-0.09517
H	0.024024	-0.169135	-0.043362
H	0.025466	-0.064261	0.016371
H	-0.080294	-0.194097	-0.060528
H	0.003157	-0.037208	-0.266662
H	-0.034749	-0.208833	0.016089
H	0.004222	0.156852	0.063441
H	-0.169431	-0.080728	-0.244008
H	-0.189922	-0.197016	-0.053019
H	-0.323164	-0.285671	-0.16319
H	-0.19027	-0.263708	-0.138393
H	0.160969	-0.191424	-0.150255
H	0.047916	0.232873	0.113959
H	0	-0.280892	-0.00115
H	-0.144082	-0.005017	0.109814
H	0.055655	-0.071001	0.022064
H	0.385184	-0.24264	-0.111226
H	-0.481947	-0.05349	0.13198
H	0.019724	-0.021503	-0.063278
H	0.17243	0.202994	0.088295
H	0.034719	-0.093875	0.291451
H	0.039159	0.162223	0.038634
H	0	-0.094677	-0.095134
H	-0.297794	0.141907	0.150786
H	-0.268632	0.071934	-0.027364
H	0.039595	0.068404	0.050065
H	-0.101522	-0.115891	-0.060473
H	0	-0.052237	-0.14147
H	0.370715	0.025745	-0.046344
H	-0.304603	0.004983	0.058021
H	-0.217867	0.132315	0.072661
H	0	0.002234	-0.111426
H	-0.048547	-0.038822	0.01067
H	0.231106	-0.00356	-0.216556
H	-0.023608	-0.097892	-0.26067
H	0	-0.020295	-0.011387
H	-0.120675	0.185794	-0.002852
H	0.03926	-0.018934	-0.00702
H	0.024846	-0.115998	-0.151578

H	-0.179414	0.236628	-0.013466

Atom	**$Au_{11}(PPh_3)_7Cl_3$** Charge (e^-)	**$Au_{11}(PPh_3)_7Br_3$** Charge (e^-)	**$Au_{11}(PPh_3)_7I_3$** Charge (e^-)
Au	0.238015	0.280155	0.280232
Au	0.038966	0.014689	0.006833
Au	0.056172	0.02606	0.057753
Au	0.008517	-0.016216	0.116695
Au	0.069724	0.036607	0.065583
Au	-0.05809	0.003934	0.077599
Au	-0.016558	0.004554	-0.011381
Au	0.044419	0.034016	0.029065
Au	-0.091665	0.001332	0.067821
Au	-0.057309	0.007554	0.068829
Au	0.048578	0.046256	0.047518
X	0.539389	0.448788	0.33939
X	0.579506	0.471512	0.360669
X	0.5448	0.458402	0.339582
P	-0.146352	-0.089397	-0.160549
P	-0.10995	-0.029241	-0.063432
P	0.086937	0.146882	-0.027013
P	0.262937	-0.026195	0.070401
P	-0.049774	0.096629	0.04492
P	0.082601	-0.034906	-0.05136
P	-0.155994	-0.065745	-0.077648
C	0.202078	-0.066527	0.178975
C	0	0.18576	0
C	-0.408734	-0.033602	-0.161115
C	-0.338834	0	0.204399
C	-0.22361	0.436709	-0.322101
C	0.21485	-0.097807	0.051871
C	0.320491	0.131632	-0.073268
C	0	0.033488	-0.132477
C	0.31078	0.00886	0.264145
C	-0.206526	-0.178198	0
C	0.129866	0.246994	-0.099387
C	0.039531	0	-0.023612
C	0.277677	0.285789	0.024458
C	0.035646	0.085413	0
C	0.079801	-0.025818	-0.045666
C	0	0	-0.05354
C	-0.030178	-0.029023	0.198505
C	0	0	-0.231298
C	0	0.24086	0
C	0.098065	0	0.369041
C	0.07465	-0.263591	0.03336
C	0.417618	-0.024253	0.045658
C	-0.180641	0.359589	0.0133
C	-0.097037	-0.039647	-0.073021
C	-0.058141	0.279572	-0.139838

C	0.543763	0	0.223372
C	0.139309	-0.337061	0.099012
C	0.477997	0	-0.41106
C	-0.082462	0.021772	0.327517
C	-0.06254	0.042842	-0.212461
C	0.527482	0.018414	0
C	-0.284704	0.122256	-0.327367
C	-0.227723	-0.473369	0
C	0.154373	0.647447	0.019396
C	-0.060582	0	0.405955
C	-0.005068	-0.166305	-0.256956
C	0.363251	0.07419	0.204492
C	0	0	-0.115467
C	-0.147803	-0.121072	0.338464
C	0	-0.136713	0
C	0.031654	-0.102459	0.058044
C	-0.415703	0	-0.308135
C	0.037668	-0.058602	0.219402
C	0	0	-0.169266
C	-0.124234	0.334529	0
C	0	0	-0.001142
C	0.058946	-0.088718	0
C	0.269552	-0.108088	0.154182
C	-0.12589	0	0
C	0.219444	-0.287989	0.041584
C	-0.168908	0.423459	0.052509
C	0	-0.185271	0
C	0.005548	-0.161371	-0.16812
C	0.39858	0.140087	0.261042
C	0.220267	0.086782	0.134591
C	-0.302877	-0.155208	-0.224016
C	-0.270974	-0.094355	-0.330948
C	0	0	0
C	-0.406165	-0.114875	0.178605
C	0.018809	0	0
C	0.194168	0.260569	0.282593
C	-0.167503	-0.328699	-0.079259
C	-0.064663	-0.047775	0.039542
C	0	0	0
C	0.05888	0.023288	-0.023397
C	-0.272052	0	-0.212593
C	0.117009	0.032506	0
C	0	0	0.160548
C	0.121304	-0.257366	-0.140344
C	0	0.216741	0.176608
C	-0.147418	0	0
C	-0.05245	-0.347125	0.049799
C	-0.193004	-0.035103	0
C	-0.029767	0.070959	0.08437
C	-0.034397	0	0.05263
C	0.176585	-0.351911	0.05385
C	0	0.264683	-0.081326
C	-0.090122	-0.279216	0.014044
C	-0.014621	0	-0.07381
C	0.174584	-0.222325	-0.143043
C	0	-0.06088	0.087623

C	0.026135	-0.088802	-0.20122
C	-0.222083	0	0
C	-0.124162	0.275987	-0.106538
C	0	-0.089732	0.134436
C	-0.166027	-0.107877	-0.103196
C	-0.048855	0.034285	0.455003
C	0	-0.087902	0
C	-0.068366	0.044864	-0.335676
C	0.102007	0	0.06847
C	0	-0.327094	0
C	-0.071376	-0.014363	-0.020621
C	0.201633	0.035151	0.312634
C	0	0	0
C	0.098737	-0.160504	-0.396654
C	-0.220458	0.398105	-0.113393
C	0.232521	0.099762	0.231702
C	0.104113	0.045057	0.0992
C	0.03432	0.148245	0.154668
C	0.058816	0.00413	-0.003294
C	0.017477	-0.243092	-0.030253
C	0	0.348337	0.255568
C	0.064522	0	0
C	-0.053507	-0.457682	-0.381256
C	0.156668	0	0.003904
C	0	0	0
C	0.263239	0.389292	0.05452
C	-0.001843	0	0
C	-0.146881	0.069716	-0.022432
C	0.140576	0	0.219759
C	0	0.284844	0
C	-0.258748	-0.222308	-0.165967
C	0.238781	0.149701	0.398555
C	0.126382	-0.185887	0
C	0.039804	0	0.092004
C	0.125249	0.108178	0.216481
C	0	0	0.157784
C	-0.094742	-0.028064	0
C	0.175033	0.23772	0.135081
C	-0.023845	-0.102488	-0.128288
C	0	0.115533	0
C	-0.183296	0	-0.346815
C	-0.12925	-0.084651	-0.175157
C	0	0	0.300194
C	0.114031	0.020047	0.295517
C	-0.173682	0.029624	0.098922
H	-0.089272	-0.034053	-0.104974
H	-0.068328	-0.174515	-0.042866
H	-0.203935	-0.097663	-0.119526
H	-0.126624	0.015738	-0.000408
H	0.024253	0.113197	-0.003483
H	-0.113296	-0.046362	-0.152519
H	-0.057267	-0.127607	-0.041057
H	-0.01977	0.037692	-0.090876
H	-0.156678	-0.027271	-0.147888
H	-0.119657	-0.239445	-0.347248
H	-0.063233	-0.031306	-0.033219

H	0.079585	-0.047185	-0.207829
H	-0.035229	0.194499	0.032854
H	0.045197	-0.049111	-0.03193
H	-0.041632	-0.069554	-0.221556
H	0.050943	-0.106499	0.046671
H	0.285007	0.051711	0.178318
H	0.192002	0.081677	0.06184
H	0.029435	0.117764	-0.33913
H	-0.035177	-0.053777	-0.042579
H	-0.459234	-0.222084	-0.084086
H	-0.330115	-0.060563	-0.08283
H	-0.093228	0.023599	0.205665
H	-0.422229	-0.066671	-0.105675
H	0.082204	-0.048611	-0.142596
H	-0.028388	-0.050419	0.093213
H	0.16423	0.16069	0.024193
H	-0.111826	-0.051034	-0.200424
H	0.00743	-0.002364	-0.000232
H	0.002076	0.051517	-0.10273
H	-0.020854	0.023843	0.039302
H	-0.01568	-0.009046	-0.057912
H	-0.041166	-0.02683	0.15639
H	0.012789	-0.009797	-0.019577
H	-0.115607	-0.078499	-0.201251
H	-0.185937	0.115234	0.044485
H	-0.154583	0.062202	-0.02897
H	-0.272936	-0.179849	-0.217191
H	0.089604	-0.395719	-0.182476
H	-0.018067	0.164644	0.082918
H	-0.140248	-0.034305	0.009264
H	-0.068143	-0.098939	0.06429
H	0.002548	0.039157	-0.002485
H	0.021804	-0.048877	0.074232
H	-0.048369	-0.039324	0.024886
H	-0.206932	-0.0302	-0.025375
H	0.059506	-0.00451	-0.12608
H	0.062345	0.020411	-0.131883
H	-0.181314	0.041736	-0.127642
H	-0.067926	0.082594	-0.125313
H	-0.009931	-0.209436	0.208298
H	-0.029051	-0.070199	-0.09524
H	0.198176	0.054557	-0.010613
H	-0.030285	0.049582	-0.213746
H	0.037173	-0.00283	-0.077309
H	-0.04911	-0.155457	-0.001564
H	-0.117666	-0.059118	-0.204947
H	-0.073132	0.11936	0.025099
H	-0.229345	0.144344	-0.052124
H	-0.082779	-0.018789	0.060545
H	0.040253	-0.070522	-0.117771
H	-0.021846	-0.142718	-0.238484
H	0.181307	0.151413	0.136639
H	-0.089339	0.009672	-0.111564
H	-0.059987	-0.173118	0.09168
H	-0.110334	-0.151049	-0.130693
H	-0.219873	-0.210127	-0.261804

H	-0.113008	0.102032	-0.158833
H	-0.292994	-0.233504	0.00301
H	0.210442	-0.019447	-0.063581
H	-0.075905	-0.076543	-0.427825
H	-0.15299	-0.070654	-0.025477
H	-0.146343	-0.089221	-0.052428
H	0.035372	-0.137575	-0.113281
H	-0.117953	0.000371	-0.026774
H	-0.28814	-0.378565	-0.06531
H	-0.091262	0.292237	0.097229
H	-0.066989	-0.263037	-0.156925
H	-0.16903	-0.212592	-0.138543
H	0.053929	0.084234	0.01183
H	-0.181759	-0.180446	-0.124545
H	-0.053419	-0.190562	-0.059022
H	-0.185757	-0.170657	-0.058205
H	-0.077	-0.185377	-0.149664
H	-0.187718	-0.073128	-0.145529
H	-0.139233	-0.163697	0.064415
H	-0.203868	-0.285639	-0.031087
H	-0.156796	0.076066	0.053346
H	0.026486	0.10507	-0.060742
H	-0.150933	-0.132721	-0.258562
H	-0.165553	0.013403	-0.15535
H	-0.032997	-0.033858	0.064101
H	-0.036144	-0.031729	0.002201
H	0.082493	0.140678	-0.036712
H	-0.083951	-0.040128	-0.228294
H	-0.158092	-0.292603	0.103805
H	-0.041885	-0.208637	-0.008575
H	-0.060067	0.091626	-0.121151
H	0.04603	-0.038216	-0.227286
H	-0.221928	-0.045055	0.180689
H	0.319259	-0.030364	0.138782
H	-0.072605	-0.10998	-0.114335
H	0.261539	-0.027384	-0.138113
H	0.007857	-0.366643	-0.155704
H	-0.014617	0.00039	0.21735

Table A4. Life time (τ) of emissions of AuNCs.

AuNP	Φ (a.u.)	τ_{obs} (μs)	τ_{rad} (μs)
$Au_{11}(PPh_3)_8Cl_2^+$	0.023%	2.1	9130
$Au_{11}(PPh_3)_8Br_2^+$	0.067%	2.8	4180
$Au_{11}(PPh_3)_8I_2^+$	0.339%	3.4	1003

τ_{obs}: Observed lifetime

τ_{rad}: Radiative lifetime

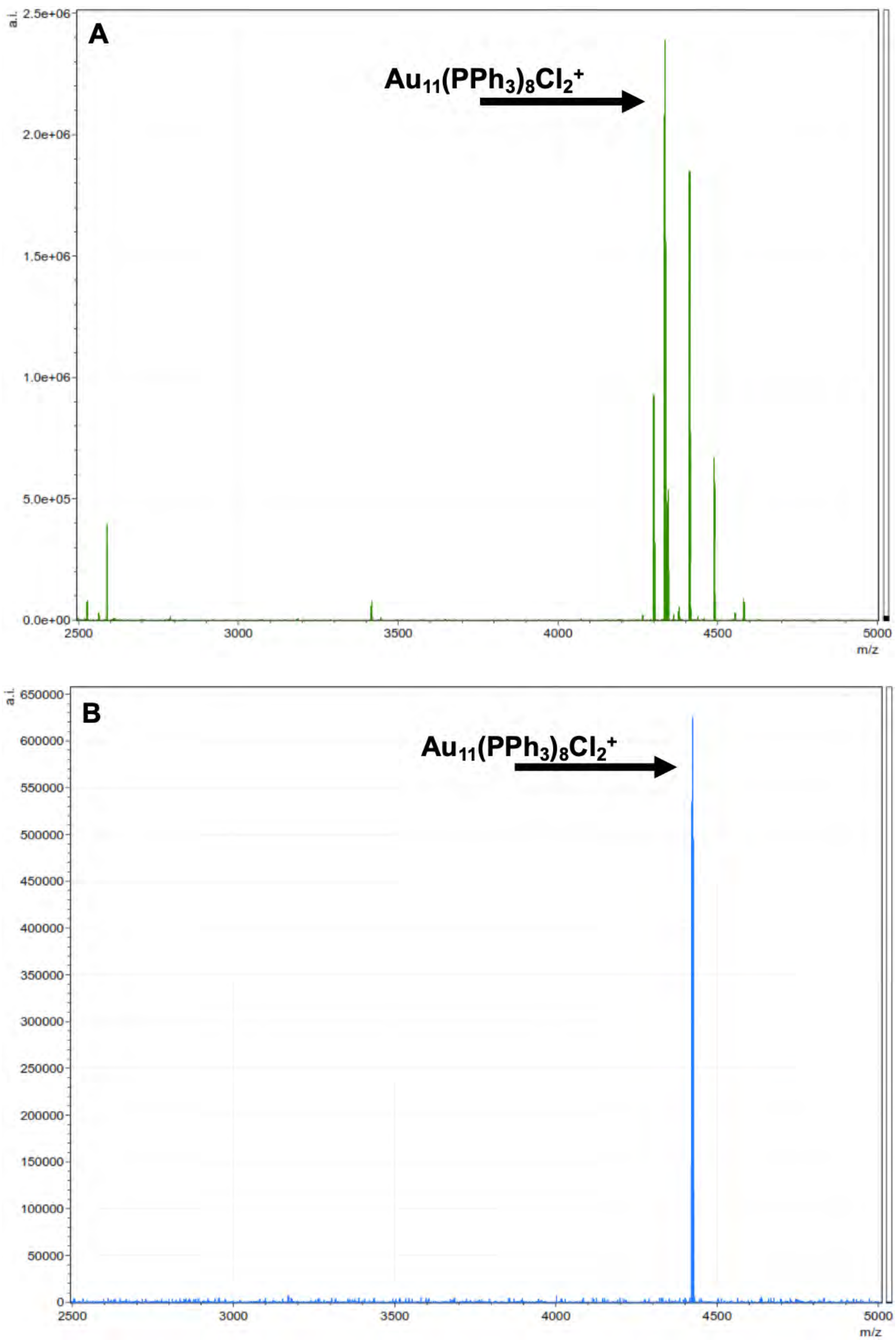
A
B
$Au_{11}(PPh_3)_8Cl_2^+$
$Au_{11}(PPh_3)_8Cl_2^+$
a.i.
m/z
2500
3000
3500
4000
4500
5000

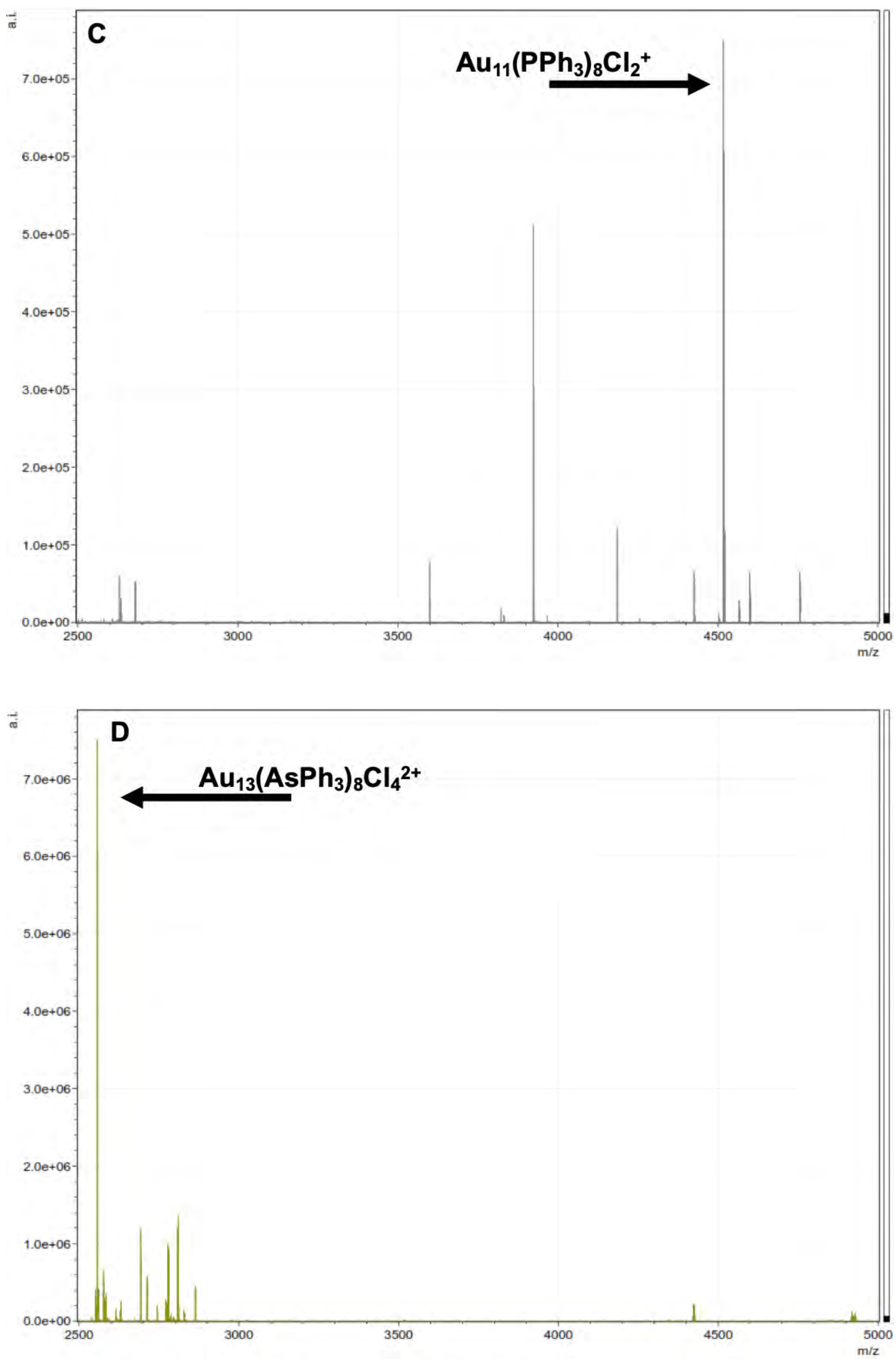

Figure A1. ESI spectrum showing the existence of A) $Au_{11}(PPh_3)_8Cl_2^+$, B) $Au_{11}(PPh_3)_8Br_2^+$, and C) $Au_{11}(PPh_3)_8I_2^+$, and D) $Au_{13}(AsPh_3)_8Cl_4^+$.

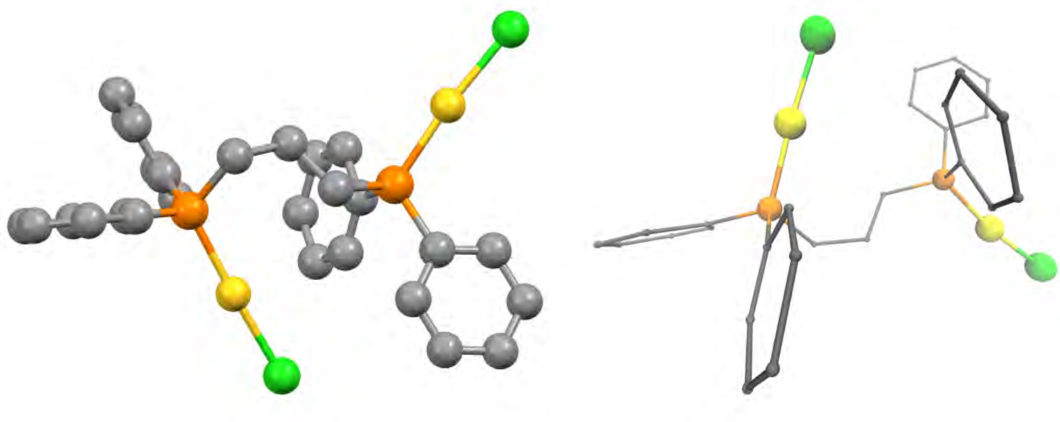

Figure A2. The crystal and computation structure of dppp.

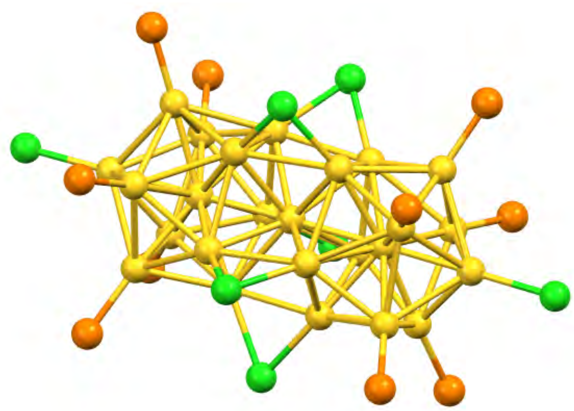

Figure A3. Crystal structure of decomposed product $Au_{25}NC$ from $Au11(PPh_3)_7Cl_3$. Purified $Au_{11}(PPh_3)_7Cl_3$ solution was left to decompose after three months, other impurities were removed and the major product $Au_{25}NC$ was crystalized. X-ray diffraction data suggests that the $Au_{25}NC$ is passivated with phosphine and halide ligands.

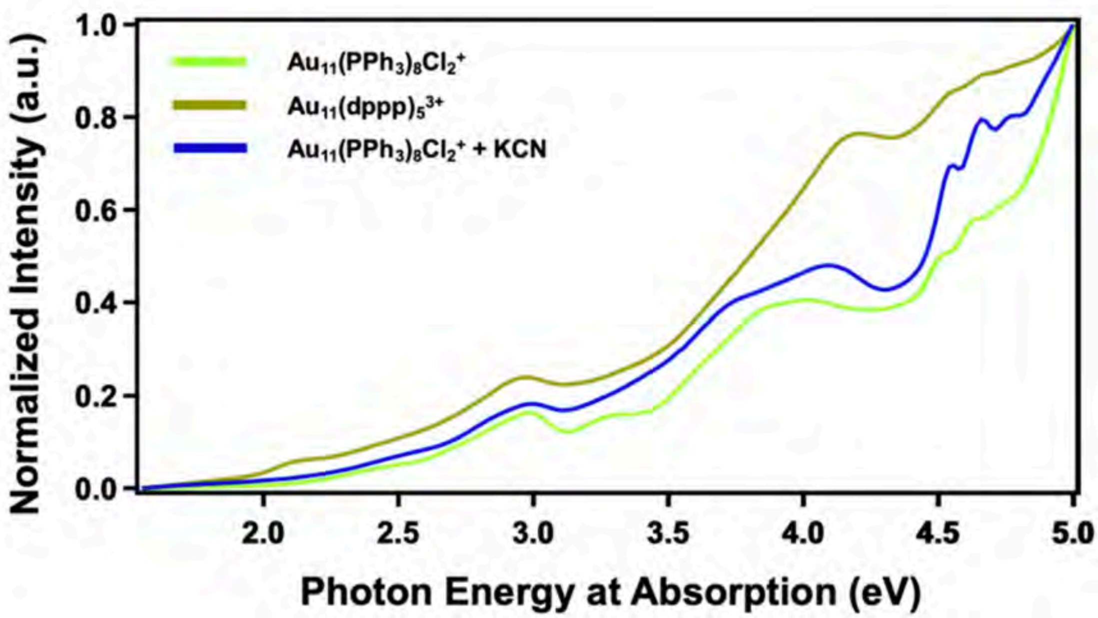

Figure A4. Absorption spectrum of $Au_{11}(dppp)_5^+$ and $Au_{11}NC$ with CN^-. Comparing to the $Au_{11}(PPh_3)_8Cl_2^+$, the other AuNCs has similar absorption features, especially near 3.0 and 4.0 eV.

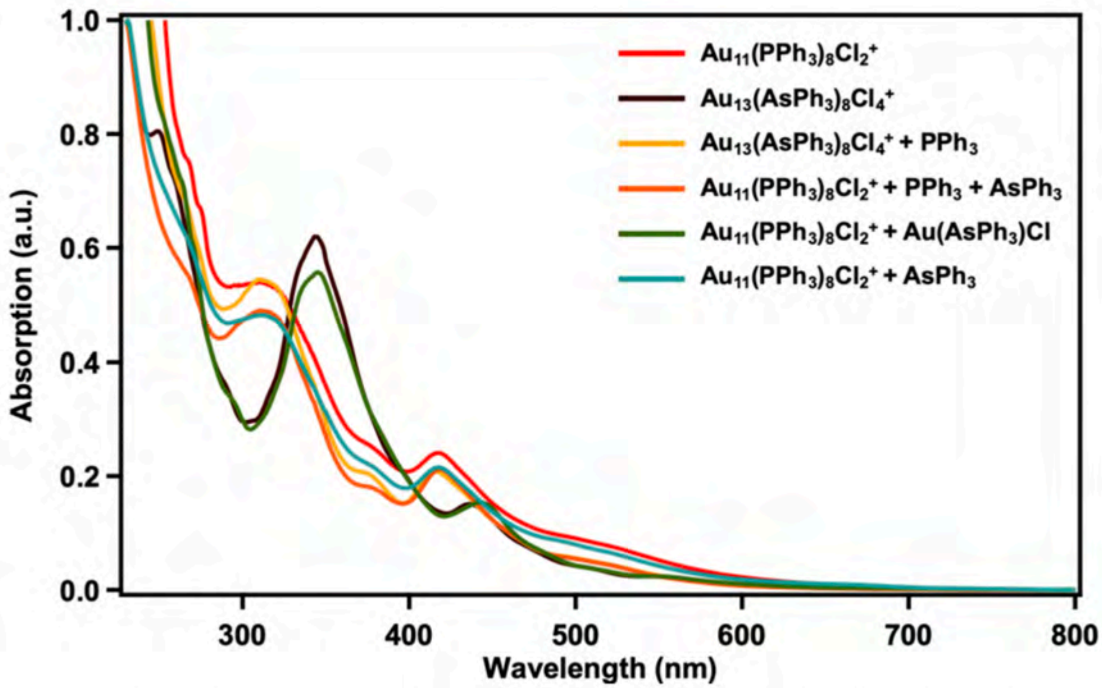

Figure A5. Absorption spectrum of $Au_{11}NCs$ with addition of other ligands. In the presence of PPh_3 ligands, the $Au_{13}(AsPh_3)_8Cl_4^+$ seems to produce $Au_{11}NCs$, whereas $AsPh_3$ ligands does not indicate any changes in the absorption features of $Au_{11}(PPh_3)_2Cl_2^+$. Interestingly, in the presence of $Au(AsPh_3)Cl$, $Au_{11}(PPh_3)_8Cl_2^+$ appears to show absorption features that resemble $Au_{13}NCs$.

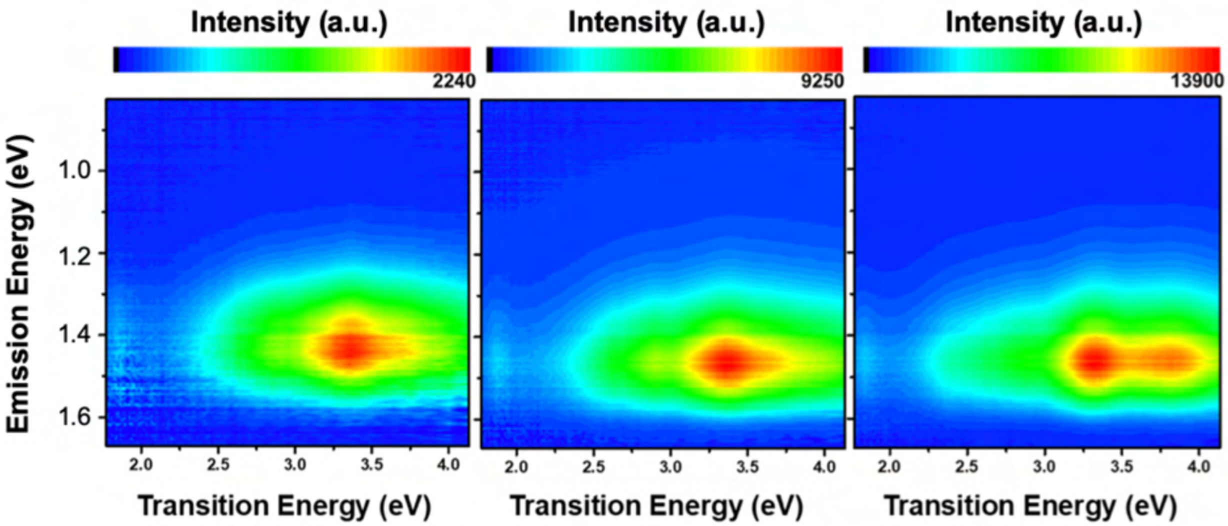

Figure A6. Emission maps of Au_{11}NCs in DCM. Compared to the same Au_{11}NCs solvated in the ethanol, the emission maps show less pronounced features. However, the **Φ** collected from the Au_{11}NCs in DCM is much higher than that of Au_{11}NCs in ethanol.

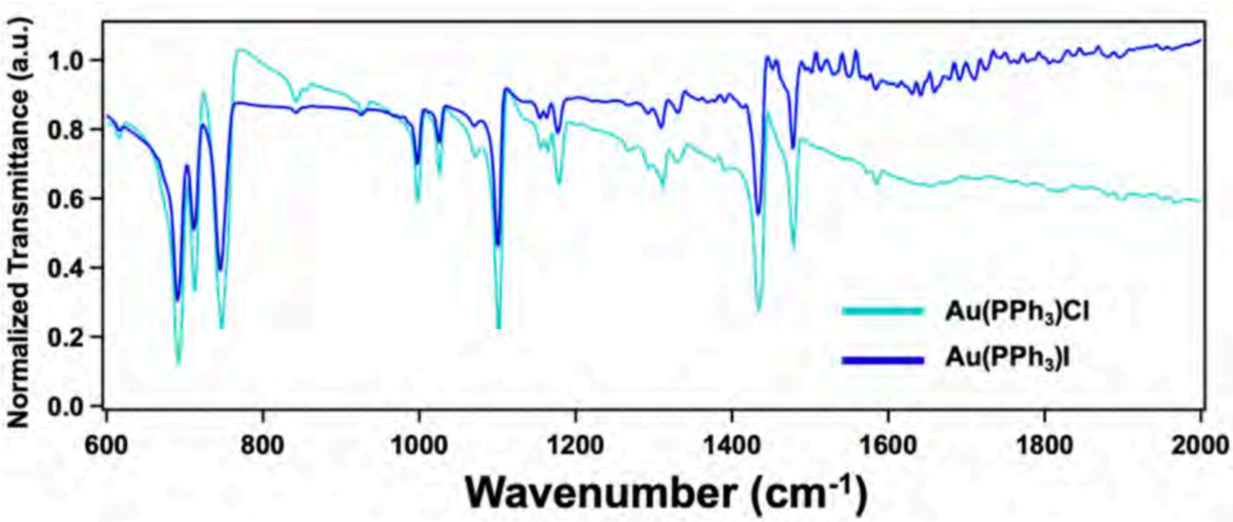

Figure A7. FTIR spectrum comparing the features in KBr pallet containing $Au(PPh_3)Cl$ and $Au(PPh_3)I$.

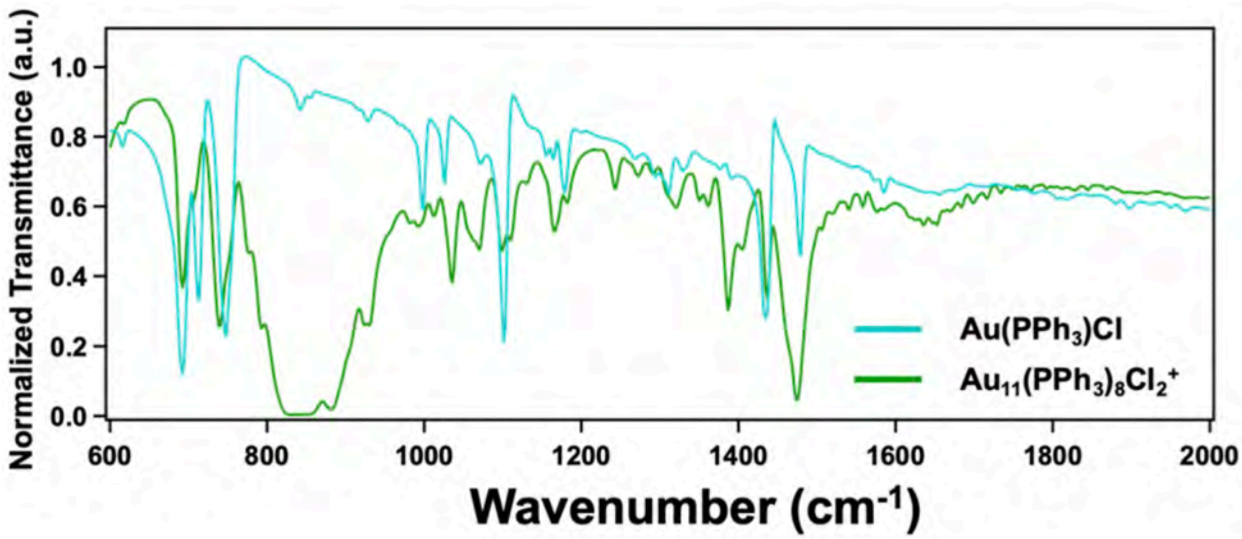

Figure A8. FTIR spectrum comparing the features in KBr pallet containing $Au(PPh_3)Cl$ and $Au_{11}(PPh_3)_8Cl_2^+$.

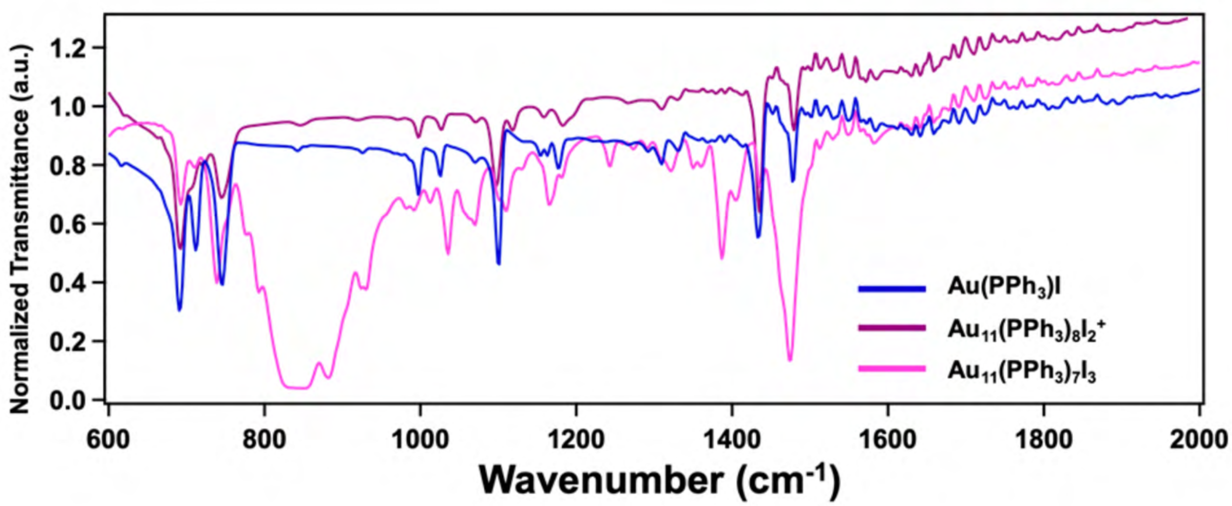

Figure A9. FTIR spectrum comparing the features in KBr pallet containing $Au(PPh_3)I$, $Au_{11}(PPh_3)_8I_2^+$, and $Au_{11}(PPh_3)_7I_3$.

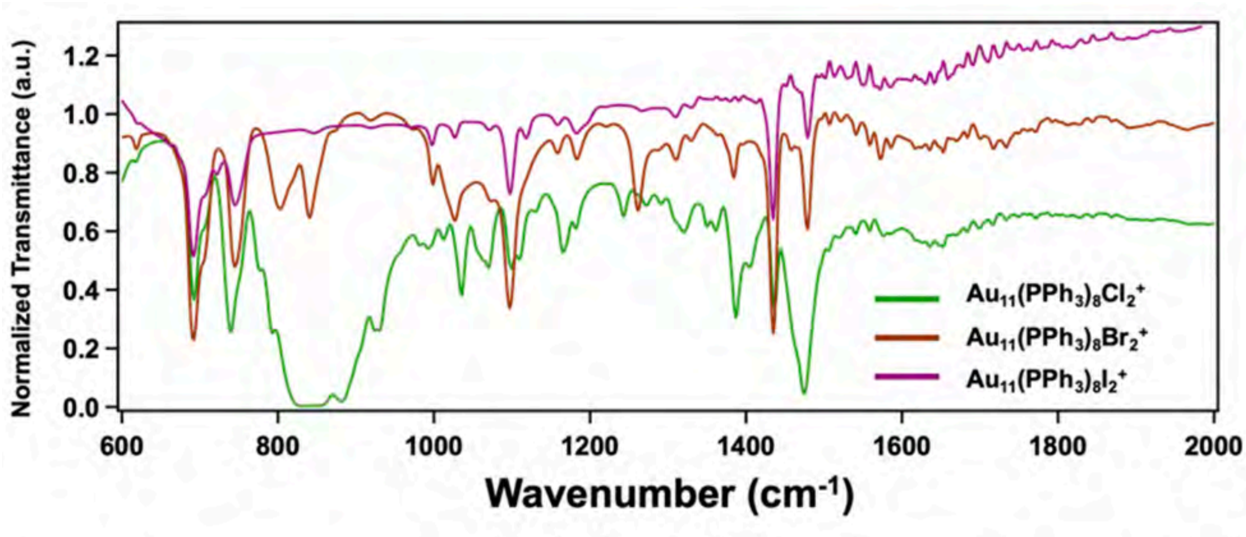

Figure A10. FTIR spectrum comparing the features in KBr pallet containing $Au_{11}(PPh_3)_8Cl_2^+$, $Au_{11}(PPh_3)_8Br_2^+$, and $Au_{11}(PPh_3)_8I_2^+$.

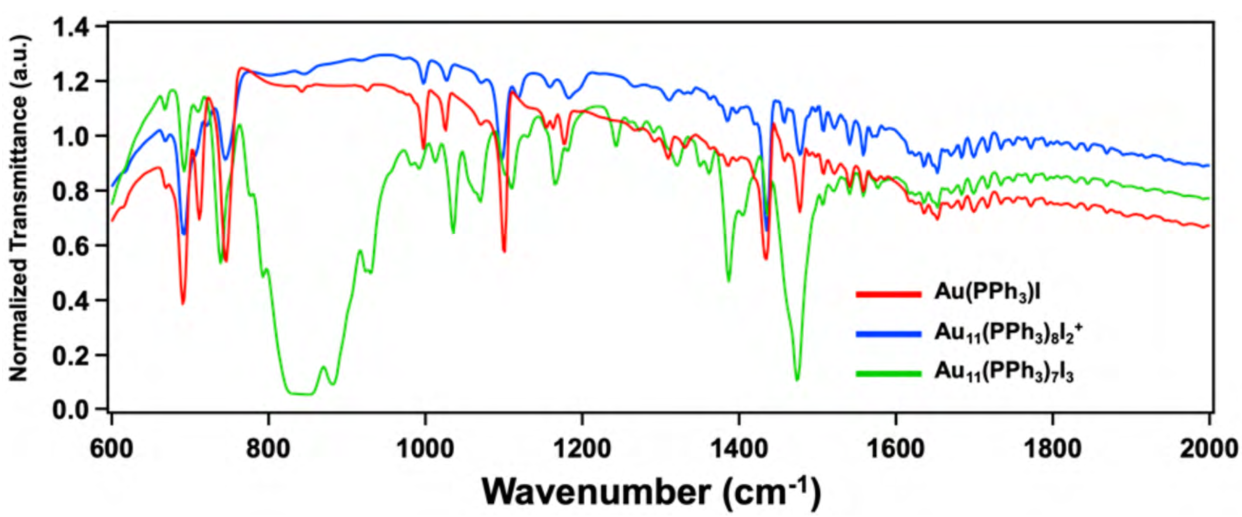

Figure A11. FTIR spectrum comparing the features in DCM solution containing $Au(PPh_3)I$, $Au_{11}(PPh_3)_8I_2^+$, and $Au_{11}(PPh_3)_7I_3$.

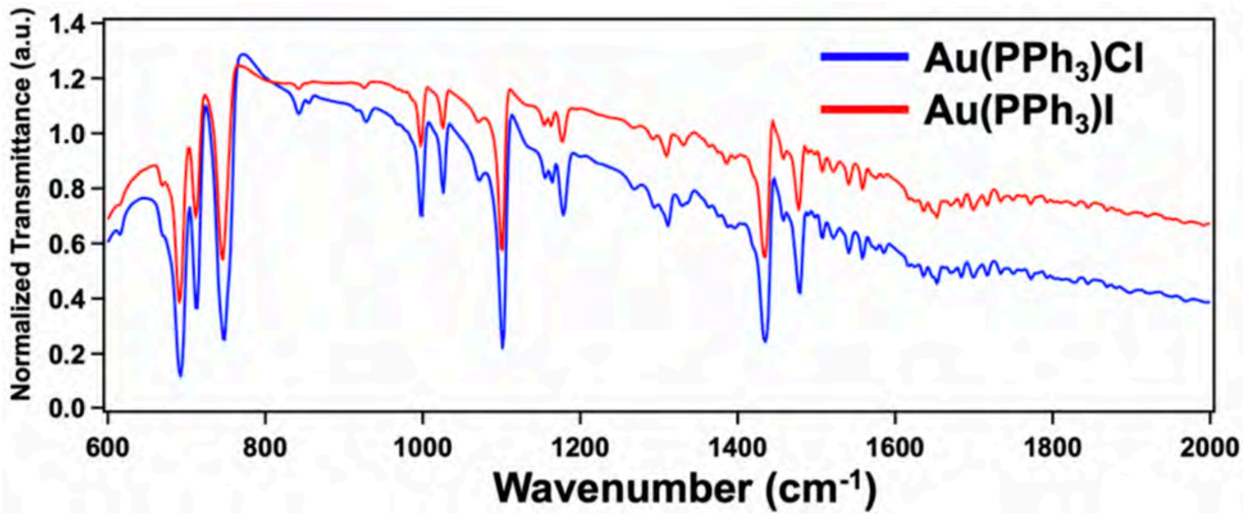

Figure A12. FTIR spectrum comparing the features in DCM solution containing $Au(PPh_3)Cl$ and $Au(PPh_3)I$.

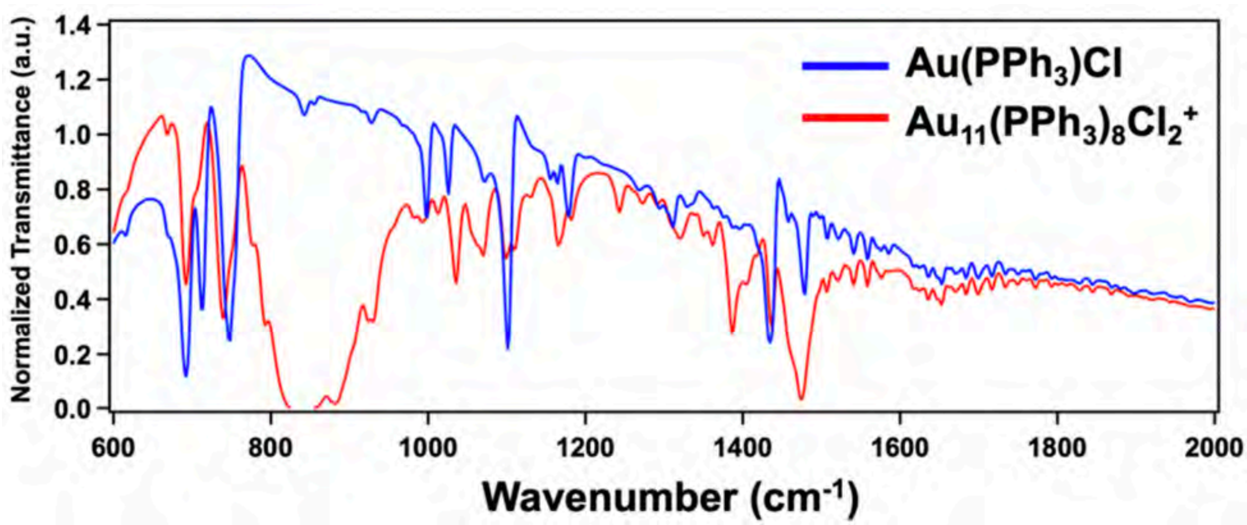

Figure A13. FTIR spectrum comparing the features in DCM solution containing $Au(PPh_3)Cl$ and $Au_{11}(PPh_3)_8Cl_2^+$.

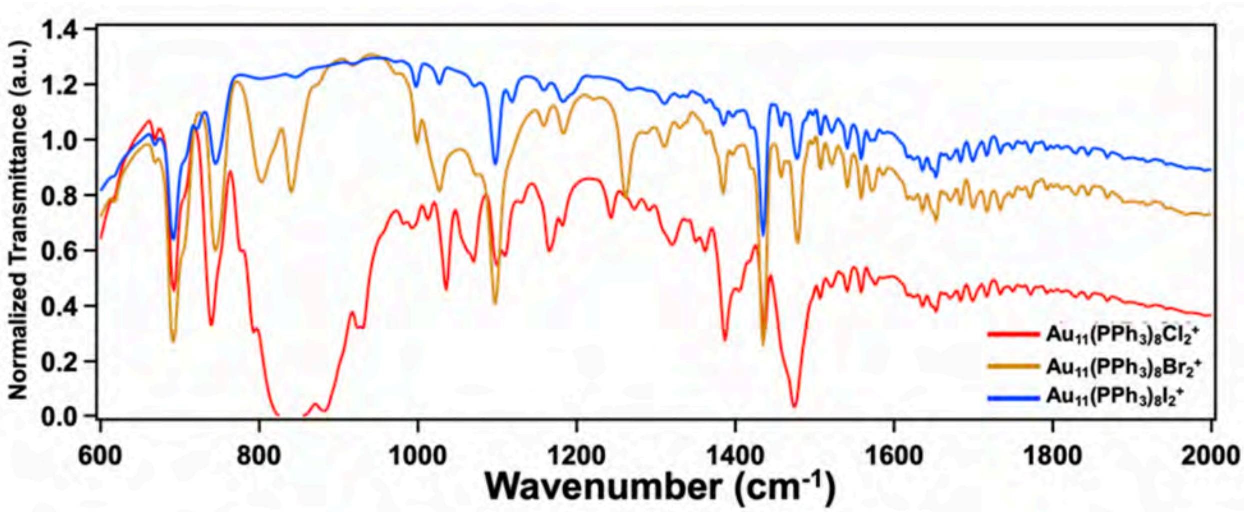

Figure A14. FTIR spectrum comparing the features in DCM solution containing $Au_{11}(PPh_3)_8Cl_2^+$, $Au_{11}(PPh_3)_8Br_2^+$, and $Au_{11}(PPh_3)_8I_2^+$.

Following **Figure**s are comparing Raman features among the Au(I) precursors and AuNCs. Lower Raman shift range contains many features resulting from metal to organic (M-S, M-P) and metal to halogen (M-X) vibrations.

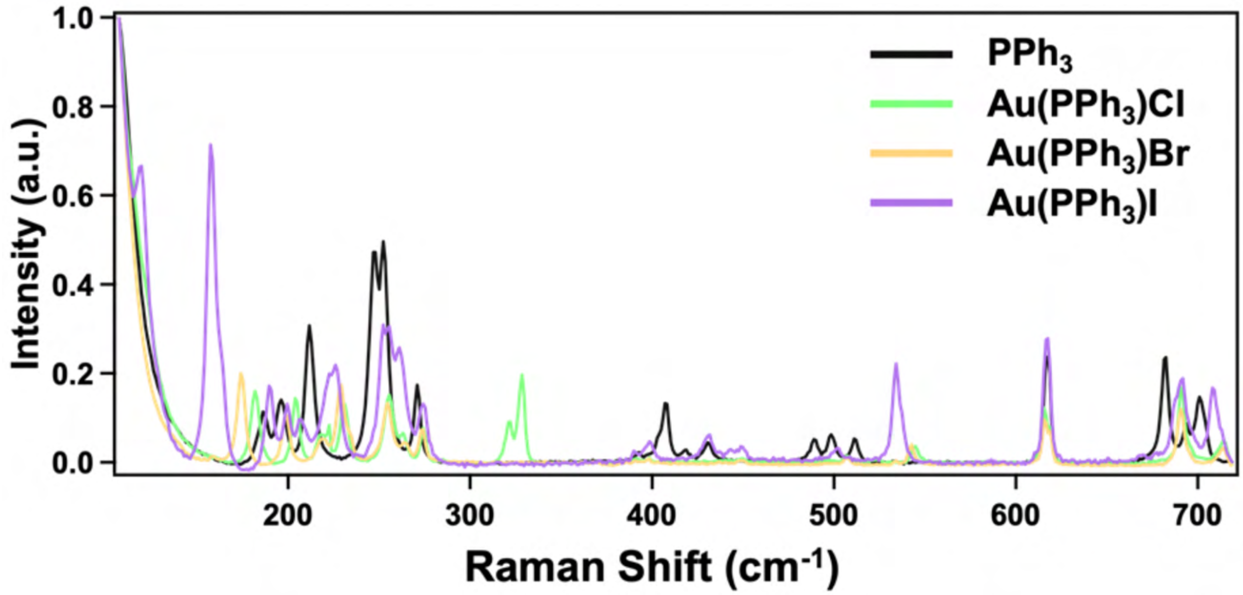

Figure A15. Raman spectra of PPh_3 and $Au(PPh_3)X$ (X = Cl, Br, I) at low Raman shifts.

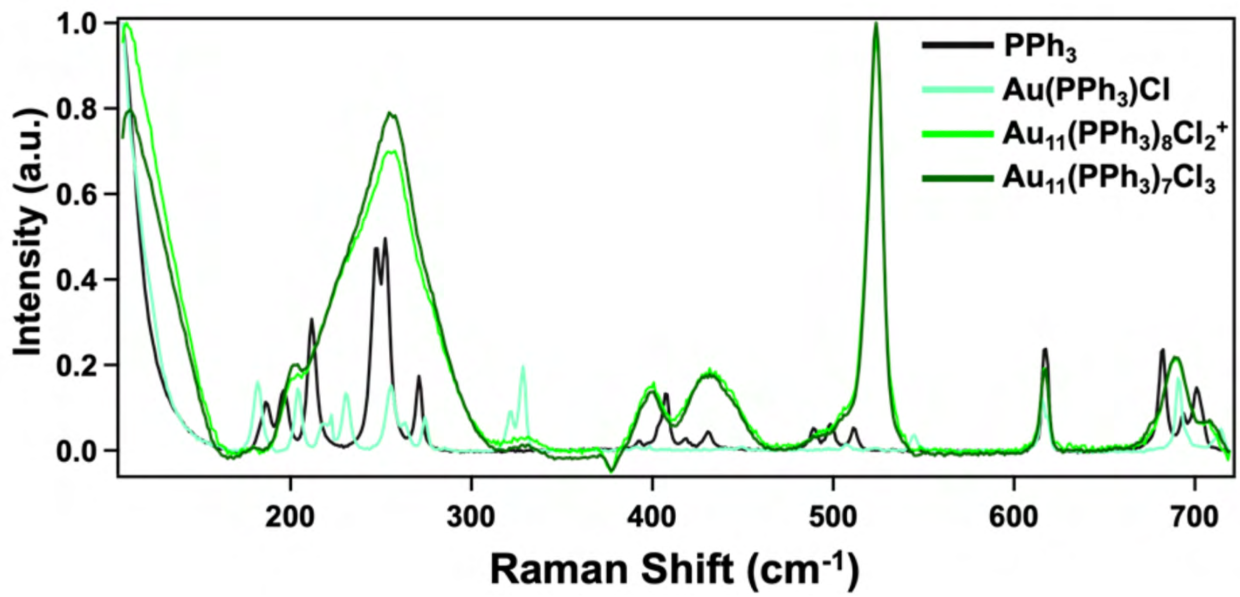

Figure A16. Raman spectra of PPh_3, $Au(PPh_3)Cl$, $Au_{11}(PPh_3)_8Cl_2^+$, and $Au_{11}(PPh_3)_7Cl_3$ at low Raman shifts.

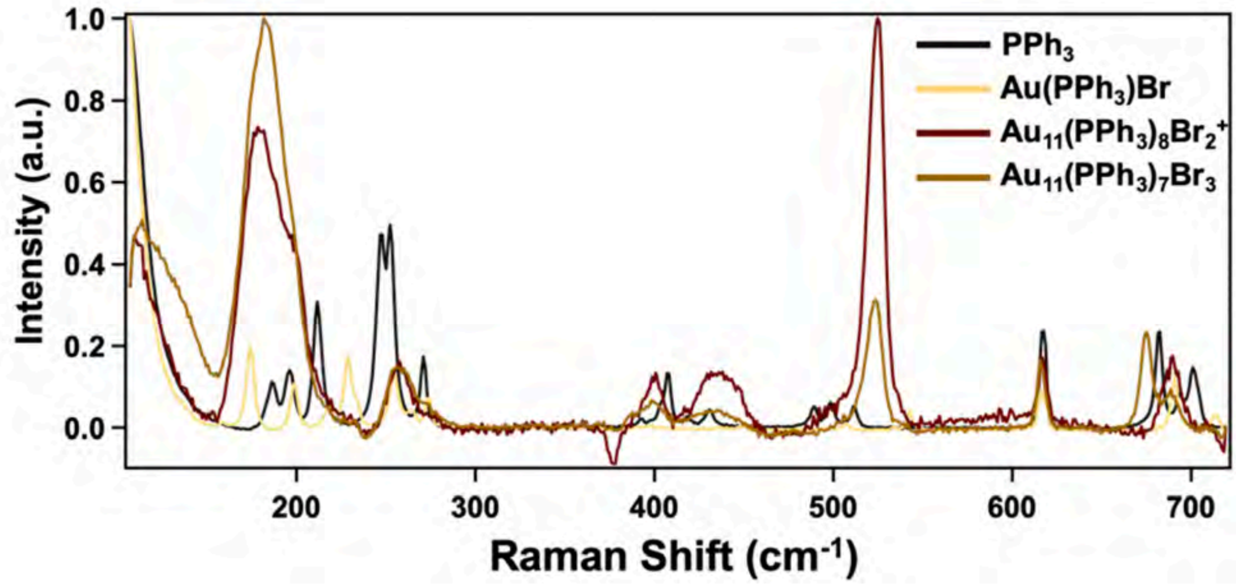

Figure A17. Raman spectra of PPh_3, $Au(PPh_3)Br$, $Au_{11}(PPh_3)_8Br_2^+$, and $Au_{11}(PPh_3)_7Br_3$ at low Raman shifts.

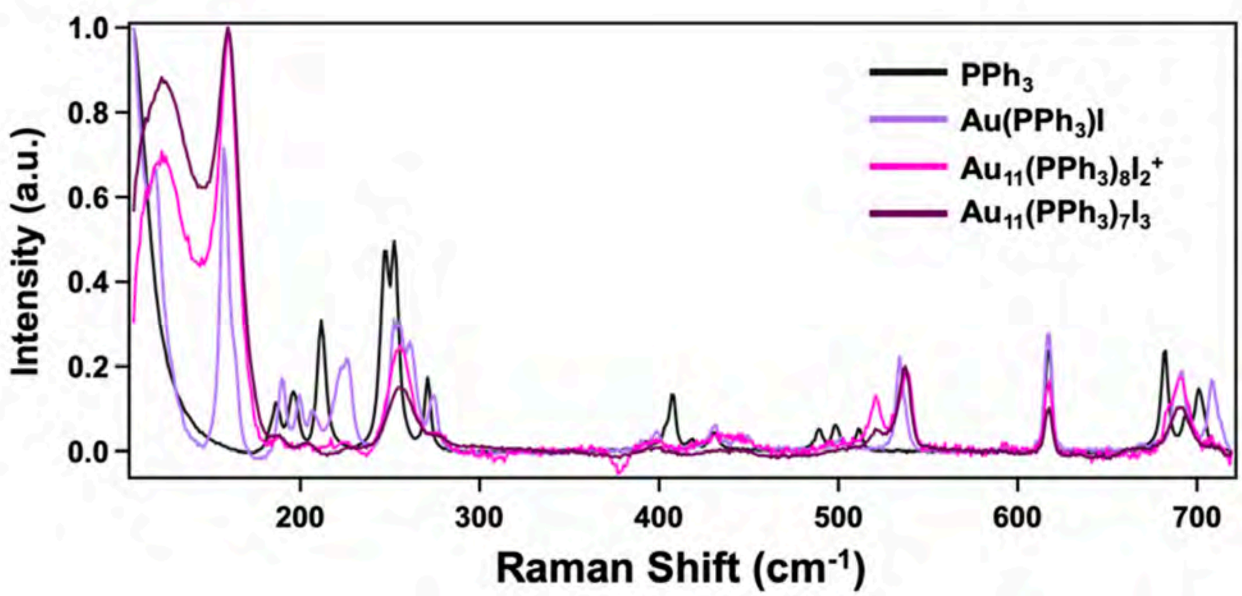

Figure A18. Raman spectra of PPh_3, $Au(PPh_3)I$, $Au_{11}(PPh_3)_8I_2^+$, and $Au_{11}(PPh_3)_7I_3$ at low Raman shifts.

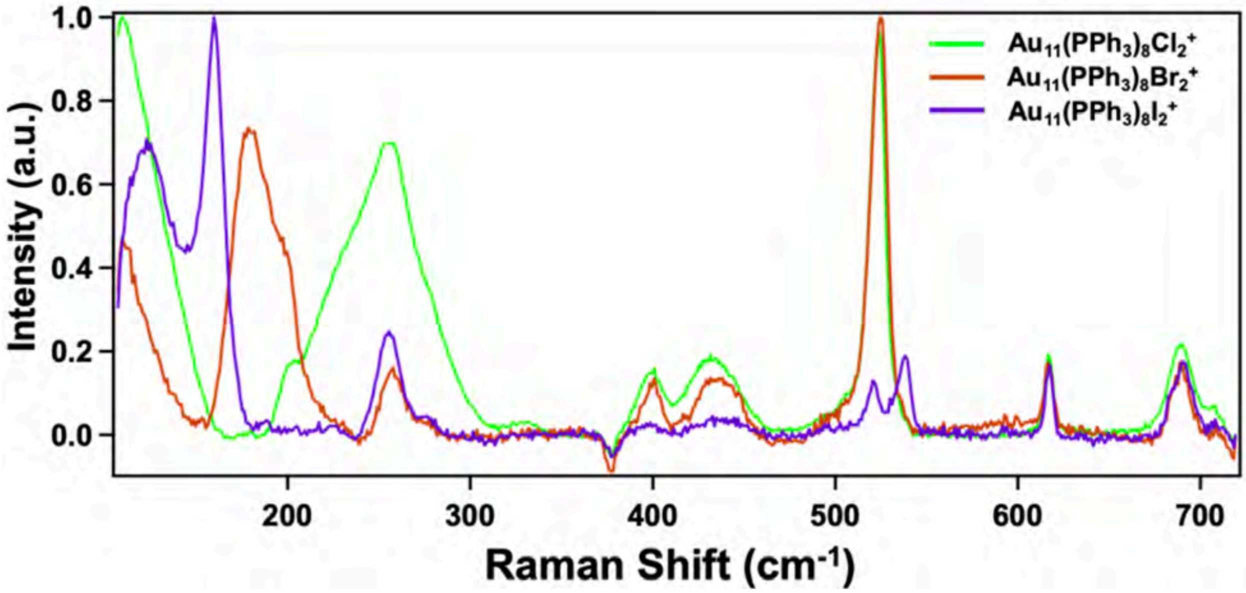

Figure A19. Raman spectra directly comparing the features of $Au_{11}(PPh_3)_8X_2^+$ (X = Cl, Br, I) in low Raman shifts.

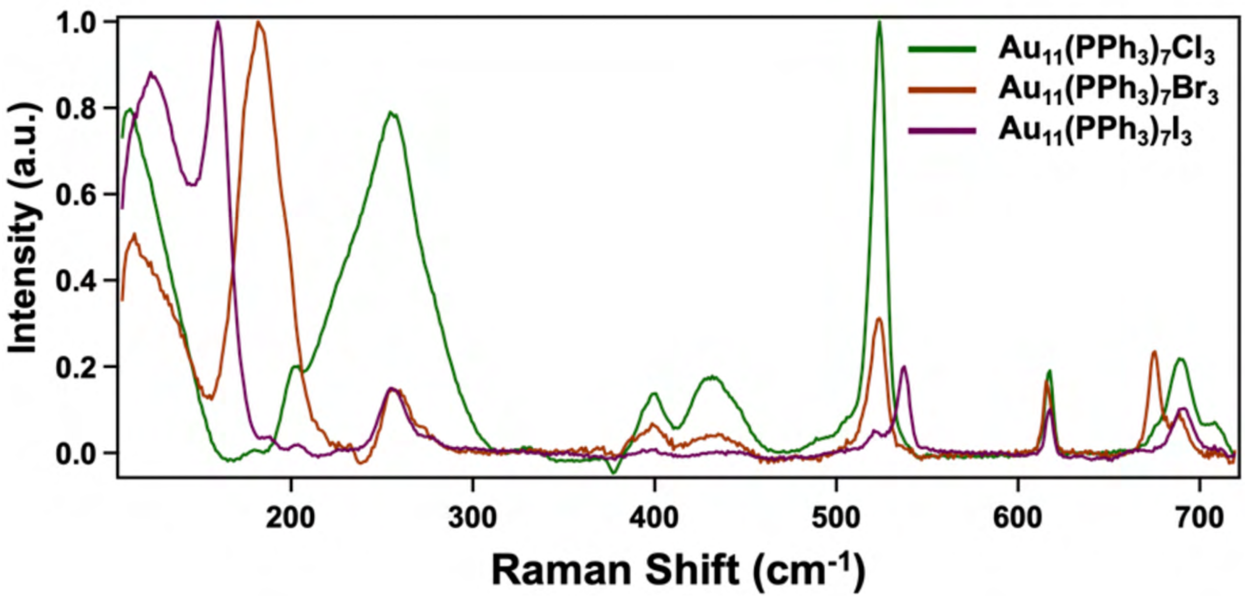

Figure A20. Raman spectra directly comparing the features of $Au_{11}(PPh_3)_7X_3$ (X = Cl, Br, I) in low Raman shifts.

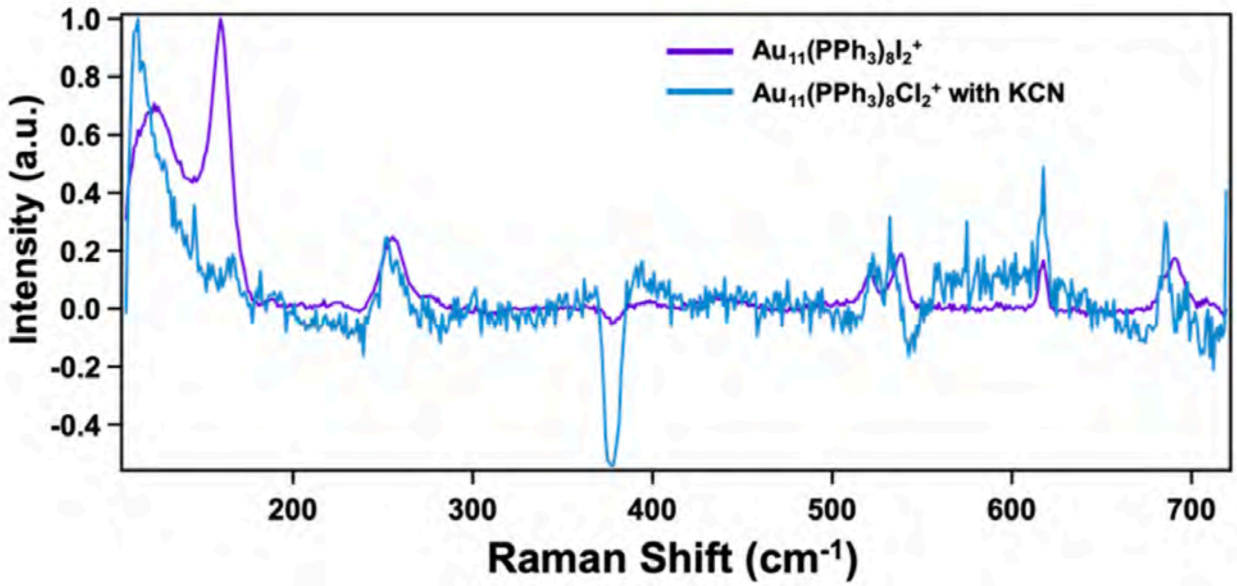

Figure A21. Raman spectra directly comparing the features between $Au_{11}(PPh_3)_8I_2^+$ and $Au_{11}(PPh_3)_8Cl_2^+$ with KCN in low Raman shifts.

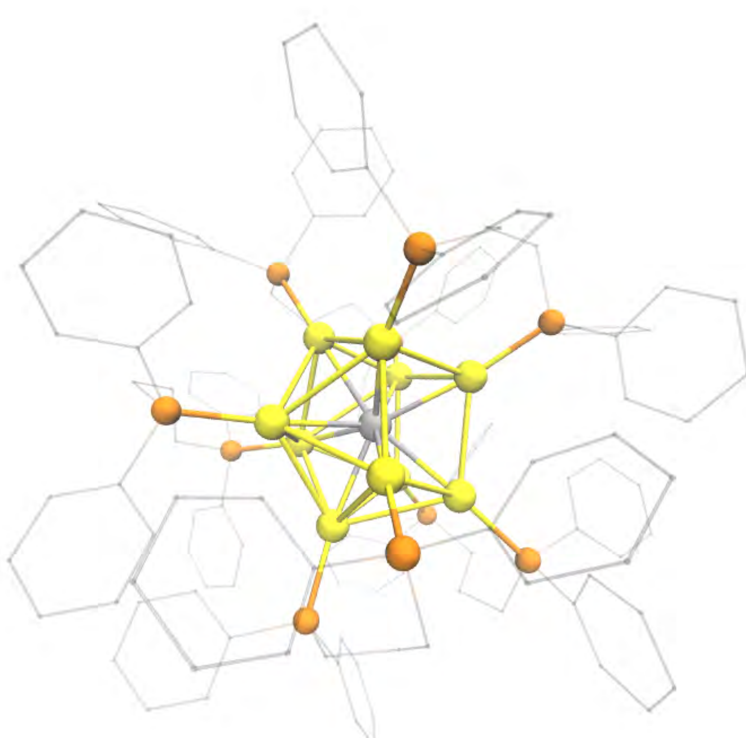

Figure A22. Fully optimized geometries of $PtAu_{10}(dppp)_5^{2+}$. The $PtAu_{10}$NC structure was based off of previously reported structure, which has much difficulty in syntheses.[81] However, this new alloy cluster can provide very important insight to the influences of the core metal in small metallic clusters.

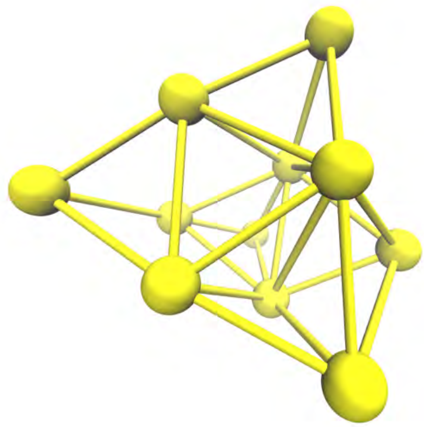

Figure A23. Fully optimized geometries of Au_{11}^{3+}. Due to the large change in the geometries of fully relaxed structure of Au_{11}^{3+} compared to the gold core in $Au_{11}(PPh_3)_8X_2^+$ or $Au_{11}(PPh_3)_7X_3$, several calculations regarding the electronic structure of the gold core was done using single point calculations.

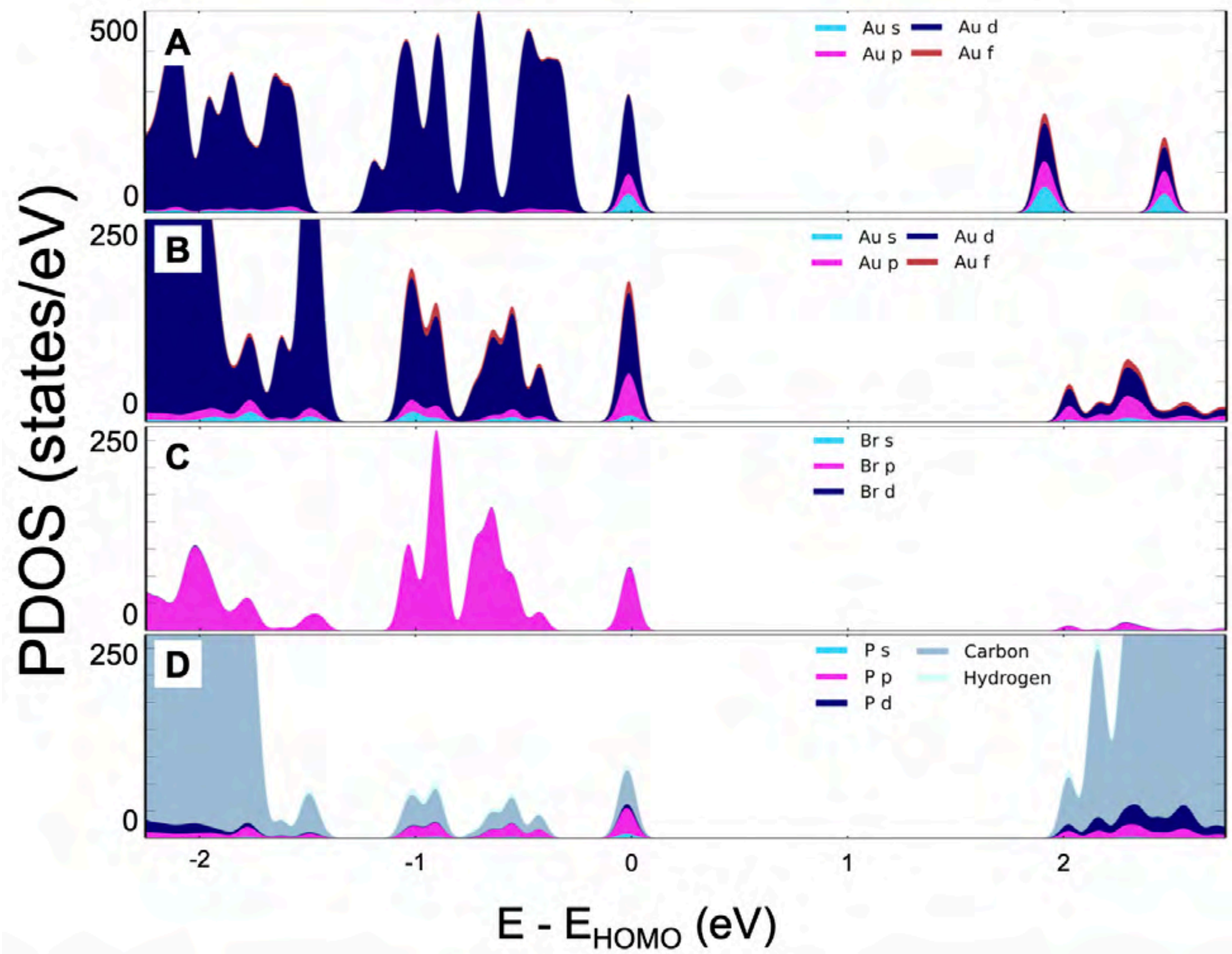

Figure A24. Orbital angular momentum PDOS of A) gold in Au_{11}^{3+}, B) gold, C) Br, and D) organic elements of PPh_3 in $Au_{11}(PPh_3)_7Br_3$. The PDOS of bare Au_{11}NCs with the same core geometry as $Au_{11}(PPh_3)_8Br_3$ is modelled in A) for comparison. Unlike the rest of the elements, the orbital angular momentums of carbon and hydrogen were combined.

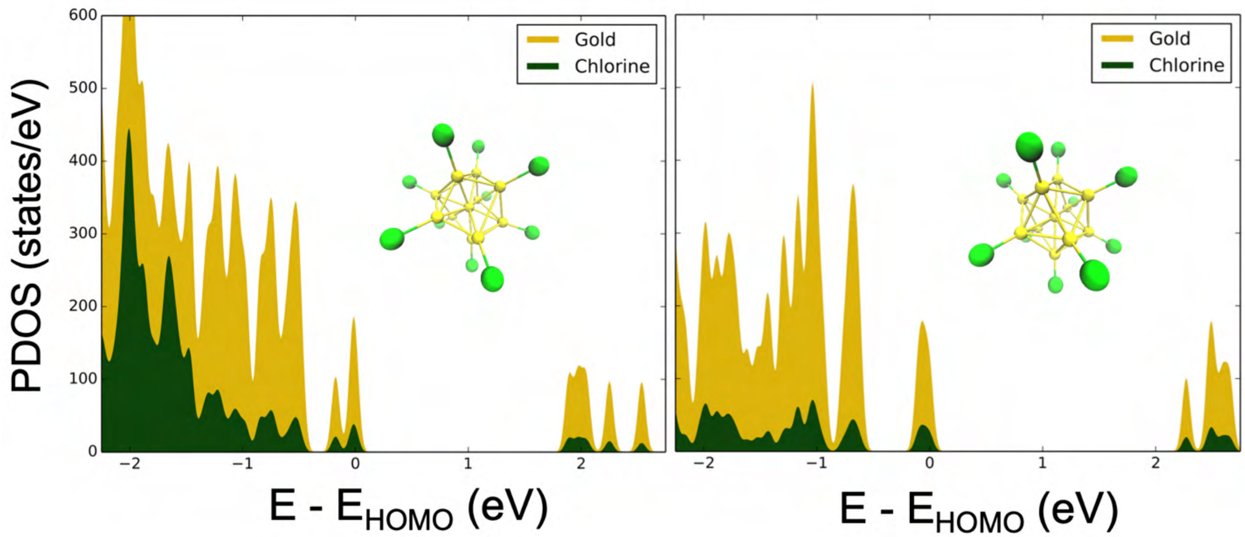

Figure A25. PDOS of theoretical compound $Au_{11}Cl_{10}^{7-}$ by substituting phosphine ligands with chlorine on the geometrically optimized $Au_{11}(PPh_3)_8Cl_2^+$ (left) and $Au_{11}(PPh_3)_7Cl_3$ (right). The insets depict the structural differences among the two compounds. With higher symmetry in the core, $Au_{11}Cl_{10}^{7-}$ derived from $Au_{11}(PPh_3)_7Cl_3$ shows features indicating much stable energy levels such as broadening of HOMO-LUMO gap.

Following **Figures** describe KS orbitals of each Au(I) precursors and AuNCs at different energy levels near their frontier orbitals. They are labeled with orbital numbers as computer output printed out. However, different orbital number could still be close enough in energy to be considered degenerate orbitals.

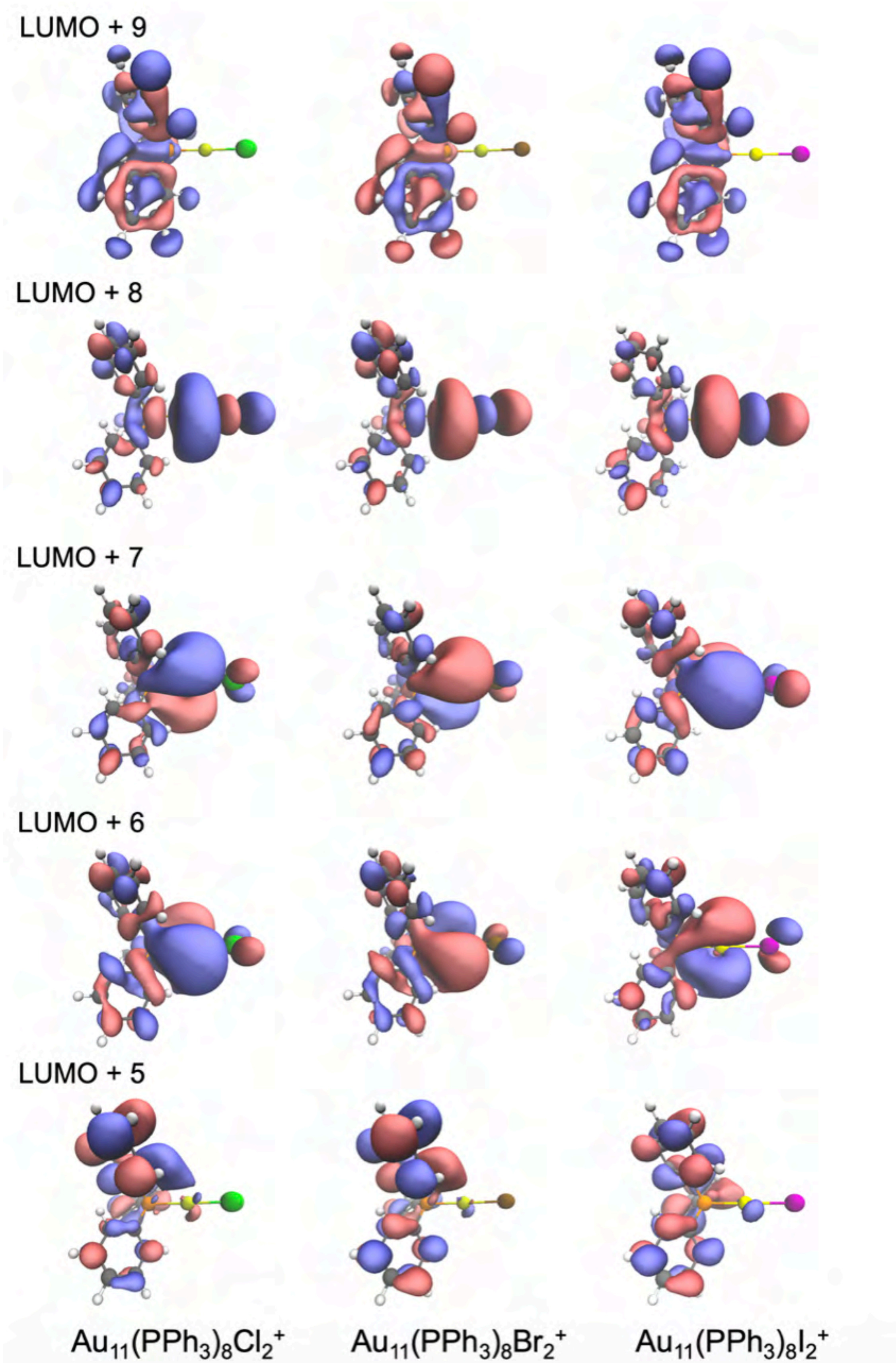

LUMO + 9
LUMO + 8
LUMO + 7
LUMO + 6
LUMO + 5
$Au_{11}(PPh_3)_8Cl_2^+$
$Au_{11}(PPh_3)_8Br_2^+$
$Au_{11}(PPh_3)_8I_2^+$

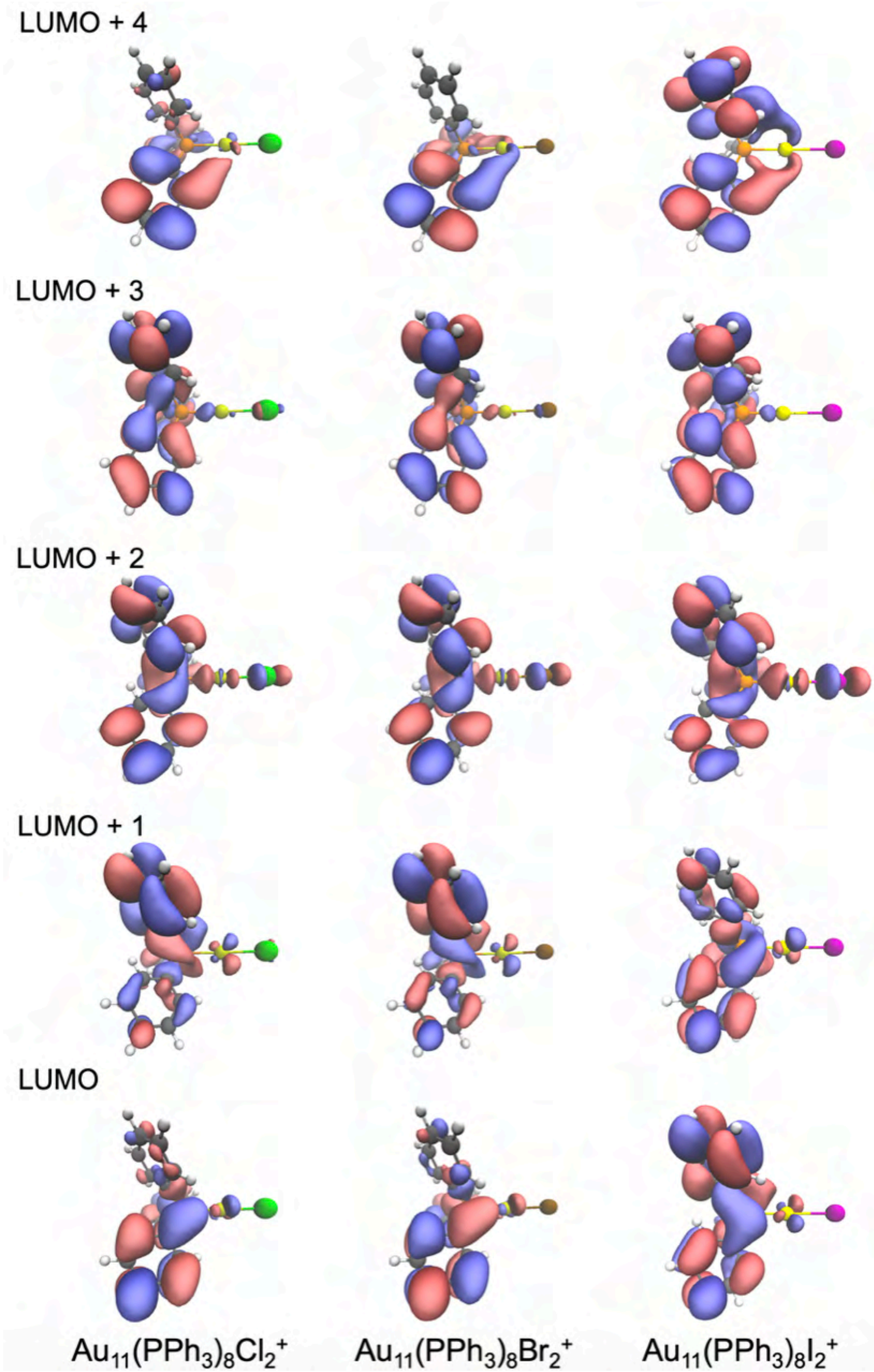
LUMO + 4
LUMO + 3
LUMO + 2
LUMO + 1
LUMO
$Au_{11}(PPh_3)_8Cl_2^+$
$Au_{11}(PPh_3)_8Br_2^+$
$Au_{11}(PPh_3)_8I_2^+$

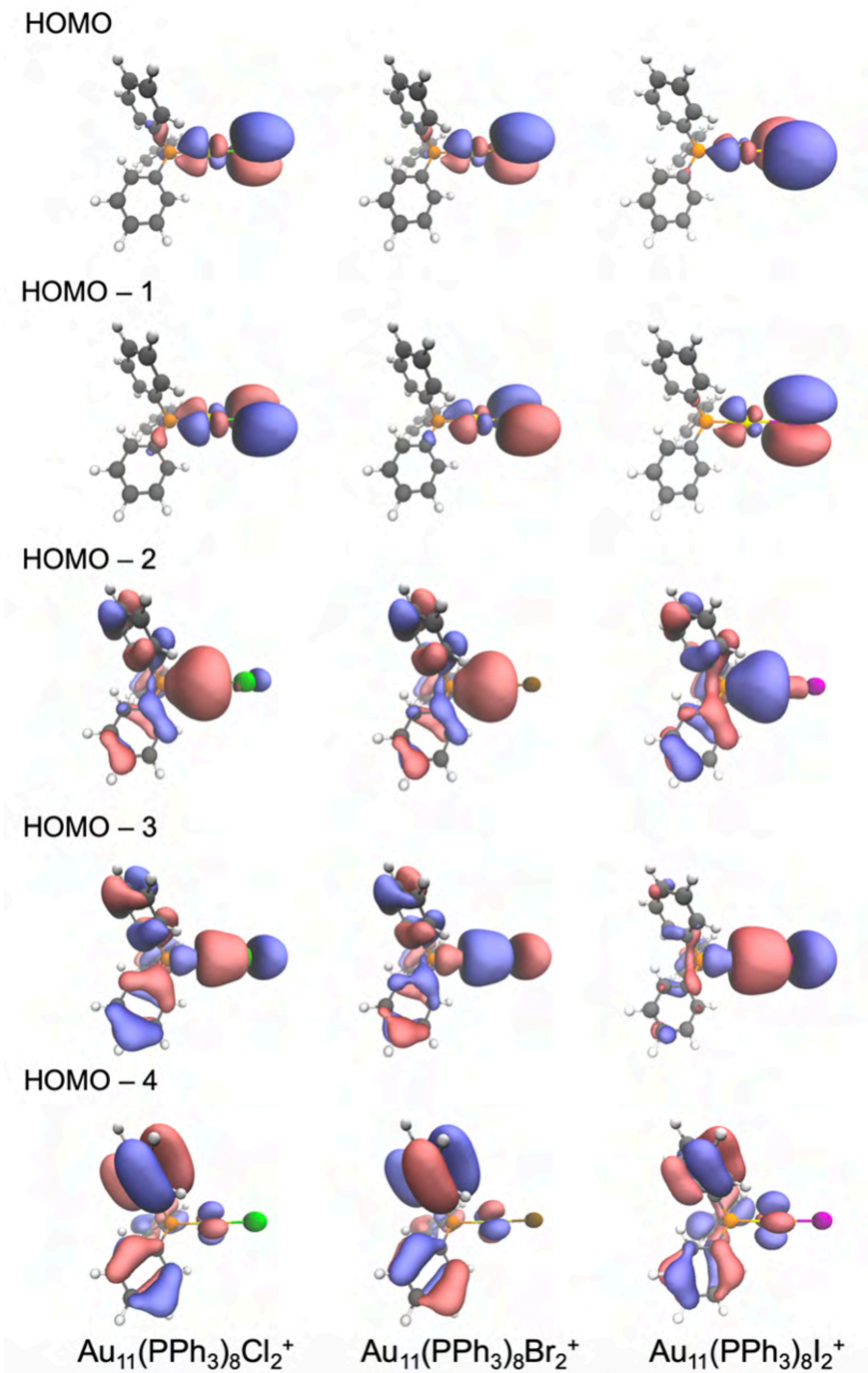
HOMO
HOMO – 1
HOMO – 2
HOMO – 3
HOMO – 4
$Au_{11}(PPh_3)_8Cl_2^+$
$Au_{11}(PPh_3)_8Br_2^+$
$Au_{11}(PPh_3)_8I_2^+$

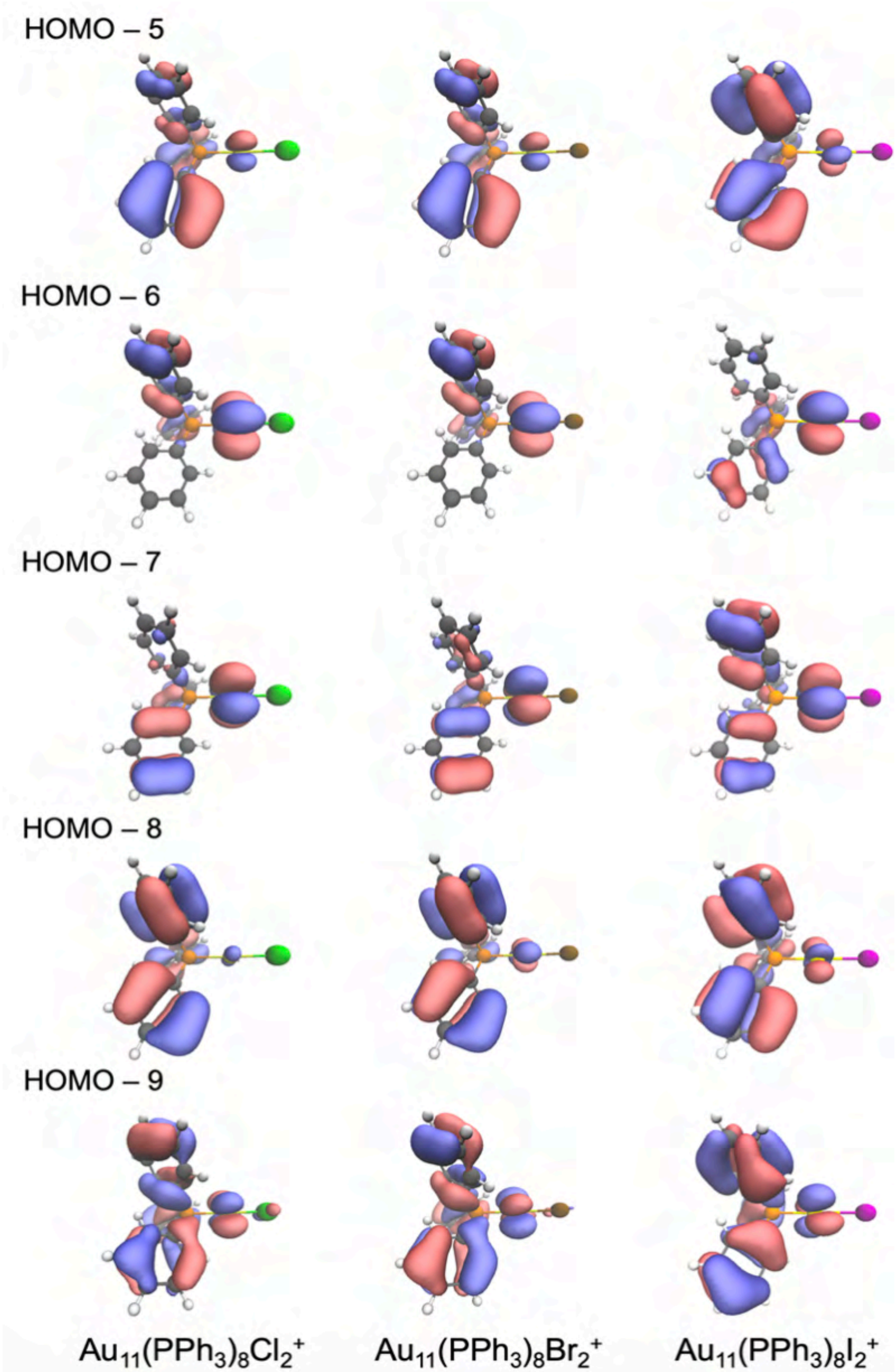

Figure A26. KS orbitals of $Au_{11}(PPh_3)_8X_2^+$ near the frontier orbitals.

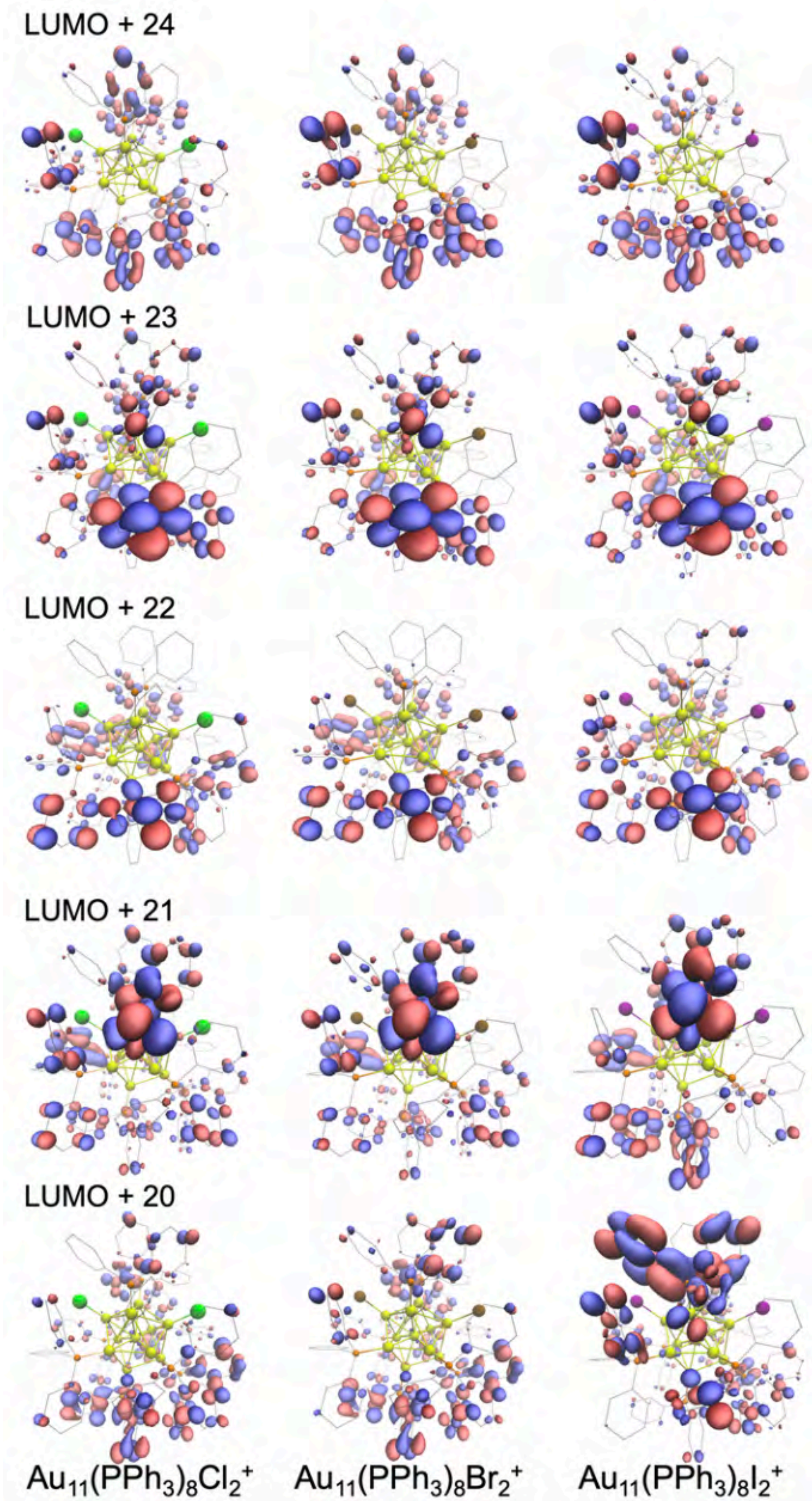

LUMO + 24
LUMO + 23
LUMO + 22
LUMO + 21
LUMO + 20
$Au_{11}(PPh_3)_8Cl_2^+$
$Au_{11}(PPh_3)_8Br_2^+$
$Au_{11}(PPh_3)_8I_2^+$

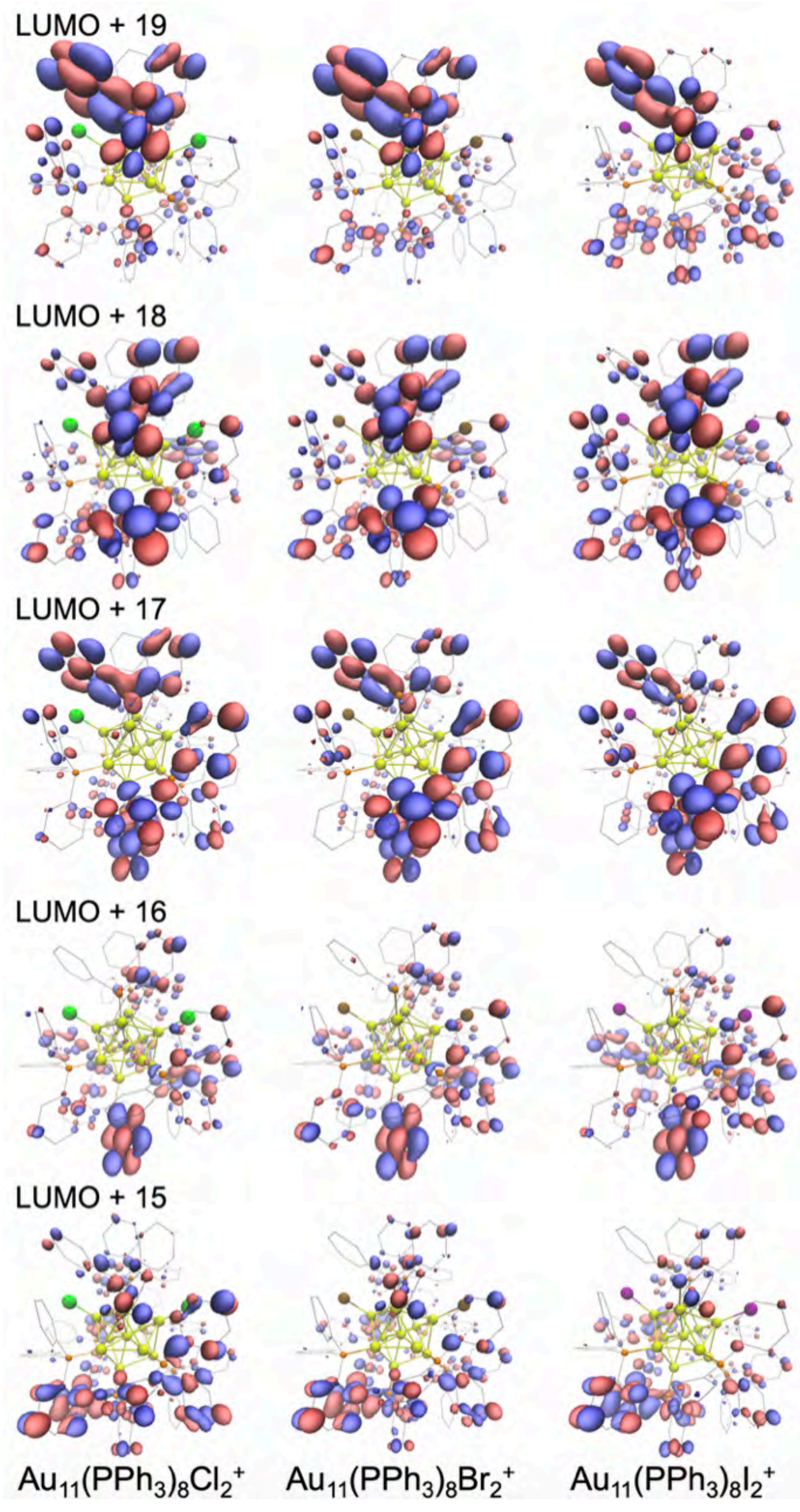
LUMO + 19
LUMO + 18
LUMO + 17
LUMO + 16
LUMO + 15
$Au_{11}(PPh_3)_8Cl_2^+$
$Au_{11}(PPh_3)_8Br_2^+$
$Au_{11}(PPh_3)_8I_2^+$

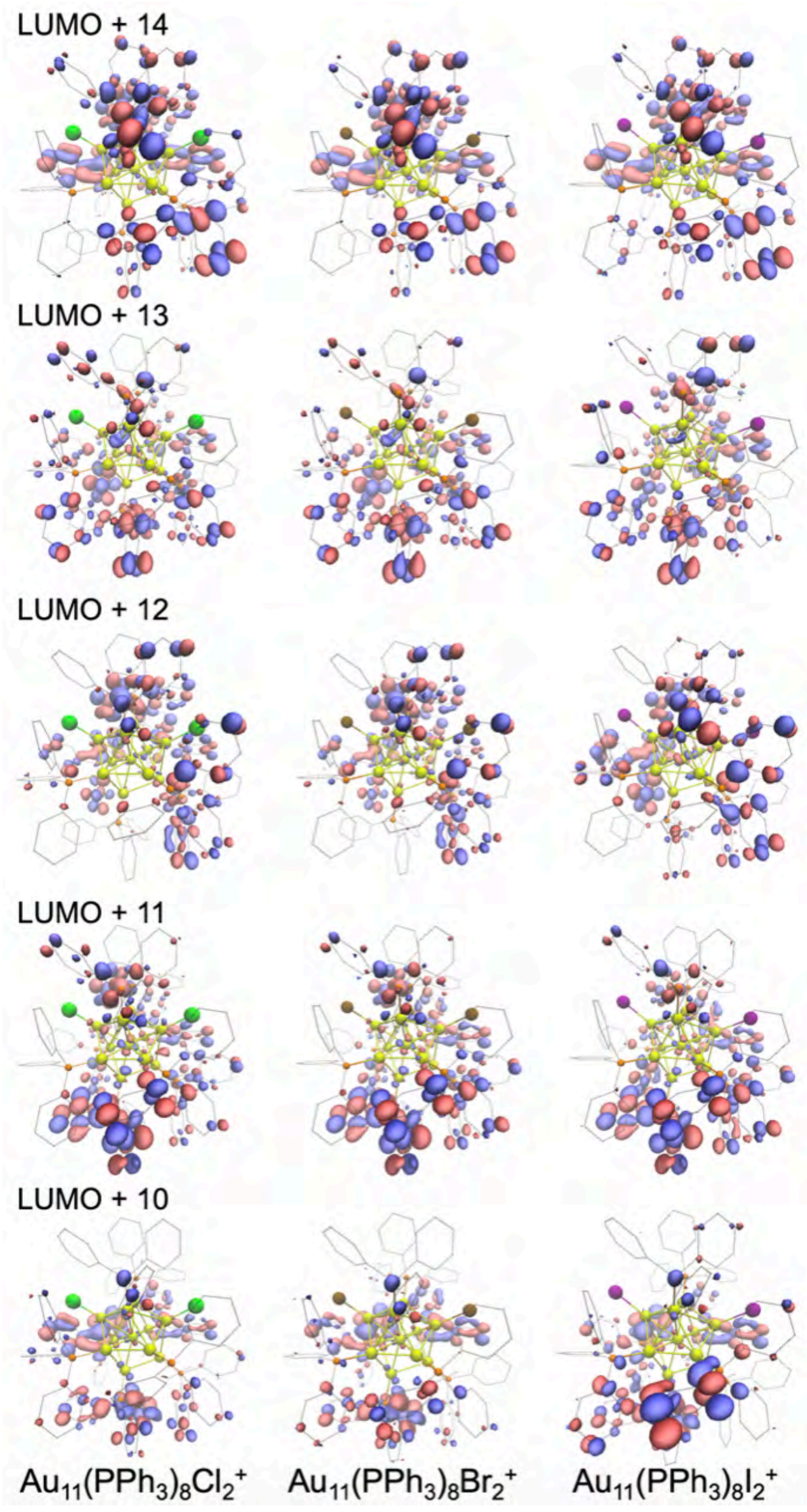
LUMO + 14
LUMO + 13
LUMO + 12
LUMO + 11
LUMO + 10
$Au_{11}(PPh_3)_8Cl_2^+$
$Au_{11}(PPh_3)_8Br_2^+$
$Au_{11}(PPh_3)_8I_2^+$

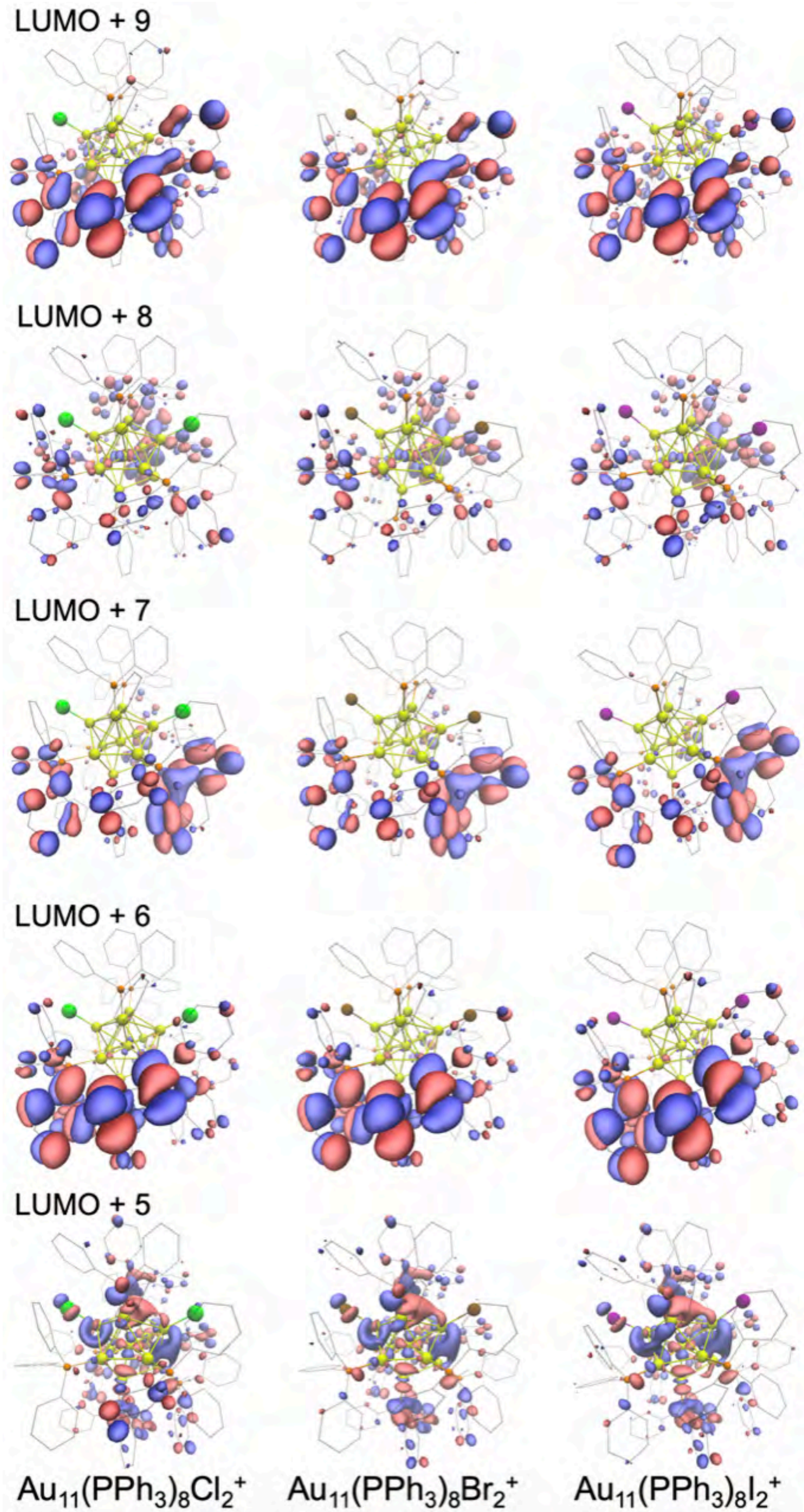
LUMO + 9
LUMO + 8
LUMO + 7
LUMO + 6
LUMO + 5
$Au_{11}(PPh_3)_8Cl_2^+$
$Au_{11}(PPh_3)_8Br_2^+$
$Au_{11}(PPh_3)_8I_2^+$

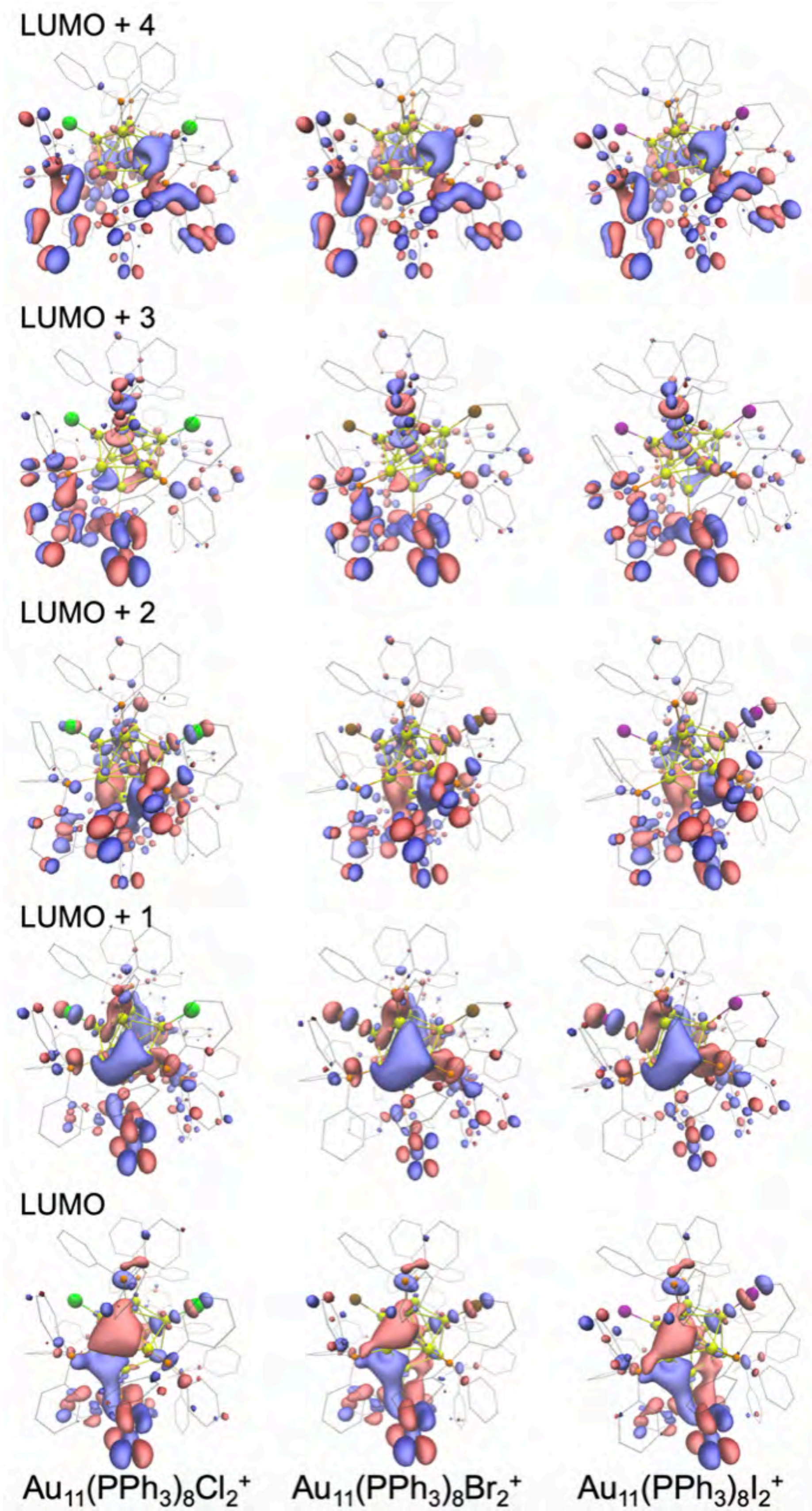
LUMO + 4
LUMO + 3
LUMO + 2
LUMO + 1
LUMO
$Au_{11}(PPh_3)_8Cl_2^+$
$Au_{11}(PPh_3)_8Br_2^+$
$Au_{11}(PPh_3)_8I_2^+$

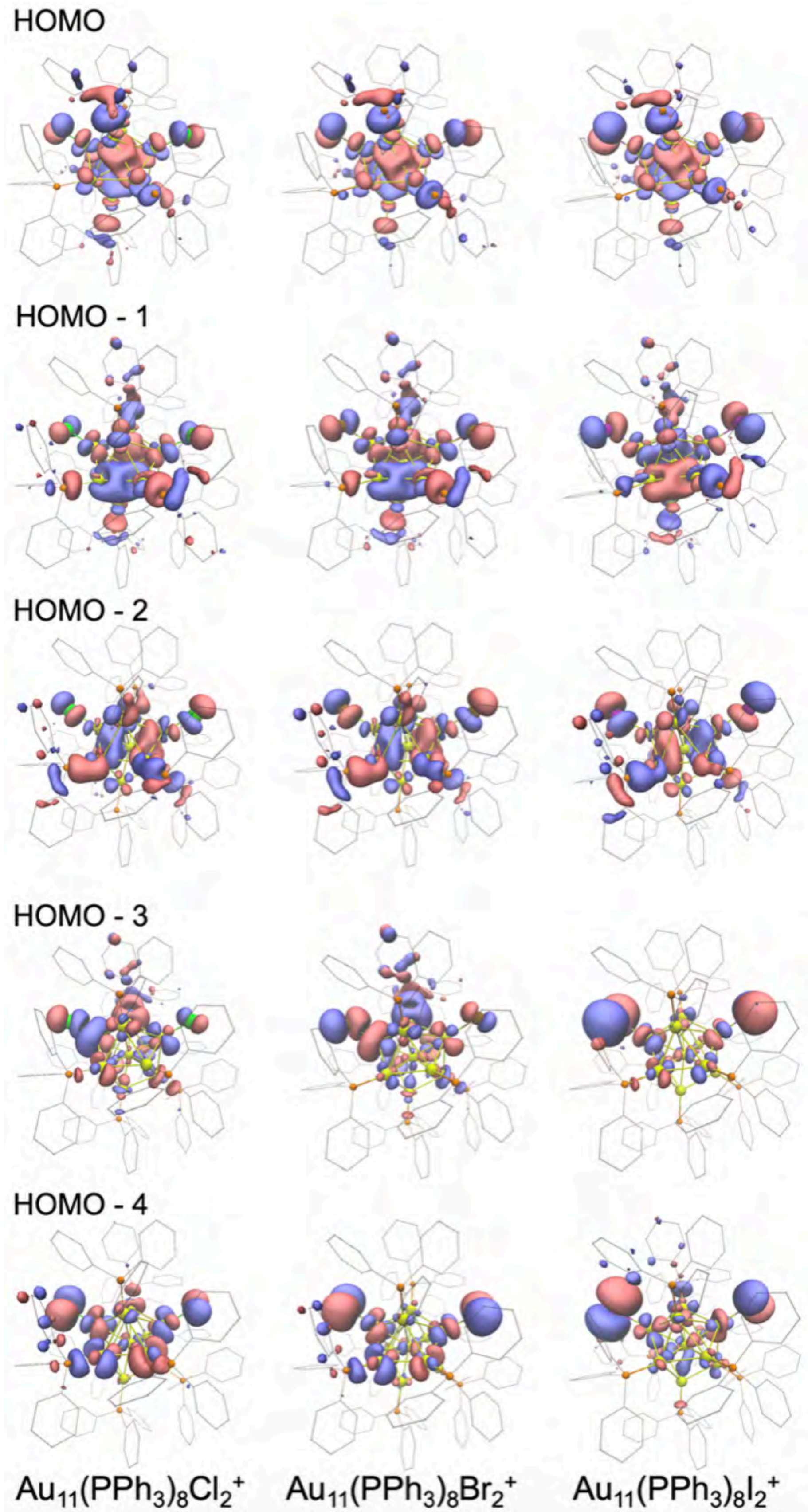
HOMO
HOMO - 1
HOMO - 2
HOMO - 3
HOMO - 4
$Au_{11}(PPh_3)_8Cl_2^+$
$Au_{11}(PPh_3)_8Br_2^+$
$Au_{11}(PPh_3)_8I_2^+$

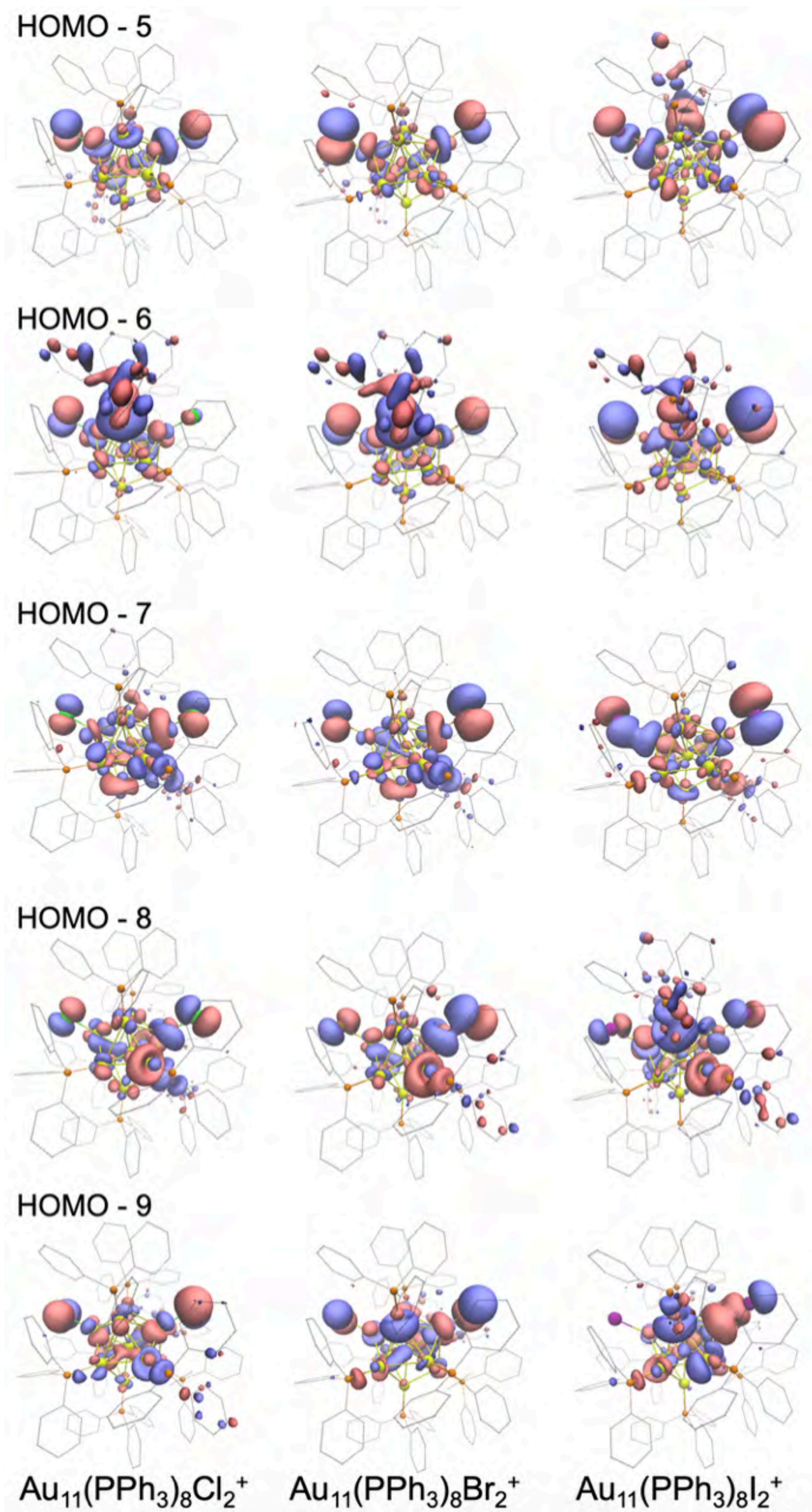
HOMO - 5
HOMO - 6
HOMO - 7
HOMO - 8
HOMO - 9
$Au_{11}(PPh_3)_8Cl_2^+$
$Au_{11}(PPh_3)_8Br_2^+$
$Au_{11}(PPh_3)_8I_2^+$

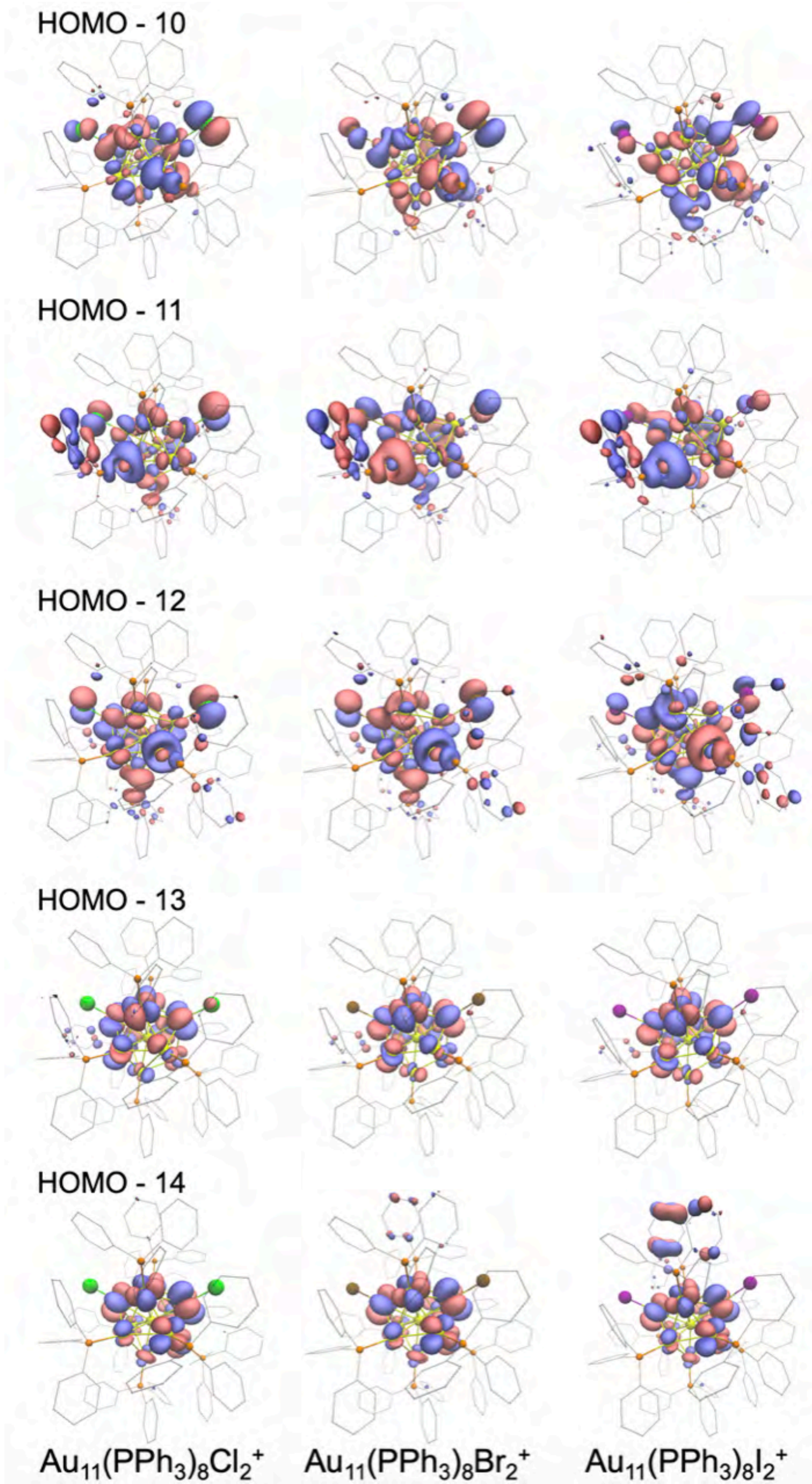
HOMO - 10
HOMO - 11
HOMO - 12
HOMO - 13
HOMO - 14
$Au_{11}(PPh_3)_8Cl_2^+$
$Au_{11}(PPh_3)_8Br_2^+$
$Au_{11}(PPh_3)_8I_2^+$

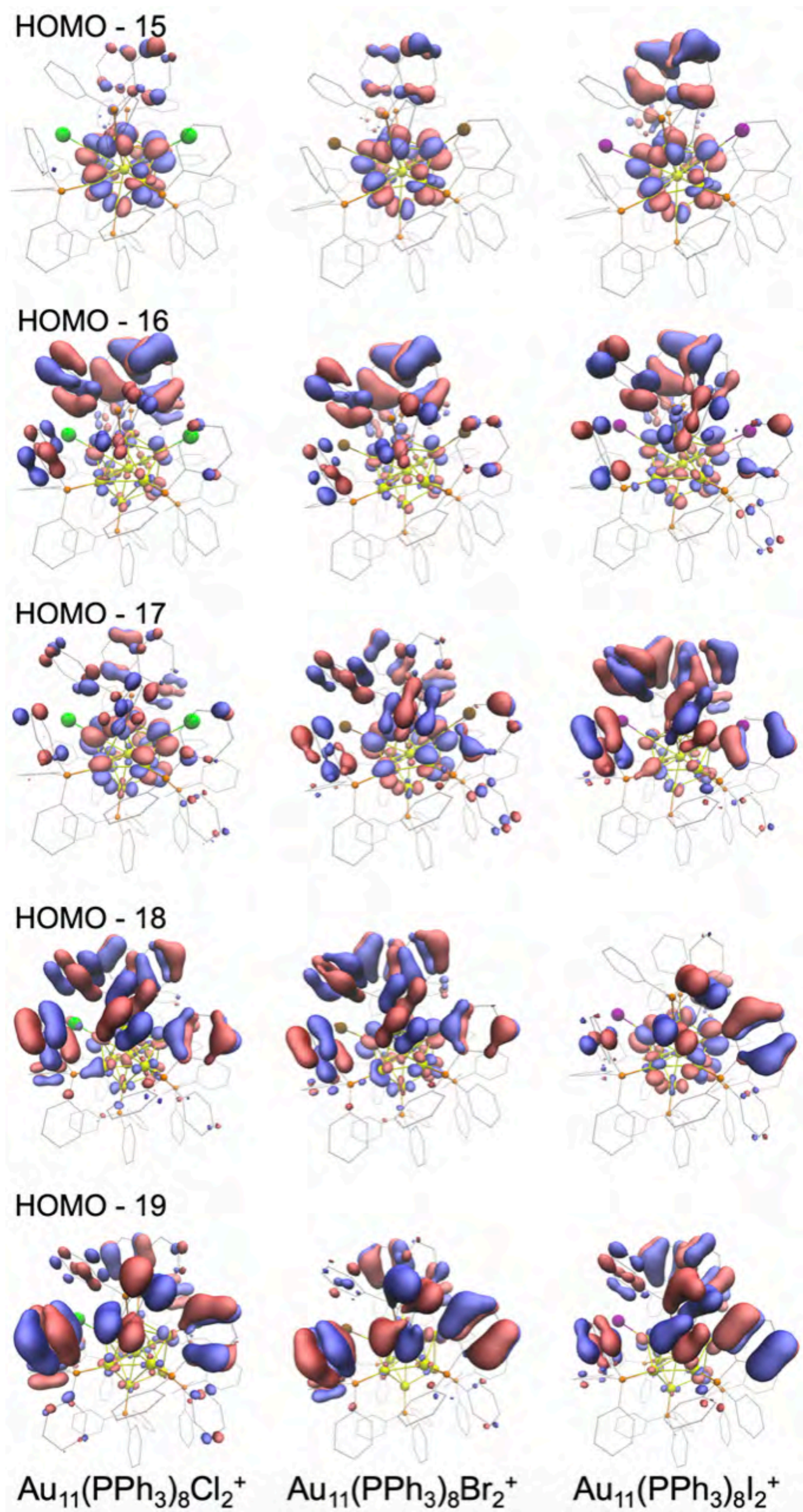
HOMO - 15
HOMO - 16
HOMO - 17
HOMO - 18
HOMO - 19
$Au_{11}(PPh_3)_8Cl_2^+$
$Au_{11}(PPh_3)_8Br_2^+$
$Au_{11}(PPh_3)_8I_2^+$

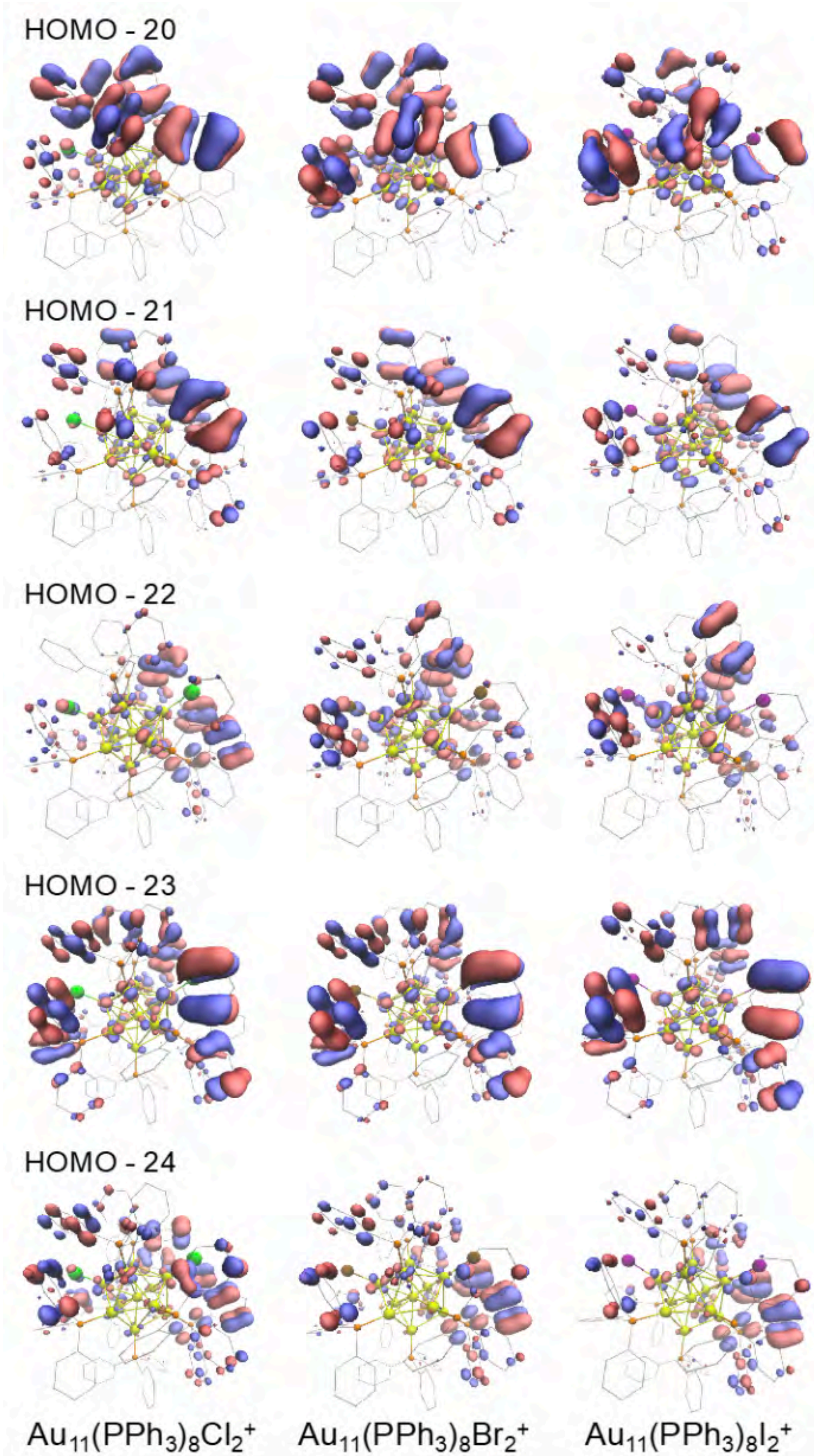

Figure A27. KS orbitals of $Au_{11}(PPh_3)_8X_2^+$ near the frontier orbitals.

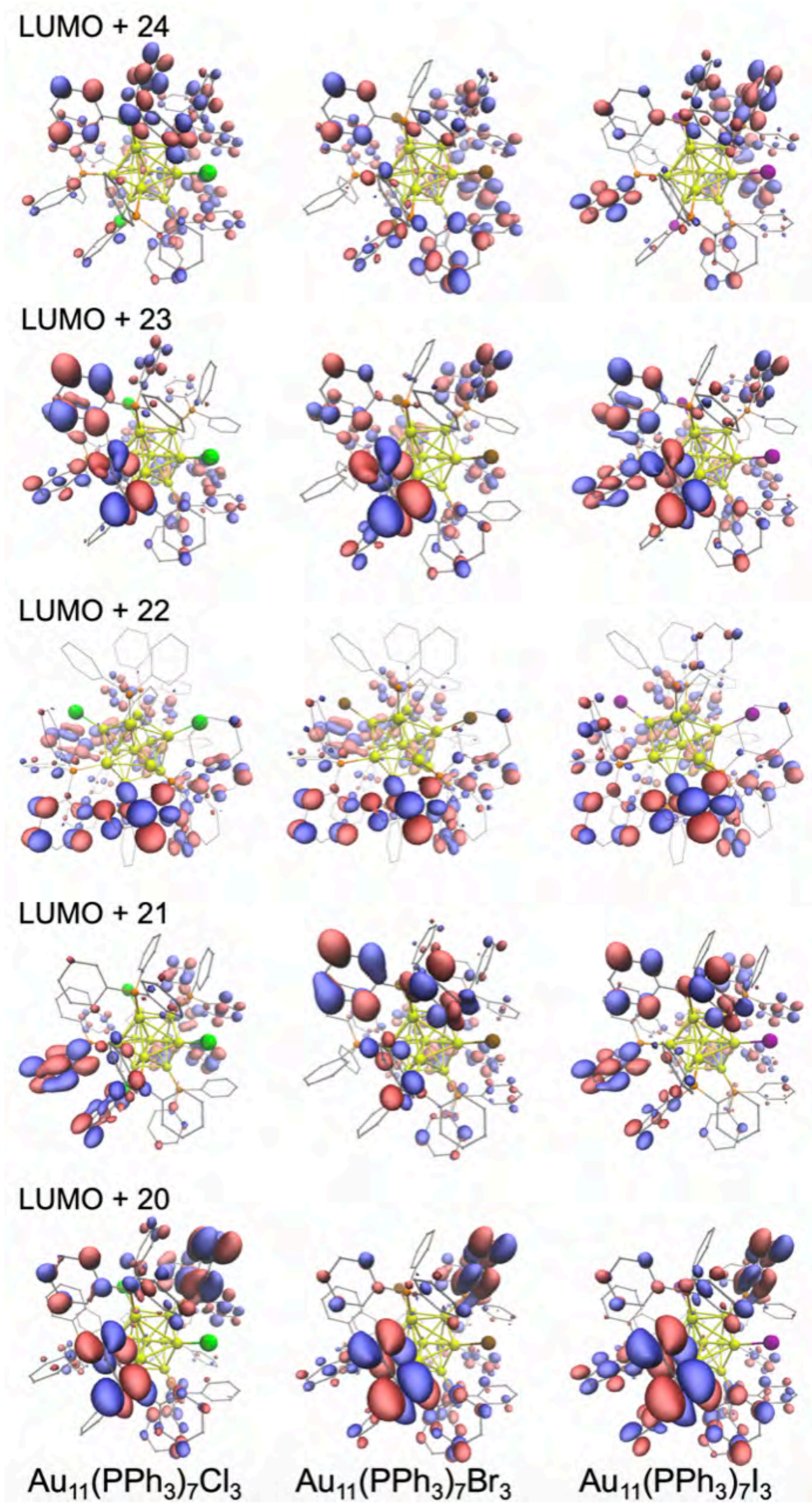

LUMO + 24
LUMO + 23
LUMO + 22
LUMO + 21
LUMO + 20
$Au_{11}(PPh_3)_7Cl_3$
$Au_{11}(PPh_3)_7Br_3$
$Au_{11}(PPh_3)_7I_3$

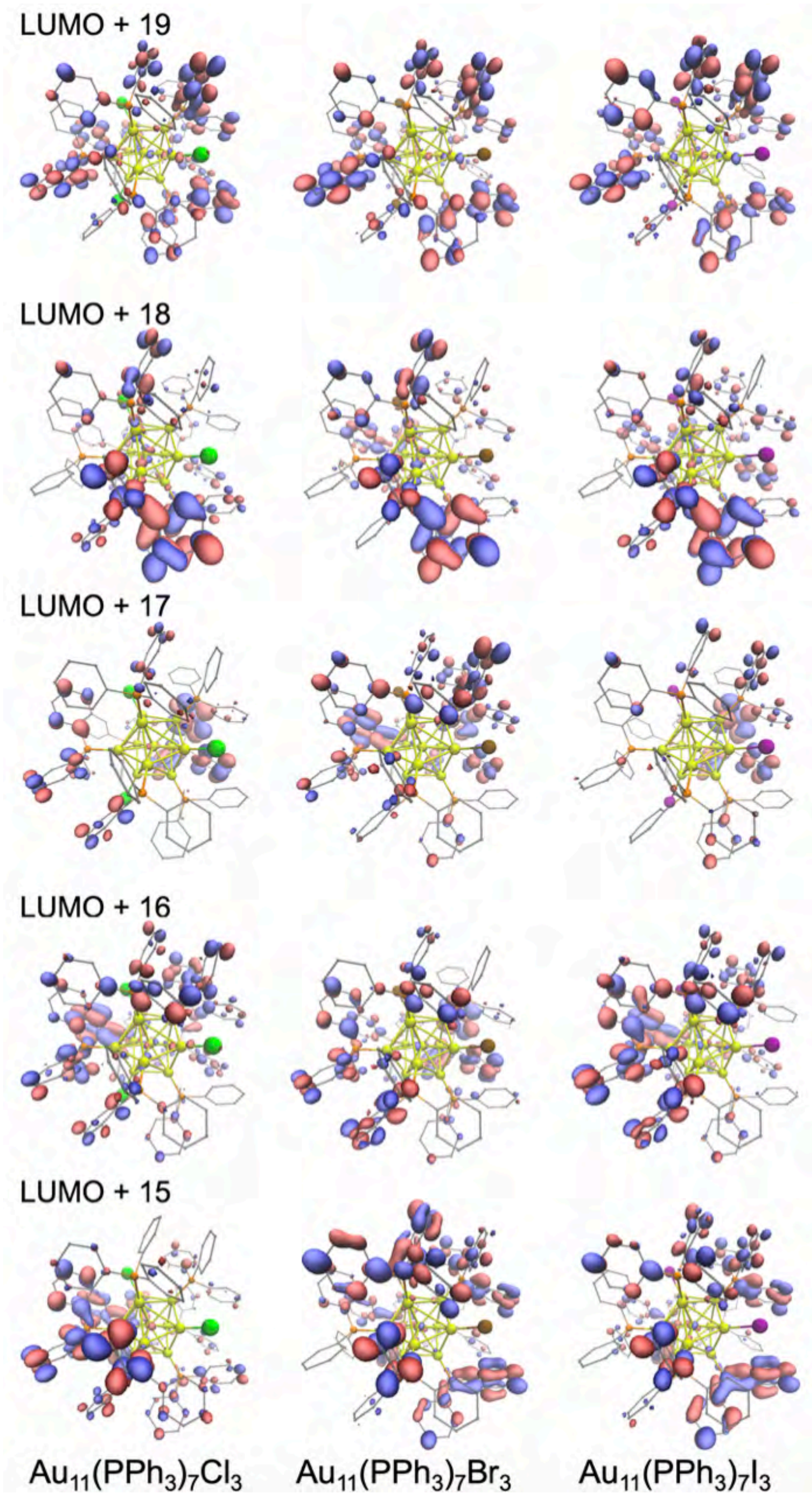
LUMO + 19
LUMO + 18
LUMO + 17
LUMO + 16
LUMO + 15
Au11(PPh3)7Cl3
Au11(PPh3)7Br3
Au11(PPh3)7I3

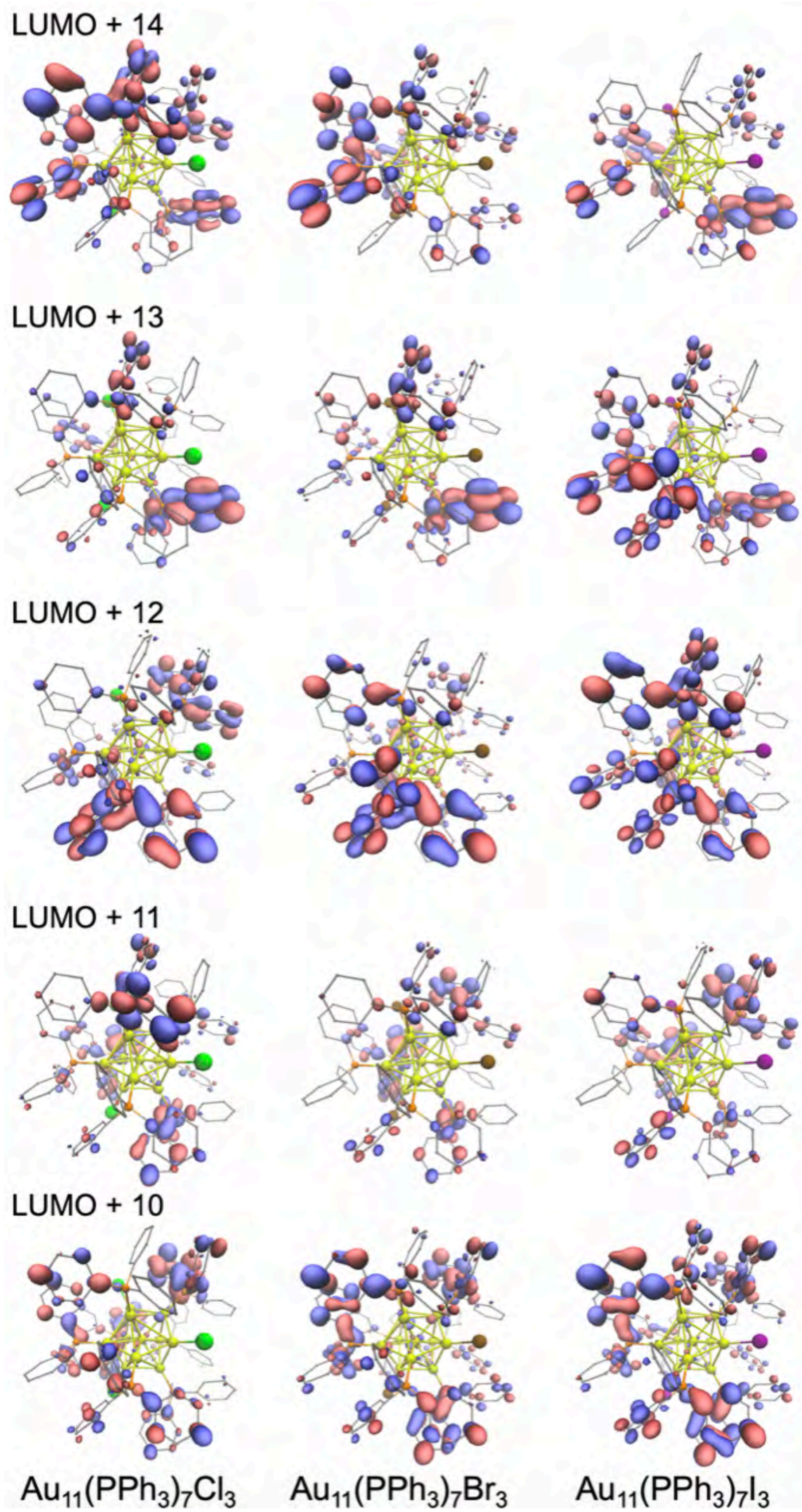

LUMO + 14
LUMO + 13
LUMO + 12
LUMO + 11
LUMO + 10
Au11(PPh3)7Cl3
Au11(PPh3)7Br3
Au11(PPh3)7I3

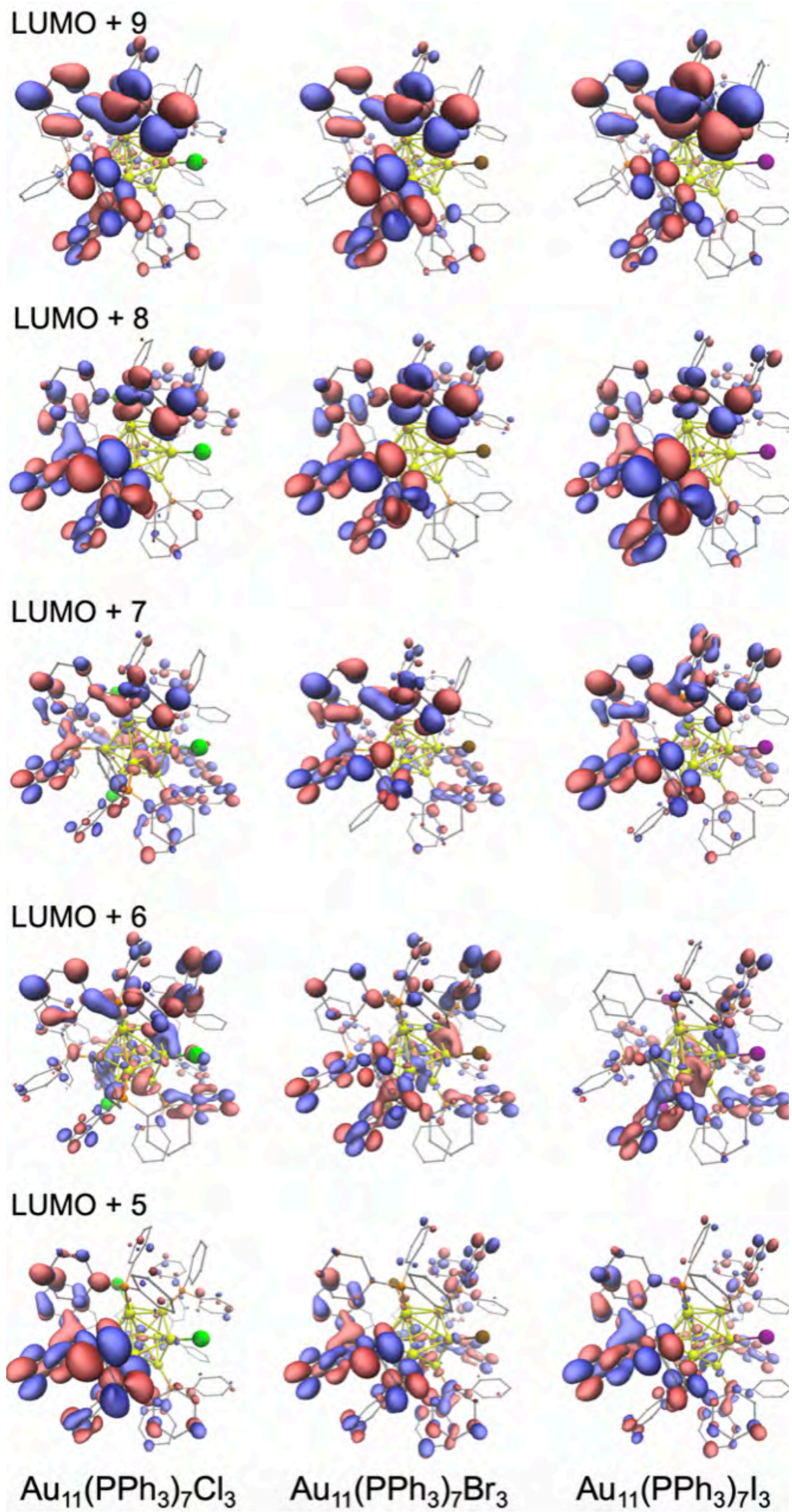

LUMO + 9
LUMO + 8
LUMO + 7
LUMO + 6
LUMO + 5
Au11(PPh3)7Cl3
Au11(PPh3)7Br3
Au11(PPh3)7I3

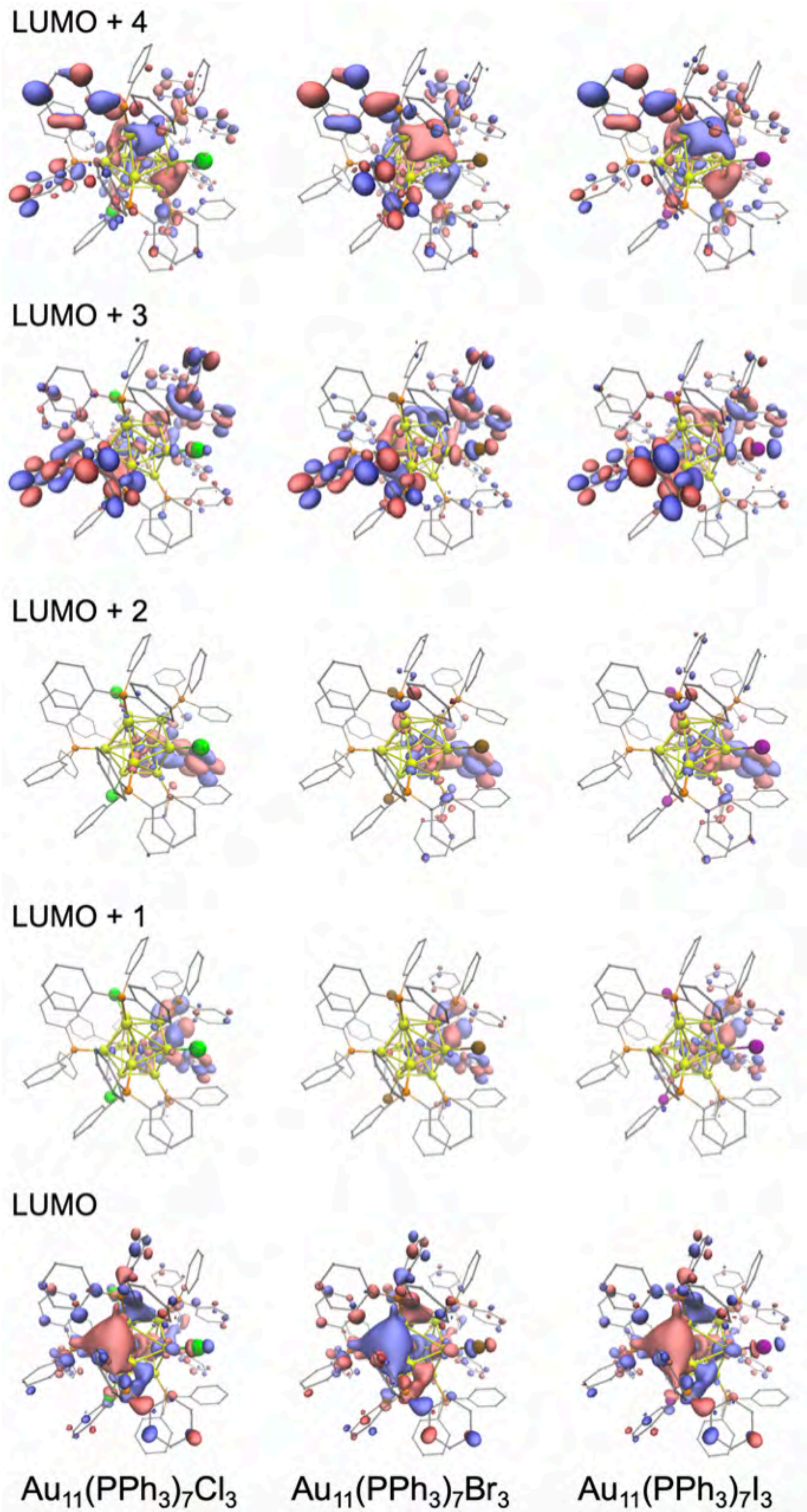
LUMO + 4
LUMO + 3
LUMO + 2
LUMO + 1
LUMO
$Au_{11}(PPh_3)_7Cl_3$
$Au_{11}(PPh_3)_7Br_3$
$Au_{11}(PPh_3)_7I_3$

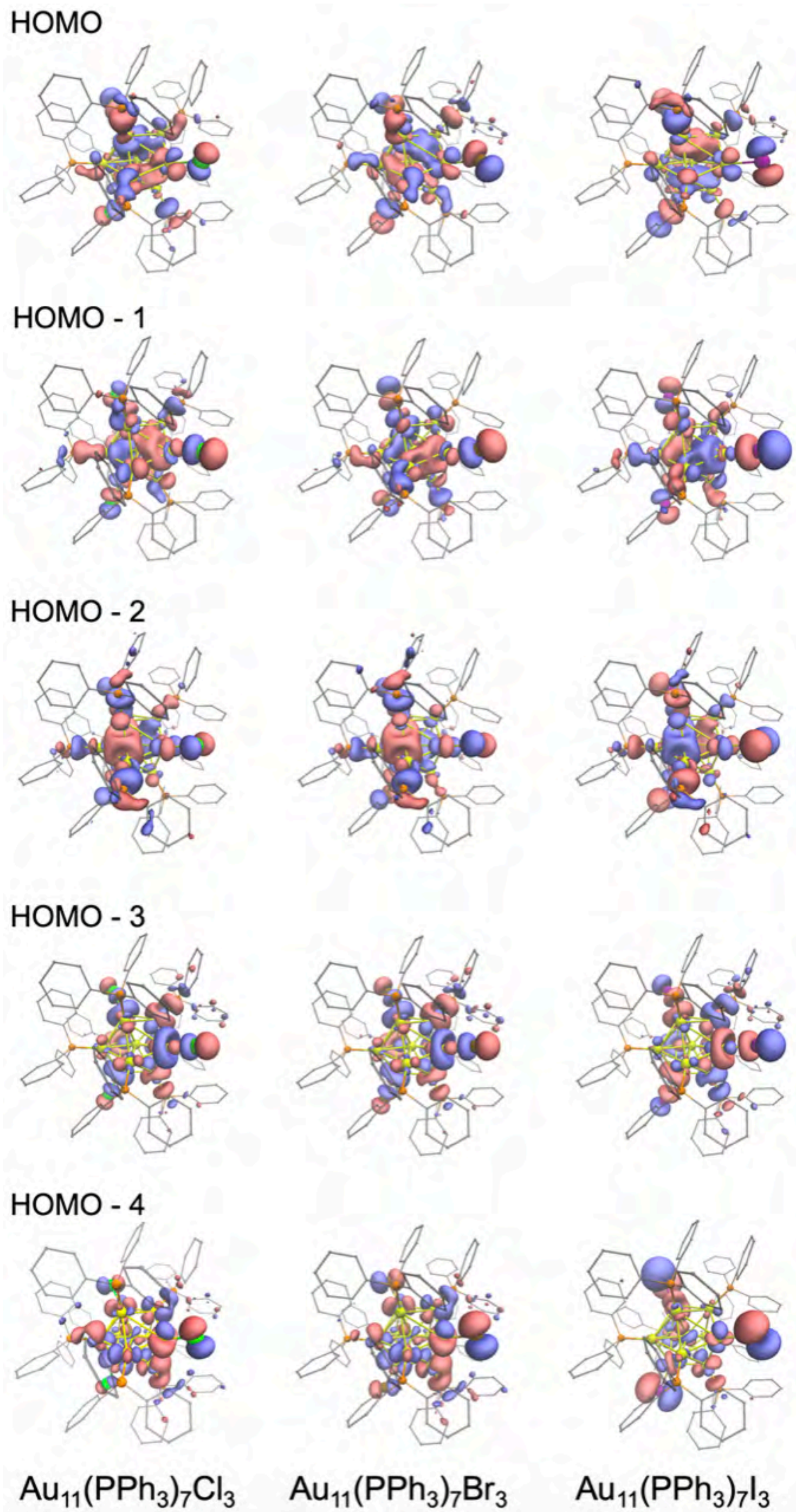
HOMO
HOMO - 1
HOMO - 2
HOMO - 3
HOMO - 4
Au11(PPh3)7Cl3
Au11(PPh3)7Br3
Au11(PPh3)7I3

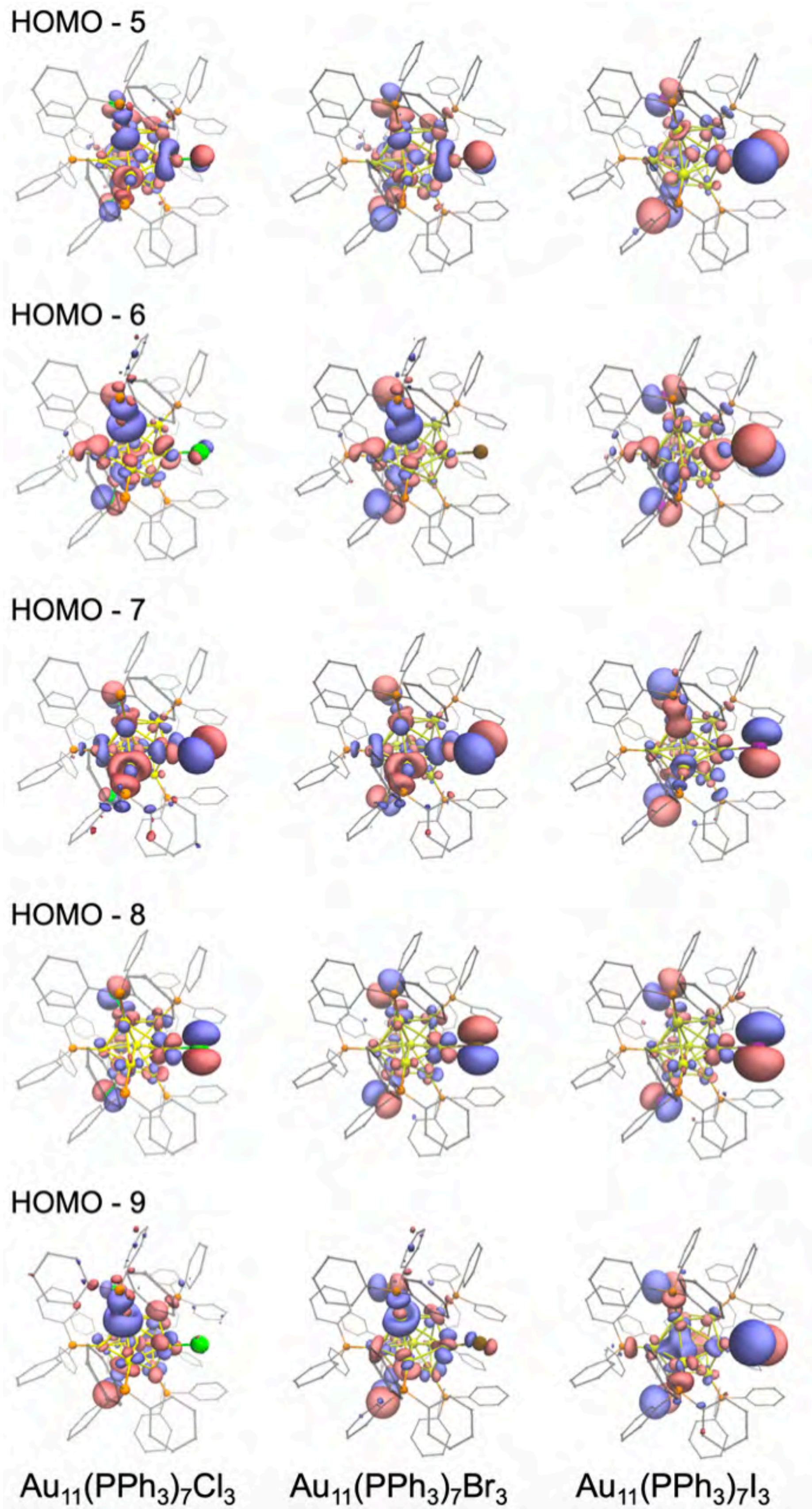

HOMO - 5
HOMO - 6
HOMO - 7
HOMO - 8
HOMO - 9
Au11(PPh3)7Cl3
Au11(PPh3)7Br3
Au11(PPh3)7I3

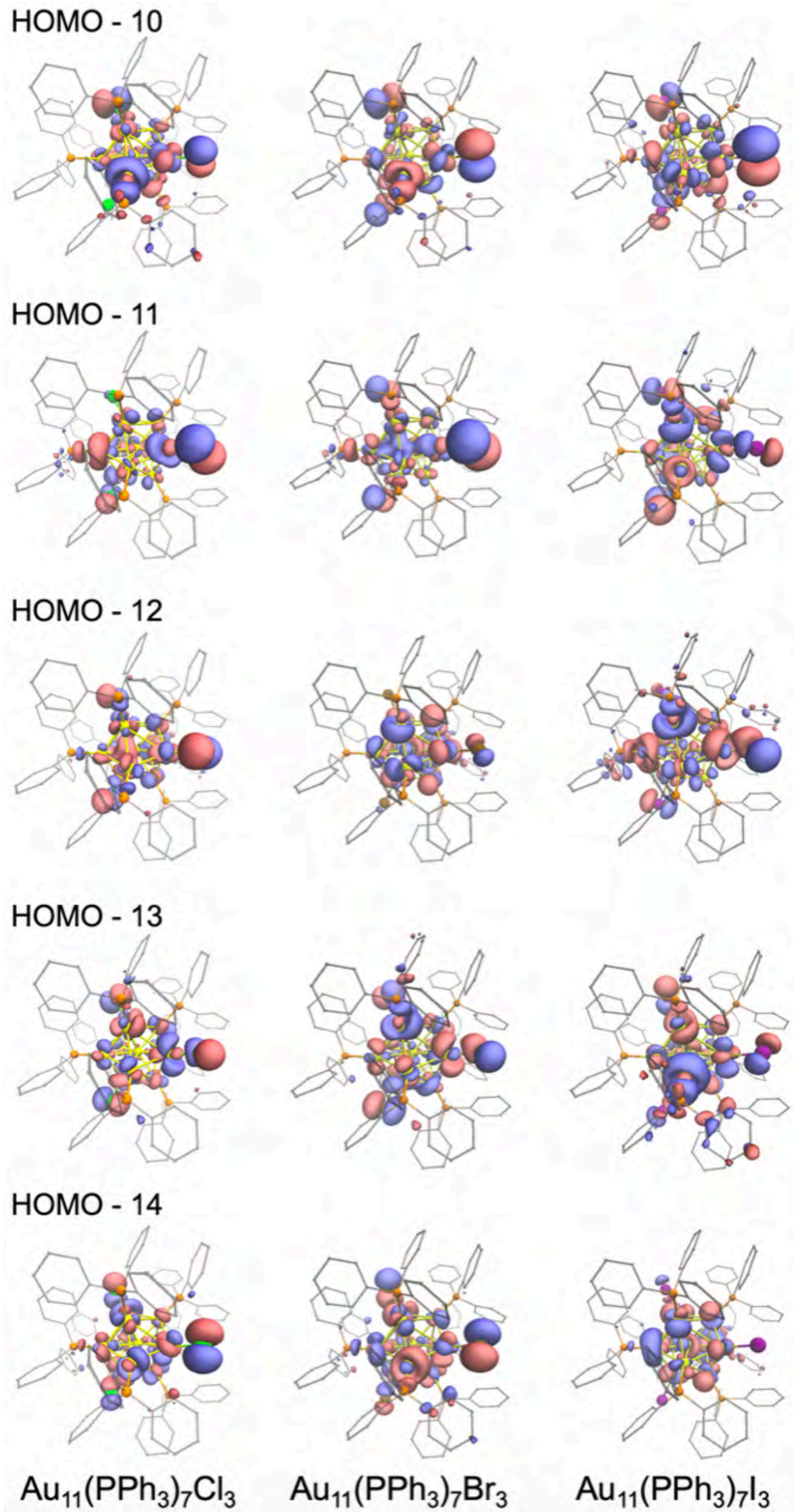
HOMO - 10
HOMO - 11
HOMO - 12
HOMO - 13
HOMO - 14
$Au_{11}(PPh_3)_7Cl_3$
$Au_{11}(PPh_3)_7Br_3$
$Au_{11}(PPh_3)_7I_3$

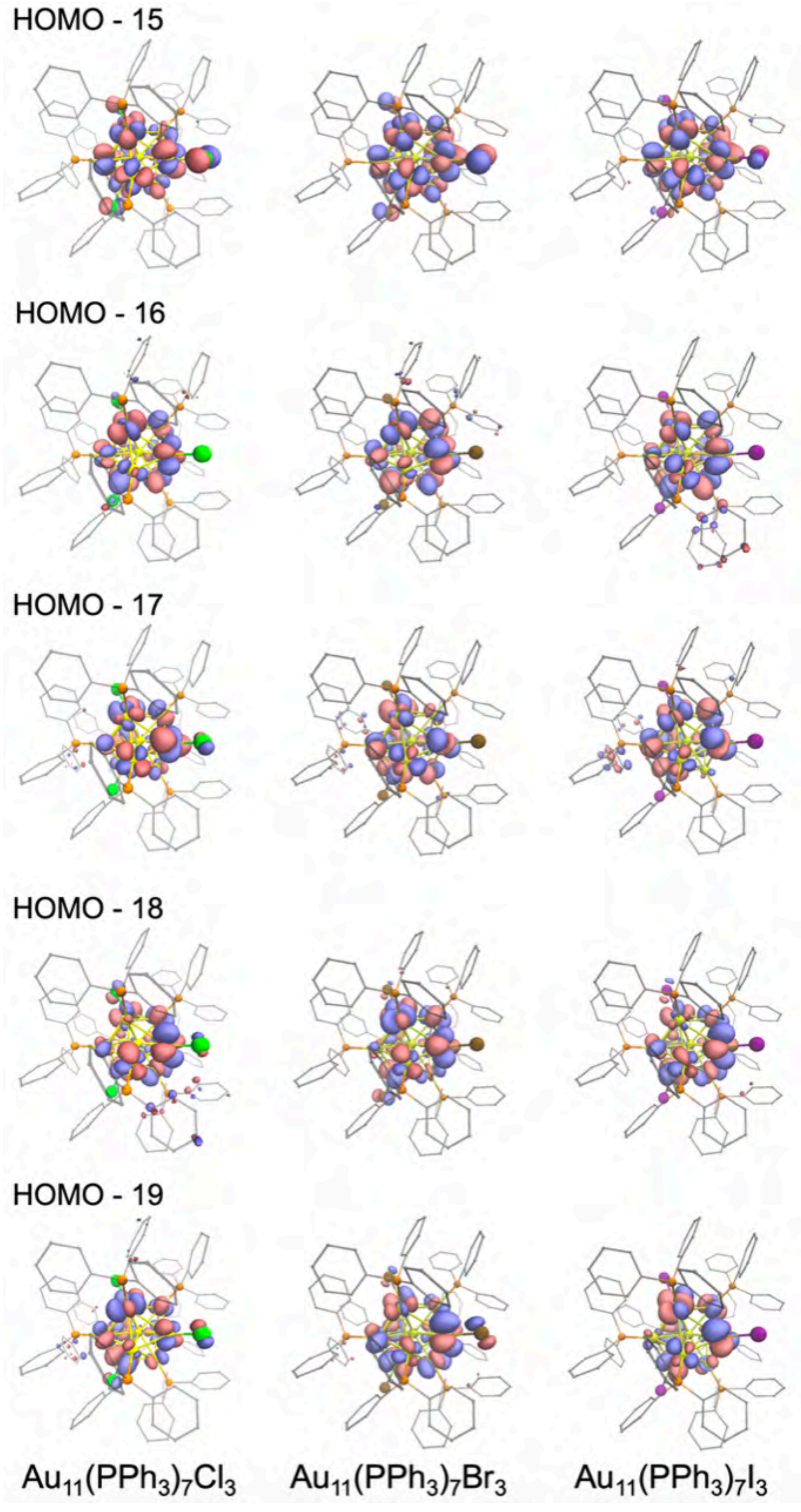
HOMO - 15
HOMO - 16
HOMO - 17
HOMO - 18
HOMO - 19
Au11(PPh3)7Cl3
Au11(PPh3)7Br3
Au11(PPh3)7I3

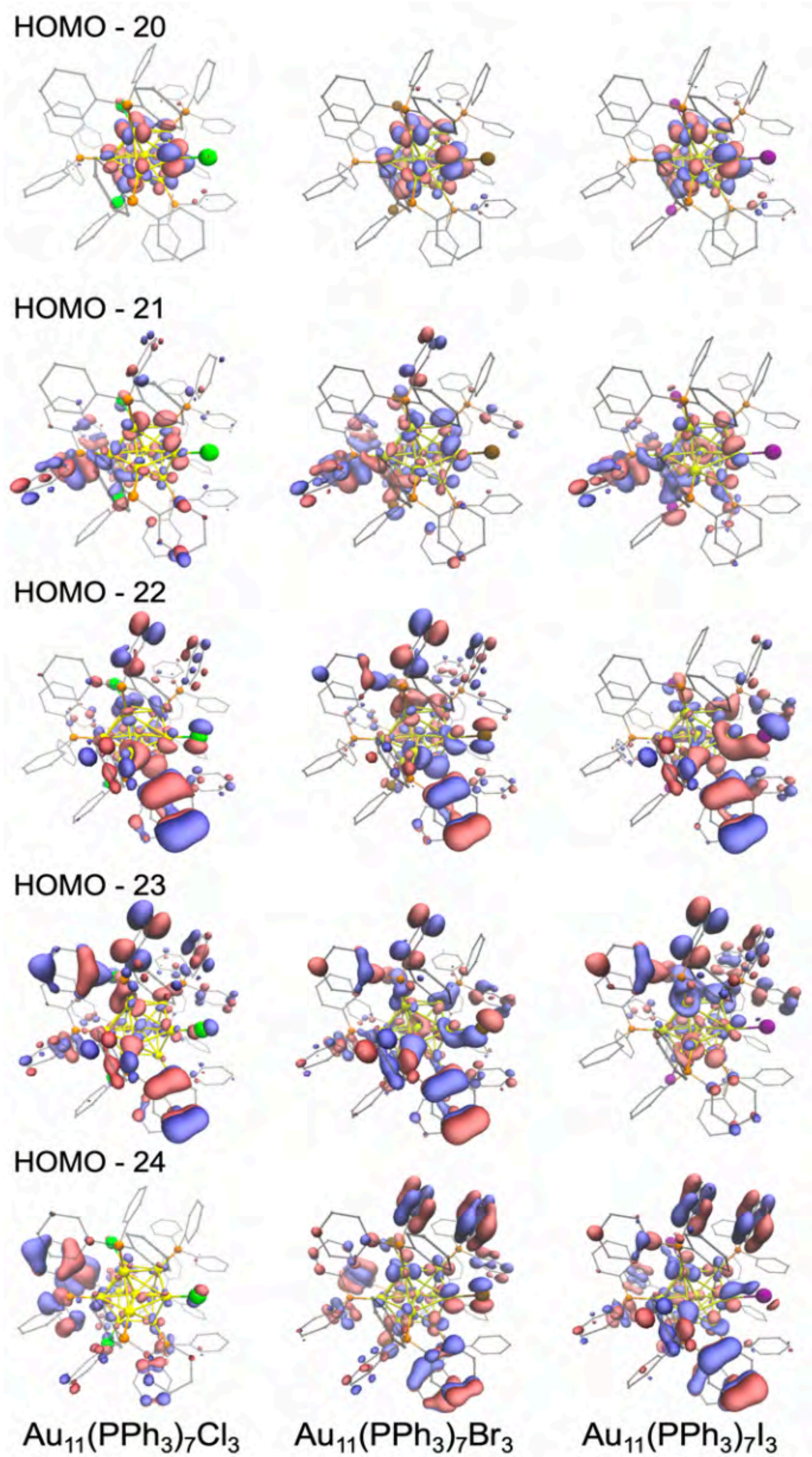

Figure A28. KS orbitals of $Au_{11}(PPh_3)_7X_3$ near the frontier orbitals.

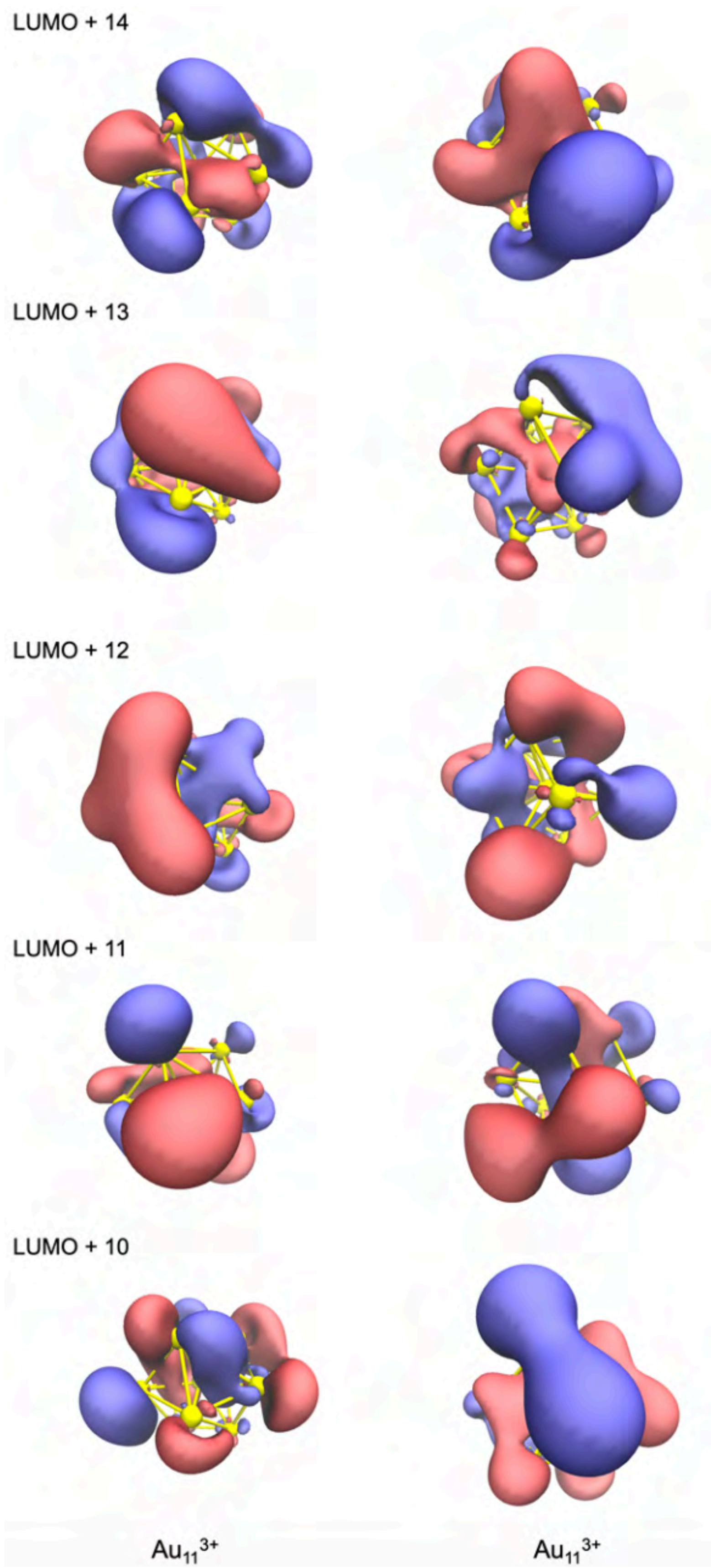

LUMO + 14
LUMO + 13
LUMO + 12
LUMO + 11
LUMO + 10
Au_{11}^{3+}
Au_{11}^{3+}

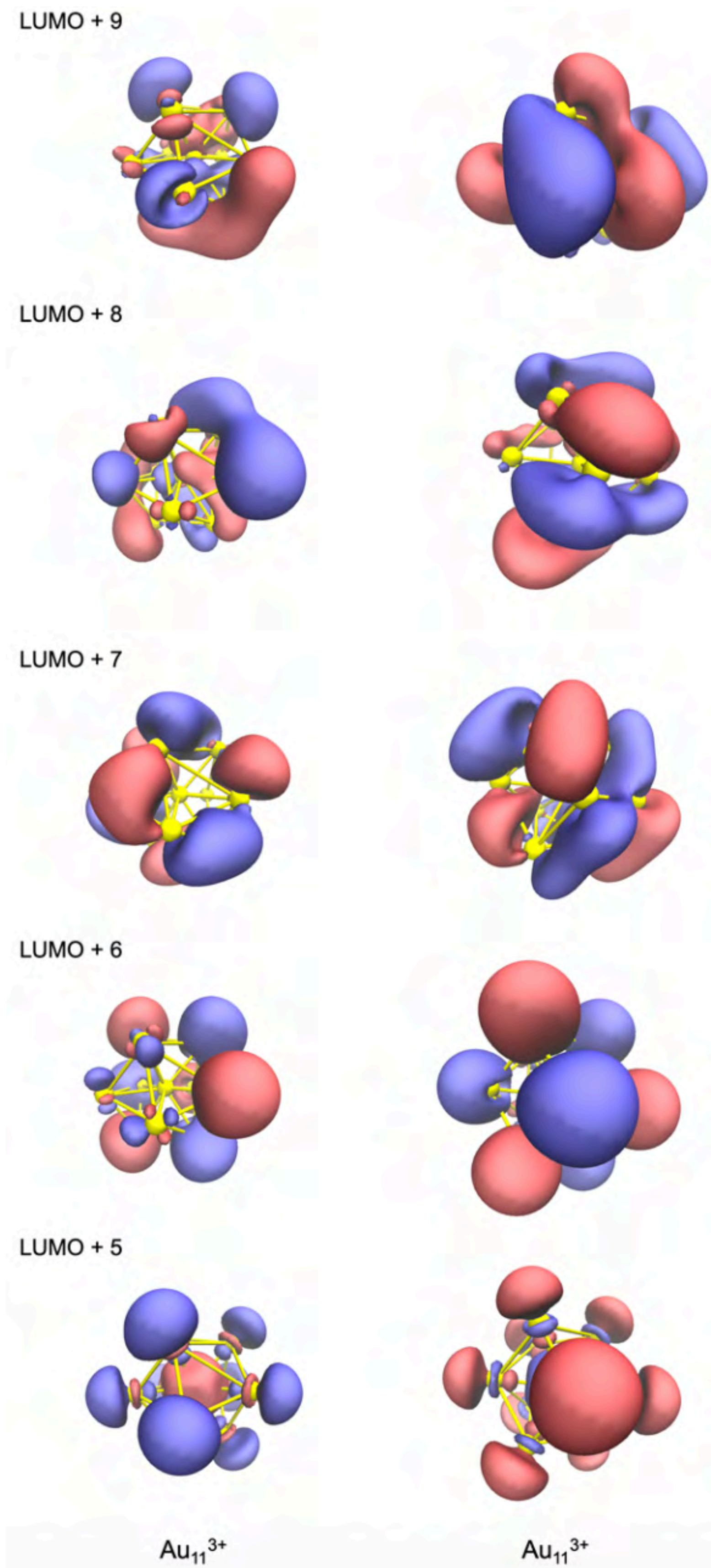
LUMO + 9
LUMO + 8
LUMO + 7
LUMO + 6
LUMO + 5
Au_{11}^{3+}
Au_{11}^{3+}

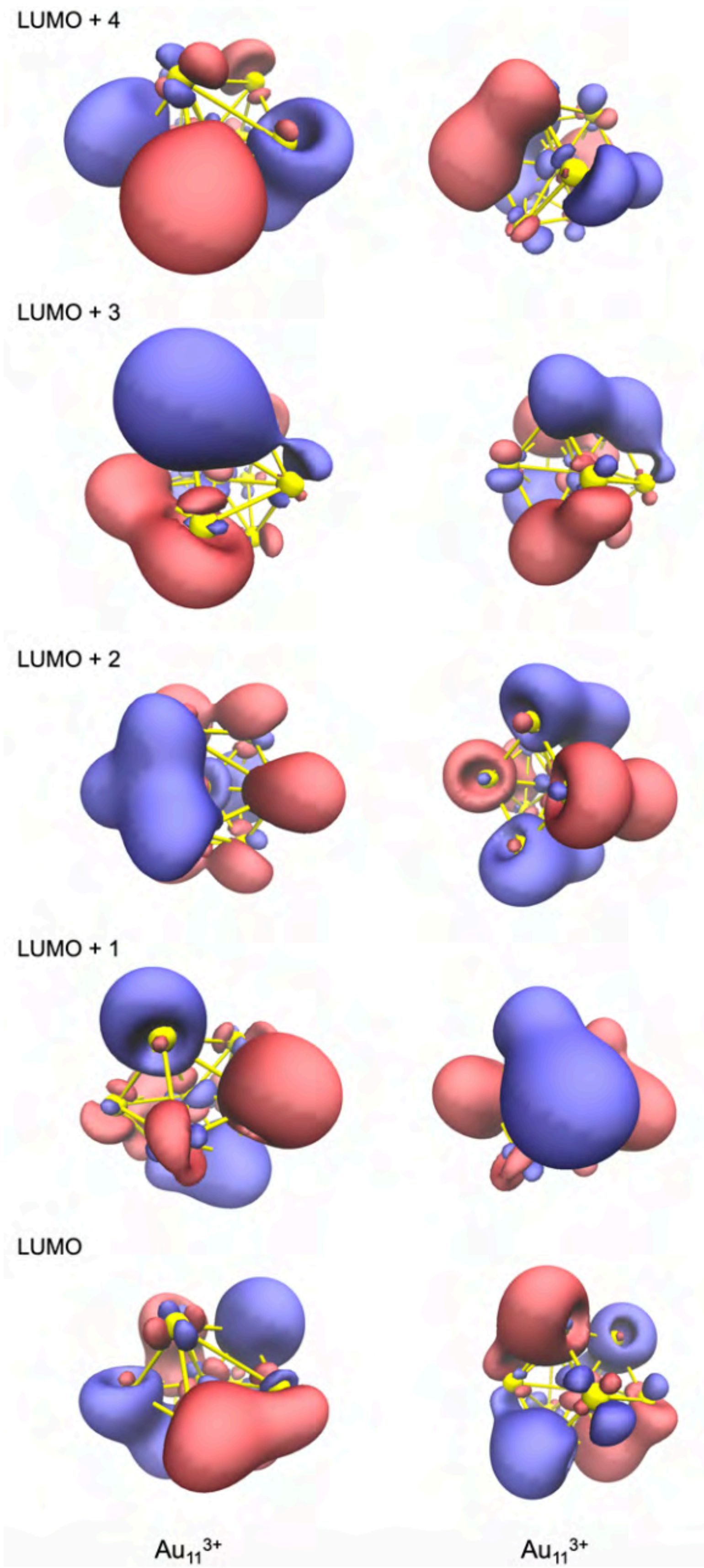
LUMO + 4
LUMO + 3
LUMO + 2
LUMO + 1
LUMO
Au_{11}^{3+}
Au_{11}^{3+}

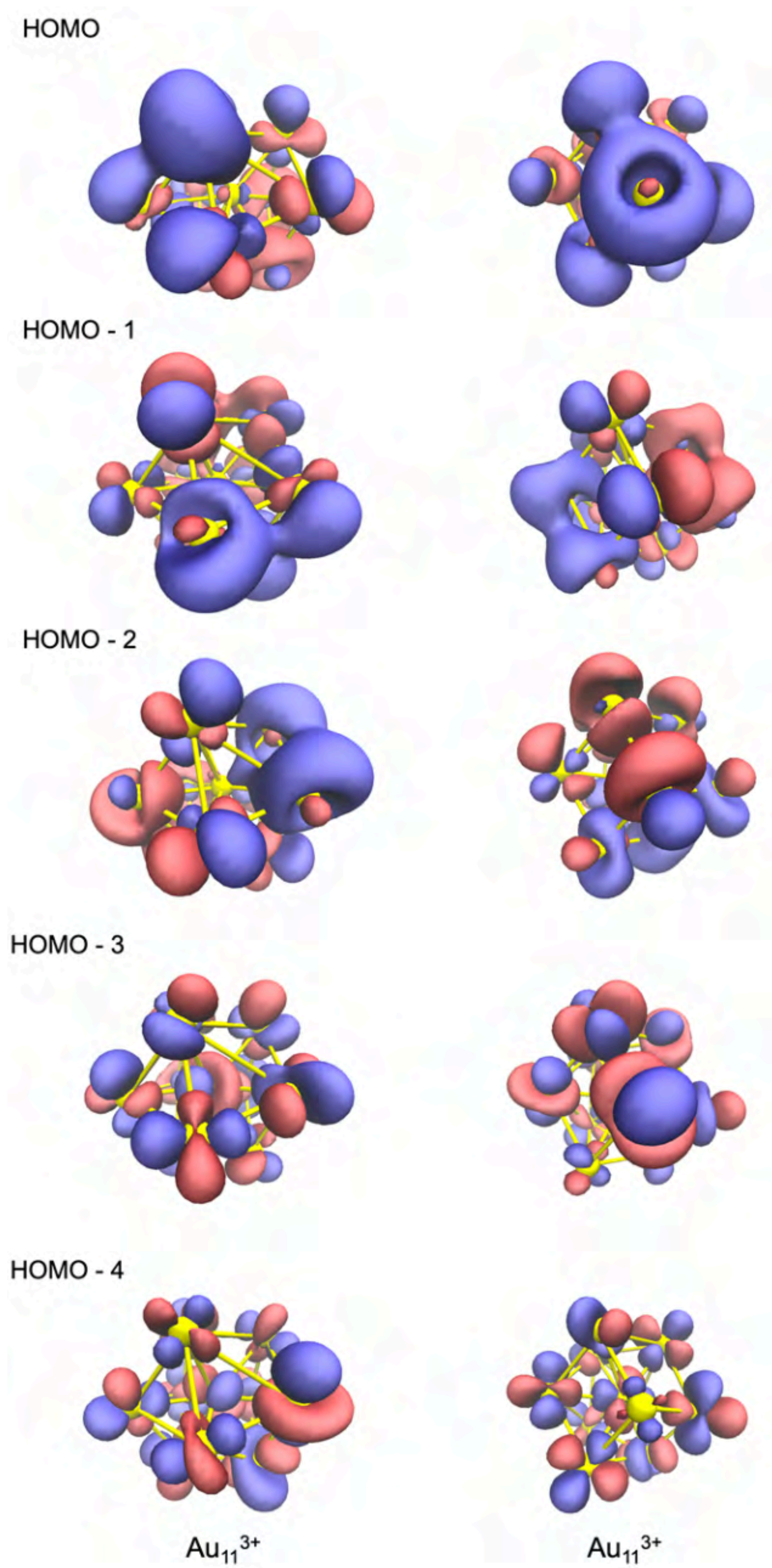
HOMO
HOMO - 1
HOMO - 2
HOMO - 3
HOMO - 4
Au_{11}^{3+}
Au_{11}^{3+}

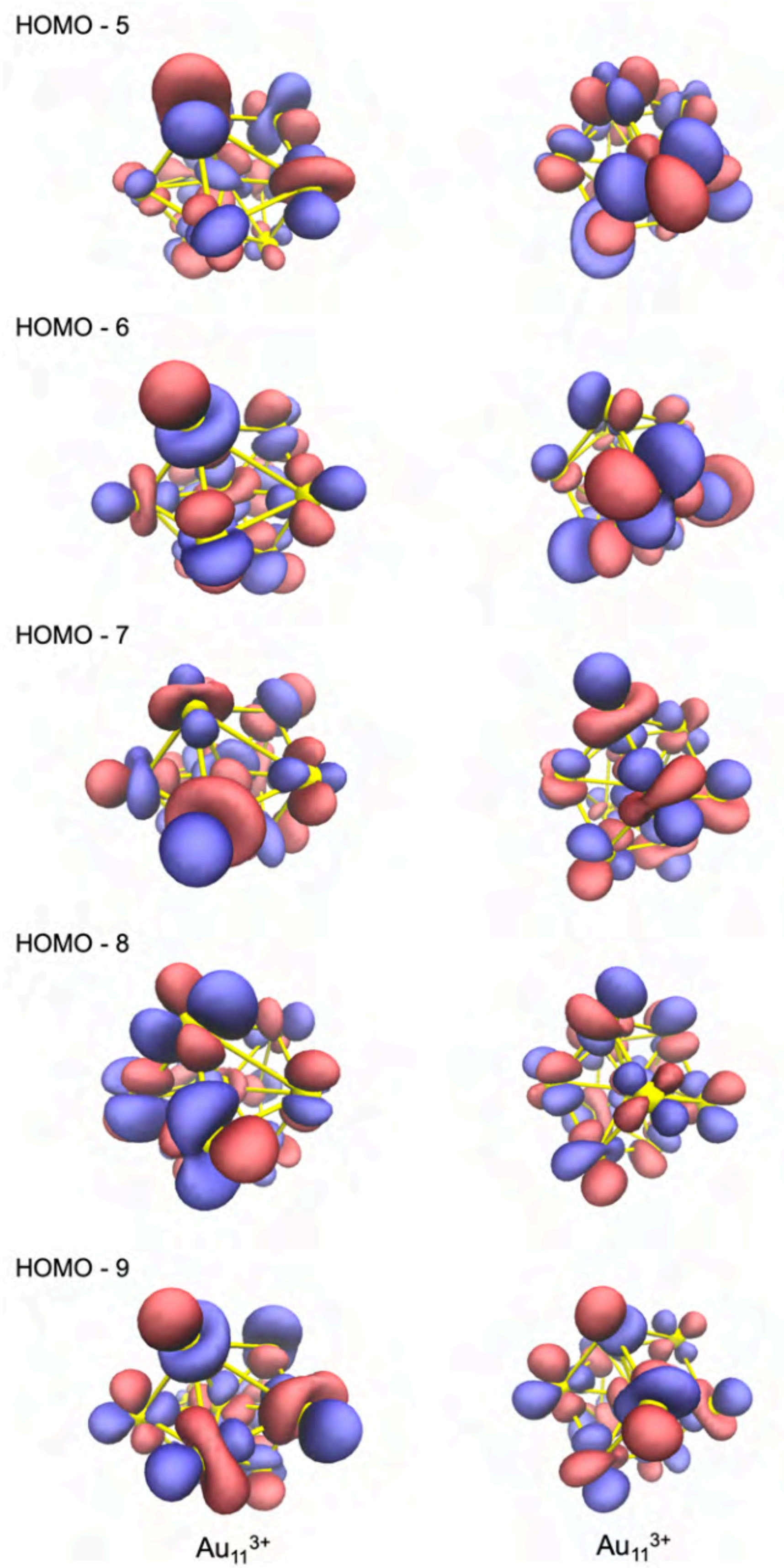
HOMO - 5
HOMO - 6
HOMO - 7
HOMO - 8
HOMO - 9
Au_{11}^{3+}
Au_{11}^{3+}

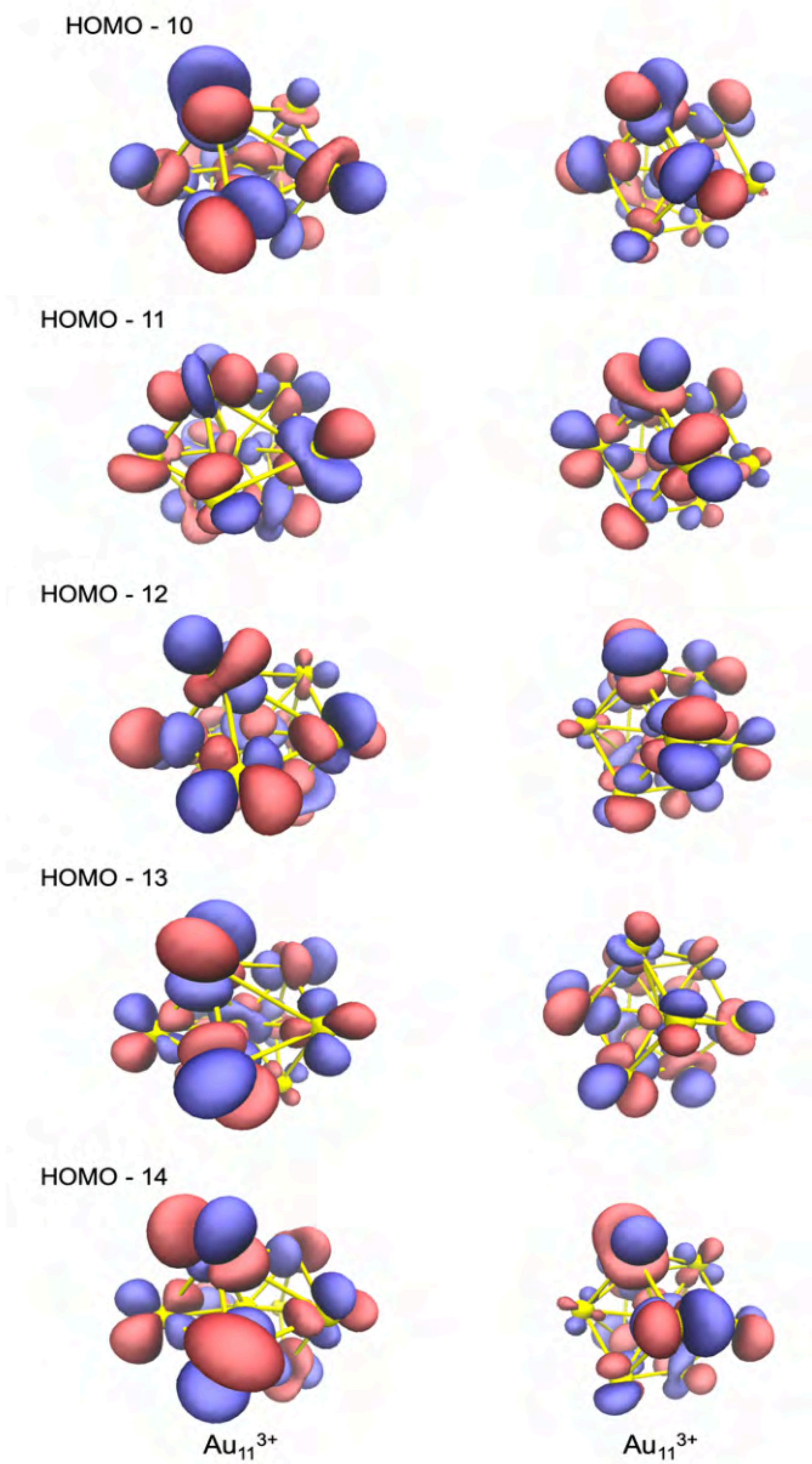

Figure A29. KS orbitals of Au_{11}^{3+} with $Au_{11}(PPh_3)_8Br_2^+$ core (left) and $Au(PPh_3)_7Br_3$ core (right) near the frontier orbitals.

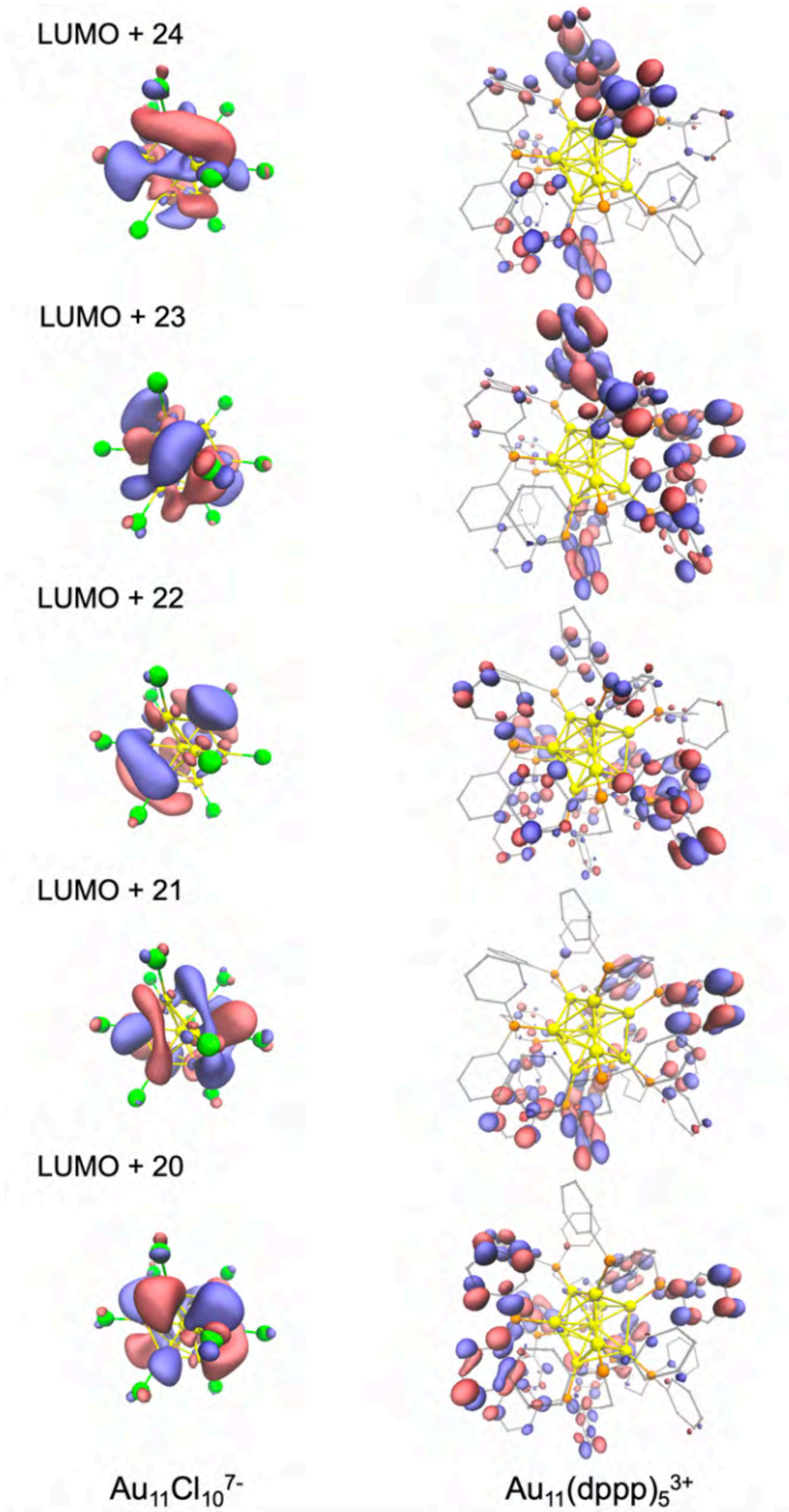
LUMO + 24
LUMO + 23
LUMO + 22
LUMO + 21
LUMO + 20
$Au_{11}Cl_{10}^{7-}$
$Au_{11}(dppp)_5^{3+}$

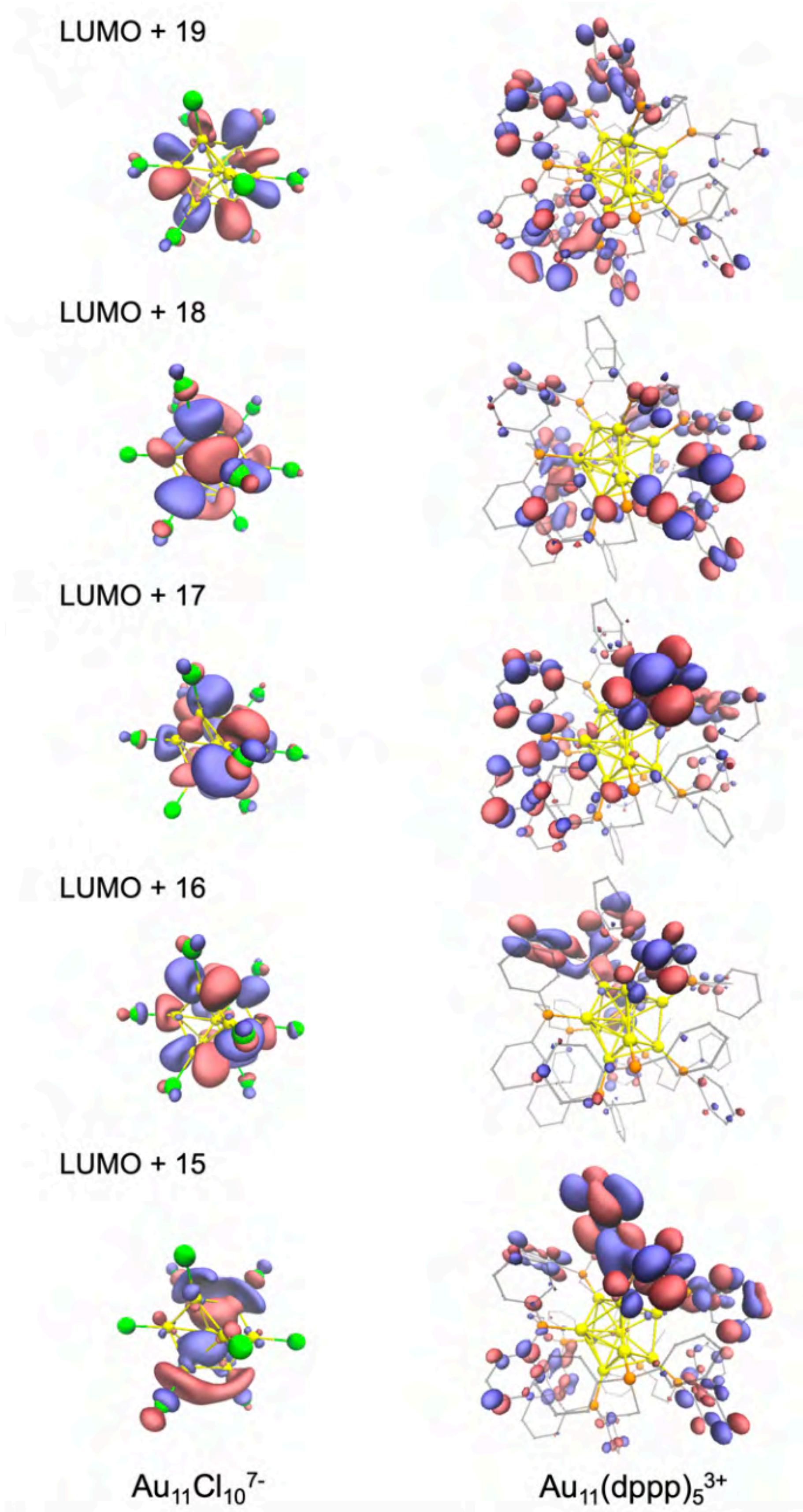
LUMO + 19
LUMO + 18
LUMO + 17
LUMO + 16
LUMO + 15
$Au_{11}Cl_{10}^{7-}$
$Au_{11}(dppp)_5^{3+}$

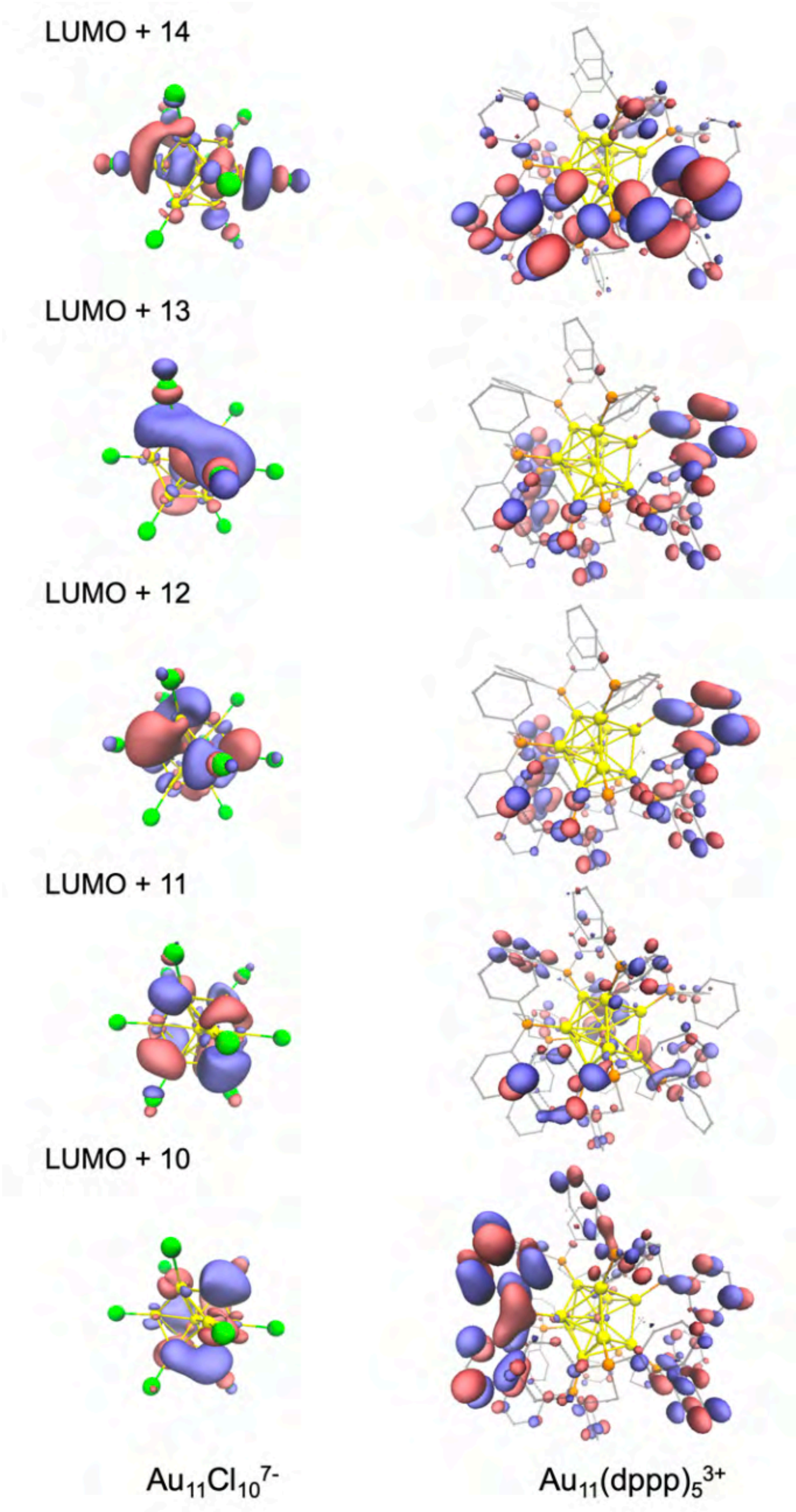
LUMO + 14
LUMO + 13
LUMO + 12
LUMO + 11
LUMO + 10
$Au_{11}Cl_{10}^{7-}$
$Au_{11}(dppp)_5^{3+}$

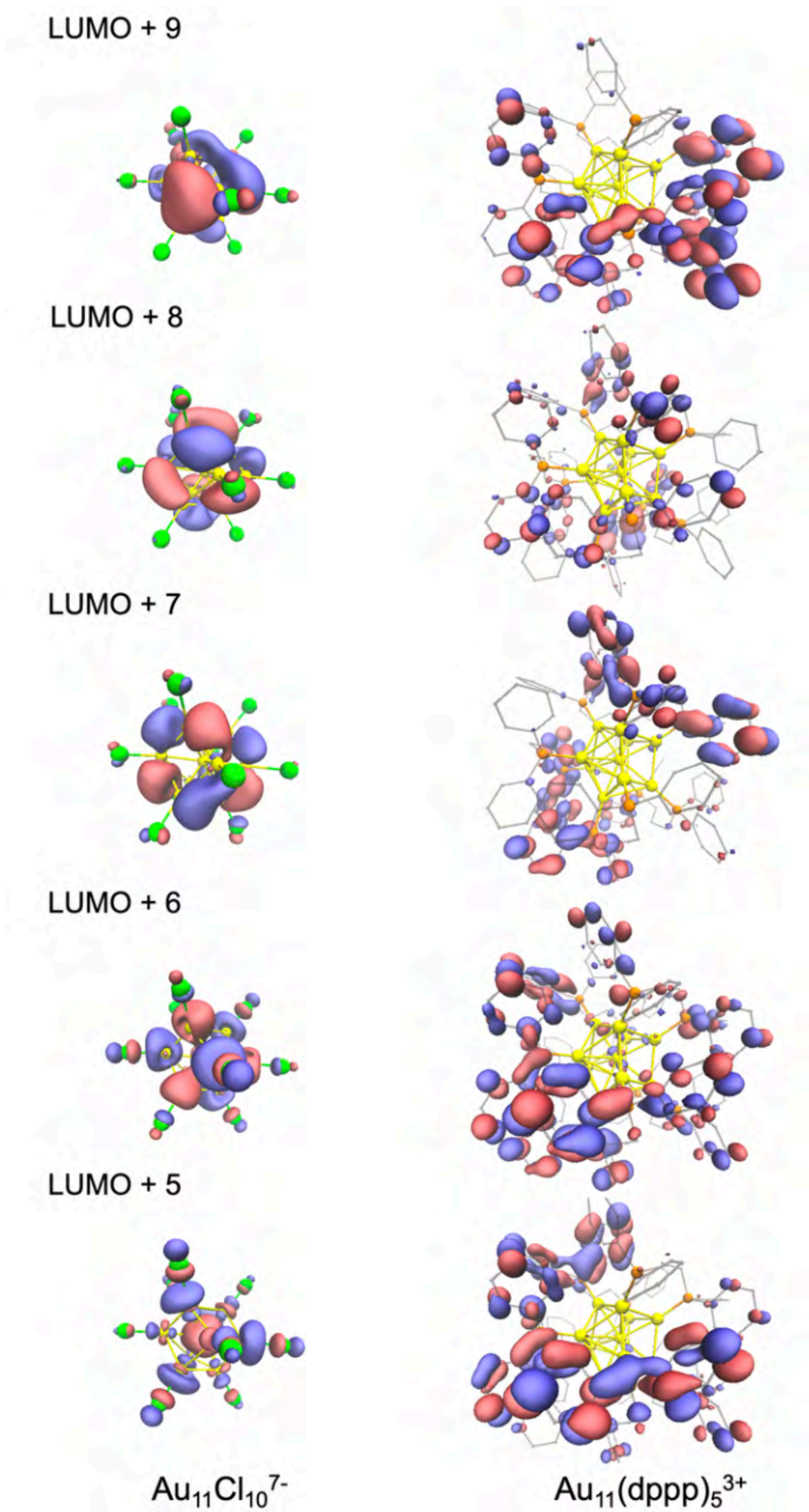
LUMO + 9
LUMO + 8
LUMO + 7
LUMO + 6
LUMO + 5
$Au_{11}Cl_{10}^{7-}$
$Au_{11}(dppp)_5^{3+}$

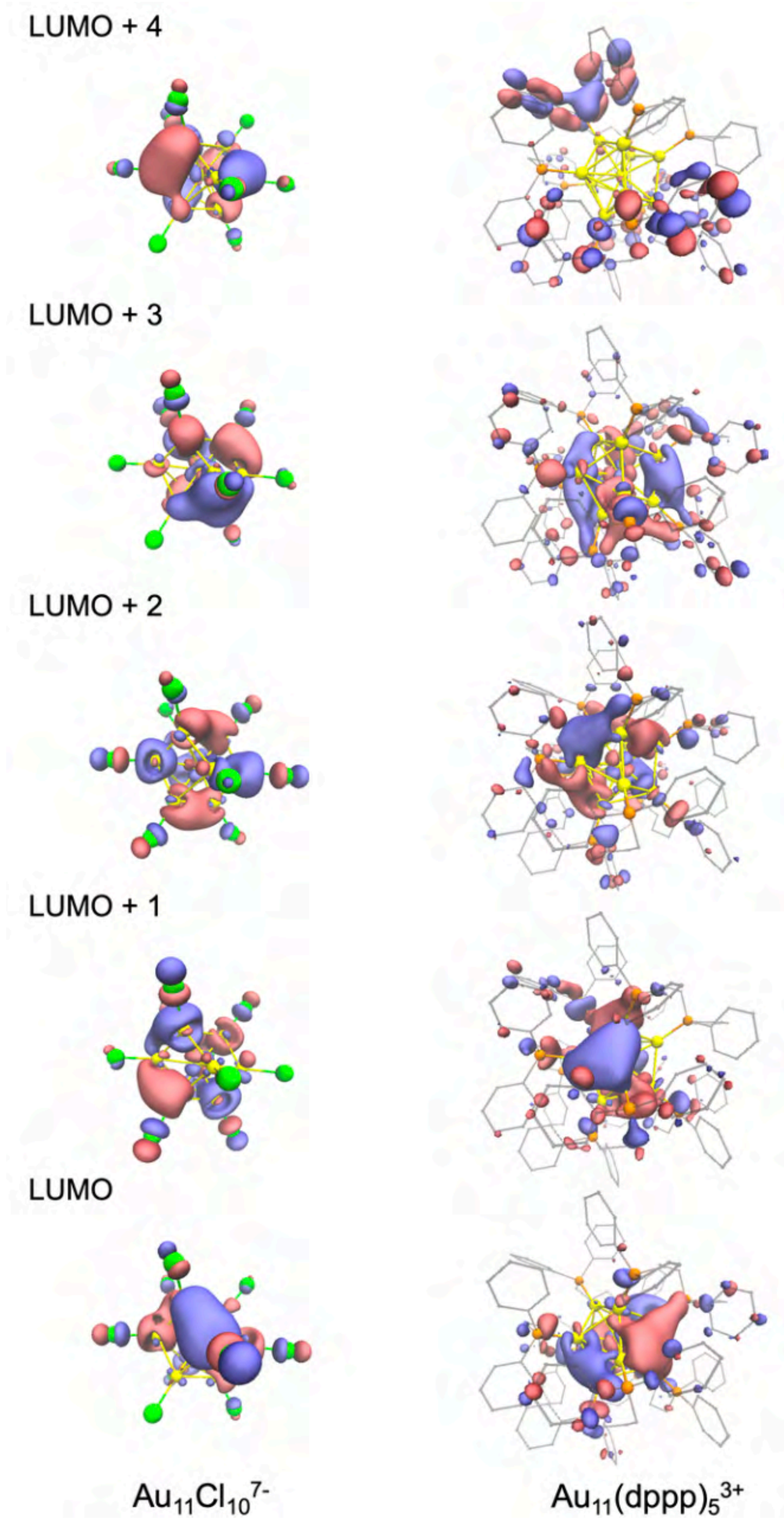
LUMO + 4
LUMO + 3
LUMO + 2
LUMO + 1
LUMO
$Au_{11}Cl_{10}^{7-}$
$Au_{11}(dppp)_5^{3+}$

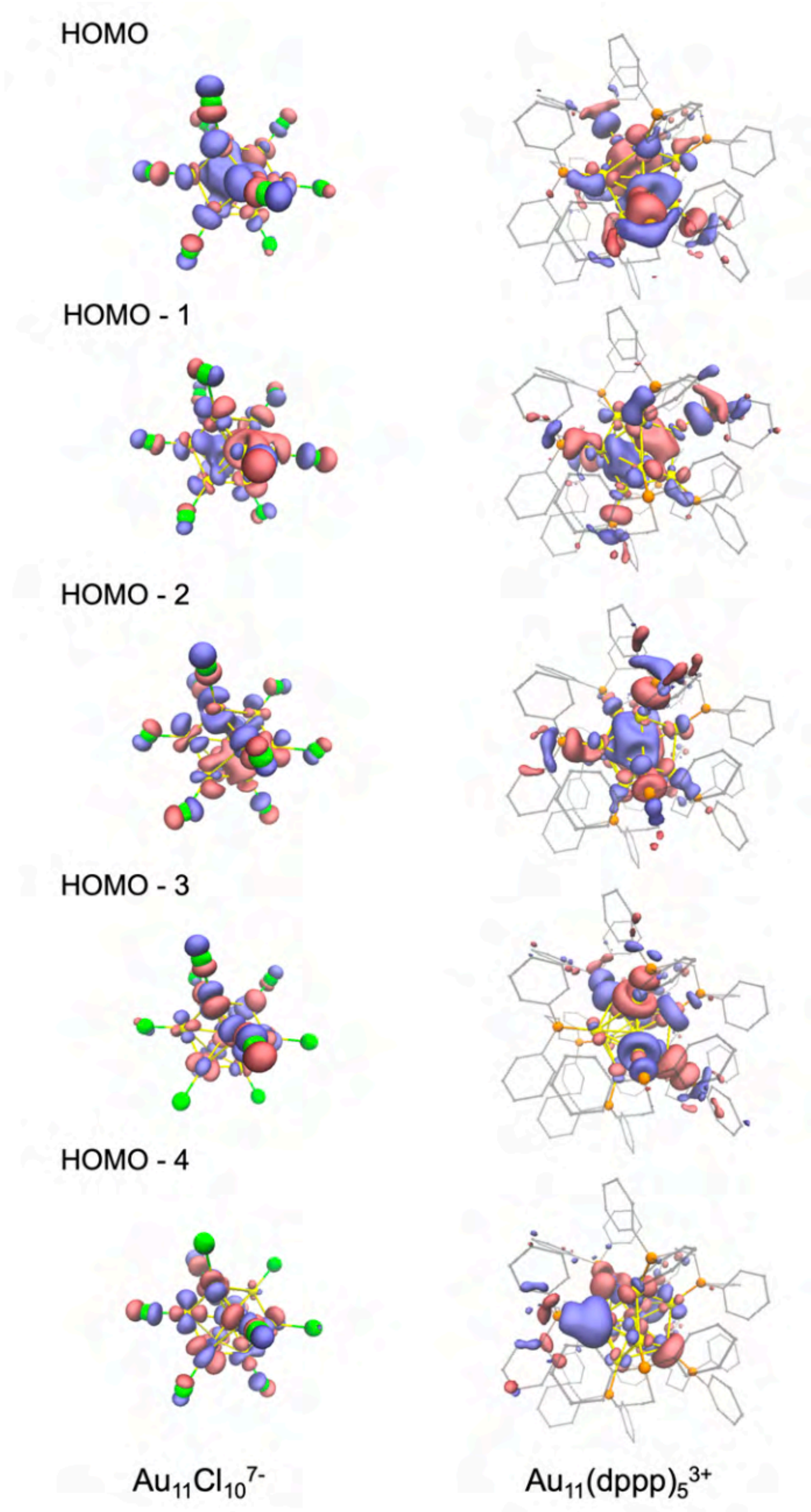
HOMO
HOMO - 1
HOMO - 2
HOMO - 3
HOMO - 4
$Au_{11}Cl_{10}^{7-}$
$Au_{11}(dppp)_5^{3+}$

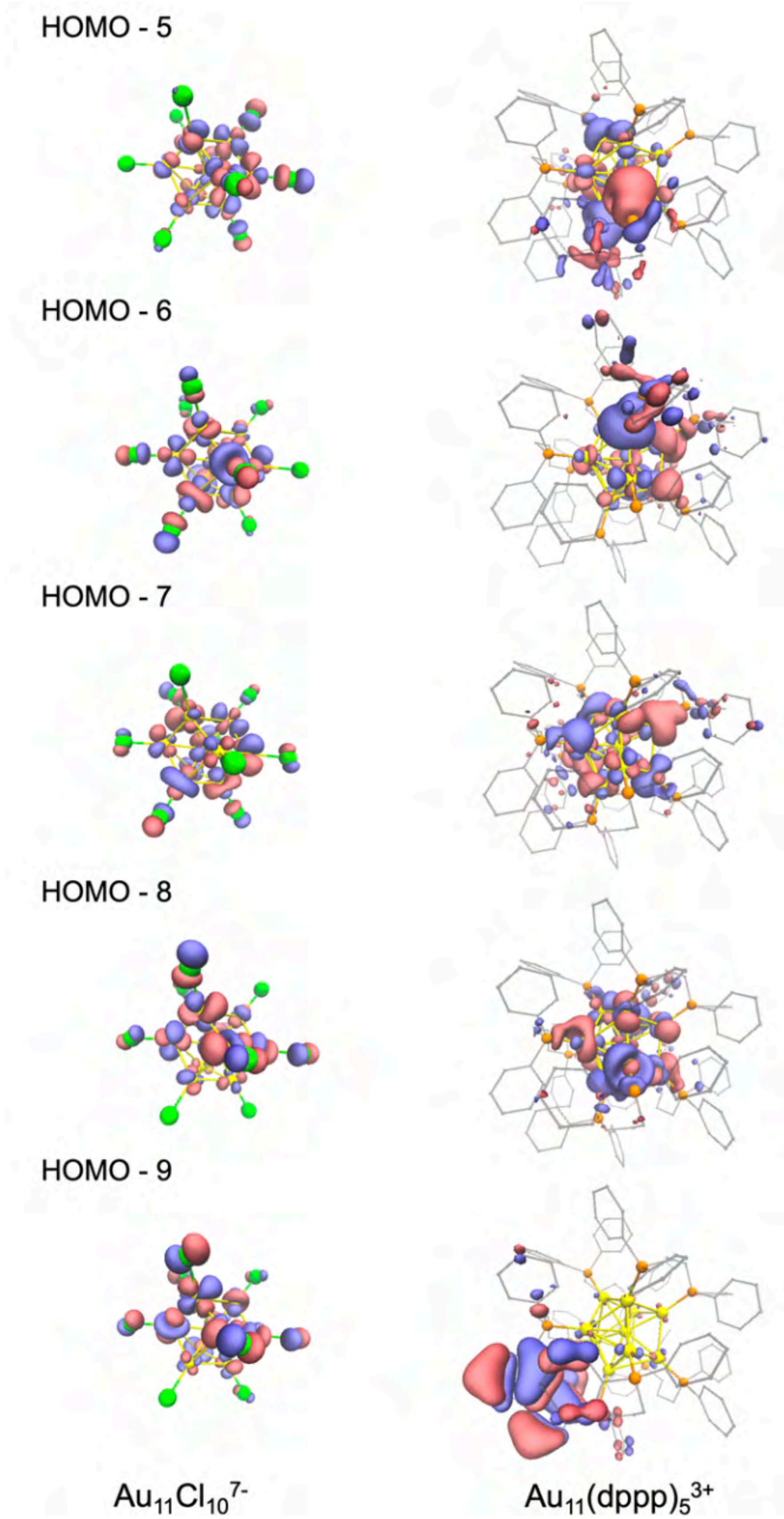
HOMO - 5
HOMO - 6
HOMO - 7
HOMO - 8
HOMO - 9
$Au_{11}Cl_{10}^{7-}$
$Au_{11}(dppp)_5^{3+}$

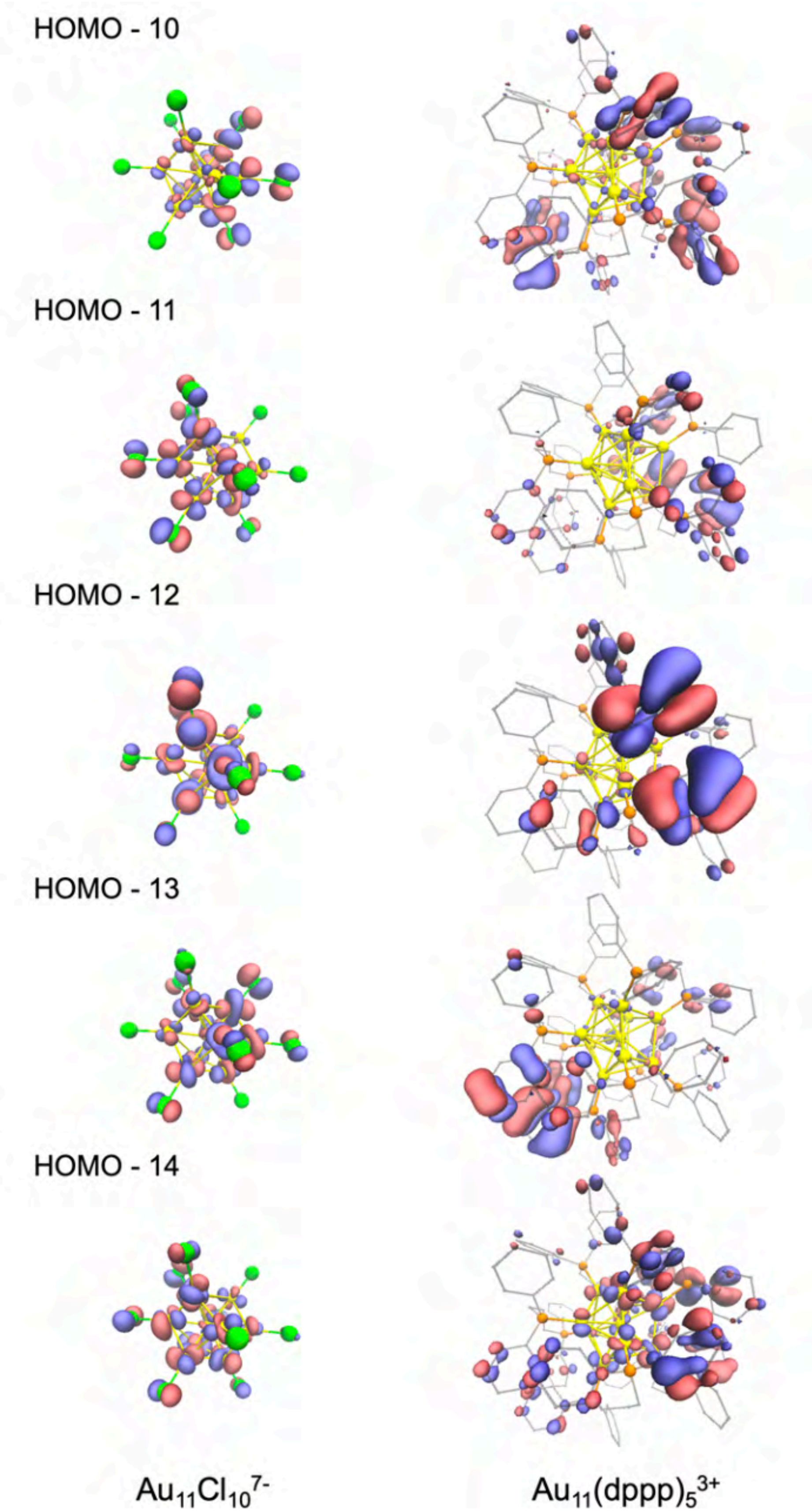
HOMO - 10
HOMO - 11
HOMO - 12
HOMO - 13
HOMO - 14
$Au_{11}Cl_{10}^{7-}$
$Au_{11}(dppp)_5^{3+}$

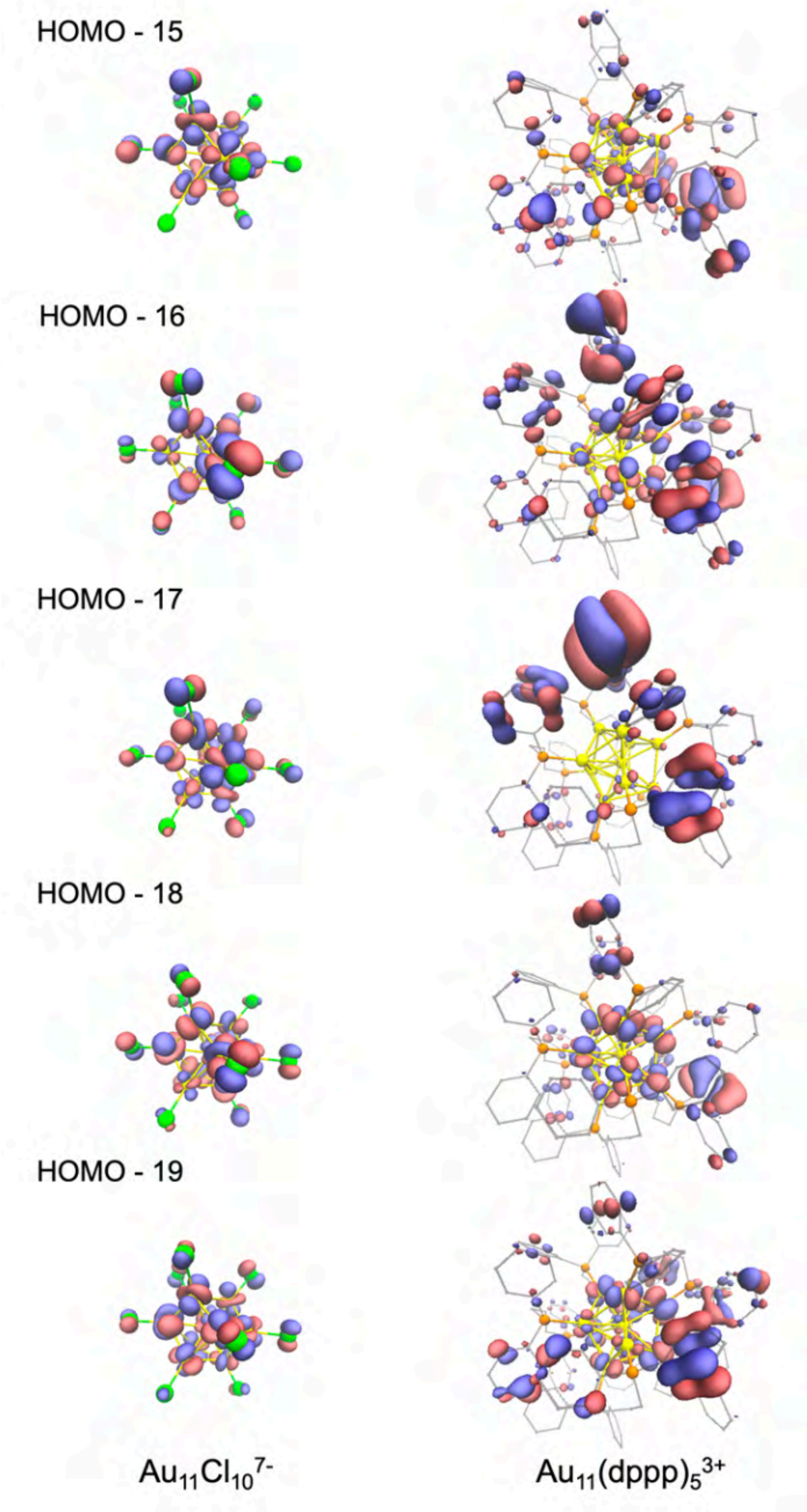
HOMO - 15
HOMO - 16
HOMO - 17
HOMO - 18
HOMO - 19
$Au_{11}Cl_{10}^{7-}$
$Au_{11}(dppp)_5^{3+}$

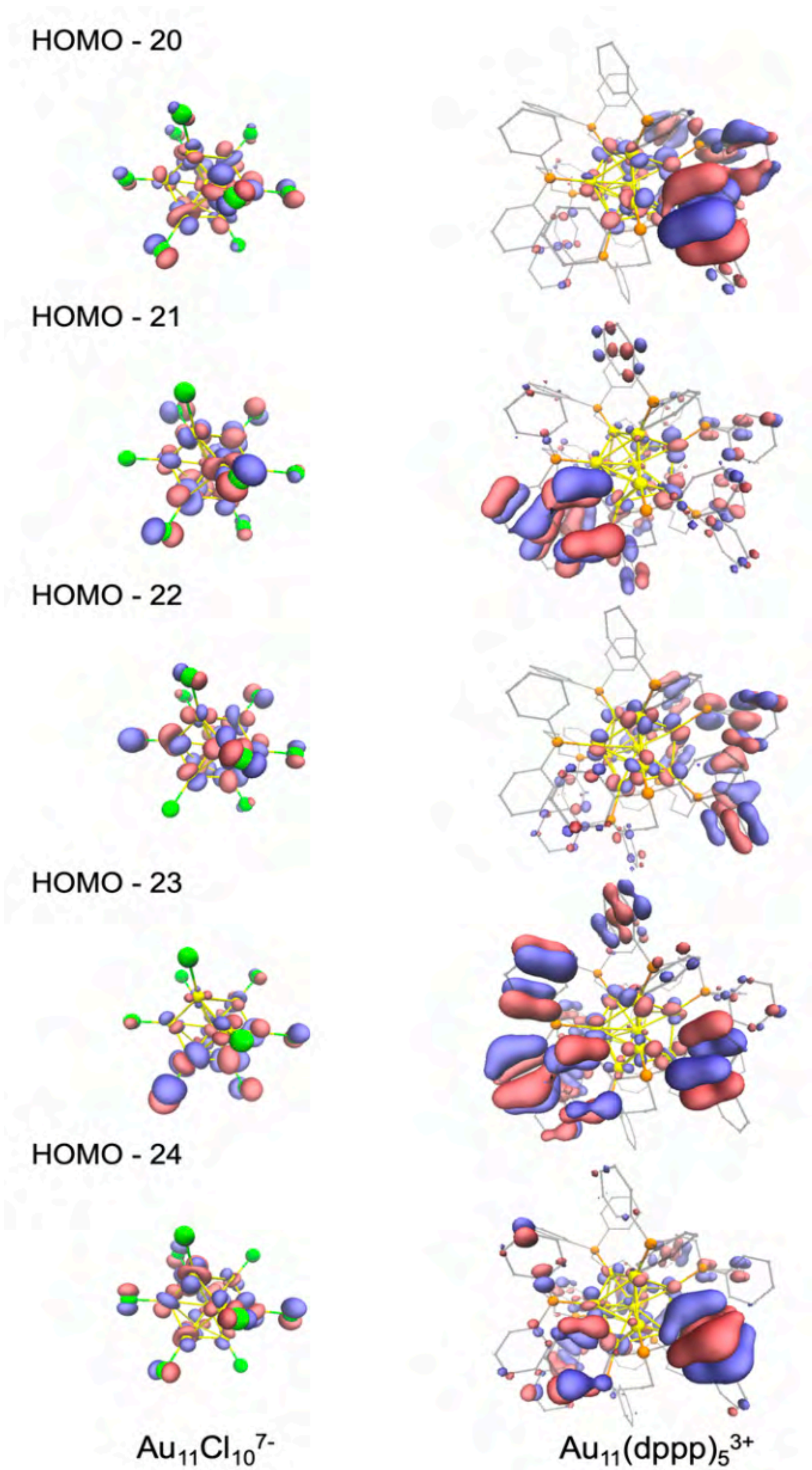

Figure A30. KS orbitals of $Au_{11}Cl_{10}^{7-}$ and $Au_{11}(dppp)_5^{3+}$ near their frontier orbitals.

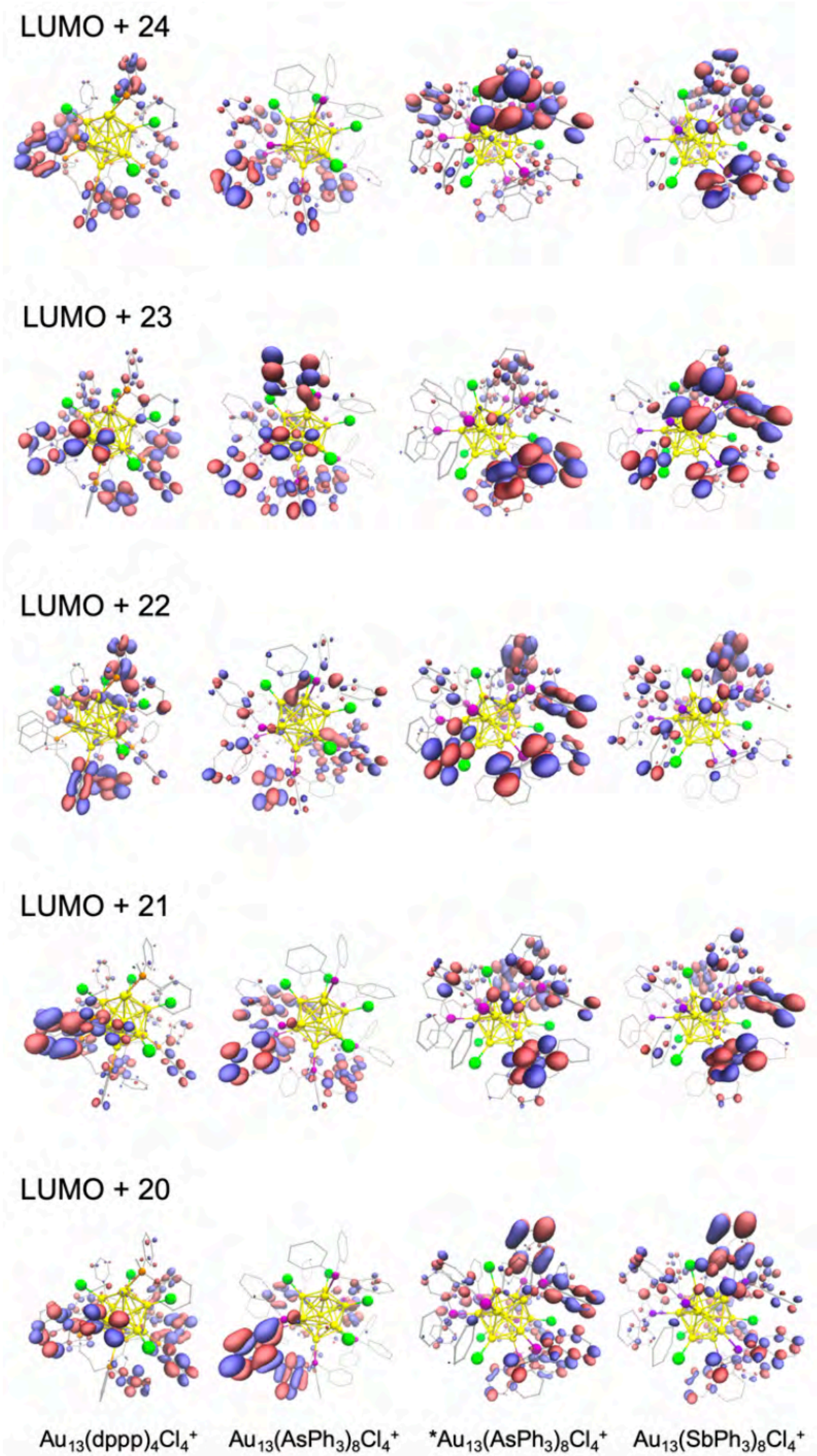
LUMO + 24
LUMO + 23
LUMO + 22
LUMO + 21
LUMO + 20
$Au_{13}(dppp)_4Cl_4^+$
$Au_{13}(AsPh_3)_8Cl_4^+$
$*Au_{13}(AsPh_3)_8Cl_4^+$
$Au_{13}(SbPh_3)_8Cl_4^+$

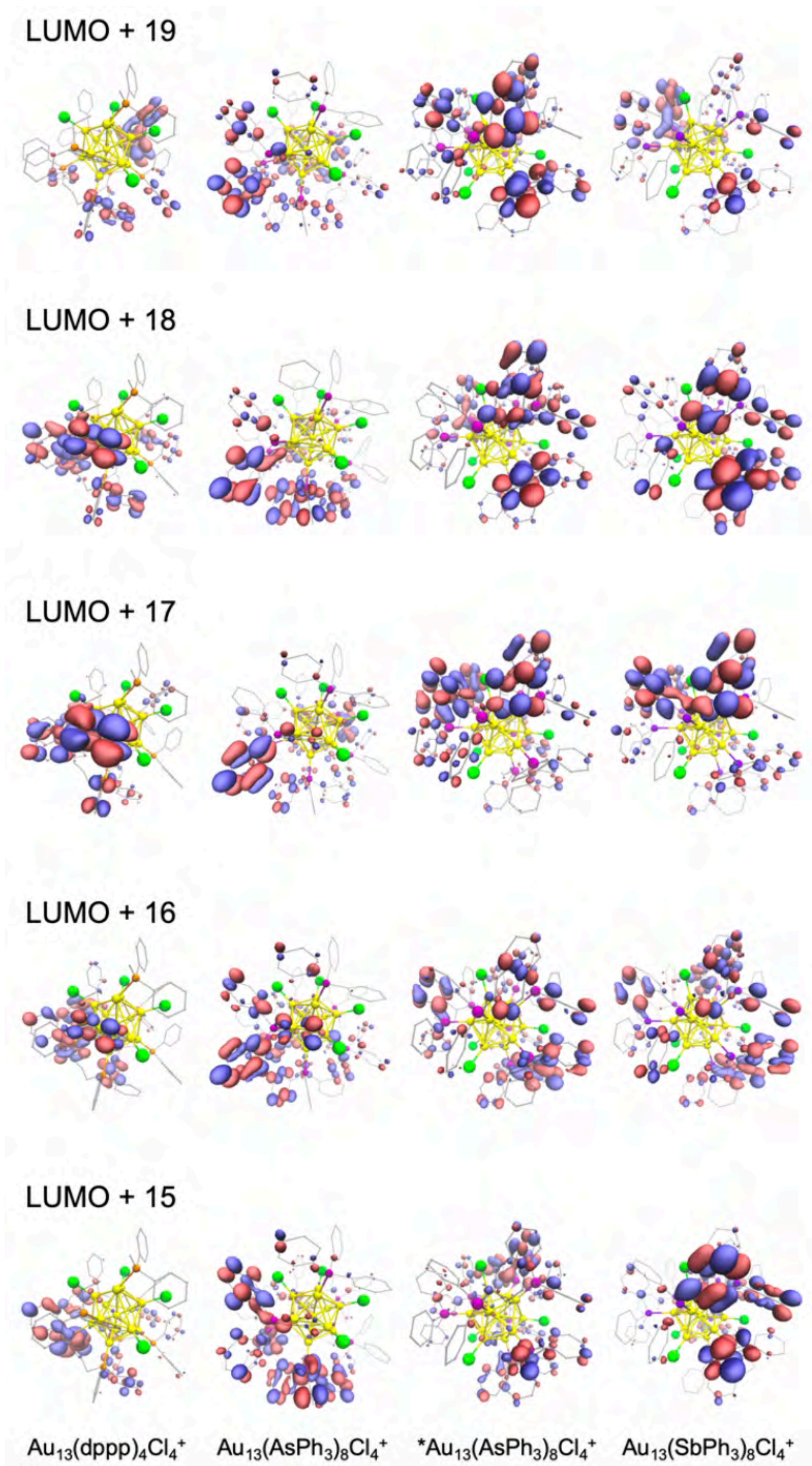
LUMO + 19
LUMO + 18
LUMO + 17
LUMO + 16
LUMO + 15
$Au_{13}(dppp)_4Cl_4^+$
$Au_{13}(AsPh_3)_8Cl_4^+$
$^*Au_{13}(AsPh_3)_8Cl_4^+$
$Au_{13}(SbPh_3)_8Cl_4^+$

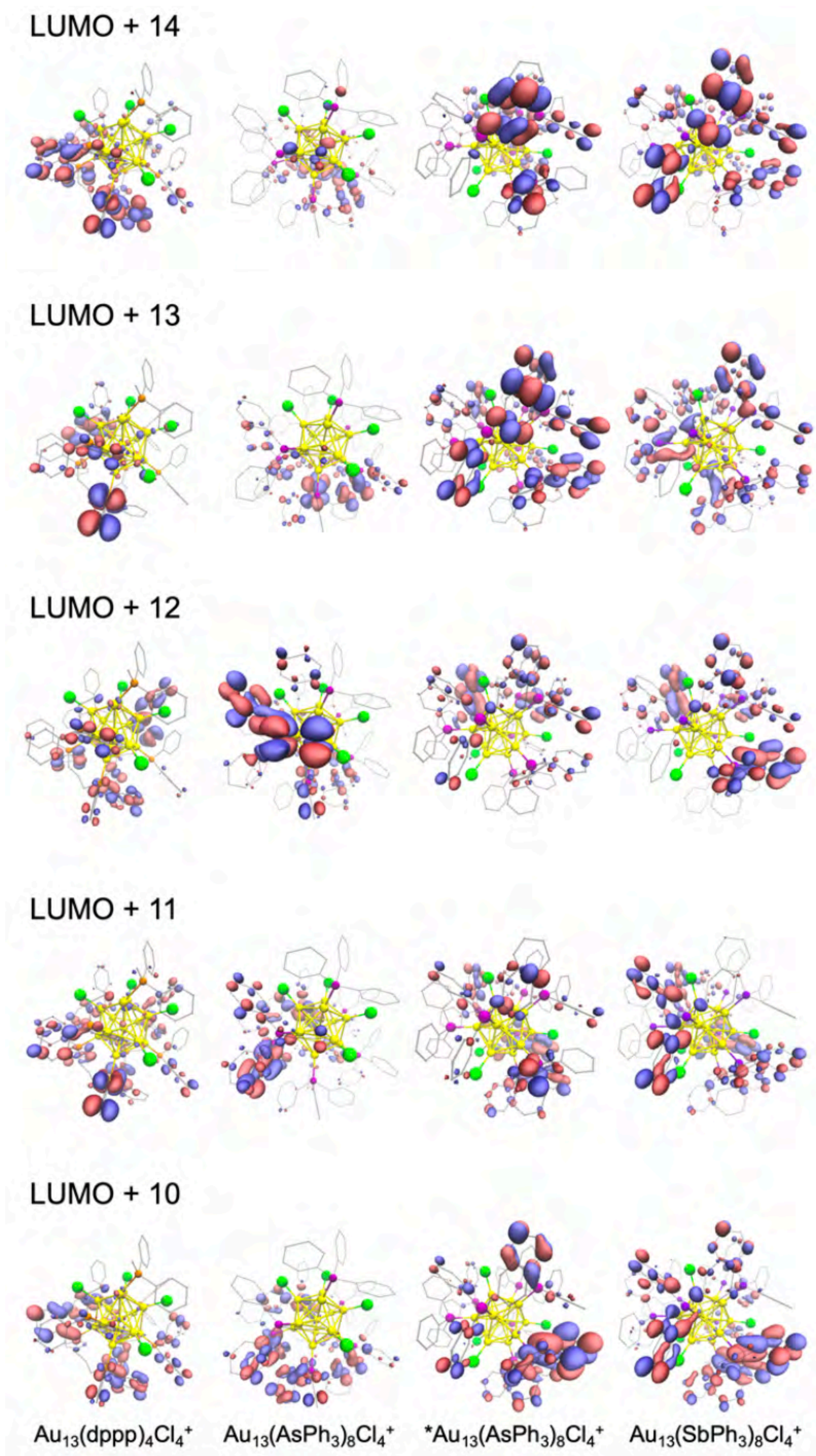
LUMO + 14
LUMO + 13
LUMO + 12
LUMO + 11
LUMO + 10
Au13(dppp)4Cl4+
Au13(AsPh3)8Cl4+
*Au13(AsPh3)8Cl4+
Au13(SbPh3)8Cl4+

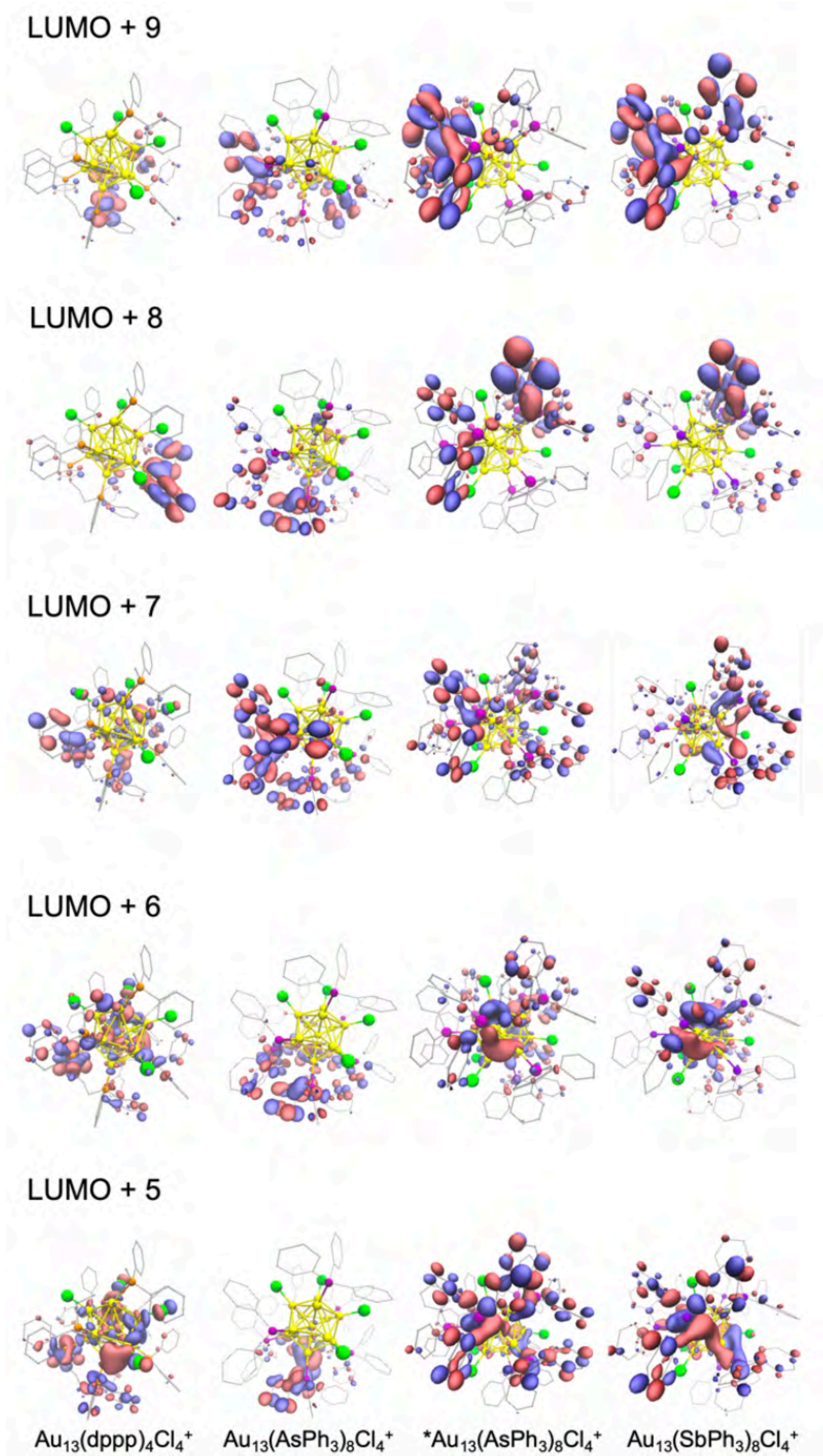
LUMO + 9
LUMO + 8
LUMO + 7
LUMO + 6
LUMO + 5
$Au_{13}(dppp)_4Cl_4^+$
$Au_{13}(AsPh_3)_8Cl_4^+$
$^*Au_{13}(AsPh_3)_8Cl_4^+$
$Au_{13}(SbPh_3)_8Cl_4^+$

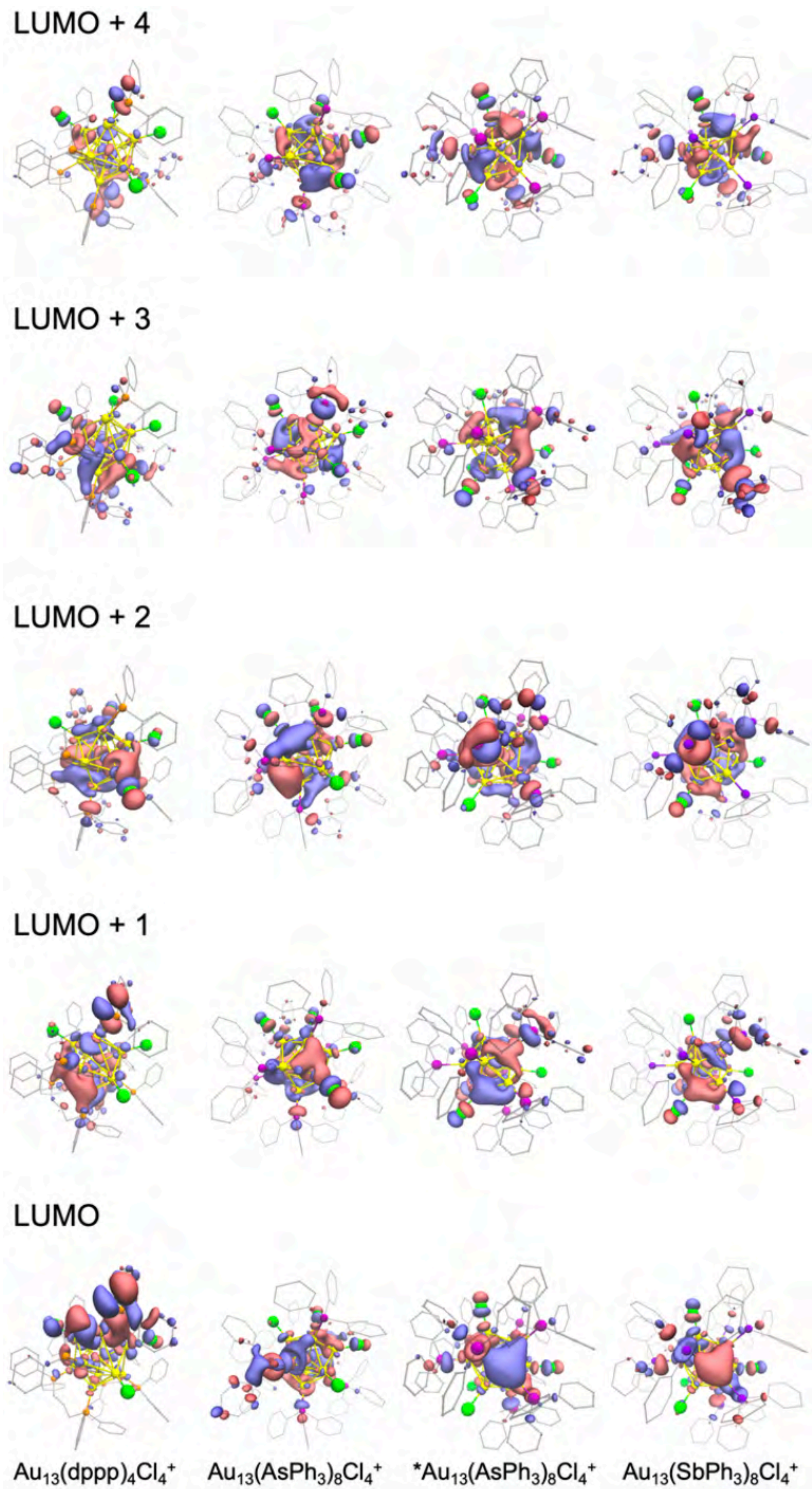

LUMO + 4
LUMO + 3
LUMO + 2
LUMO + 1
LUMO
$Au_{13}(dppp)_4Cl_4^+$
$Au_{13}(AsPh_3)_8Cl_4^+$
$*Au_{13}(AsPh_3)_8Cl_4^+$
$Au_{13}(SbPh_3)_8Cl_4^+$

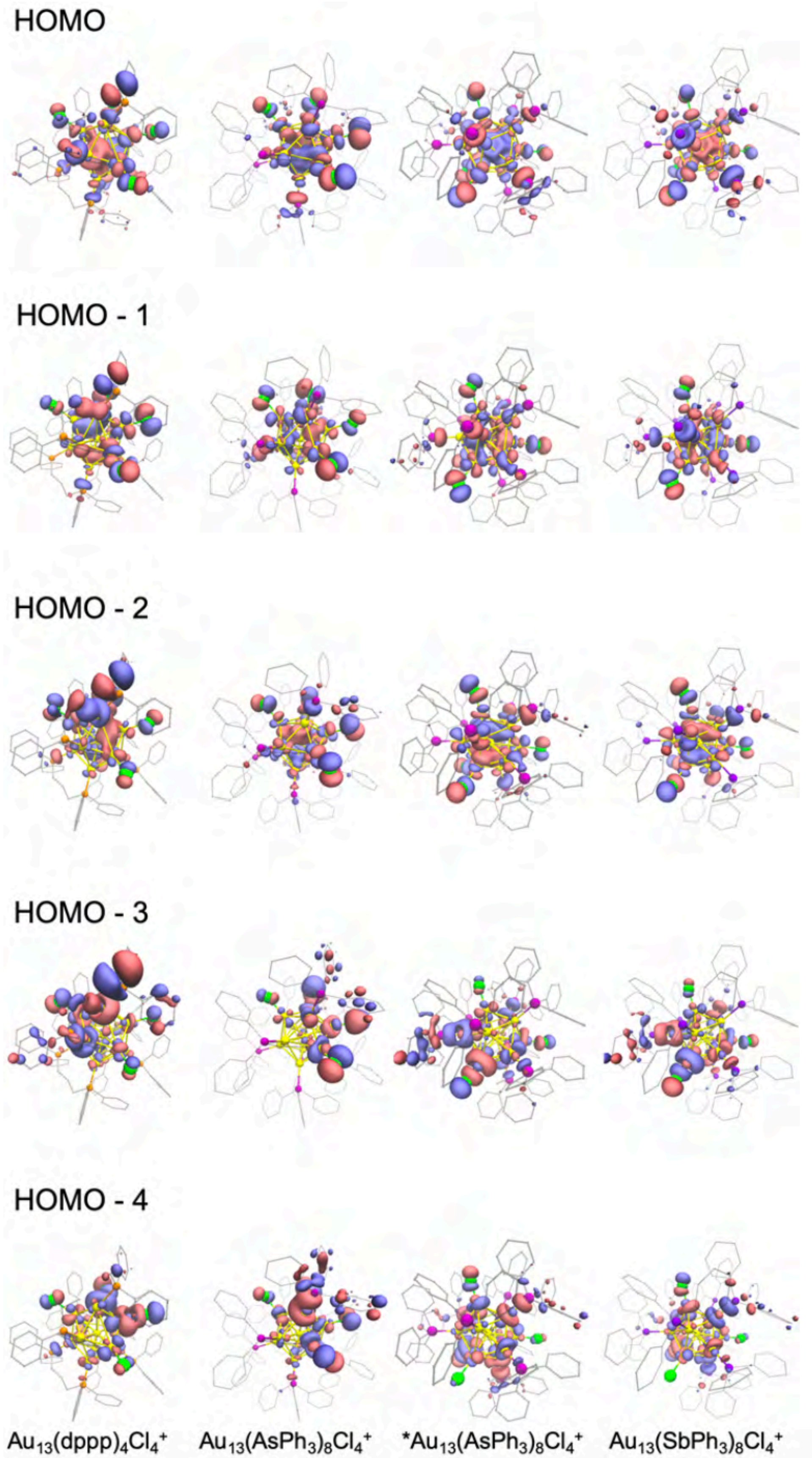
HOMO
HOMO - 1
HOMO - 2
HOMO - 3
HOMO - 4
$Au_{13}(dppp)_4Cl_4^+$
$Au_{13}(AsPh_3)_8Cl_4^+$
$*Au_{13}(AsPh_3)_8Cl_4^+$
$Au_{13}(SbPh_3)_8Cl_4^+$

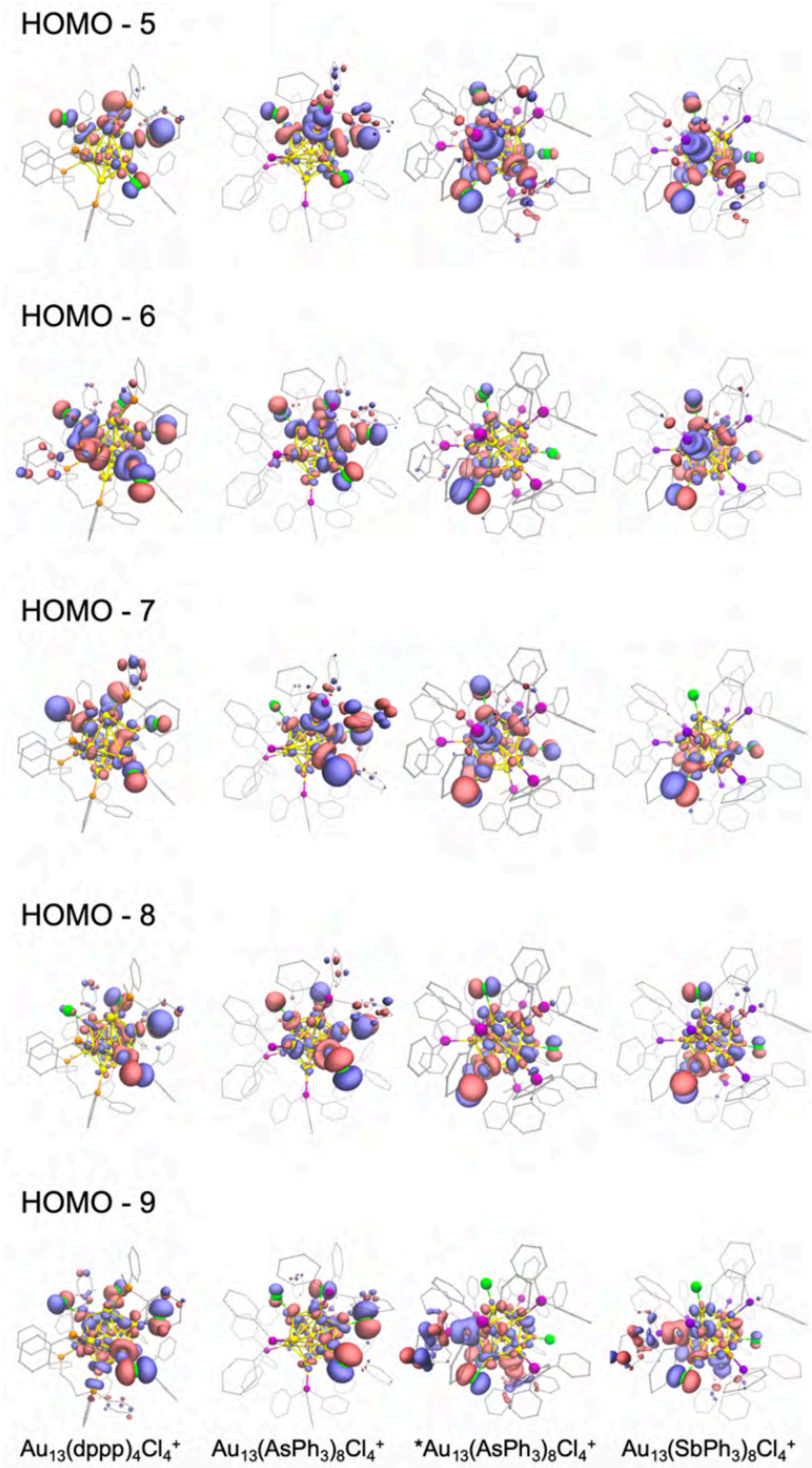

HOMO - 5
HOMO - 6
HOMO - 7
HOMO - 8
HOMO - 9
$Au_{13}(dppp)_4Cl_4^+$
$Au_{13}(AsPh_3)_8Cl_4^+$
$*Au_{13}(AsPh_3)_8Cl_4^+$
$Au_{13}(SbPh_3)_8Cl_4^+$

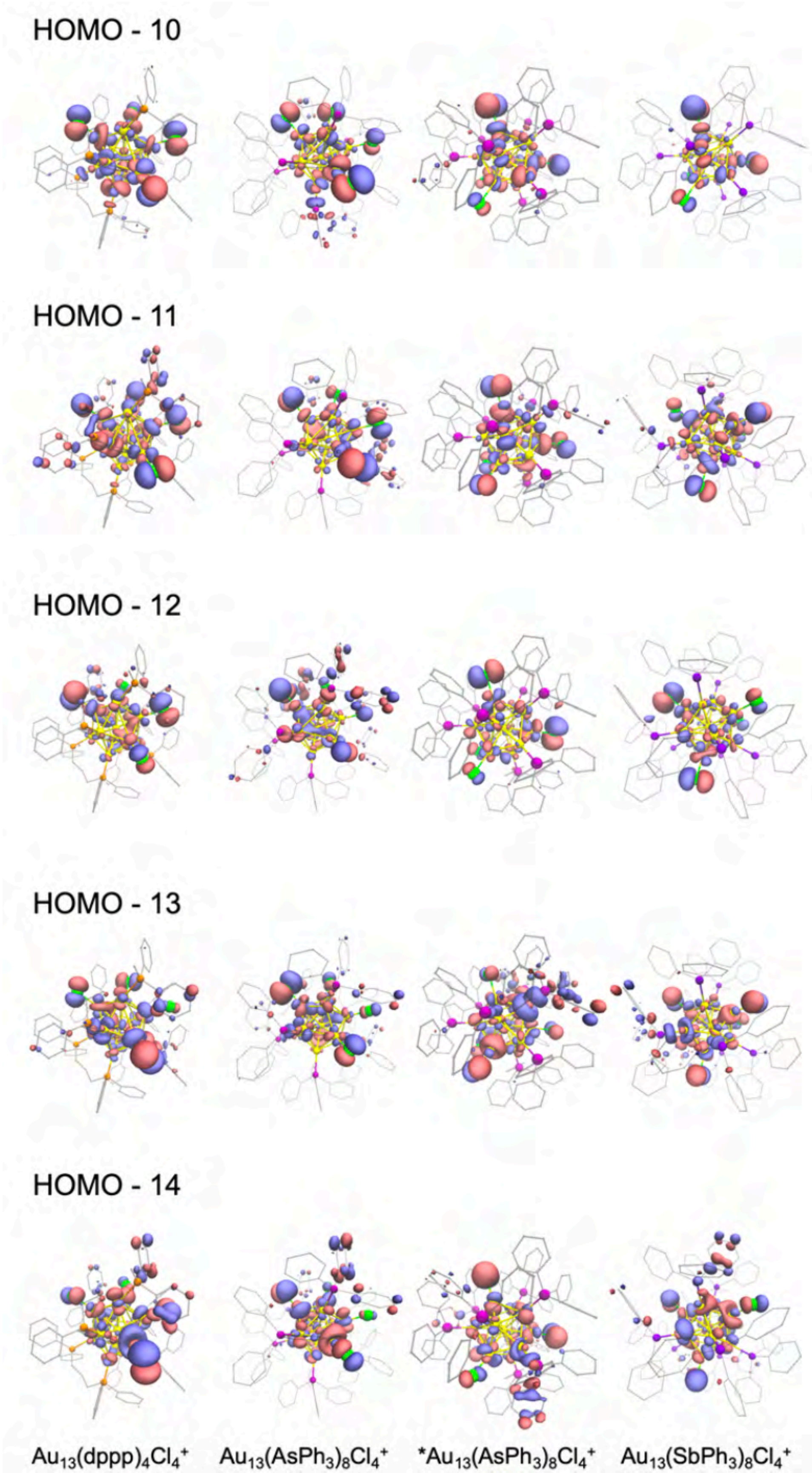
HOMO - 10
HOMO - 11
HOMO - 12
HOMO - 13
HOMO - 14
Au13(dppp)4Cl4+
Au13(AsPh3)8Cl4+
*Au13(AsPh3)8Cl4+
Au13(SbPh3)8Cl4+

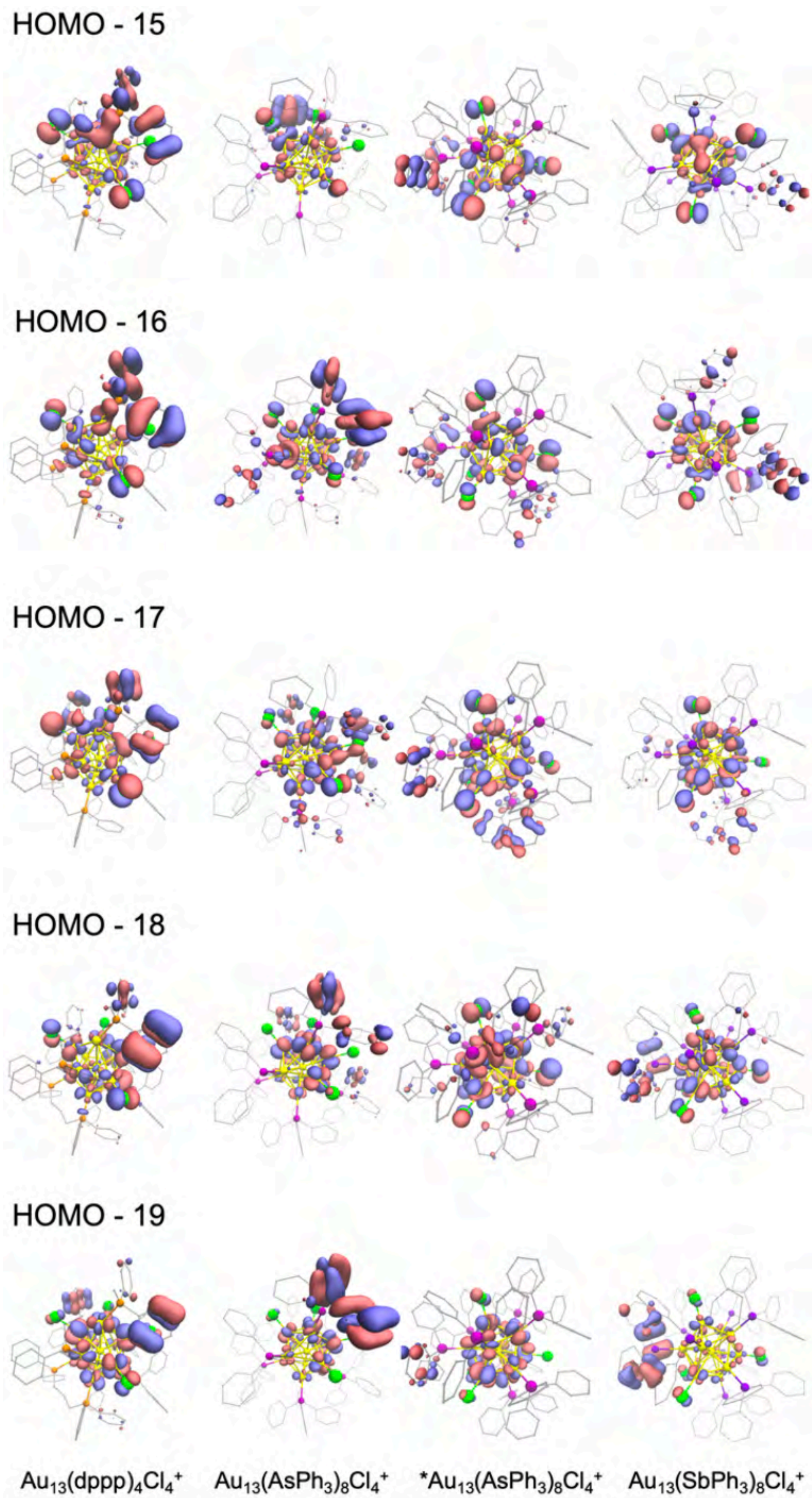
HOMO - 15
HOMO - 16
HOMO - 17
HOMO - 18
HOMO - 19
$Au_{13}(dppp)_4Cl_4^+$
$Au_{13}(AsPh_3)_8Cl_4^+$
$*Au_{13}(AsPh_3)_8Cl_4^+$
$Au_{13}(SbPh_3)_8Cl_4^+$

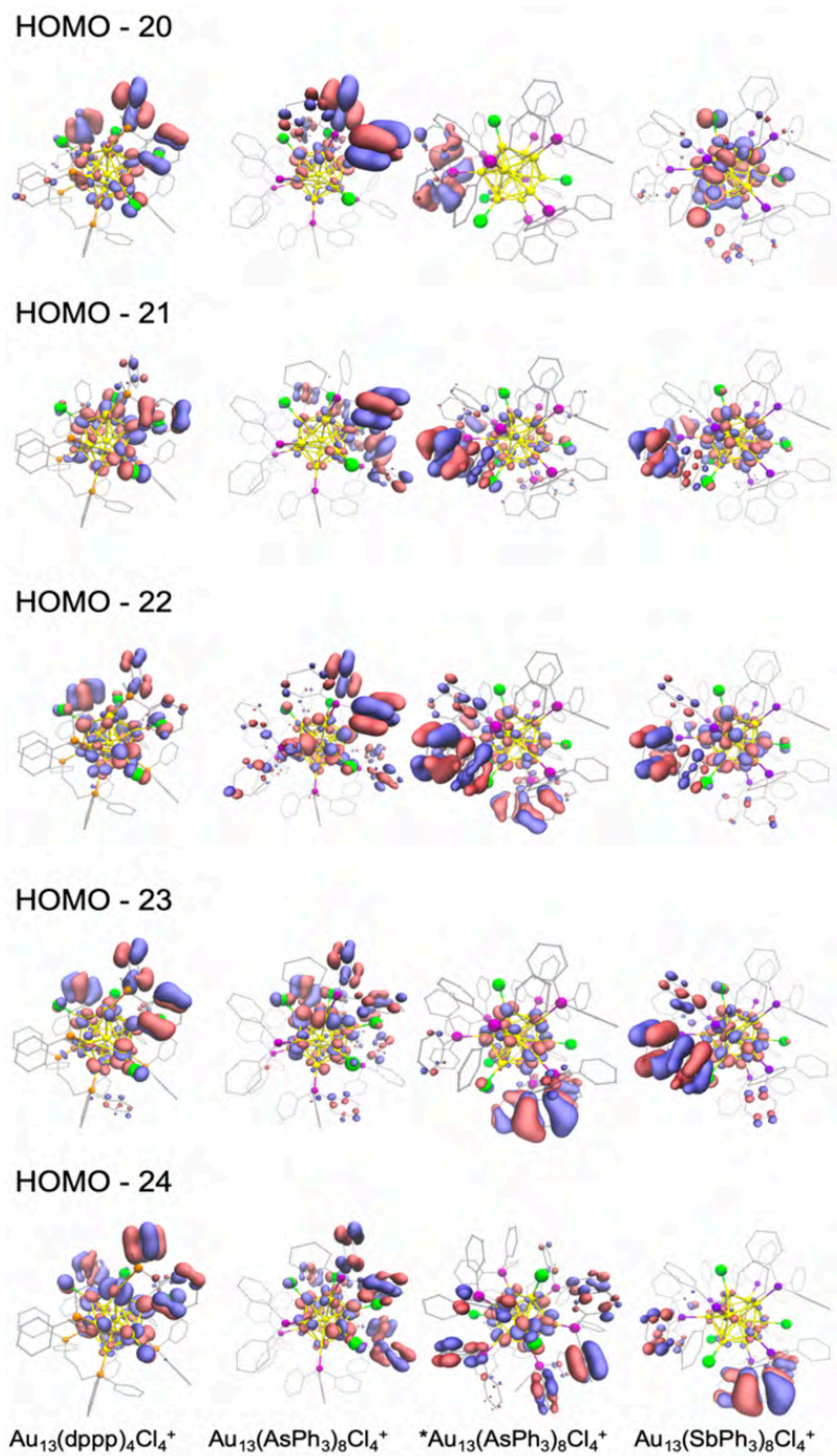

Figure A31. KS orbitals of Au_{13}NCs with different pnictide ligands. *$Au_{13}(AsPh_3)_8Cl_4^+$ represents the $Au_{13}(AsPh_3)_8Cl_4^+$ with similar halide orientation with $Au_{13}(SbPh_3)_8Cl_4^+$.

Following **Figures** are the lists of xyz coordination of geometrically optimized structures using CP2K Quickstep method. Information on the calculation method is in Computational Details section.

Coordinates of optimized structure of PPh_3

P	20.8229836	19.92949182	21.36067085
C	19.19651728	19.70273086	20.52341567
C	21.45457939	21.47218384	20.57887313
C	21.86592199	18.66031191	20.52563256
C	19.01150603	18.97267250	19.33811800
C	20.76701924	22.20643185	19.60073106
C	22.59110083	18.87814579	19.34192374
C	18.07524743	20.29322736	21.13374190
C	22.70904171	21.93673576	21.01605800
C	21.93143950	17.39444546	21.13301145
C	17.74058950	18.84919508	18.77134314
C	21.33066321	23.36524246	19.05835615
C	23.35087655	17.85044884	18.77690416
C	16.80773016	20.18181880	20.55909570
C	23.27698794	23.08354735	20.46244984
C	22.68228529	16.36525366	20.56226830
C	16.63754050	19.45755033	19.37552749
C	22.58766142	23.80329303	19.48090001
C	23.39557908	16.59081681	19.38185059
H	19.86565406	18.49697460	18.85565068
H	19.79204436	21.86500826	19.25334182
H	22.56070561	19.85582040	18.86006261
H	18.19852385	20.84371283	22.06875203
H	23.25276257	21.38479505	21.78569200
H	21.38912528	17.21688763	22.06392187
H	17.61263690	18.27670354	17.85097230
H	20.78800479	23.92101586	18.29168628
H	23.90829074	18.03245912	17.85629044
H	15.95010902	20.65208019	21.04291361
H	24.25943045	23.41837109	20.80001171
H	22.71564616	15.38703373	21.04515465
H	15.64632796	19.36152757	18.93085667
H	23.02727550	24.70508956	19.05388258
H	23.98810595	15.78947923	18.93882562

Figure A32. Optimized coordinates of PPh_3.

Coordinates of optimized structure of AuCl

Au	3.867713656	4.999999987	4.999999997
Cl	6.132203821	5.000000003	4.999999994

Figure A33. Optimized coordinates of AuCl.

Coordinates of optimized structure for Au-PPh_3

Au	9.973610909	8.495954277	8.289537581
P	8.174189928	7.180426902	7.850062329
C	8.469961483	6.195892431	6.384619955
C	8.824570125	6.853768990	5.190025803
C	8.891565248	6.120011143	4.016280563
C	8.629115800	4.744547431	4.020129752
C	8.324500683	4.083454026	5.204297333
C	8.245040639	4.808040017	6.397725383
C	6.747343897	8.244897256	7.578775361
C	6.261894066	8.968540075	8.684536208
C	5.132596464	9.766446187	8.538975204
C	4.494290030	9.856410556	7.297515428
C	4.981837883	9.148320904	6.199001695
C	6.108800340	8.337079836	6.332889361
C	7.767783622	6.164915297	9.273556448
C	6.500344089	5.545485782	9.270058651
C	6.056481413	4.879279557	10.41092411
C	6.862604313	4.855719819	11.55043707
C	8.128649091	5.452159254	11.54783856
C	8.592160047	6.105747129	10.40962925
H	9.031767631	7.924511958	5.174376878
H	9.118628078	6.597388774	3.050433670
H	8.658746594	4.220455262	3.051119993
H	8.143985630	3.008178965	5.195799508
H	7.992591064	4.301667235	7.327718250
H	6.755811204	8.893563843	9.654032299
H	4.745838535	10.32180318	9.392500935
H	3.607853196	10.47787511	7.188913493
H	4.484823758	9.221426132	5.231064756
H	6.471447075	7.771689666	5.476576066
H	5.851526023	5.614995904	8.395954256
H	5.071393961	4.414471693	10.42389510
H	6.508927083	4.438841166	12.51098605
H	8.682227050	5.461581592	12.50606906
H	9.563257862	6.601965689	10.42284818

Figure A34. Optimized coordinates of Au-PPh_3.

Coordinates of optimized structure for $Au(PPh_3)Cl$

Au	11.82402954	10.51778375	11.10076117
Cl	13.87264131	11.36042954	11.74081244
P	9.792764895	9.727331842	10.46853808
C	9.811902494	8.782042930	8.909214081
C	10.66663009	9.218085183	7.883323079
C	10.65505109	8.577411427	6.644671206
C	9.802544251	7.491860335	6.423820651
C	8.965890372	7.042741829	7.447622792
C	8.966860768	7.684003493	8.688891207
C	8.581402259	11.05922022	10.17279206
C	8.525846792	12.12526330	11.08694742
C	7.605509542	13.15666779	10.90261931
C	6.747313038	13.14337656	9.798681792
C	6.809249587	12.09306565	8.880881758
C	7.719481175	11.04948593	9.066688819
C	8.999738071	8.634327494	11.69316178
C	7.604946008	8.564099945	11.83881869
C	7.045459744	7.698379886	12.78116590
C	7.870346212	6.904281542	13.58229052
C	9.259168457	6.972919982	13.44018411
C	9.824549947	7.838589161	12.50352342
H	11.34811610	10.05133468	8.062641268
H	11.31932395	8.920188717	5.851177769
H	9.794773214	6.989801620	5.456112900
H	8.304720707	6.191921128	7.279863438
H	8.309048936	7.327905144	9.481826752
H	9.215353786	12.15353232	11.93191196
H	7.568482144	13.98207069	11.61393584
H	6.037615696	13.95729624	9.646951170
H	6.151031592	12.08396966	8.011627645
H	7.767416484	10.23702618	8.341988043
H	6.959139188	9.194509031	11.22669746
H	5.962151779	7.653228209	12.89596122
H	7.430322013	6.240585082	14.32723087
H	9.906097269	6.363947182	14.07167350
H	10.90918880	7.915623979	12.41005739

Figure A35. Optimized coordinates of $Au(PPh_3)Cl$.

Coordinates of optimized structure for $Au(PPh_3)Br$

Au	11.83711336	10.52015143	11.01079786
Br	14.01530938	11.42090904	11.64241930
P	9.786524755	9.724144885	10.42288941
C	9.781112257	8.750596527	8.878264392
C	10.57263555	9.197605834	7.805846861
C	10.56536987	8.507717265	6.592975941
C	9.784652716	7.356708000	6.445080029
C	9.007227916	6.900795943	7.512294927

C	9.001219108	7.594629055	8.725212547
C	8.587584854	11.07158328	10.14714116
C	8.477115445	12.06231066	11.13825353
C	7.570955449	13.11073136	10.98265884
C	6.780992073	13.18986570	9.829982665
C	6.899585058	12.21588159	8.836725811
C	7.796140593	11.15485992	8.993211757
C	9.007589977	8.658511507	11.68271997
C	7.612434584	8.572550759	11.82276237
C	7.057300659	7.715460866	12.77566153
C	7.886197197	6.945007139	13.59654862
C	9.274815681	7.038066577	13.46939637
C	9.835881771	7.892770573	12.51923537
H	11.20153797	10.08086376	7.930081927
H	11.18261751	8.86247119	5.767006144
H	9.788954523	6.812616754	5.499549389
H	8.403634169	5.998703821	7.405851070
H	8.397171164	7.228677267	9.555239376
H	9.108970415	12.01480342	12.02684582
H	7.490319757	13.87447726	11.75712656
H	6.081503486	14.01718569	9.702259894
H	6.296160163	12.27802842	7.930659638
H	7.883472593	10.39926659	8.212813297
H	6.961184908	9.180197916	11.19323162
H	5.974186242	7.654767550	12.88172033
H	7.449644363	6.280968599	14.34380475
H	9.927642302	6.458149722	14.12243900
H	10.92012714	7.986521135	12.43699597

Figure A36. Optimized coordinates of Au(PPh_3)Br.

Coordinates of optimized structure for Au(PPh_3)I

Au	11.74580169	10.50918284	11.05927540
I	14.00242746	11.58477694	11.80097004
P	9.700388827	9.687409942	10.42718906
C	9.712865864	8.716952329	8.884802281
C	10.50858024	9.183420944	7.824673695
C	10.53553042	8.493473379	6.613331728
C	9.783961410	7.324284640	6.455308239
C	9.001137283	6.850526835	7.510754161
C	8.962560651	7.542766332	8.723953231
C	8.532170935	11.05858015	10.13989342
C	8.435633723	12.04438785	11.13752613
C	7.571371187	13.12499075	10.97314839
C	6.811200997	13.24392331	9.804870784
C	6.919400358	12.27656809	8.803515988
C	7.772748410	11.18167076	8.969126767
C	8.897209324	8.628505239	11.67351736
C	7.500832608	8.571973907	11.80859988

C	6.927784072	7.740233205	12.77239443
C	7.738594901	6.962101493	13.60338578
C	9.129186669	7.018942117	13.47301728
C	9.709481342	7.851955001	12.51518760
H	11.11539955	10.08065245	7.959859402
H	11.15836115	8.860536739	5.797392763
H	9.816978520	6.778048433	5.511870893
H	8.422588652	5.933444945	7.395556179
H	8.359087012	7.161315097	9.547936709
H	9.053607019	11.97149445	12.03431839
H	7.502574198	13.88284143	11.75391714
H	6.142635028	14.09550807	9.671640412
H	6.339584356	12.37010522	7.885269891
H	7.854179422	10.43159861	8.182039750
H	6.863363782	9.186230352	11.17118792
H	5.843253602	7.705555768	12.87772950
H	7.284086551	6.322469404	14.36120423
H	9.765998660	6.427140071	14.13054308
H	10.79539919	7.918802138	12.42987503

Figure A37. Optimized coordinates of $Au(PPh_3)I$.

Coordinates of optimized structure for $Au_2(dppp)Cl$

Au	18.81178760	17.10617845	20.20741049
Au	20.47689569	18.31237436	22.89006972
P	19.81689284	18.34081118	18.58062543
P	19.13102072	20.14749876	22.81263871
Cl	17.53971108	15.94349358	21.76182483
Cl	21.98643901	16.54492069	22.99678456
C	19.45213272	16.45612119	16.59961522
H	19.79244071	15.75980875	17.36808272
C	19.32271441	17.82259087	16.90384671
C	21.63953036	18.32693268	18.51725863
C	21.05605926	21.57978392	24.22532366
H	21.39067158	20.59622095	24.55884959
C	19.39894949	20.13556813	18.70167230
H	20.00189335	20.66294804	17.94731812
H	18.33898397	20.25594875	18.42921628
C	17.62390352	20.06279930	23.83243987
C	19.97973818	21.67525023	23.32946578
C	18.52876308	20.46149012	21.10574631
H	17.98554853	19.53671119	20.84780119
H	17.79057105	21.27723061	21.10686082
C	18.85662196	18.70333510	15.9165403
H	18.74127034	19.76672892	16.1250456
C	22.31228602	18.88796825	17.41654717
H	21.75064245	19.29578106	16.57413792
C	16.68629769	19.05207673	23.55453102
H	16.85766722	18.33143471	22.75225399
C	24.43738562	18.34733437	18.44296884

H	25.52775050	18.35923083	18.41173236
C	21.70188081	22.73241558	24.67568032
H	22.53418178	22.64700524	25.37438593
C	21.29217896	23.98818140	24.22227020
H	21.80457536	24.88811260	24.56470293
C	19.67386602	20.71161386	20.10500238
H	20.61714143	20.29010883	20.49228950
H	19.85027175	21.79367744	20.01897700
C	15.34549996	19.77978490	25.43732411
H	14.46306436	19.66336734	26.06806715
C	23.77224725	17.78002683	19.53055981
H	24.32694406	17.34524400	20.36215832
C	19.56589185	22.94260696	22.88539960
H	18.72658846	23.04109045	22.19630826
C	23.70556473	18.89546140	17.38278029
H	24.22292301	19.32199791	16.52255697
C	22.37467720	17.75997540	19.56622992
H	21.87078699	17.29947427	20.41661594
C	17.41958948	20.91966699	24.92519457
H	18.15193627	21.69015951	25.16551968
C	16.28432668	20.77252308	25.72547005
H	16.13982770	21.43258074	26.58155614
C	15.54852811	18.92302294	24.35106998
H	14.83175652	18.13105471	24.13173651
C	20.22503116	24.09135258	23.32534491
H	19.90475098	25.07042964	22.96725320
C	18.67201151	16.86656686	14.34749660
H	18.41585861	16.49452054	13.35516365
C	18.52629332	18.22267042	14.64533707
H	18.14957903	18.91174443	13.88870395
C	19.13789565	15.98462350	15.32749652
H	19.24303676	14.92268888	15.10381907

Figure A38. Optimized coordinates of Au_2(dppp)Cl_2.

Coordinates of optimized structure for Au_2(dppp)Cl_2 in different orientation

Au	18.50448759	17.22704066	21.18348873
Au	19.94647782	23.57794497	19.73118550
Cl	18.56162878	14.92734539	20.98536623
Cl	19.04331016	24.71269311	21.54014081
P	18.51052981	19.49484879	21.30815928
P	20.79554247	22.35513435	18.00752847
C	20.05796411	20.21180406	20.63384701
H	19.98844590	21.31037062	20.72354270
H	20.88516150	19.87564422	21.27703596
C	20.29445538	19.81811319	19.17176639
H	20.58760336	18.75864754	19.12328687
H	19.35858351	19.89810888	18.59630782
C	21.37924615	20.66929592	18.49169873
H	21.73235130	20.18335996	17.56959009

H	22.25014615	20.78954040	19.15277176
C	18.33619513	20.20620520	22.97365461
C	17.57436782	19.49655556	23.91687988
H	17.16212821	18.52151303	23.65336374
C	17.35030228	20.03228453	25.18537215
H	16.75034299	19.47674600	25.90659607
C	17.89505762	21.27338909	25.52917768
H	17.71637382	21.69107334	26.52077878
C	18.66731344	21.97616712	24.60184181
H	19.09421940	22.94732842	24.85462365
C	18.88563618	21.45037068	23.32650767
H	19.46381696	22.04092136	22.61746919
C	17.20186176	20.27471603	20.29379332
C	16.80883799	21.60724576	20.49961221
H	17.27497747	22.21599011	21.27406121
C	15.80080387	22.16580291	19.71032430
H	15.49693692	23.19882942	19.88479089
C	15.18651701	21.40626974	18.71031670
H	14.38646643	21.84023819	18.10850167
C	15.59066919	20.08838471	18.48587235
H	15.12480663	19.49360526	17.69944089
C	16.58951655	19.52150670	19.27904012
H	16.88771832	18.48293678	19.12543209
C	19.58514435	22.03437581	16.68371072
C	18.25257038	22.43915711	16.84852304
H	17.95210163	22.94620099	17.76574770
C	17.31262324	22.18567835	15.84694210
H	16.27997511	22.50498728	15.98711238
C	17.69428833	21.52228465	14.68079770
H	16.95981006	21.32599246	13.89890291
C	19.02068530	21.10821320	14.51305391
H	19.32059869	20.58960412	13.60167526
C	19.96421274	21.36291330	15.50779689
H	20.99889967	21.04920327	15.36145197
C	22.23096311	23.12965312	17.19398039
C	22.03998316	23.96690754	16.08307859
H	21.04277690	24.09390284	15.66203600
C	23.12395923	24.63317500	15.50933053
H	22.95906771	25.28377957	14.64963173
C	24.40807425	24.46935015	16.03448493
H	25.25161210	24.99568398	15.58721448
C	24.60548082	23.63997660	17.14128969
H	25.60456596	23.51030178	17.55884814
C	23.52278693	22.97852264	17.72446989
H	23.69494750	22.35535439	18.60186485

Figure A39. Optimized coordinates of $Au_2(dppp)Cl_2$ in different orientation.

Coordinates of optimized structure for $Au(SbPh_3)Cl$

Au	11.98610360	10.56495925	11.19289660

Cl	14.03368463	11.37871839	11.85303448
As	9.845260712	9.737669161	10.52009399
C	9.812498447	8.686281042	8.866116224
C	10.64981585	9.078138859	7.814493515
C	10.59639309	8.393752048	6.597327934
C	9.723063435	7.313292160	6.438062206
C	8.901145231	6.915880847	7.495340777
C	8.941350812	7.602796467	8.711406147
C	8.505162022	11.12664613	10.16868182
C	8.348521299	12.14620521	11.11599211
C	7.409037739	13.15605104	10.89647069
C	6.644407831	13.15920850	9.725648817
C	6.812593672	12.14753401	8.778099639
C	7.740076240	11.12447955	8.997972252
C	8.963502701	8.585003373	11.83618765
C	7.568692239	8.534986291	11.94021656
C	6.976071406	7.685944315	12.87899725
C	7.774222158	6.894694314	13.70973135
C	9.166928295	6.953157005	13.60799411
C	9.765794725	7.799675159	12.67203677
H	11.34723915	9.907435730	7.945819318
H	11.24399009	8.700360811	5.775679389
H	9.687696407	6.774348549	5.491080754
H	8.226464980	6.066537729	7.379956175
H	8.300027868	7.289722925	9.535096763
H	8.965621433	12.16254296	12.01599178
H	7.283349026	13.94910275	11.63438831
H	5.922208485	13.95681716	9.547458578
H	6.229022774	12.15657657	7.856726543
H	7.872703072	10.34179051	8.251180823
H	6.944998858	9.165900779	11.30553785
H	5.889607192	7.650928169	12.96620900
H	7.309427526	6.240330485	14.44746498
H	9.791501006	6.348112257	14.26575354
H	10.85322277	7.858826237	12.60187792

Figure A40. Coordinates for optimized structure of $Au(AsPh_3)Cl$.

Coordinates of optimized structure for $Au(SbPh_3)Cl$

Au	11.98610360	10.56495925	11.19289660
Cl	14.03368463	11.37871839	11.85303448
As	9.845260712	9.737669161	10.52009399
C	9.812498447	8.686281042	8.866116224
C	10.64981585	9.078138859	7.814493515
C	10.59639309	8.393752048	6.597327934
C	9.723063435	7.313292160	6.438062206
C	8.901145231	6.915880847	7.495340777
C	8.941350812	7.602796467	8.711406147
C	8.505162022	11.12664613	10.16868182
C	8.348521299	12.14620521	11.11599211

C	7.409037739	13.15605104	10.89647069
C	6.644407831	13.15920850	9.725648817
C	6.812593672	12.14753401	8.778099639
C	7.740076240	11.12447955	8.997972252
C	8.963502701	8.585003373	11.83618765
C	7.568692239	8.534986291	11.94021656
C	6.976071406	7.685944315	12.87899725
C	7.774222158	6.894694314	13.70973135
C	9.166928295	6.953157005	13.60799411
C	9.765794725	7.799675159	12.67203677
H	11.34723915	9.907435730	7.945819318
H	11.24399009	8.700360811	5.775679389
H	9.687696407	6.774348549	5.491080754
H	8.226464980	6.066537729	7.379956175
H	8.300027868	7.289722925	9.535096763
H	8.965621433	12.16254296	12.01599178
H	7.283349026	13.94910275	11.63438831
H	5.922208485	13.95681716	9.547458578
H	6.229022774	12.15657657	7.856726543
H	7.872703072	10.34179051	8.251180823
H	6.944998858	9.165900779	11.30553785
H	5.889607192	7.650928169	12.96620900
H	7.309427526	6.240330485	14.44746498
H	9.791501006	6.348112257	14.26575354
H	10.85322277	7.858826237	12.60187792

Figure A41. Coordinates for optimized structure of $Au(SbPh_3)Cl$.

Coordinates of optimized structure for $Au(BiPh_3)Cl$

Au	12.34779549	10.87947780	11.40561352
Cl	14.21617587	11.91207817	12.25335204
Bi	10.07385420	9.855379535	10.52988960
C	9.912574484	8.642074431	8.628695550
C	10.66894235	9.001965903	7.509479033
C	10.56751252	8.244586828	6.337358279
C	9.723284648	7.131723521	6.292400847
C	8.977594877	6.771798645	7.417588064
C	9.069441309	7.527438885	8.591980135
C	8.503910037	11.43706911	10.18449942
C	8.300989473	12.38873939	11.19004724
C	7.377956431	13.41983550	10.99026510
C	6.675438097	13.50627459	9.784941167
C	6.885054429	12.55507027	8.783197331
C	7.798072424	11.51211934	8.981107081
C	8.956505586	8.494040255	11.93441532
C	7.559642414	8.522800469	11.96546721
C	6.868928549	7.650320906	12.81419225
C	7.575278948	6.757836968	13.62498594
C	8.972345638	6.738670582	13.59442670
C	9.668490404	7.607701347	12.74810849

H	11.34609700	9.857849359	7.539252191
H	11.15691666	8.523418167	5.463094478
H	9.652887371	6.539093245	5.380316432
H	8.323907420	5.898777719	7.388053971
H	8.490058090	7.235417845	9.468705746
H	8.860107283	12.34465027	12.12648187
H	7.217394244	14.16035858	11.77492383
H	5.970116405	14.32158662	9.621856898
H	6.344580943	12.62446926	7.838159807
H	7.959161827	10.77682317	8.190924680
H	7.003929045	9.224989827	11.34177434
H	5.778735408	7.671670175	12.84116847
H	7.036260172	6.079823222	14.28775589
H	9.526619871	6.046883606	14.22913304
H	10.75959803	7.588085569	12.73817945

Figure A42. Optimized coordinates of $Au(BiPh_3)Cl$.

Coordinates of optimized structure for Au_{11}^{3+}

Au	21.40353316	19.63679396	21.54486392
Au	19.2134999	23.04088317	18.69991458
Au	19.17821652	20.32315852	17.89578355
Au	18.76576921	18.84592723	20.48898181
Au	19.44962396	21.70085924	21.18856689
Au	17.19240366	21.1534543	19.65946803
Au	21.1811281	18.50411054	18.83638821
Au	18.70718476	17.61087964	18.01917487
Au	19.11882095	19.72513255	23.0820024
Au	21.48174163	21.47768993	19.17052184
Au	23.49434261	19.70685889	19.74363861

Figure A43. Coordinates for optimized structure of Au_{11}^{3+}.

Coordinates of optimized structure for $Au_{11}(PPh_3)_7Cl_2^+$

Au	19.90878	20.20860	20.12783
Au	18.57571	22.25516	18.72639
Au	20.77734	20.55001	17.52964
Au	18.61293	17.98236	21.08659
Au	19.11329	22.46111	21.62666
Au	17.18870	20.51274	20.62269
Au	20.87281	17.81588	19.13147
Au	18.26080	19.04658	18.18610
Au	20.30302	20.02215	22.80413
Au	21.46482	22.45803	19.74169
Au	22.54641	19.77612	20.56160
P	17.23159	23.74818	17.54564

P	21.38772	20.73102	15.28201
P	14.96831	20.45002	21.29208
P	17.71404	15.96224	21.83998
P	20.70259	20.00272	25.10978
P	21.66683	15.75992	18.34990
P	24.83922	19.38193	20.72198
P	22.51519	24.53333	19.99405
Cl	16.80397	18.05433	16.53924
Cl	18.48206	24.45624	22.79456
C	19.43811	24.57130	16.10881
H	19.96330	24.41158	17.05161
C	20.13975	24.99783	14.98402
H	21.21286	25.17276	15.05330
C	19.47397	25.17066	13.76762
H	20.03002	25.48403	12.88326
C	18.10228	24.92382	13.68042
H	17.58359	25.04443	12.72872
C	17.39126	24.50538	14.80718
H	16.32446	24.29585	14.72705
C	18.05678	24.32736	16.02824
C	16.44793	26.46609	17.77910
H	16.55168	26.54126	16.69594
C	16.02050	27.57383	18.51407
H	15.77549	28.50339	17.99833
C	15.92242	27.49796	19.90845
H	15.59688	28.36835	20.48029
C	16.27056	26.31672	20.56784
H	16.25436	26.25249	21.65627
C	16.68270	25.20240	19.83620
H	16.97948	24.29627	20.36301
C	16.75921	25.26440	18.43906
C	14.51347	23.74969	16.74471
H	14.51472	24.82548	16.91998
C	13.35889	23.13037	16.26339
H	12.47315	23.73152	16.05439
C	13.33355	21.74708	16.06069
H	12.42822	21.26712	15.68573
C	14.46152	20.97776	16.35657
H	14.46345	19.89531	16.22224
C	15.61946	21.59290	16.83524
H	16.48959	20.97774	17.07112
C	15.66001	22.98484	17.01627
C	23.06713	22.86550	15.93439
H	22.94777	22.51452	16.96172
C	23.88573	23.96531	15.66243
H	24.42966	24.44354	16.47703
C	24.00687	24.44098	14.35479
H	24.64358	25.30103	14.14285
C	23.30641	23.81494	13.31857
H	23.38926	24.18978	12.29763
C	22.49673	22.71032	13.58527
H	21.94430	22.23929	12.77253
C	22.37936	22.21889	14.89559
C	18.70171	21.11590	14.63923
H	18.59605	21.39788	15.68690
C	17.58617	21.10237	13.80148

H	16.61289	21.38268	14.20294
C	17.71498	20.70429	12.47062
H	16.83990	20.68421	11.81959
C	18.96295	20.30848	11.97619
H	19.06403	19.97731	10.94188
C	20.07989	20.31564	12.81092
H	21.03977	19.96444	12.43054
C	19.95738	20.73422	14.14896
C	23.62710	19.45843	14.04789
H	24.09727	20.43841	13.96732
C	24.27644	18.33410	13.52898
H	25.26011	18.44490	13.07047
C	23.66654	17.07993	13.58712
H	24.17331	16.20564	13.17767
C	22.40521	16.94612	14.17602
H	21.92233	15.97141	14.23147
C	21.76143	18.05983	14.71051
H	20.77995	17.94732	15.17222
C	22.36346	19.32906	14.63961
C	20.11542	15.63596	23.21729
H	20.51030	16.33027	22.47352
C	20.93274	15.18225	24.25270
H	21.96673	15.52341	24.30608
C	20.42223	14.31774	25.22293
H	21.05816	13.97337	26.03975
C	19.08793	13.90384	25.15496
H	18.68224	13.23538	25.91528
C	18.26267	14.36343	24.12678
H	17.21332	14.06687	24.10393
C	18.77198	15.23372	23.14671
C	17.61217	13.33786	20.75786
H	17.88999	12.96673	21.74462
C	17.36291	12.43487	19.72226
H	17.43369	11.36284	19.91206
C	17.03307	12.90203	18.44606
H	16.84535	12.19534	17.63689
C	16.95485	14.27642	18.20652
H	16.71530	14.65762	17.21422
C	17.20216	15.18431	19.23688
H	17.15196	16.25485	19.03094
C	17.52381	14.71912	20.52207
C	15.10821	15.01828	22.49913
H	15.26915	14.20047	21.79725
C	13.93595	15.06303	23.25717
H	13.19169	14.27408	23.14124
C	13.71653	16.10798	24.15891
H	12.80262	16.13370	24.75367
C	14.65967	17.13160	24.27932
H	14.48886	17.96968	24.95533
C	15.82861	17.09320	23.51995
H	16.55728	17.89779	23.60740
C	16.07567	16.02496	22.64573
C	15.99791	20.47324	23.88645
H	16.96499	20.35834	23.39203
C	15.93131	20.55922	25.27786
H	16.84625	20.49477	25.86602

C	14.69758	20.73162	25.90921
H	14.64681	20.79719	26.99677
C	13.53024	20.83825	25.14481
H	12.56791	20.99609	25.63314
C	13.59426	20.75956	23.75239
H	12.68543	20.88401	23.16193
C	14.82834	20.55255	23.11250
C	13.11789	18.27687	21.36307
H	12.77567	18.63569	22.33242
C	12.51812	17.15254	20.79250
H	11.70976	16.64887	21.32295
C	12.95442	16.66809	19.55538
H	12.48162	15.78744	19.11846
C	14.00297	17.30564	18.88916
H	14.37616	16.93902	17.93211
C	14.61001	18.42508	19.45822
H	15.43962	18.90076	18.93449
C	14.16752	18.92402	20.69479
C	12.81158	21.58098	19.84553
H	12.59580	20.57686	19.48233
C	12.01010	22.65304	19.44668
H	11.17174	22.47317	18.77288
C	12.28010	23.94374	19.90391
H	11.64992	24.77745	19.59247
C	13.36696	24.16776	20.75418
H	13.59554	25.17611	21.09793
C	14.17427	23.10522	21.15572
H	15.02592	23.28662	21.81423
C	13.89043	21.80074	20.71451
C	19.60801	15.79320	16.47317
H	19.24226	16.65978	17.02527
C	18.91180	15.36906	15.33882
H	18.02321	15.92529	15.03821
C	19.36328	14.26340	14.61728
H	18.82476	13.93259	13.72802
C	20.51745	13.58448	15.02889
H	20.87738	12.72351	14.46381
C	21.21947	14.01271	16.15576
H	22.12989	13.49074	16.45057
C	20.76529	15.12417	16.88941
C	23.96986	16.92698	17.28397
H	23.37587	17.84021	17.26138
C	25.27177	16.92449	16.77898
H	25.68339	17.84146	16.36152
C	26.03577	15.75586	16.81620
H	27.05335	15.75575	16.42309
C	25.49903	14.58961	17.37020
H	26.09501	13.67663	17.41293
C	24.19692	14.58604	17.87000
H	23.79250	13.67679	18.31528
C	23.41725	15.75338	17.81670
C	20.82410	13.27826	19.43465
H	20.16108	13.18112	18.57616
C	20.87586	12.25650	20.38672
H	20.25592	11.36950	20.25347
C	21.71293	12.36973	21.49697

H	21.75332	11.56999	22.23732
C	22.49378	13.51818	21.66254
H	23.14450	13.62022	22.53042
C	22.44448	14.54346	20.72136
H	23.05897	15.43415	20.86025
C	21.62061	14.42098	19.58761
C	18.75852	18.05726	25.57096
H	18.99818	17.72319	24.56152
C	17.78809	17.38861	26.31895
H	17.28200	16.52470	25.89131
C	17.45587	17.83779	27.59901
H	16.68576	17.32305	28.17463
C	18.10327	18.95377	28.13714
H	17.84274	19.31338	29.13341
C	19.08614	19.61601	27.40014
H	19.58338	20.48768	27.82354
C	19.42253	19.16898	26.11068
C	19.91078	22.63309	25.45147
H	19.24700	22.44549	24.60711
C	19.87814	23.88182	26.07385
H	19.19237	24.63781	25.69205
C	20.74324	24.15769	27.13501
H	20.71979	25.13451	27.61966
C	21.65393	23.18629	27.56496
H	22.33754	23.39950	28.38770
C	21.69203	21.93542	26.94489
H	22.40351	21.18378	27.28674
C	20.81423	21.65101	25.88438
C	24.73230	18.00559	26.20345
H	25.69108	17.55351	26.45949
C	24.69466	19.19124	25.46190
H	25.61759	19.66461	25.12789
C	23.46964	19.76671	25.12636
H	23.45002	20.67995	24.52983
C	22.26701	19.17916	25.55933
C	22.31005	17.98670	26.29680
H	21.38574	17.51793	26.63373
C	23.54016	17.40204	26.61024
H	23.56536	16.47836	27.19051
C	22.46616	24.02638	22.74922
H	22.09742	23.03628	22.47459
C	22.69710	24.33870	24.08977
C	23.12752	25.61626	24.44838
H	23.29868	25.85604	25.49843
C	23.31753	26.59216	23.46451
H	23.63701	27.59740	23.74177
C	23.09476	26.28304	22.12418
H	23.23243	27.05274	21.36484
C	22.68300	24.99127	21.75644
C	20.38874	26.30136	19.91506
H	20.08427	25.83466	20.85501
C	19.59181	27.29802	19.35459
H	18.67909	27.59976	19.86564
C	19.94336	27.88587	18.13692
H	19.30801	28.65792	17.70155
C	21.09732	27.46873	17.47063

H	21.36549	27.90810	16.50926
C	21.90438	26.47221	18.0229
H	22.79161	26.13998	17.4848
C	21.56515	25.89576	19.25735
C	24.88875	25.90159	19.18412
H	24.35617	26.84041	19.33263
C	26.22751	25.92701	18.79369
H	26.72705	26.88492	18.64399
C	26.93174	24.73215	18.60475
H	27.97984	24.75816	18.30419
C	26.28850	23.50940	18.79875
H	26.82487	22.57232	18.65556
C	24.94322	23.48227	19.17152
H	24.43337	22.52847	19.30718
C	24.23144	24.67226	19.37403
C	25.03647	20.18122	18.04967
H	23.95262	20.30392	18.11388
C	25.71223	20.51447	16.87293
H	25.15138	20.91084	16.02872
C	27.09561	20.34930	16.78574
H	27.62084	20.60863	15.86583
C	27.80815	19.86049	17.88611
H	28.88987	19.73311	17.82726
C	27.14036	19.55242	19.07213
H	27.71277	19.20248	19.93122
C	25.74560	19.70355	19.16226
C	25.92567	16.75458	20.44140
H	26.25512	17.02363	19.43941
C	26.17745	15.46715	20.92522
H	26.70542	14.75365	20.29242
C	25.75171	15.09651	22.20208
H	25.96117	14.09470	22.57790
C	25.04064	16.00964	22.98821
H	24.69356	15.73240	23.98452
C	24.76955	17.28752	22.50462
H	24.19969	17.98594	23.11662
C	25.23740	17.68069	21.23697
C	25.16883	21.69749	22.21895
H	24.21033	21.97995	21.78155
C	25.83587	22.58186	23.06800
H	25.39658	23.55709	23.27820
C	27.05026	22.20620	23.64739
H	27.57424	22.89514	24.31095
C	27.58996	20.94156	23.38501
H	28.53098	20.64128	23.84793
C	26.92689	20.05835	22.53156
H	27.34199	19.06624	22.34859
C	25.71514	20.43791	21.93134
H	22.54900	23.62244	24.81782

Figure A44. Coordinates for optimized structure of $Au_{11}(PPh_3)_8Cl_2^+$.

Coordinates of optimized structure for $Au_{11}(PPh_3)_7Br_2^+$

Au	19.89617	20.21644	20.12296
Au	18.55133	22.28956	18.74422
Au	20.76615	20.57044	17.52986
Au	18.61325	17.98608	21.07610
Au	19.08383	22.44425	21.64370
Au	17.16955	20.50396	20.61478
Au	20.85933	17.81502	19.10858
Au	18.25180	19.06407	18.17525
Au	20.30463	20.03656	22.80666
Au	21.44694	22.46757	19.74494
Au	22.53352	19.77577	20.53705
P	17.22770	23.80559	17.55660
P	21.37653	20.73889	15.27997
P	14.95438	20.44411	21.31207
P	17.71597	15.96673	21.83780
P	20.71583	19.99658	25.11631
P	21.68824	15.75722	18.34489
P	24.82681	19.37765	20.70533
P	22.51126	24.53781	19.99550
Br	16.76240	18.06202	16.37870
Br	18.32678	24.49255	22.91018
C	19.44729	24.59155	16.11570
H	19.96805	24.43536	17.06149
C	20.15759	25.00001	14.98933
H	21.23169	25.16599	15.06166
C	19.49817	25.16771	13.76892
H	20.05922	25.46732	12.88276
C	18.12386	24.93412	13.68113
H	17.60819	25.05168	12.72736
C	17.40403	24.53412	14.80961
H	16.33479	24.33735	14.72952
C	18.06400	24.35959	16.03437
C	16.50148	26.54188	17.75402
H	16.64751	26.60825	16.67520
C	16.06357	27.66074	18.46507
H	15.85395	28.59067	17.93499
C	15.90499	27.59359	19.85426
H	15.56717	28.47120	20.40793
C	16.20516	26.40991	20.53262
H	16.13764	26.35273	21.61926
C	16.63229	25.28555	19.82423
H	16.88910	24.37580	20.36557
C	16.76694	25.33878	18.43124
C	14.51625	23.87948	16.75507
H	14.55431	24.95508	16.92502
C	13.33989	23.29786	16.28075
H	12.47482	23.92795	16.07094
C	13.26654	21.91564	16.08586
H	12.34441	21.46429	15.71641
C	14.36997	21.11127	16.38083
H	14.33279	20.02932	16.24963
C	15.55116	21.68843	16.85111
H	16.40209	21.04615	17.08446
C	15.63847	23.07891	17.02652

C	23.06331	22.86582	15.93279
H	22.94093	22.51392	16.95950
C	23.88476	23.96390	15.66235
H	24.42865	24.44067	16.47783
C	24.00832	24.44007	14.35497
H	24.64619	25.29958	14.14398
C	23.30751	23.81598	13.31765
H	23.39195	24.19083	12.29682
C	22.49537	22.71263	13.58262
H	21.94293	22.24186	12.76959
C	22.37514	22.22160	14.89281
C	18.69355	21.14456	14.64131
H	18.59298	21.43986	15.68578
C	17.57556	21.13121	13.80707
H	16.60572	21.42297	14.20860
C	17.69629	20.72105	12.47956
H	16.81949	20.70336	11.83085
C	18.93899	20.30946	11.98547
H	19.03455	19.96924	10.95374
C	20.05843	20.31375	12.81679
H	21.01443	19.95194	12.43684
C	19.94363	20.74556	14.15104
C	23.61858	19.46206	14.05432
H	24.08975	20.44157	13.97440
C	24.27047	18.33636	13.54115
H	25.25658	18.44601	13.08771
C	23.66001	17.08242	13.59865
H	24.16898	16.20687	13.19419
C	22.39714	16.94995	14.18411
H	21.91433	15.97536	14.24101
C	21.75066	18.06502	14.71259
H	20.76736	17.95505	15.17147
C	22.35126	19.33461	14.63970
C	20.11710	15.63944	23.21423
H	20.51222	16.33136	22.46827
C	20.93369	15.18756	24.25100
H	21.96798	15.52723	24.30270
C	20.42255	14.32737	25.22461
H	21.05827	13.98513	26.04260
C	19.08789	13.91468	25.15751
H	18.68164	13.24846	25.91928
C	18.26320	14.37165	24.12770
H	17.21358	14.07613	24.10522
C	18.77319	15.23918	23.14545
C	17.62097	13.34072	20.75679
H	17.89968	12.97041	21.74366
C	17.37470	12.43757	19.72050
H	17.44825	11.36582	19.90991
C	17.04199	12.90338	18.44445
H	16.85512	12.19571	17.63566
C	16.96073	14.27779	18.20521
H	16.71837	14.65922	17.21354
C	17.20601	15.18572	19.23595
H	17.15418	16.25674	19.03176
C	17.52771	14.72162	20.52147
C	15.11334	15.01844	22.50104

H	15.27548	14.20043	21.79967
C	13.94289	15.06024	23.26191
H	13.20078	14.26911	23.14834
C	13.72152	16.10530	24.16298
H	12.80794	16.12957	24.75871
C	14.66231	17.13135	24.28045
H	14.49112	17.96928	24.95622
C	15.82977	17.09632	23.5186
H	16.55632	17.90322	23.60375
C	16.07811	16.02814	22.64468
C	15.99845	20.48838	23.89725
H	16.96220	20.38074	23.39512
C	15.94155	20.57936	25.28849
H	16.86174	20.52572	25.86919
C	14.71228	20.74439	25.92972
H	14.67136	20.81398	27.01768
C	13.53779	20.83913	25.17505
H	12.57916	20.99217	25.67214
C	13.59177	20.75546	23.78243
H	12.67653	20.87152	23.20015
C	14.82273	20.55541	23.13286
C	13.10069	18.27592	21.40731
H	12.76150	18.64666	22.37307
C	12.50104	17.14287	20.85497
H	11.69580	16.64489	21.39533
C	12.93528	16.64124	19.62504
H	12.46413	15.75321	19.20098
C	13.97964	17.27274	18.94714
H	14.34522	16.89627	17.99131
C	14.58625	18.40140	19.49799
H	15.41127	18.87452	18.96409
C	14.14943	18.91451	20.73016
C	12.80141	21.56652	19.85848
H	12.59379	20.56158	19.49265
C	11.99795	22.63409	19.45328
H	11.16624	22.45175	18.77234
C	12.25893	23.92551	19.91323
H	11.62790	24.75733	19.59776
C	13.33954	24.15427	20.77089
H	13.56033	25.16342	21.11694
C	14.14959	23.09561	21.17868
H	14.99584	23.28035	21.84353
C	13.87364	21.79054	20.73425
C	19.66266	15.72997	16.42225
H	19.26812	16.59737	16.95310
C	19.00204	15.27140	15.27952
H	18.10790	15.79971	14.94765
C	19.49152	14.16341	14.58673
H	18.97859	13.80537	13.69272
C	20.64798	13.51427	15.03677
H	21.03704	12.65002	14.49680
C	21.31557	13.97702	16.17078
H	22.22730	13.47685	16.49676
C	20.82457	15.09221	16.87402
C	23.98047	16.93684	17.28096
H	23.37253	17.84059	17.24357

C	25.28218	16.94668	16.77651
H	25.68162	17.86318	16.34670
C	26.06517	15.79191	16.82970
H	27.08175	15.80250	16.43472
C	25.54735	14.62554	17.40086
H	26.15702	13.72252	17.45566
C	24.24464	14.60914	17.90057
H	23.85511	13.69895	18.35718
C	23.44485	15.76304	17.82969
C	20.84219	13.28049	19.43162
H	20.18338	13.18402	18.56998
C	20.89029	12.25888	20.38347
H	20.26986	11.37271	20.24803
C	21.72298	12.37200	21.49697
H	21.75735	11.57361	22.23888
C	22.50204	13.52069	21.66594
H	23.14605	13.62368	22.53857
C	22.46074	14.54442	20.72251
H	23.07730	15.43331	20.86181
C	21.64143	14.42133	19.58566
C	18.76614	18.05687	25.56943
H	19.01039	17.72329	24.56082
C	17.78975	17.39035	26.31155
H	17.28370	16.52867	25.87986
C	17.45132	17.83895	27.59024
H	16.67496	17.32702	28.16018
C	18.10033	18.95173	28.13313
H	17.83656	19.31025	29.12879
C	19.09013	19.61159	27.40286
H	19.58848	20.48030	27.83159
C	19.43093	19.16561	26.11376
C	19.89481	22.59789	25.54466
H	19.20240	22.41057	24.72347
C	19.85335	23.82852	26.19969
H	19.12985	24.57346	25.86989
C	20.75512	24.10384	27.22985
H	20.72523	25.06797	27.73918
C	21.70973	23.14957	27.59589
H	22.42262	23.36379	28.39318
C	21.75340	21.91361	26.94677
H	22.49337	21.17176	27.24587
C	20.83834	21.63016	25.91805
C	24.73804	17.98451	26.20152
H	25.69532	17.52966	26.45864
C	24.70372	19.16693	25.45426
H	25.62771	19.63638	25.11794
C	23.48003	19.74306	25.11563
H	23.46197	20.65369	24.51445
C	22.27654	19.16257	25.55566
C	22.31578	17.97494	26.30057
H	21.39006	17.51376	26.64457
C	23.54454	17.38720	26.61333
H	23.56702	16.46698	27.19890
C	22.44628	24.02935	22.75016
H	22.07511	23.04078	22.47237
C	22.66704	24.34070	24.09282

H	22.48550	23.58741	24.85693
C	23.10210	25.61554	24.45523
H	23.26515	25.85471	25.50692
C	23.30888	26.58937	23.47261
H	23.63224	27.59252	23.75234
C	23.09703	26.28135	22.13005
H	23.24736	27.04984	21.37177
C	22.67861	24.99259	21.75890
C	20.39241	26.31390	19.91686
H	20.09043	25.85157	20.85933
C	19.59652	27.31134	19.35727
H	18.68654	27.61687	19.87107
C	19.94780	27.89793	18.13899
H	19.31343	28.67121	17.70438
C	21.09930	27.47707	17.47120
H	21.36682	27.91579	16.50947
C	21.90465	26.47838	18.02255
H	22.79073	26.14520	17.48324
C	21.56638	25.90399	19.25819
C	24.88534	25.90441	19.18503
H	24.35307	26.84366	19.33289
C	26.22424	25.92950	18.79467
H	26.72301	26.88761	18.64433
C	26.92905	24.73462	18.60661
H	27.97739	24.76094	18.30585
C	26.28537	23.51221	18.80140
H	26.82197	22.57510	18.65911
C	24.93961	23.48519	19.17339
H	24.42868	22.53180	19.30912
C	24.22779	24.67520	19.37547
C	25.03618	20.18896	18.03926
H	23.95203	20.31189	18.10023
C	25.71625	20.53045	16.86727
H	25.15886	20.93476	16.02455
C	27.09926	20.36154	16.78219
H	27.62828	20.62717	15.86607
C	27.80690	19.86135	17.88064
H	28.88802	19.72960	17.82312
C	27.13552	19.54635	19.06285
H	27.70411	19.18588	19.92007
C	25.74097	19.70126	19.15036
C	25.92751	16.75352	20.44060
H	26.26352	17.02088	19.44016
C	26.18508	15.47008	20.93236
H	26.72544	14.75861	20.30801
C	25.75191	15.10130	22.20732
H	25.96566	14.10255	22.58945
C	25.02539	16.01210	22.98224
H	24.67262	15.73634	23.97680
C	24.74935	17.28633	22.49164
H	24.17002	17.98344	23.09624
C	25.22669	17.67837	21.22678
C	25.15005	21.69410	22.20569
H	24.19018	21.97486	21.76976
C	25.82037	22.58120	23.04986
H	25.37970	23.55570	23.26044

C	27.03903	22.20983	23.62227
H	27.56510	22.90087	24.28202
C	27.57970	20.94562	23.35893
H	28.52321	20.64770	23.81748
C	26.91324	20.05929	22.51173
H	27.32828	19.06695	22.32908
C	25.69781	20.43555	21.91688

Figure A45. Optimized coordinates of $Au_{11}(PPh_3)_8Br_2^+$.

Coordinates of optimized structure for $Au_{11}(PPh_3)_7I_2^+$

Au	19.86107	20.21703	20.07714
Au	18.53173	22.32829	18.70266
Au	20.74929	20.56179	17.49071
Au	18.59352	17.98639	21.02445
Au	18.99795	22.42221	21.61701
Au	17.12523	20.47235	20.50098
Au	20.84138	17.82051	19.04055
Au	18.23668	19.03823	18.10561
Au	20.25118	20.03826	22.77988
Au	21.39262	22.47070	19.72953
Au	22.48539	19.76325	20.54283
P	17.22377	23.83504	17.47364
P	21.35911	20.74036	15.23833
P	14.92233	20.42822	21.23486
P	17.70922	15.96522	21.78386
P	20.66214	19.96768	25.09719
P	21.70889	15.76315	18.31192
P	24.78090	19.36106	20.71895
P	22.44283	24.54374	19.99575
I	16.69825	18.00194	16.15135
I	18.05952	24.52890	22.98499
C	19.43533	24.58376	15.98383
H	19.97663	24.42995	16.91823
C	20.11958	24.99107	14.83959
H	21.19520	25.15823	14.88902
C	19.43451	25.15837	13.63315
H	19.97695	25.45710	12.73549
C	18.05803	24.92639	13.57596
H	17.52005	25.04416	12.63443
C	17.36489	24.53012	14.72134
H	16.29329	24.33747	14.66606
C	18.05044	24.35702	15.93299
C	16.53929	26.57813	17.57524
H	16.74686	26.61326	16.50547
C	16.06694	27.71753	18.22838
H	15.89466	28.63307	17.66031
C	15.82207	27.68810	19.60590
H	15.45853	28.58203	20.11411
C	16.06278	26.51837	20.32925

H	15.91649	26.49079	21.40977
C	16.52194	25.37234	19.67820
H	16.72436	24.47035	20.25447
C	16.75136	25.39156	18.29732
C	14.50728	23.91220	16.67403
H	14.54677	24.98992	16.83112
C	13.33084	23.32752	16.20412
H	12.46644	23.95707	15.98838
C	13.25626	21.94335	16.02283
H	12.33397	21.48915	15.65854
C	14.35879	21.14114	16.32515
H	14.32084	20.05810	16.20314
C	15.53932	21.72270	16.79113
H	16.39052	21.08310	17.03128
C	15.62863	23.11332	16.95436
C	23.04488	22.86089	15.91580
H	22.91420	22.50275	16.93930
C	23.86908	23.95980	15.65797
H	24.40628	24.43326	16.48000
C	24.00293	24.44176	14.35368
H	24.64287	25.30187	14.15263
C	23.31014	23.82442	13.30684
H	23.40114	24.20712	12.28942
C	22.49474	22.72057	13.55889
H	21.94607	22.25618	12.7396
C	22.36414	22.22288	14.86605
C	18.68755	21.18994	14.61356
H	18.60300	21.48236	15.66013
C	17.56247	21.19890	13.78987
H	16.60058	21.50447	14.19999
C	17.66398	20.78689	12.46124
H	16.77893	20.77940	11.82382
C	18.89409	20.35765	11.95289
H	18.97226	20.01679	10.91981
C	20.02148	20.34102	12.77396
H	20.96790	19.96639	12.38225
C	19.92527	20.76874	14.11088
C	23.59843	19.46593	14.00706
H	24.06210	20.44798	13.91679
C	24.25836	18.33932	13.50718
H	25.24244	18.45146	13.04965
C	23.65722	17.08190	13.58079
H	24.17375	16.20491	13.18973
C	22.39476	16.94668	14.16634
H	21.92011	15.96868	14.23344
C	21.73994	18.06312	14.68221
H	20.75777	17.95039	15.14308
C	22.33280	19.33572	14.59754
C	20.13113	15.65166	23.12884
H	20.51157	16.35225	22.38326
C	20.96312	15.20428	24.15479
H	21.99313	15.55831	24.19968
C	20.47274	14.33094	25.12712
H	21.12003	13.99292	25.93736
C	19.14466	13.89830	25.06893
H	18.75321	13.22117	25.82910

C	18.30415	14.35381	24.05131
H	17.25803	14.04519	24.03686
C	18.79100	15.23666	23.07130
C	17.56523	13.34077	20.73139
H	17.81919	12.98103	21.72858
C	17.31287	12.42639	19.70736
H	17.35461	11.35619	19.91534
C	17.01586	12.88134	18.41842
H	16.82604	12.16489	17.61826
C	16.97044	14.25312	18.15356
H	16.75350	14.62341	17.15139
C	17.21684	15.17199	19.17458
H	17.18936	16.24084	18.95513
C	17.50801	14.71911	20.47149
C	15.10988	15.02385	22.48141
H	15.25287	14.21025	21.77095
C	13.95088	15.07019	23.25916
H	13.19889	14.28763	23.14930
C	13.75158	16.11119	24.16959
H	12.84576	16.13958	24.77671
C	14.70170	17.12906	24.28128
H	14.54681	17.96371	24.96546
C	15.85596	17.08978	23.50127
H	16.58866	17.89136	23.58124
C	16.08396	16.02590	22.61600
C	16.00100	20.47383	23.81317
H	16.96209	20.34589	23.31059
C	15.94645	20.56829	25.20465
H	16.86502	20.49504	25.78678
C	14.72057	20.75910	25.84587
H	14.68128	20.83156	26.93344
C	13.54716	20.88009	25.09351
H	12.59164	21.05432	25.58955
C	13.59905	20.79366	23.70208
H	12.68841	20.92923	23.11727
C	14.82416	20.56288	23.05311
C	13.03845	18.28872	21.42327
H	12.71071	18.69706	22.37789
C	12.42303	17.14086	20.92102
H	11.61720	16.67223	21.48703
C	12.84355	16.58706	19.70815
H	12.36065	15.68838	19.32238
C	13.88815	17.18106	18.99673
H	14.24061	16.76281	18.05292
C	14.51022	18.32416	19.49896
H	15.33658	18.76955	18.94329
C	14.08639	18.89191	20.71164
C	12.75800	21.56682	19.81159
H	12.53741	20.56288	19.44990
C	11.94945	22.63920	19.42840
H	11.10235	22.46249	18.76470
C	12.22466	23.92708	19.89008
H	11.58996	24.76201	19.59100
C	13.32235	24.14859	20.72823
H	13.55085	25.15528	21.07676
C	14.13613	23.08488	21.11413

H	14.99193	23.26452	21.76888
C	13.84588	21.78303	20.66826
C	19.72026	15.64947	16.34869
H	19.29417	16.51946	16.85055
C	19.10116	15.15031	15.19926
H	18.20471	15.64889	14.82874
C	19.63439	14.04103	14.54298
H	19.15564	13.65483	13.64243
C	20.79108	13.42610	15.03869
H	21.21549	12.56081	14.52753
C	21.41519	13.92785	16.17979
H	22.32685	13.45412	16.54215
C	20.88387	15.04955	16.84238
C	23.99275	16.94873	17.23708
H	23.37773	17.84723	17.18177
C	25.29446	16.95928	16.73258
H	25.68889	17.87171	16.28932
C	26.08525	15.81112	16.79968
H	27.09929	15.82227	16.39793
C	25.57625	14.64913	17.38926
H	26.19243	13.75116	17.45631
C	24.27678	14.63432	17.89630
H	23.89551	13.73064	18.37177
C	23.46939	15.78212	17.81045
C	20.80221	13.33363	19.44083
H	20.12238	13.25494	18.59335
C	20.82121	12.32473	20.40699
H	20.15524	11.46852	20.29835
C	21.67914	12.41443	21.50281
H	21.69313	11.62545	22.25543
C	22.51474	13.52730	21.63925
H	23.17963	13.61286	22.49801
C	22.50047	14.53971	20.68231
H	23.15691	15.40296	20.79898
C	21.65360	14.44003	19.56433
C	18.73281	18.00043	25.54698
H	18.96016	17.68790	24.52777
C	17.78614	17.30264	26.29892
H	17.28478	16.44053	25.86219
C	17.47147	17.72137	27.59329
H	16.72274	17.18172	28.17422
C	18.10938	18.83927	28.13895
H	17.85869	19.17869	29.14489
C	19.07003	19.52999	27.39837
H	19.55989	20.40181	27.83033
C	19.39167	19.11079	26.09555
C	19.84220	22.55611	25.64404
H	19.11090	22.38869	24.85305
C	19.83151	23.76841	26.33491
H	19.08756	24.51885	26.06893
C	20.78561	24.01973	27.32368
H	20.78047	24.96962	27.85958
C	21.75553	23.05678	27.61822
H	22.50601	23.24815	28.38673
C	21.76430	21.83764	26.93749
H	22.51523	21.08872	27.18639

C	20.80493	21.58028	25.94287
C	24.70599	17.99755	26.18949
H	25.66841	17.56288	26.46119
C	24.65656	19.16625	25.42177
H	25.57537	19.64067	25.07816
C	23.42729	19.72233	25.07077
H	23.40176	20.62364	24.45648
C	22.22978	19.13451	25.51700
C	22.28345	17.95797	26.27794
H	21.36227	17.49003	26.62431
C	23.51850	17.38956	26.60318
H	23.54817	16.47621	27.19952
C	22.36694	24.00191	22.73557
H	22.00451	23.01646	22.43646
C	22.57632	24.28852	24.08505
H	22.39557	23.52020	24.83453
C	22.99648	25.56106	24.47254
H	23.15046	25.78206	25.52941
C	23.20149	26.55613	23.51032
H	23.51182	27.55701	23.81266
C	23.00606	26.27047	22.15920
H	23.16177	27.05252	21.41627
C	22.59809	24.98516	21.76299
C	20.35622	26.36827	19.90859
H	20.06874	25.95269	20.87632
C	19.55821	27.34644	19.31836
H	18.65990	27.68481	19.83299
C	19.89298	27.87019	18.06659
H	19.25849	28.62830	17.60710
C	21.02539	27.40370	17.39674
H	21.27857	27.79357	16.41030
C	21.82837	26.41999	17.97666
H	22.69801	26.04838	17.43612
C	21.50754	25.90804	19.24481
C	24.81089	25.90723	19.17984
H	24.27291	26.84473	19.31705
C	26.15087	25.93296	18.79295
H	26.64793	26.89131	18.63720
C	26.85699	24.73780	18.61353
H	27.90712	24.76481	18.32043
C	26.21578	23.51403	18.80920
H	26.75463	22.57774	18.66849
C	24.87117	23.48643	19.18144
H	24.36066	22.53307	19.31868
C	24.15854	24.67720	19.37864
C	24.98064	20.16764	18.05316
H	23.89417	20.26734	18.11539
C	25.64923	20.51321	16.87673
H	25.08136	20.89458	16.03040
C	27.03556	20.37614	16.79140
H	27.55574	20.64492	15.87138
C	27.75863	19.90605	17.89358
H	28.84303	19.80431	17.83625
C	27.09584	19.58378	19.07918
H	27.67342	19.24661	19.94006
C	25.69707	19.70293	19.16652

C	25.92665	16.75813	20.44725
H	26.26536	17.03995	19.45149
C	26.20627	15.47652	20.93164
H	26.76505	14.77995	20.30644
C	25.77182	15.09061	22.20095
H	26.00528	14.09453	22.57840
C	25.02269	15.98095	22.97758
H	24.66739	15.68931	23.96686
C	24.72308	17.25185	22.49268
H	24.12550	17.93187	23.09898
C	25.19920	17.66278	21.23291
C	25.08743	21.67702	22.21924
H	24.13003	21.95416	21.77626
C	25.74725	22.56699	23.06820
H	25.30295	23.54065	23.27630
C	26.96231	22.19887	23.65143
H	27.48274	22.89205	24.31309
C	27.50869	20.93582	23.39497
H	28.45008	20.64154	23.86136
C	26.85233	20.04585	22.54272
H	27.27140	19.05473	22.36422
C	25.64102	20.41888	21.93710

Figure A46. Optimized coordinates of $Au_{11}(PPh_3)_8I_2^+$.

Coordinates of optimized structure for $Au_{11}(PPh_3)_7Cl_3$

Au	19.98971627	20.19912856	19.87655613
Au	19.58353254	18.92271761	22.28971813
Au	19.20128704	21.84526822	21.93151249
Au	21.81690058	22.25344552	19.87327386
Au	21.58161141	20.17161425	17.75142331
Au	19.05516892	22.75569063	19.14897558
Au	17.36409180	19.90638850	20.62253502
Au	18.54597021	20.40185580	17.54576347
Au	22.20523644	19.98319071	21.61227136
Au	18.66484780	17.87081332	18.98604684
Au	21.45964855	17.89001674	19.72397718
Cl	17.98830582	24.85567090	18.57877751
Cl	23.96129010	20.05578788	23.28293830
Cl	17.60467925	15.72805417	18.56158680
P	18.97772399	23.33563847	23.69455055
P	23.41314626	23.92594053	20.00625766
P	22.92035671	20.13056398	15.86922474
P	15.05801207	19.97360780	20.81914952
P	19.31018635	17.40903887	24.02424804
P	17.24143986	20.66700712	15.63824971
P	22.59273114	15.86969468	19.61928749
C	19.90346949	22.81210245	25.17899349
C	19.56439125	23.23355128	26.47606281
C	20.29220589	22.76869805	27.57373488

C	21.35669240	21.87930081	27.38801483
C	21.69945917	21.45959747	26.10031698
C	20.97498491	21.92233920	25.00085244
C	23.58370681	24.64529514	21.67269542
C	23.83181378	26.01133931	21.87667784
C	24.02804615	26.49688698	23.17039453
C	23.97615844	25.62988305	24.26500129
C	23.71257106	24.27188519	24.06655678
C	23.50864151	23.77973821	22.77669650
C	17.24544328	23.52798813	24.24183055
C	16.73828148	24.73500473	24.74637630
C	15.40106834	24.81929718	25.14363551
C	14.56404993	23.70431276	25.04386944
C	15.06216651	22.50236490	24.53309640
C	16.39163988	22.41980155	24.12311080
C	26.76715886	17.70671494	16.68533923
C	26.26129701	17.74333477	15.38288982
C	25.11056664	18.48285794	15.09819229
C	24.46555370	19.19735804	16.12013350
C	24.98505123	19.16253324	17.42624777
C	26.13016327	18.41903683	17.70493384
C	17.92934510	16.25121758	23.72723315
C	17.53199321	16.02839506	22.39912400
C	16.47542890	15.16307705	22.11336944
C	15.80356990	14.51535128	23.15243273
C	16.19012537	14.73504832	24.47845356
C	17.24509737	15.60207453	24.76861293
C	21.72037032	25.61300711	18.60564381
C	23.06519236	25.32546066	18.88914066
C	24.07658387	26.11527841	18.31916843
C	23.74018771	27.18282495	17.48333164
C	22.39840832	27.46879974	17.20974986
C	21.38867966	26.68119758	17.77143870
C	18.94874574	18.19045750	25.63610340
C	18.29043033	19.43047357	25.63740582
C	17.95182492	20.05273663	26.83822110
C	18.29094116	19.45160484	28.05292933
C	18.97343280	18.23163479	28.06111893
C	19.30175874	17.59946958	26.85948752
C	14.42983449	21.68399441	20.94598622
C	15.28818171	22.72324160	20.55301890
C	14.89669954	24.05675109	20.68212953
C	13.63875923	24.36299263	21.20618121
C	12.77286420	23.33441474	21.59294471
C	13.16400442	22.00036357	21.46829356
C	22.90323066	16.02583419	16.86496534
C	22.66353111	15.15492708	17.93985384
C	22.46195247	13.79010273	17.68541847
C	22.51059061	13.30819834	16.37509748
C	22.76223654	14.17776640	15.31119478
C	22.95929463	15.53941843	15.56002871
C	21.94101082	14.33096842	24.84614511
C	23.16746854	14.99928556	24.82403679
C	23.21284109	16.36727228	24.53987168
C	22.03253329	17.06627434	24.29311426
C	20.79533418	16.39980948	24.33138985

C	20.75397357	15.02314160	24.59530848
C	22.37999677	19.66161023	13.11732216
C	22.07366103	19.35228981	14.45189042
C	21.03667270	18.44369228	14.73214125
C	20.32225079	17.85113538	13.69179175
C	20.63390763	18.16125574	12.36552906
C	21.66188184	19.06461141	12.07879453
C	14.33883804	23.15930612	17.04967441
C	15.54754283	22.49461928	16.84293296
C	15.60781142	21.41389591	15.94639761
C	14.44640444	20.99803524	15.27864490
C	13.24136877	21.67216411	15.48937651
C	13.18574595	22.75434292	16.37135871
C	20.27125039	25.83164850	24.15457338
C	19.52459558	25.02330341	23.28464029
C	19.16758627	25.51089367	22.01565236
C	19.54089925	26.79666903	21.62889537
C	20.27553413	27.60445381	22.50166269
C	20.63950346	27.12064424	23.76080032
C	13.05307743	17.78433752	17.28405125
C	14.14305925	17.23018542	17.96209021
C	14.72548457	17.91761262	19.02430721
C	14.21860694	19.16833498	19.42015161
C	13.14047293	19.73260621	18.72477198
C	12.55911479	19.03475429	17.66293332
C	22.65174940	13.58563584	21.29743241
C	21.86711554	14.53647428	20.62750877
C	20.46697483	14.42286442	20.64196699
C	19.86315341	13.34967191	21.29781988
C	20.64672886	12.39102142	21.94554818
C	22.03862640	12.51333245	21.94936720
C	13.10817464	18.59180201	22.35415168
C	12.66149332	17.95707647	23.51496373
C	13.51146980	17.82453283	24.61748918
C	14.81894901	18.31207301	24.55291673
C	15.27112303	18.93619860	23.39061465
C	14.41555554	19.10090132	22.29074497
C	25.09133391	23.34635270	19.57622671
C	26.57621703	22.39563798	17.90568047
C	26.09578629	23.18936664	20.54364057
C	17.20234792	22.57205105	13.52594929
C	17.97407193	21.74955055	14.36135121
C	19.36920906	21.73880647	14.21726602
C	19.98462244	22.51603413	13.23676095
C	19.21138312	23.32501537	12.39974752
C	17.82215546	23.35461988	12.54942112
C	25.34124665	22.94089314	18.25274756
C	27.57523462	22.24067774	18.87272205
C	27.33056681	22.64030154	20.18797693
C	24.14934341	24.40372406	14.58579612
C	22.95470443	24.17298239	15.27314589
C	22.59678761	22.87511735	15.63916994
C	23.43137146	21.79199195	15.31049331
C	24.63468419	22.03094692	14.62572117
C	24.98878869	23.33294442	14.26329284
C	24.63689274	17.00745615	21.10257817

C	25.95434993	17.20664629	21.51404333
C	26.98078869	16.43018865	20.96749062
C	26.68613226	15.46007402	20.00353228
C	25.36875066	15.26159224	19.58446041
C	24.33452190	16.03226758	20.13854285
C	16.86189148	17.92370370	15.57780314
C	16.68132082	16.67267693	14.98825138
C	16.56853603	16.56696955	13.59912633
C	16.63844889	17.71522449	12.80285358
C	16.82597913	18.96933816	13.39027795
C	16.93594263	19.08038676	14.78602114
H	22.25280996	13.10548124	18.50702966
H	23.03439121	17.09034038	17.05735949
H	23.13642683	16.23002345	14.73608590
H	22.79065529	13.79789192	14.28883048
H	22.34307003	12.24695771	16.18664534
H	25.14573606	14.52045614	18.81605301
H	27.48726171	14.86159999	19.56676716
H	28.01365497	16.58740851	21.28319235
H	26.16081358	17.98727190	22.24760546
H	23.84961573	17.63787541	21.51818130
H	23.73759418	13.68183955	21.30703863
H	19.84480529	15.15458275	20.12318397
H	18.77579404	13.27390220	21.29979244
H	20.17179153	11.55168648	22.45640271
H	22.65307135	11.77466580	22.46610658
H	24.09081415	14.44849752	25.01009142
H	24.16265576	16.90033347	24.48764352
H	22.08728775	18.12874266	24.04986057
H	21.90604273	13.25860986	25.04099321
H	19.80347236	14.48982856	24.58599136
H	18.03508653	16.54219168	21.57807290
H	16.19385148	15.01012901	21.07032208
H	14.97141923	13.84464055	22.93260530
H	15.66161491	14.23769387	25.29338596
H	17.52455068	15.78619438	25.80660629
H	19.84919237	16.65607962	26.87207323
H	18.07452362	19.91868155	24.68679930
H	17.44673585	21.01842848	26.81713389
H	19.25888762	17.77129043	29.00823896
H	18.04114527	19.94440394	28.99349314
H	13.15941822	17.32252150	25.51955029
H	15.49854320	18.19086044	25.39667430
H	16.30512877	19.27358871	23.31275913
H	12.44768139	18.67138792	21.48940059
H	11.64710266	17.55649852	23.55445602
H	16.28144495	22.49588536	20.16177750
H	12.49216174	21.20842705	21.80065312
H	11.79308162	23.57238730	22.01043528
H	15.59297698	24.83751133	20.37144125
H	13.33473216	25.40420386	21.32544555
H	15.59840580	17.48726607	19.51709501
H	14.56954597	16.27421800	17.65745598
H	12.60342078	17.25125034	16.44510501
H	11.72820160	19.48330186	17.11761902
H	12.76833194	20.72103078	18.99396702

H	14.48269357	20.14510883	14.60082749
H	12.34286288	21.34517751	14.96441676
H	12.24232881	23.27762514	16.53561717
H	16.44105449	22.83170845	17.37208626
H	14.30339642	23.99136376	17.75233985
H	16.97848451	17.98707546	16.66047114
H	16.66224486	15.79102227	15.63003303
H	16.44101806	15.58839339	13.13299780
H	16.55890434	17.63459930	11.71763269
H	16.90746201	19.85677937	12.76196110
H	16.11934702	22.60908476	13.64552389
H	19.96894062	21.12229836	14.8864436
H	21.07000010	22.50163234	13.14103214
H	19.69136157	23.94110749	11.63794164
H	17.21540607	23.99546351	11.90818962
H	20.76755083	18.22595257	15.76746046
H	23.15887915	20.39063081	12.88921543
H	21.89571648	19.31950513	11.04410007
H	19.50541238	17.16730576	13.92282577
H	20.05963355	17.71201770	11.55414532
H	26.75112989	17.17660219	14.58988614
H	27.64978629	17.10803692	16.91381309
H	24.69997046	18.48023552	14.08770013
H	24.46914567	19.68906764	18.23107835
H	26.50258058	18.37346750	18.72819601
H	25.30820282	21.20321953	14.39881010
H	25.92951233	23.51236149	13.74048053
H	21.68395647	22.70483666	16.21287243
H	22.31066132	25.00549352	15.55504942
H	24.43350497	25.42222813	14.31835258
H	20.92282126	24.99038830	19.01427812
H	25.12410650	25.88570732	18.51688744
H	24.53150247	27.79013401	17.04107450
H	22.14260956	28.29772441	16.54742206
H	20.33587258	26.87177130	17.55793842
H	24.56531886	23.04395294	17.49506604
H	26.74893193	22.07679192	16.87781014
H	28.53736840	21.80350704	18.60138729
H	28.10246117	22.52372673	20.94959475
H	25.91415891	23.48519080	21.57591413
H	23.86602428	26.69496891	21.02892546
H	23.31047675	22.71607459	22.63221253
H	23.65541741	23.58543267	24.91127484
H	24.12684744	26.01509921	25.27482564
H	24.21672345	27.56059610	23.32307896
H	19.26733090	27.14717618	20.63298009
H	20.58019721	28.60605936	22.19405164
H	21.22850147	27.74184588	24.43651363
H	20.58068770	25.45060937	25.12759921
H	18.61883887	24.88470999	21.31026058
H	17.38229250	25.61311429	24.80779716
H	16.76901513	21.50404561	23.66787722
H	14.41219225	21.63406916	24.42375155
H	13.51837807	23.77761826	25.34551081
H	15.01105050	25.76477291	25.52354234
H	20.01913014	23.09271452	28.57923707

H	18.72082632	23.90790327	26.63045038
H	21.90976325	21.50424627	28.25043137
H	22.52254961	20.76444021	25.92706043
H	21.23684352	21.56822738	24.00209357

Figure A47. Optimized coordinates of $Au_{11}(PPh_3)_7Cl_3$.

Coordinates of optimized structure for $Au_{11}(PPh_3)_7Br_3$

Au	19.98281808	20.18493335	19.86088833
Au	19.66380762	18.94052888	22.28832719
Au	19.18614221	21.83123302	21.91053130
Au	21.76634310	22.29248635	19.83556161
Au	21.57121183	20.17295132	17.74069273
Au	19.01733342	22.72619317	19.10519847
Au	17.36812531	19.85629733	20.62832074
Au	18.54000664	20.35218807	17.51928860
Au	22.26790732	20.00883268	21.52354407
Au	18.68509150	17.84348760	18.96375873
Au	21.48471819	17.88005357	19.70399098
Br	17.91655129	24.92963828	18.41943166
Br	24.19320853	20.17009321	23.19845361
Br	17.58404917	15.58963016	18.46455333
P	18.97516517	23.32877688	23.66899209
P	23.37307348	23.96048788	19.93789094
P	22.93703078	20.12649017	15.88530519
P	15.06084595	19.93894129	20.84777304
P	19.42291163	17.44349097	24.03813228
P	17.22166016	20.63472892	15.62497762
P	22.60331534	15.84472799	19.61267052
C	19.90614788	22.81764453	25.15660026
C	19.56108813	23.24831505	26.44895911
C	20.28925606	22.80041434	27.55285010
C	21.36335371	21.92116628	27.37914082
C	21.71060825	21.48842539	26.09681429
C	20.98307273	21.93126600	24.99088880
C	23.56232724	24.71348097	21.58971909
C	23.97426310	26.04425724	21.76216822
C	24.17828728	26.55158029	23.04626028
C	23.98077959	25.73526987	24.16385329
C	23.56111176	24.41408801	23.99610497
C	23.34106080	23.90460000	22.71533021
C	17.25262613	23.52930823	24.24082418
C	16.76090353	24.74012792	24.75106778
C	15.44316529	24.82158762	25.20656176
C	14.61012051	23.70062134	25.15739541
C	15.08792382	22.49817228	24.62900806
C	16.39875309	22.41774559	24.16255592
C	26.75328224	17.67620814	16.76994534
C	26.24066642	17.68381483	15.46988985
C	25.10292473	18.43605220	15.17037511

C	24.47380024	19.18965750	16.17366017
C	24.99558819	19.17946745	17.48028886
C	26.13111034	18.42533477	17.77277021
C	18.03139820	16.29439683	23.76339809
C	17.58257726	16.10389242	22.44652853
C	16.49417996	15.27078321	22.18416448
C	15.84102096	14.62493475	23.23638381
C	16.28512313	14.80588109	24.55020347
C	17.37389144	15.63765193	24.81661994
C	21.71406637	25.65309373	18.51710040
C	23.05509159	25.35077464	18.80243116
C	24.07667155	26.13117147	18.23731544
C	23.75309651	27.20427333	17.40365624
C	22.41415202	27.50498538	17.12898415
C	21.39475984	26.72800199	17.68669539
C	19.05690269	18.22842422	25.64500407
C	18.33187836	19.43023453	25.64380391
C	17.96231401	20.03412029	26.84450234
C	18.33633002	19.45412524	28.05957488
C	19.08463424	18.27370274	28.06888569
C	19.44572244	17.66042513	26.86736620
C	14.44463880	21.64904837	21.02819115
C	15.29079492	22.69613935	20.63258983
C	14.88480943	24.02471879	20.76562835
C	13.62695676	24.31764547	21.29773514
C	12.77708153	23.27928544	21.69494799
C	13.18204038	21.94987643	21.56589456
C	22.93618879	15.94569812	16.86014081
C	22.63983555	15.10193275	17.94299175
C	22.35975567	13.74829589	17.70246963
C	22.38799662	13.24832534	16.39772458
C	22.69072484	14.09161473	15.32630376
C	22.96501018	15.44280195	15.56084729
C	22.03530116	14.36176603	24.89043304
C	23.26797844	15.01718382	24.83705442
C	23.32210270	16.38025504	24.52969902
C	22.14634604	17.08687257	24.28121679
C	20.90447767	16.43283829	24.34647231
C	20.85313789	15.06331909	24.64182245
C	22.39419453	19.66665727	13.12849635
C	22.10924777	19.33764953	14.46281937
C	21.09111866	18.40792696	14.74266209
C	20.37289800	17.81495561	13.70508991
C	20.65959835	18.14886384	12.37949089
C	21.67019156	19.07135684	12.09285037
C	14.27376360	23.03599471	17.12066982
C	15.48597059	22.37777845	16.91074722
C	15.57594400	21.35360313	15.95315048
C	14.43339203	20.97619020	15.23205535
C	13.22425162	21.64164549	15.44568017
C	13.14357108	22.67532890	16.38276254
C	20.27312685	25.82980116	24.09095115
C	19.52524937	25.00910775	23.23465180
C	19.17351189	25.47683046	21.95689989
C	19.54861320	26.75625942	21.55069880
C	20.28567805	27.57631785	22.41014375

C	20.64862172	27.11035734	23.67661723
C	12.97222448	17.94742364	17.24123510
C	14.07147807	17.35130825	17.86723072
C	14.67593169	17.97404097	18.95744895
C	14.18184948	19.20084756	19.43406122
C	13.08775111	19.80366975	18.79687295
C	12.48462065	19.17047086	17.70693917
C	22.66312764	13.55959791	21.29234962
C	21.87952923	14.53394500	20.65431339
C	20.47921974	14.45844079	20.72804899
C	19.87119392	13.40434208	21.40966545
C	20.65244494	12.42308317	22.02574209
C	22.04659096	12.50605757	21.97093488
C	13.12916599	18.50635741	22.35582089
C	12.68059648	17.86665698	23.51349430
C	13.52124512	17.75078070	24.62450312
C	14.82285845	18.25567862	24.57043135
C	15.27532606	18.88812847	23.41314370
C	14.42653320	19.04034513	22.30582765
C	25.03089381	23.31509161	19.52804255
C	26.56935542	22.42648523	17.86986221
C	25.92411223	22.93598950	20.54252542
C	17.18107953	22.65540384	13.62439992
C	17.95039271	21.75390507	14.37607846
C	19.33611902	21.68556276	14.16290476
C	19.93945505	22.48863182	13.19584213
C	19.16803343	23.37569373	12.43968620
C	17.79074052	23.46093376	12.65985387
C	25.36085453	23.04572192	18.18731795
C	27.46142987	22.06338162	18.88334184
C	27.13279472	22.31698966	20.21636752
C	24.15643570	24.39432954	14.58298656
C	22.95530832	24.16404523	15.25913876
C	22.59884604	22.86741389	15.63124979
C	23.44185633	21.78574533	15.31979223
C	24.64789188	22.02360563	14.64096538
C	25.00109939	23.32414183	14.27325898
C	24.69319681	16.94150954	21.07556679
C	26.01816222	17.09844895	21.48306227
C	27.02028502	16.30040836	20.92237885
C	26.69273183	15.35285139	19.94647433
C	25.36747763	15.19344252	19.53511319
C	24.35654370	15.98426451	20.10473080
C	16.85042702	17.88609266	15.46780184
C	16.67019680	16.65970847	14.82776719
C	16.57475290	16.60383050	13.43420029
C	16.66272814	17.78065486	12.68340245
C	16.84504980	19.01068121	13.32030939
C	16.93520725	19.07183905	14.72062084
H	22.10777704	13.08649344	18.53074312
H	23.13257157	17.00268367	17.04023726
H	23.18395355	16.11411455	14.73067369
H	22.70202483	13.70047889	14.30790351
H	22.16207259	12.19592163	16.22100453
H	25.12124744	14.46785569	18.75888769
H	27.47390231	14.73767091	19.49691758

H	28.05817671	16.42346783	21.23633573
H	26.24960047	17.86510227	22.22419096
H	23.92555799	17.59090217	21.49943106
H	23.75098571	13.62277189	21.25696189
H	19.86007758	15.20835095	20.23325821
H	18.78294121	13.36092610	21.45566901
H	20.17474110	11.59833343	22.55697752
H	22.66079189	11.74989571	22.46245858
H	24.18930647	14.46196308	25.01969585
H	24.27630630	16.90346167	24.46043322
H	22.20545602	18.14381487	24.01517410
H	21.99087101	13.29450745	25.10893089
H	19.89698467	14.54052135	24.65921416
H	18.06911266	16.62279131	21.61834971
H	16.17337940	15.14137338	21.14931972
H	14.97912974	13.98678838	23.03553516
H	15.77398070	14.30697724	25.37526329
H	17.69692987	15.79167134	25.84702659
H	20.03918348	16.74520142	26.87871672
H	18.08417771	19.90090803	24.69200340
H	17.40318366	20.96966138	26.82466594
H	19.39441244	17.82939959	29.01593521
H	18.06225893	19.93438249	28.99987397
H	13.16851752	17.24704853	25.52527859
H	15.49786833	18.14314221	25.41891913
H	16.30495917	19.24085425	23.34567482
H	12.47719324	18.57443286	21.48361345
H	11.67253860	17.45032304	23.54392849
H	16.28236819	22.47828877	20.23068166
H	12.52217115	21.14898374	21.90121479
H	11.79798115	23.50583829	22.11955784
H	15.56565373	24.81525976	20.44636944
H	13.30985380	25.35516963	21.41328267
H	15.55731385	17.51639650	19.40919549
H	14.48763260	16.41187116	17.50210288
H	12.50763039	17.46663284	16.37918211
H	11.64084212	19.64925822	17.20938669
H	12.72128805	20.77354636	19.13191096
H	14.48745719	20.16326349	14.50752131
H	12.34005497	21.34479376	14.87945949
H	12.19665266	23.19310626	16.54388715
H	16.36622222	22.68066680	17.47988835
H	14.22294286	23.82861339	17.86705374
H	16.95635207	17.90827373	16.55330354
H	16.63368088	15.75487874	15.43597029
H	16.44287654	15.64378477	12.93256911
H	16.59734740	17.74255588	11.59484961
H	16.93612566	19.92050812	12.72600413
H	16.10794809	22.73485264	13.79745639
H	19.93835325	21.00540418	14.76472961
H	21.01736176	22.42879255	13.04517916
H	19.64236518	24.00874063	11.68828479
H	17.18600607	24.16144106	12.08220271
H	20.83607701	18.17586374	15.77830493
H	23.15938120	20.40903057	12.89753361
H	21.88576518	19.34278032	11.05859896

H	19.57024754	17.11581478	13.93906170
H	20.08175909	17.70185993	11.56946784
H	26.71600014	17.08788435	14.68964885
H	27.62724347	17.06870981	17.00896648
H	24.68939849	18.41514501	14.16113987
H	24.49381664	19.73744334	18.27247312
H	26.51049095	18.40264588	18.79392468
H	25.32545030	21.19579860	14.42616267
H	25.94595194	23.50272732	13.75796999
H	21.68115986	22.69682307	16.19694809
H	22.30591236	24.99622111	15.52858382
H	24.44227906	25.41234484	14.31525401
H	20.91046871	25.03895341	18.92669170
H	25.12175766	25.89385927	18.43966890
H	24.55101441	27.80546153	16.96504908
H	22.16810795	28.34014108	16.47137619
H	20.34423326	26.92945333	17.47219002
H	24.66791080	23.30879522	17.38930599
H	26.80278260	22.21701520	16.82550294
H	28.40503484	21.57609595	18.63449989
H	27.81424460	22.02374299	21.01565135
H	25.67311136	23.10294516	21.58902016
H	24.12788277	26.68728458	20.89543687
H	23.01971760	22.86946802	22.59177197
H	23.39276957	23.76986713	24.85929332
H	24.14403424	26.13399752	25.16633523
H	24.49135811	27.58906132	23.17165936
H	19.27583159	27.08871010	20.54850798
H	20.59366614	28.57128565	22.08539947
H	21.24463269	27.73684258	24.34093315
H	20.58086117	25.46346694	25.07043816
H	18.62476297	24.83985625	21.26163650
H	17.40256378	25.62178696	24.77709924
H	16.76093235	21.49988715	23.69889520
H	14.43727682	21.62674557	24.55418480
H	13.58029668	23.76966620	25.51033454
H	15.06443902	25.76771908	25.59599493
H	20.00961720	23.13252615	28.55392376
H	18.71205679	23.91754262	26.59504025
H	21.91989026	21.56314572	28.24645904
H	22.54217253	20.80082103	25.93546679
H	21.24631310	21.56408756	23.99686192

Figure A48. Optimized coordinates of $Au_{11}(PPh_3)_7Br_3^+$.

Coordinates of optimized structure for $Au_{11}(PPh_3)_7I_3$

Au	19.97284678	20.18288515	19.87458029
Au	19.59515456	18.89093997	22.27922073
Au	19.20790257	21.84618767	21.91457887
Au	21.77990492	22.2803023	19.82991513

Au	21.57565522	20.14738497	17.75481323
Au	19.02509876	22.72350078	19.07879061
Au	17.34901441	19.90958673	20.61259995
Au	18.55009583	20.31718735	17.50986290
Au	22.23388964	19.99762300	21.57153918
Au	18.66159805	17.83248202	18.98123432
Au	21.45843810	17.86755344	19.76366357
I	17.88367197	25.03710420	18.24479968
I	24.32555746	20.17320443	23.29093705
I	17.61412811	15.39973556	18.40786675
P	18.96975424	23.32497425	23.68953352
P	23.39892261	23.94623771	19.94820078
P	22.92086515	20.11983627	15.87510699
P	15.04194494	19.99660275	20.84340066
P	19.34315819	17.41013418	24.05324170
P	17.29207228	20.60109634	15.56908807
P	22.59911614	15.84681277	19.62863796
C	19.86300459	22.79737254	25.19056507
C	19.50351689	23.24711884	26.47195589
C	20.21808300	22.81652854	27.59027548
C	21.29377940	21.93525838	27.44095051
C	21.65509721	21.48361117	26.16991408
C	20.93968788	21.90826294	25.04882523
C	23.55365418	24.70544407	21.60014523
C	23.97636475	26.03284135	21.77500617
C	24.15361225	26.54499928	23.06115474
C	23.91869708	25.73709902	24.17763634
C	23.48798088	24.42032337	24.00777255
C	23.29321071	23.90728915	22.72451058
C	17.23341996	23.52593376	24.21692794
C	16.71974670	24.74119627	24.69365188
C	15.38251096	24.82746303	25.08936505
C	14.55214423	23.70581464	25.01880976
C	15.05717318	22.49534459	24.53663118
C	16.38589856	22.41095296	24.12490900
C	26.76750635	17.70076449	16.69725237
C	26.26179032	17.73984103	15.39505723
C	25.11417899	18.48323874	15.11029232
C	24.47037653	19.19792240	16.13199755
C	24.99089777	19.16419242	17.43805196
C	26.13507086	18.41837156	17.71606651
C	17.94968745	16.25047379	23.83319793
C	17.50088506	15.99248802	22.52838346
C	16.42628365	15.12848401	22.31188463
C	15.78574945	14.52268632	23.39539742
C	16.23008003	14.77115265	24.69788916
C	17.30718105	15.63131606	24.91855715
C	21.79750973	25.68870385	18.50881388
C	23.12462136	25.34334495	18.80700910
C	24.17594298	26.08948035	18.25002696
C	23.89704491	27.17139679	17.41256640
C	22.57250367	27.51678948	17.12629784
C	21.52315118	26.77319090	17.67490223
C	19.01036189	18.22842131	25.65164704
C	18.31328273	19.44628058	25.65078660
C	17.97247622	20.06779055	26.85184072

C	18.35335939	19.49185502	28.06668973
C	19.07833407	18.29703004	28.07473170
C	19.40555875	17.66430905	26.87405345
C	14.40795723	21.70292373	21.00241255
C	15.25035288	22.76171360	20.62627230
C	14.81498313	24.08327090	20.73584128
C	13.53760558	24.36038849	21.22702718
C	12.69209268	23.31216889	21.60439128
C	13.12357104	21.98898318	21.49451881
C	22.85896359	16.01821385	16.87330863
C	22.60358526	15.14552099	17.94345863
C	22.37036546	13.78740277	17.68409183
C	22.40832263	13.31067225	16.37172923
C	22.68068966	14.17952450	15.31261248
C	22.90505050	15.53611565	15.56657550
C	21.94658385	14.30052480	24.85597561
C	23.18048481	14.95350229	24.81857268
C	23.23633651	16.32310039	24.54605779
C	22.06167214	17.03721557	24.31552480
C	20.81821693	16.38625440	24.36080260
C	20.76486797	15.00960495	24.62560786
C	22.38837680	19.63870487	13.11566426
C	22.08759290	19.33492163	14.45287611
C	21.06001660	18.41760184	14.73749790
C	20.35438332	17.80533214	13.70293962
C	20.65889450	18.11107509	12.37488970
C	21.67450714	19.02612275	12.08279084
C	14.22750350	22.86873183	17.02505373
C	15.45763430	22.23394120	16.85264339
C	15.62196418	21.28040070	15.83688354
C	14.53323413	20.94246541	15.01703154
C	13.30433291	21.58019051	15.19599156
C	13.15150743	22.54783971	16.19375380
C	20.21752203	25.82715322	24.23789403
C	19.54156229	25.01241512	23.31741748
C	19.28474305	25.49312748	22.02306684
C	19.69187188	26.77492871	21.65762800
C	20.36502983	27.5849912	22.57656179
C	20.62505689	27.10997373	23.86421504
C	13.00454174	17.93160496	17.24850666
C	14.05517335	17.32400191	17.94330074
C	14.64139802	17.97245481	19.02716271
C	14.17575048	19.23486411	19.43496858
C	13.13061161	19.84699856	18.72996959
C	12.54784254	19.19077012	17.64231321
C	22.77521092	13.50464834	21.20946452
C	21.94533687	14.49954630	20.66900967
C	20.55579261	14.41518677	20.84520797
C	20.00168833	13.32876597	21.52348819
C	20.82796089	12.32613637	22.03702989
C	22.21471325	12.41996392	21.88614349
C	13.11382337	18.57462994	22.36999035
C	12.67467548	17.92258339	23.52382914
C	13.52823696	17.78070249	24.62197835
C	14.83359978	18.27280366	24.55504022
C	15.27842766	18.91429104	23.39926438

C	14.41686365	19.09375414	22.30603099
C	25.06952161	23.32476737	19.55428376
C	26.57285497	22.36330116	17.90681709
C	26.04669007	23.14090364	20.54329208
C	17.30733411	22.61101099	13.55076781
C	18.05301969	21.74140502	14.36112622
C	19.44920413	21.70896478	14.23315861
C	20.08998891	22.50657791	13.28652692
C	19.34385720	23.36302659	12.47369221
C	17.95457126	23.41931885	12.61290355
C	25.33930212	22.92260921	18.23410303
C	27.55045392	22.19336202	18.89257319
C	27.28217574	22.58001404	20.20692694
C	24.09252046	24.40671996	14.59505187
C	22.91230308	24.16366345	15.30061367
C	22.57575018	22.86178700	15.67055624
C	23.41373282	21.78701623	15.32492606
C	24.60208494	22.03731883	14.61962205
C	24.93536280	23.34356132	14.25547356
C	24.72093459	16.88429932	21.08292640
C	26.05356020	17.01181437	21.47461550
C	27.04038951	16.23614171	20.85870416
C	26.69158535	15.33902168	19.84396892
C	25.35920390	15.20973850	19.44704271
C	24.36412670	15.97880866	20.07217315
C	16.82669340	17.87449213	15.37099136
C	16.59534509	16.66714573	14.71187705
C	16.56528852	16.62671321	13.31471338
C	16.77431093	17.79677448	12.57850766
C	17.00773731	19.00776220	13.23404547
C	17.02525117	19.05471658	14.63671337
H	22.15165611	13.10342261	18.50346504
H	23.01433649	17.07883966	17.07114557
H	23.10107067	16.22599386	14.74643611
H	22.70814305	13.80298365	14.28923076
H	22.21952727	12.25378676	16.17884378
H	25.09342867	14.52014461	18.64524826
H	27.46013909	14.73811799	19.35545326
H	28.08339026	16.33614527	21.16386584
H	26.30609430	17.73792286	22.24859881
H	23.96282709	17.51377380	21.55149022
H	23.85723198	13.57461657	21.09707681
H	19.90412444	15.18375025	20.42839156
H	18.91971529	13.27564871	21.64752814
H	20.39323467	11.47647173	22.56607653
H	22.86534549	11.64763270	22.29849146
H	24.10086260	14.39179904	24.98653739
H	24.19096081	16.84726403	24.49214956
H	22.12227579	18.10071522	24.07845532
H	21.90108657	13.22821173	25.04769853
H	19.80859491	14.48773869	24.63602172
H	17.98015524	16.47765460	21.67579209
H	16.10109311	14.94309524	21.28732332
H	14.93446869	13.86154776	23.22612893
H	15.73259979	14.29895677	25.54622369
H	17.63609759	15.83212233	25.93879863

H	19.97715621	16.73547738	26.88426422
H	18.06447952	19.91830805	24.70017688
H	17.43191653	21.01369228	26.83359545
H	19.39525205	17.85416526	29.02003780
H	18.10369458	19.98397503	29.00776295
H	13.18349860	17.26650985	25.52017441
H	15.51866789	18.13943932	25.39204868
H	16.31260901	19.25108093	23.32075269
H	12.45138567	18.65902952	21.50731842
H	11.66397181	17.51432912	23.56192827
H	16.25640201	22.55847627	20.25335663
H	12.46337833	21.17968072	21.80795162
H	11.69640022	23.52508040	21.99607584
H	15.48730949	24.88523316	20.42761211
H	13.20344553	25.39444512	21.32602865
H	15.48679221	17.50473147	19.53431039
H	14.44910267	16.35530704	17.63477500
H	12.55414464	17.43044472	16.39047681
H	11.74550299	19.67989005	17.09015874
H	12.78331365	20.84016563	19.01273903
H	14.64598562	20.18534984	14.24066835
H	12.46228086	21.31707918	14.55401129
H	12.18970716	23.04570269	16.32753100
H	16.29751538	22.49867001	17.49589239
H	14.11917615	23.61241594	17.81459550
H	16.87630072	17.88698219	16.46088883
H	16.46652337	15.76052684	15.30420491
H	16.39024123	15.68193814	12.79753358
H	16.76346582	17.76956880	11.48768766
H	17.18896650	19.91415894	12.65583101
H	16.22410379	22.66561432	13.65914027
H	20.02892247	21.05788167	14.88648713
H	21.17514939	22.47055236	13.19906740
H	19.84599000	23.99566468	11.74027693
H	17.36879717	24.09909174	11.99294796
H	20.79129517	18.20657118	15.77405984
H	23.15861657	20.37379543	12.87830771
H	21.90205029	19.27757050	11.04623755
H	19.54730467	17.11295739	13.94064648
H	20.09014357	17.64849676	11.56709951
H	26.74851401	17.17250743	14.60125350
H	27.64576137	17.09515386	16.92481648
H	24.70407150	18.48299628	14.09993640
H	24.47897472	19.69462592	18.24289688
H	26.51155000	18.37581976	18.73791274
H	25.27768979	21.21594624	14.37701563
H	25.86458891	23.53308845	13.71682178
H	21.67377694	22.68093609	16.25794898
H	22.26378749	24.98804950	15.59322250
H	24.36541704	25.42832223	14.32791550
H	20.97094048	25.09795119	18.90736161
H	25.21017703	25.81641065	18.46197862
H	24.71933850	27.74502608	16.98233021
H	22.35981993	28.36039477	16.46745985
H	20.48299305	27.01018367	17.44645708
H	24.57945259	23.03904517	17.46219437

H	26.76135091	22.04570149	16.88109817
H	28.51289297	21.74662452	18.63872287
H	28.03378405	22.43966182	20.98449307
H	25.84251044	23.41857335	21.57666763
H	24.15907365	26.66906498	20.90932079
H	22.95742815	22.87780731	22.59736045
H	23.29071503	23.78313165	24.87029382
H	24.05953453	26.13978881	25.18223863
H	24.47236751	27.58023010	23.19074849
H	19.49229279	27.12112509	20.64306871
H	20.70484505	28.57923908	22.28248140
H	21.16822570	27.73056467	24.57730568
H	20.44986218	25.45380375	25.23496747
H	18.78686879	24.86059198	21.28585779
H	17.35990868	25.62319442	24.73603648
H	16.76684027	21.48596811	23.69179761
H	14.41308826	21.62015753	24.45289132
H	13.50736368	23.77934373	25.32345535
H	14.98800451	25.77959629	25.44655966
H	19.92670977	23.16312531	28.58259122
H	18.65329324	23.91918396	26.59636180
H	21.84095052	21.59116757	28.31983602
H	22.49016501	20.79605241	26.03091449
H	21.21544718	21.52965261	24.06235788

Figure A49. Optimized coordinates of $Au_{11}(PPh_3)_7I_3^+$.

Coordinates of optimized structure for $Au_{11}(PPh_3)_8(CN)_2^+$

Au	19.87857	20.19839	20.09123
Au	18.54521	22.24519	18.68830
Au	20.74716	20.53999	17.49198
Au	18.58233	17.97204	21.04872
Au	19.07889	22.46783	21.59609
Au	17.15818	20.50270	20.58612
Au	20.84139	17.80578	19.09378
Au	18.24250	19.04175	18.16208
Au	20.27308	20.01260	22.76595
Au	21.43458	22.44721	19.70454
Au	22.51538	19.76666	20.52483
P	17.19912	23.73886	17.50722
P	21.35670	20.72084	15.24308
P	14.93605	20.43988	21.25464
P	17.68293	15.95150	21.80301
P	20.67151	19.99223	25.07338
P	21.63674	15.74890	18.31225
P	24.80901	19.37116	20.68396
P	22.48445	24.52388	19.95636
C	16.78970	18.63716	16.73265
C	18.52381	24.46173	22.55902
C	19.40727	24.56093	16.07109

H	19.93256	24.40127	17.01396
C	20.10878	24.98751	14.94608
H	21.18202	25.16245	15.01565
C	19.44341	25.16030	13.72957
H	19.99921	25.47368	12.84554
C	18.07131	24.91354	13.64241
H	17.55273	25.03408	12.69112
C	17.36017	24.49488	14.76949
H	16.29363	24.28541	14.68959
C	18.02659	24.31679	15.99094
C	16.41691	26.45580	17.74134
H	16.52088	26.53072	16.65828
C	15.98989	27.56338	18.47645
H	15.74469	28.49294	17.96055
C	15.89164	27.48736	19.87068
H	15.56618	28.35787	20.44265
C	16.23886	26.30621	20.53071
H	16.22423	26.24245	21.61892
C	16.65180	25.19341	19.79890
H	16.94860	24.28551	20.32533
C	16.72906	25.25359	18.40204
C	14.48225	23.73956	16.70692
H	14.48400	24.81507	16.88231
C	13.32828	23.12010	16.22551
H	12.44234	23.72127	16.01678
C	13.30344	21.73734	16.02329
H	12.39746	21.25671	15.64812
C	14.42990	20.96824	16.31939
H	14.43296	19.88517	16.18403
C	15.58686	21.58413	16.79731
H	16.45810	20.96836	17.03306
C	15.62974	22.97432	16.97868
C	23.03651	22.85515	15.89707
H	22.91701	22.50412	16.92406
C	23.85497	23.95490	15.62532
H	24.39882	24.43320	16.43940
C	23.97627	24.43059	14.31741
H	24.61271	25.29062	14.10523
C	23.27540	23.80463	13.28073
H	23.35841	24.17938	12.25999
C	22.46594	22.69988	13.54713
H	21.91349	22.22891	12.73492
C	22.34847	22.20851	14.85801
C	18.67105	21.10573	14.60176
H	18.56523	21.38765	15.64915
C	17.55534	21.09223	13.76406
H	16.58215	21.37197	14.16528
C	17.68442	20.69404	12.43270
H	16.80914	20.67376	11.78212
C	18.93194	20.29822	11.93887
H	19.03322	19.96695	10.90426
C	20.04921	20.30513	12.77329
H	21.00894	19.95416	12.39281
C	19.92625	20.72377	14.11145
C	23.59658	19.44822	14.01005
H	24.06638	20.42798	13.92966

C	24.24596	18.32382	13.49152
H	25.22926	18.43450	13.03278
C	23.63543	17.06944	13.54925
H	24.14253	16.19525	13.14006
C	22.37454	16.93593	14.13864
H	21.89157	15.96103	14.19382
C	21.73103	18.04958	14.67273
H	20.74921	17.93699	15.13452
C	22.33247	19.31847	14.60231
C	20.08486	15.62559	23.17934
H	20.47956	16.31984	22.43588
C	20.90229	15.17195	24.21497
H	21.93588	15.51302	24.26844
C	20.39113	14.30732	25.18531
H	21.02734	13.96301	26.00207
C	19.05753	13.89352	25.11699
H	18.65146	13.22499	25.87761
C	18.23221	14.35306	24.08886
H	17.18256	14.05648	24.06623
C	18.74096	15.22326	23.10904
C	17.58154	13.32779	20.72059
H	17.85915	12.95643	21.70698
C	17.33198	12.42455	19.68465
H	17.40283	11.35251	19.87439
C	17.00228	12.89151	18.40874
H	16.81450	12.18495	17.59924
C	16.92424	14.26635	18.16853
H	16.68435	14.64683	17.17650
C	17.17122	15.17370	19.19859
H	17.12118	16.24460	18.99378
C	17.49321	14.70928	20.48411
C	15.07778	15.00791	22.46151
H	15.23827	14.19009	21.75964
C	13.90496	15.05256	23.21980
H	13.16087	14.26376	23.10357
C	13.68606	16.09770	24.12115
H	12.77176	16.12334	24.71599
C	14.62904	17.12131	24.24196
H	14.45808	17.95925	24.91765
C	15.79795	17.08266	23.48238
H	16.52644	17.88739	23.56983
C	16.04451	16.01477	22.60782
C	15.96677	20.46294	23.84893
H	16.93416	20.34787	23.35448
C	15.90085	20.54894	25.24035
H	16.81539	20.48442	25.82841
C	14.66640	20.72128	25.87129
H	14.61599	20.78690	26.95912
C	13.49987	20.82791	25.10688
H	12.53712	20.98575	25.59548
C	13.56316	20.74917	23.71448
H	12.65468	20.87361	23.12428
C	14.79821	20.54221	23.07448
C	13.08689	18.26643	21.32512
H	12.74488	18.62531	22.29477
C	12.48757	17.14214	20.75461

H	11.67889	16.63843	21.28535
C	12.92361	16.65775	19.51820
H	12.45087	15.77708	19.08077
C	13.97289	17.29525	18.85168
H	14.34491	16.92887	17.89410
C	14.57867	18.41444	19.42128
H	15.40820	18.89059	18.89717
C	14.13714	18.91358	20.65702
C	12.78085	21.57066	19.80820
H	12.56499	20.56655	19.44466
C	11.97903	22.64258	19.40912
H	11.14102	22.46283	18.73523
C	12.24917	23.93312	19.86631
H	11.61915	24.76713	19.55480
C	13.33627	24.15776	20.71681
H	13.56481	25.16573	21.06026
C	14.14369	23.09458	21.11801
H	14.99494	23.27640	21.77667
C	13.85979	21.79046	20.67658
C	19.57651	15.78245	16.43499
H	19.21168	16.64980	16.98811
C	18.88096	15.35944	15.30142
H	17.99200	15.91479	14.99993
C	19.33262	14.25306	14.57930
H	18.79399	13.92225	13.69045
C	20.48619	13.57417	14.99155
H	20.84653	12.71321	14.42621
C	21.18887	14.00243	16.11815
H	22.09902	13.48044	16.41304
C	20.73483	15.11399	16.85226
C	23.93907	16.91643	17.24609
H	23.34496	17.83003	17.22364
C	25.24076	16.91398	16.74164
H	25.65278	17.83096	16.32396
C	26.00517	15.74571	16.77843
H	27.02251	15.74540	16.38541
C	25.46842	14.57894	17.33226
H	26.06424	13.66635	17.37526
C	24.16631	14.57547	17.83236
H	23.76175	13.66645	18.27762
C	23.38645	15.74315	17.77915
C	20.79363	13.26815	19.39715
H	20.13027	13.17072	18.53850
C	20.85994	12.26716	20.35291
C	21.68251	12.36019	21.45950
H	21.72247	11.55957	22.19964
C	22.46299	13.50784	21.62507
H	23.11361	13.60986	22.49276
C	22.41364	14.53317	20.68334
H	23.02819	15.42378	20.82257
C	21.58952	14.41050	19.54963
C	18.72744	18.04706	25.53376
H	18.96737	17.71282	24.52385
C	17.75753	17.37816	26.28164
H	17.25119	16.51434	25.85365
C	17.42490	17.82730	27.56159

H	16.65494	17.31261	28.13699
C	18.07227	18.94330	28.09933
H	17.81193	19.30296	29.09572
C	19.05561	19.60561	27.36245
H	19.55251	20.47733	27.78598
C	19.39152	19.15866	26.07320
C	19.88040	22.62351	25.41410
H	19.21596	22.43482	24.56907
C	19.84668	23.87171	26.03581
H	19.16124	24.62795	25.65396
C	20.71277	24.14708	27.09763
H	20.68891	25.12419	27.58189
C	21.62289	23.17591	27.52711
H	22.30678	23.38915	28.35008
C	21.66152	21.92502	26.90726
H	22.37263	21.17339	27.24909
C	20.78325	21.64034	25.84597
C	24.70191	17.99515	26.16588
H	25.66029	17.54310	26.42189
C	24.66349	19.18088	25.42430
H	25.58681	19.65420	25.09022
C	23.43870	19.75631	25.08874
H	23.41929	20.66962	24.49224
C	22.23606	19.16887	25.52168
C	22.27925	17.97629	26.25925
H	21.35490	17.50763	26.59607
C	23.50975	17.39177	26.57263
H	23.53448	16.46797	27.15285
C	22.43524	24.01579	22.71127
H	22.06681	23.02590	22.43697
C	22.66654	24.32843	24.05256
H	22.49865	23.57291	24.81743
C	23.09669	25.60573	24.41098
H	23.26788	25.84570	25.46078
C	23.28667	26.58177	23.42702
H	23.60603	27.58701	23.70414
C	23.06405	26.27281	22.08640
H	23.20158	27.04239	21.32731
C	22.65218	24.98073	21.71883
C	20.35841	26.29093	19.87743
H	20.05361	25.82496	20.81727
C	19.56048	27.28761	19.31716
H	18.64845	27.58935	19.82821
C	19.91274	27.87549	18.09917
H	19.27723	28.64748	17.66394
C	21.06641	27.45827	17.43264
H	21.33472	27.89777	16.47162
C	21.87346	26.46180	17.98483
H	22.76073	26.12966	17.44720
C	21.53418	25.88525	19.21972
C	24.85756	25.89128	19.14667
H	24.32539	26.82998	19.29489
C	26.19706	25.91675	18.75606
H	26.69619	26.87458	18.60630
C	26.90081	24.72193	18.56709
H	27.94904	24.74781	18.26665

C	26.25761	23.49907	18.76119
H	26.79411	22.56192	18.61788
C	24.91252	23.47171	19.13391
H	24.40254	22.51811	19.26951
C	24.20032	24.66138	19.33648
C	25.00571	20.17090	18.01197
H	23.92185	20.29348	18.07621
C	25.68103	20.50401	16.83569
H	25.12063	20.90042	15.99110
C	27.06438	20.33889	16.74836
H	27.59003	20.59826	15.82816
C	27.77748	19.85006	17.84877
H	28.85897	19.72277	17.78959
C	27.10995	19.54214	19.03447
H	27.68188	19.19210	19.89352
C	25.71509	19.69307	19.12464
C	25.89497	16.74428	20.40343
H	26.22438	17.01330	19.40179
C	26.14644	15.45693	20.88770
H	26.67463	14.74332	20.25484
C	25.72110	15.08625	22.16414
H	25.93039	14.08423	22.54029
C	25.00979	15.99933	22.95088
H	24.66279	15.72197	23.94680
C	24.73866	17.27709	22.46715
H	24.16891	17.97555	23.07906
C	25.20655	17.67052	21.19952
C	25.13774	21.68709	22.18127
H	24.17964	21.96959	21.74389
C	25.80533	22.57154	23.03053
H	25.36578	23.54668	23.24058
C	27.01972	22.19592	23.60987
H	27.54341	22.88471	24.27334
C	27.55927	20.93132	23.34724
H	28.50013	20.63093	23.81031
C	26.89605	20.04770	22.49401
H	27.31121	19.05589	22.31099
C	25.68388	20.42747	21.89363
N	16.07982	18.31944	15.86002
N	18.12103	25.52481	23.29108
H	20.24536	11.38157	20.22665

Figure A50. Optimized coordinates of $Au_{11}(PPh_3)_8(CN)_2^+$.

Coordination of optimized structure for $Au_{11}(dppp)_5^{3+}$

Au	19.66715	20.17576	20.05392
Au	17.51003	19.58978	18.37143
Au	17.25234	20.28302	21.40015
Au	18.16299	22.46074	19.60968
Au	20.33646	21.62324	17.78268

Au	20.22171	18.61643	17.87305
Au	21.78416	18.42440	20.41756
Au	18.56327	17.60912	20.26974
Au	19.86548	19.02825	22.57225
Au	19.73352	21.94875	22.15158
Au	22.09113	21.39688	20.16515
P	15.34700	19.37850	17.50734
P	15.07527	20.48502	22.22662
P	16.97081	24.31819	18.82506
P	20.24295	22.91024	15.81679
P	21.29800	17.31556	16.26681
P	23.48003	16.80477	20.34142
P	17.98825	15.48694	21.05456
P	20.09364	17.84277	24.58118
P	20.50174	23.53870	23.68724
P	23.97932	22.70701	20.61507
C	14.90930	20.44965	16.10847
C	13.71165	21.17823	16.02404
H	12.98076	21.14401	16.83237
C	13.43862	21.94553	14.88783
H	12.50617	22.50727	14.82628
C	14.34671	21.97864	13.82513
H	14.12264	22.56883	12.93599
C	15.54027	21.25281	13.90315
H	16.25840	21.27762	13.08310
C	15.82544	20.50220	15.04262
H	16.77105	19.96184	15.11208
C	14.92607	17.68756	16.97082
C	15.68659	16.61594	17.46456
H	16.54542	16.82056	18.10684
C	15.34774	15.30149	17.14014
H	15.93597	14.47700	17.54334
C	14.25806	15.04938	16.30383
H	13.99135	14.02315	16.04913
C	13.50947	16.11338	15.78878
H	12.66429	15.91705	15.12840
C	13.83671	17.42942	16.12023
C	14.17896	19.71859	18.89558
H	13.14343	19.51601	18.57992
H	14.437800	18.93801	19.62871
C	14.33556	21.11417	19.51839
H	13.75469	21.84761	18.94016
H	15.38671	21.43939	19.44766
C	13.89425	21.21391	20.98719
H	12.89418	20.77986	21.13297
H	13.81994	22.27481	21.26215
C	14.35436	18.94386	22.87625
C	12.97253	18.69887	22.95915
H	12.25144	19.40180	22.54056
C	12.50158	17.54592	23.59081
H	11.42822	17.36348	23.65028
C	13.39993	16.63244	24.15127
H	13.02581	15.73779	24.64946
C	14.77365	16.85957	24.05577
H	15.47935	16.14286	24.47575
C	15.24830	18.00133	23.41229

H	16.32122	18.17290	23.32080
C	15.00353	21.65999	23.62999
C	16.11508	22.47767	23.89357
H	17.02294	22.36406	23.29594
C	16.06333	23.43567	24.90880
H	16.92928	24.07206	25.09477
C	14.90248	23.58241	25.67238
H	14.85703	24.33531	26.45986
C	13.79874	22.75679	25.43053
H	12.89641	22.85998	26.03400
C	13.84771	21.79721	24.41708
H	12.98335	21.15400	24.24839
C	15.43131	24.71894	19.71188
C	14.26865	25.17840	19.06947
H	14.23585	25.29076	17.98584
C	13.13418	25.50114	19.81808
H	12.23806	25.86115	19.31181
C	13.14937	25.37591	21.21018
H	12.26433	25.63741	21.79087
C	14.30043	24.91397	21.85507
H	14.31864	24.80018	22.93927
C	15.43146	24.57920	21.11007
H	16.31580	24.19338	21.61648
C	17.96404	25.85170	18.91360
C	19.33291	25.77712	19.21874
H	19.78324	24.80327	19.42485
C	20.10868	26.93740	19.25327
H	21.17123	26.87408	19.49157
C	19.52714	28.17930	18.98925
H	20.13318	29.08535	19.01438
C	18.16119	28.26158	18.69910
H	17.70169	29.23030	18.50129
C	17.38173	27.10528	18.66274
H	16.31460	27.18343	18.44870
C	16.47847	24.13745	17.05056
H	15.53918	23.56311	17.05615
H	16.25777	25.13314	16.63486
C	17.50318	23.37871	16.19785
H	17.66905	22.39476	16.66684
H	17.05067	23.16741	15.22007
C	18.84476	24.09970	15.99398
H	19.10076	24.73179	16.85332
H	18.82411	24.76189	15.11535
C	21.66063	23.98886	15.43855
C	21.92746	25.06778	16.30237
H	21.29054	25.25064	17.16872
C	23.00070	25.92170	16.05343
H	23.19223	26.75820	16.72626
C	23.82483	25.71097	14.94381
H	24.65994	26.38378	14.74828
C	23.57477	24.63332	14.09066
H	24.21264	24.46676	13.22193
C	22.50335	23.77002	14.33707
H	22.31762	22.93428	13.66297
C	19.82864	21.99117	14.30086
C	19.62788	20.60520	14.37047

H	19.77301	20.08856	15.32109
C	19.24369	19.89218	13.23301
C	19.05972	20.55739	12.01959
H	18.76784	19.99989	11.12863
C	19.25589	21.94134	11.94281
H	19.11491	22.46172	10.99538
C	19.63497	22.65886	13.07725
H	19.79065	23.73644	13.00461
C	20.19702	16.20991	15.33550
C	18.82239	16.50582	15.31726
H	18.44884	17.35820	15.88925
C	17.93803	15.70450	14.59413
H	16.87352	15.93864	14.59545
C	18.41573	14.59530	13.89050
H	17.72408	13.96614	13.32903
C	19.77996	14.28672	13.91160
H	20.15187	13.41936	13.36578
C	20.66924	15.08919	14.63006
H	21.73071	14.83733	14.63433
C	22.22945	18.32724	15.07459
C	22.89683	19.45624	15.58291
H	22.82248	19.70271	16.64403
C	23.63125	20.27887	14.73119
H	24.14757	21.14651	15.14036
C	23.69317	19.99734	13.36295
H	24.26257	20.64494	12.69511
C	23.02161	18.88476	12.85158
H	23.06180	18.66549	11.78442
C	22.29390	18.04780	13.70175
H	21.76858	17.18734	13.28721
C	22.58762	16.29442	17.09269
H	23.11439	15.67364	16.35242
H	23.31864	17.04328	17.43209
C	22.03387	15.46861	18.26547
H	21.12603	15.95006	18.66298
H	21.71147	14.48208	17.90400
C	23.00284	15.25904	19.43710
H	23.91977	14.74025	19.11668
H	22.50884	14.62274	20.18761
C	24.05167	16.21699	21.96891
C	24.58082	14.93128	22.17609
H	24.63428	14.21066	21.35978
C	25.05239	14.56073	23.43761
H	25.46758	13.56381	23.58759
C	25.00146	15.46639	24.50193
H	25.38087	15.17696	25.48233
C	24.46499	16.74249	24.30674
H	24.40604	17.44906	25.13507
C	23.98810	17.11434	23.04869
H	23.54997	18.10286	22.90198
C	24.97931	17.43772	19.50793
C	26.14971	16.66448	19.42181
H	26.20231	15.68103	19.89114
C	27.26430	17.15616	18.74156
H	28.16693	16.54810	18.67334
C	27.22668	18.42538	18.15295

H	28.10026	18.80490	17.62188
C	26.07353	19.20673	18.25071
H	26.04286	20.20272	17.80908
C	24.95342	18.71491	18.92392
H	24.05020	19.32564	18.99853
C	16.20361	15.12319	21.10576
C	15.29033	16.11772	20.72778
H	15.66665	17.10160	20.44630
C	13.92103	15.85135	20.71287
H	13.22069	16.62924	20.40913
C	13.45121	14.59402	21.09302
H	12.38099	14.38532	21.08732
C	14.35460	13.59880	21.48241
H	13.98887	12.61564	21.78019
C	15.72628	13.85597	21.48166
H	16.42026	13.06083	21.75781
C	18.69661	14.12059	20.08380
C	19.13887	12.91153	20.64505
H	19.14501	12.76833	21.72627
C	19.56581	11.86952	19.81694
H	19.90414	10.93188	20.25858
C	19.54684	12.02137	18.42712
H	19.86852	11.19984	17.78603
C	19.11782	13.22626	17.86249
H	19.11023	13.35806	16.77999
C	18.70680	14.27313	18.68642
H	18.40387	15.22344	18.24377
C	18.58042	15.32569	22.79215
H	18.03790	16.12913	23.31555
H	18.23257	14.38037	23.23679
C	20.10153	15.50806	22.93108
H	20.46746	16.18150	22.13789
H	20.60598	14.54422	22.76679
C	20.56897	16.07421	24.28053
H	21.66856	16.07593	24.30154
H	20.24018	15.44657	25.12215
C	18.59555	17.85844	25.62271
C	18.25795	16.83550	26.52487
H	18.86854	15.93595	26.60723
C	17.12879	16.95839	27.33812
H	16.87621	16.15866	28.03497
C	16.33021	18.10375	27.26750
H	15.45022	18.19467	27.90449
C	16.65397	19.12283	26.36809
H	16.02393	20.00916	26.28647
C	17.77220	18.99508	25.54489
H	18.00153	19.76918	24.81113
C	21.42566	18.49081	25.64781
C	21.68277	17.95023	26.91877
H	21.04941	17.16039	27.32451
C	22.75370	18.42594	27.67758
H	22.95219	17.99832	28.66071
C	23.56625	19.45022	27.17999
H	24.40135	19.81977	27.77627
C	23.30086	20.00659	25.92655
H	23.92454	20.81091	25.53820

C	22.23390	19.53075	25.16240
H	22.02301	19.96421	24.18265
C	19.49108	25.05027	23.78358
C	18.70968	25.39704	22.67004
H	18.68838	24.73453	21.80276
C	17.96322	26.57572	22.67204
H	17.37018	26.83985	21.79632
C	17.97285	27.40604	23.79485
H	17.38509	28.32452	23.79960
C	18.73600	27.05783	24.91453
H	18.74152	27.70384	25.79270
C	19.49789	25.88756	24.91195
H	20.08659	25.62347	25.79120
C	20.72542	22.95502	25.39126
C	21.77699	23.38282	26.21865
H	22.52759	24.08353	25.85391
C	21.87310	22.90890	27.52868
H	22.69271	23.24513	28.16419
C	20.92780	22.00819	28.02561
H	21.01061	21.63903	29.04797
C	19.88265	21.57428	27.20653
H	19.15017	20.85798	27.57894
C	19.78362	22.04387	25.89751
H	18.97691	21.69629	25.25208
C	22.16793	24.07964	23.11976
H	22.58881	24.82193	23.81364
H	22.78523	23.17229	23.19996
C	22.15189	24.61919	21.67924
H	21.37505	24.09210	21.10122
H	21.86329	25.68068	21.69227
C	23.47955	24.46512	20.92216
H	24.30458	25.01181	21.40292
H	23.37640	24.89364	19.91315
C	25.19460	22.82244	19.26244
C	24.71453	22.94495	17.94679
H	23.64006	22.94748	17.75248
C	25.61235	23.05398	16.88386
H	25.23097	23.17433	15.87054
C	26.99043	23.01944	17.11973
H	27.68869	23.09633	16.28570
C	27.47123	22.88217	18.42424
H	28.54481	22.85201	18.61198
C	26.57876	22.78769	19.49486
H	26.96550	22.67923	20.50759
C	24.94019	22.14275	22.05807
C	25.06787	20.75728	22.26312
H	24.55133	20.06361	21.59777
C	25.85460	20.27051	23.30726
H	25.95513	19.19500	23.45057
C	26.50851	21.15670	24.16769
H	27.12197	20.77440	24.98412
C	26.37826	22.53477	23.97827
H	26.89180	23.23137	24.64135
C	25.60379	23.02701	22.92527
H	25.53335	24.10505	22.78310

H	19.09560	18.87242	13.28946

Figure A51. Optimized coordinates of $Au_{11}(dppp)_5^{3+}$.

Coordination of initial structure of $Au_{11}Cl_{10}^{7-}$

Au	19.90877862	20.20860000	20.12783347
Au	18.57571110	22.25515720	18.72639437
Au	20.77733884	20.55000886	17.52964060
Au	18.61293008	17.98235738	21.08658713
Au	19.11329412	22.46110961	21.62665890
Au	17.18870331	20.51274013	20.62268542
Au	20.87280640	17.81588265	19.13147075
Au	18.26079751	19.04658317	18.18609700
Au	20.30301829	20.02215082	22.80412635
Au	21.46481518	22.45802711	19.74168940
Au	22.54640946	19.77611583	20.56159637
Cl	17.23159045	23.74818132	17.54564242
Cl	21.38771830	20.73101799	15.28201322
Cl	14.96830787	20.45002078	21.29207907
Cl	17.71404467	15.96223573	21.83997948
Cl	20.70258666	20.00272345	25.10977731
Cl	21.66682796	15.75992247	18.34989879
Cl	24.83922288	19.38192574	20.72198439
Cl	22.51518825	24.53332764	19.99405288
Cl	16.80397020	18.05432516	16.53923938
Cl	18.48205773	24.45623838	22.79456221

Figure A52. Initial coordinates of $Au_{11}Cl_{10}^{7-}$.

Coordination of optimized structure of $Au_{11}Cl_{10}^{7-}$

Au	19.9005844	20.12694349	19.84019069
Au	18.64754691	22.48465266	18.80879879
Au	20.27014874	20.84765808	16.99897946
Au	18.34691343	17.84309274	20.57977411
Au	18.98746657	22.16734026	21.74903309
Au	17.08542967	20.48072865	20.41584243
Au	21.07987938	17.59468947	19.48569461
Au	18.83465921	18.43079947	17.76167935
Au	20.70730549	19.96237557	22.52719508
Au	21.67572810	22.20309557	19.12824732
Au	22.72651003	19.81189488	20.49655680
Cl	17.36190372	24.56028034	17.79444664
Cl	20.91991526	21.18386213	14.32457889

Cl	14.43258650	20.56473559	20.73153731
Cl	17.08727833	15.82622935	21.73748689
Cl	21.20576014	19.50148370	25.10287067
Cl	22.33082690	15.30967082	19.11002314
Cl	25.44283201	19.52765738	20.88963265
Cl	23.32585304	24.23360560	18.84653198
Cl	17.61128947	17.08678112	15.80355819
Cl	18.55950050	24.12514231	23.53555272

Figure A53. Optimized coordinates of $Au_{11}Cl_{10}^{7-}$.

Coordination of optimized structure of $Au_{13}(dppp)_4Cl_4^+$

Au	19.74181150	20.93314088	17.70234836
Au	20.78095250	18.06445542	17.66079940
Au	20.97404680	19.71075077	19.92237540
Au	22.67039405	20.46864052	17.71116459
Au	18.36045798	18.87749001	19.28831329
Au	20.24777910	17.00575029	20.54886144
Au	23.17766398	18.12584146	19.35438041
Au	21.42075636	22.52348488	19.63600178
Au	20.96472976	21.86346974	22.47507085
Au	23.34101831	20.80251394	20.89256725
Au	18.81269992	21.52832967	20.46527702
Au	19.52468715	19.23839778	22.22457693
Au	22.28355857	18.37993689	22.09561660
Cl	25.63916246	21.42533073	21.01372409
Cl	21.86718281	24.47424187	18.37070739
Cl	23.07274786	17.02399931	23.90764568
Cl	16.84127883	22.78084176	21.01474861
P	23.60770803	21.69095915	15.93695536
P	19.69689876	14.80092166	21.09511532
P	24.90172822	16.75343047	18.63277417
P	18.34752938	19.73594045	24.14264142
P	16.33112547	17.73004954	19.15804666
P	22.51244454	23.29448747	23.98168565
P	21.41928212	16.89817801	15.73860097
P	18.82697264	22.31721141	16.06118975
C	22.23147702	22.64386311	15.17188732
C	24.40458544	20.74795705	14.58897693
C	24.16118925	20.99715189	13.22872871
H	23.46272662	21.77533463	12.92476966
C	24.81843209	20.25601387	12.24243980
H	24.61257115	20.45642522	11.19004338
C	25.74333308	19.27329769	12.60251457
H	26.26337194	18.70116793	11.83259353
C	26.01050290	19.03713372	13.95493957
H	26.74383849	18.28738366	14.25153895
C	25.34093085	19.76131077	14.94073604
H	25.55062786	19.56427086	15.99221205
C	24.89857341	22.87603498	16.42454205

C	25.20083901	23.03678786	17.78260413
H	24.65855516	22.47527133	18.54246934
C	26.22232375	23.90443114	18.17289245
H	26.45952884	23.99405230	19.23340471
C	26.93524140	24.62528816	17.21276604
H	27.72906192	25.30780194	17.51901426
C	26.63702439	24.46787436	15.85347258
H	27.19801287	25.02284668	15.10039409
C	25.62731969	23.59129253	15.45768165
H	25.42215891	23.45058413	14.39509831
C	21.00850170	13.70167068	20.46775513
C	22.27333940	13.79725830	21.08066637
H	22.42428626	14.45974240	21.93573248
C	23.34444201	13.05739110	20.58253354
H	24.31747296	13.13342326	21.06674837
C	23.18019233	12.23897202	19.46023241
H	24.02648084	11.66986943	19.07332605
C	21.93520140	12.15939854	18.83538653
H	21.79873016	11.53866712	17.94926168
C	20.85206394	12.88342099	19.34085000
H	19.89306838	12.81107489	18.83207654
C	19.60693256	14.47471927	22.88477985
C	19.82651286	15.50771240	23.80590383
H	20.10608627	16.50101890	23.45617212
C	19.70677721	15.26134476	25.17717101
H	19.89346559	16.06986851	25.88434387
C	19.36347235	13.98752414	25.63123821
H	19.26712882	13.79556573	26.70046373
C	19.15494104	12.94851540	24.71588320
H	18.89649489	11.94953387	25.06895891
C	19.27957915	13.18711404	23.34773137
H	19.12894640	12.36860734	22.64174700
C	18.07410840	14.17142972	20.43407704
C	17.38508417	15.14940351	19.46752502
C	25.65545701	15.71353752	19.93084992
C	25.29665695	15.93687503	21.26658142
H	24.54891184	16.68860306	21.51908271
C	25.88824421	15.19363419	22.29045131
H	25.57793918	15.38168031	23.31868480
C	26.84703216	14.22582313	21.98504503
H	27.31316307	13.64624527	22.78262546
C	27.21540583	14.00002642	20.65268433
H	27.97036423	13.25037817	20.41204871
C	26.62510041	14.74075945	19.62920501
H	26.94169294	14.56614278	18.59976688
C	26.30398471	17.70882798	17.96898468
C	26.46584480	19.02333846	18.43832998
H	25.74811994	19.45980486	19.13445604
C	27.55502646	19.79248332	18.02579491
H	27.65208350	20.81040067	18.40319766
C	28.49044864	19.25831833	17.13737167
H	29.33592745	19.86091189	16.80432002
C	28.34279979	17.94624830	16.67447904
H	29.07963899	17.52146472	15.99183356
C	27.25801602	17.17067805	17.08853589
H	27.16718004	16.14588930	16.72634003

C	24.34927379	15.53462041	17.35036769
C	18.21907997	21.56450816	24.14475861
C	19.13972664	19.30279623	25.72115171
C	20.47888692	18.88817917	25.73246782
H	21.02211577	18.75356845	24.79680295
C	21.12027306	18.61602808	26.94337111
H	22.16006844	18.28694716	26.92890991
C	20.42600741	18.75302104	28.14672868
H	20.92415153	18.53725144	29.09295137
C	19.08524201	19.15910096	28.14117463
H	18.54052898	19.26058201	29.08012416
C	18.44165878	19.43518915	26.93436222
H	17.39540447	19.74500119	26.93353913
C	16.68818796	19.00691865	24.17167805
C	15.54880806	19.72244371	23.76989836
H	15.62265003	20.77530093	23.50047668
C	14.31473576	19.07276009	23.68598942
H	13.43634146	19.63666746	23.37171089
C	14.20748790	17.71324430	23.98206074
H	13.24236195	17.20841321	23.90947233
C	15.34357066	16.99545280	24.37172025
H	15.27029775	15.93273784	24.60725014
C	16.57707394	17.63518149	24.46606892
H	17.45897040	17.06533832	24.76130794
C	20.96778591	15.13626654	15.53868208
C	19.92473021	14.64412435	16.33747175
H	19.49319137	15.29214352	17.10093664
C	19.43811005	13.34881774	16.15197820
H	18.60397108	12.99260864	16.75806032
C	20.01615755	12.51415721	15.19380267
H	19.63723826	11.50219011	15.04882239
C	21.07656427	12.98474982	14.41155099
H	21.53266177	12.33590408	13.66294501
C	21.53848130	14.29266688	14.56805667
H	22.33363431	14.65527177	13.91665530
C	23.24762241	17.10505702	15.51113979
C	24.22928606	15.98752514	15.88829211
C	20.68804331	17.68194827	14.25233936
C	19.51159736	18.42860018	14.41605178
H	19.12597579	18.60740786	15.42021522
C	18.84039695	18.94977869	13.30882230
H	17.91097182	19.49996726	13.45765456
C	19.35903294	18.75991004	12.02649347
H	18.83621393	19.16308721	11.15877949
C	20.55021250	18.04648701	11.85585451
H	20.96271093	17.90223627	10.85690211
C	21.20813058	17.50263580	12.95967973
H	22.12447099	16.93371804	12.79942074
C	14.88250224	18.63502860	19.77148618
C	14.95702505	20.03696169	19.77496905
H	15.88399806	20.54036505	19.50019904
C	13.85616676	20.80267961	20.16195134
H	13.94787271	21.88878382	20.17604481
C	12.66819798	20.17361139	20.53807676
H	11.80219036	20.76885612	20.83124149
C	12.59111883	18.77645367	20.55757638

H	11.66942801	18.28327413	20.86995832
C	13.69475084	18.00667272	20.18799326
H	13.62218353	16.91904441	20.22995114
C	15.89624810	17.10663428	17.49322787
C	16.93684439	16.92534893	16.56779212
H	17.95127039	17.22454295	16.84148954
C	16.68132066	16.38307413	15.30706129
H	17.50298040	16.24371460	14.60420600
C	15.37769084	16.02929700	14.95118065
H	15.17435796	15.61086255	13.96495214
C	14.33209121	16.22414101	15.85854508
H	13.31068866	15.95971691	15.58168494
C	14.58598939	16.76041174	17.12313910
H	13.75803988	16.92416334	17.81221335
C	16.51621096	16.20156532	20.17823391
C	19.75799851	22.31035409	14.45808107
C	21.17380933	21.72606453	14.53645664
C	18.66590548	24.02596874	16.64663244
C	19.26255683	25.13154337	16.02691529
H	19.86020339	25.01791486	15.12310518
C	19.11491108	26.40455000	16.58180993
H	19.59030740	27.25950107	16.10063823
C	18.38247199	26.58042849	17.75737045
H	18.28177064	27.57579014	18.19197444
C	17.79442934	25.47793452	18.38380864
H	17.24197417	25.59060099	19.31677522
C	17.93349147	24.20748800	17.83257443
H	17.48577639	23.35757563	18.34802241
C	17.13577951	21.84141399	15.56684481
C	16.35351462	22.70846651	14.78598793
H	16.72751124	23.70092490	14.52973242
C	15.08854043	22.31013002	14.35367238
H	14.48503013	22.98982165	13.75086824
C	14.59317523	21.04853290	14.70188107
H	13.60107291	20.74350144	14.36695679
C	15.36106783	20.18767883	15.48888062
H	14.97244918	19.21023770	15.77280073
C	16.62841786	20.58386327	15.92375508
H	17.22268313	19.92357066	16.55814740
C	21.92956616	23.77169166	25.48145863
C	19.58775266	22.23215657	24.13056080
C	22.93212591	24.71891077	22.94391113
C	23.57079596	24.52082176	21.71088344
H	23.80807244	23.51516391	21.36561625
C	23.92941688	25.61664652	20.92576263
H	24.39860725	25.44293814	19.95902871
C	23.65496350	26.91296871	21.36202742
H	23.93572779	27.76509643	20.74290644
C	23.01952705	27.11609133	22.59162770
H	22.81261960	28.12806888	22.94058198
C	22.65998196	26.02667144	23.38476950
H	22.19538890	26.19801745	24.35374229
C	23.95114197	22.22849285	24.23009990
C	25.21733017	22.82567053	24.33411738
H	25.33190298	23.90049972	24.19317286
C	26.32730837	22.03122178	24.61358103

H	27.31163125	22.49477390	24.68991127
C	26.18291319	20.65079880	24.77874157
H	27.06188117	20.03386789	24.97459023
C	24.92359448	20.05835203	24.67398840
H	24.80255114	18.97916318	24.77206900
C	23.80246749	20.84520140	24.40088105
H	22.82239265	20.37503337	24.30490671
H	21.21458899	24.58439838	25.59512518
H	22.04046958	23.08227931	26.31653181
H	17.66310945	21.88293721	25.04565736
H	17.63249628	21.85970575	23.26020900
H	19.48188648	23.32207189	24.06093306
H	20.19875588	21.97293645	25.00159842
H	21.47461292	21.44509891	13.51772287
H	21.12224286	20.77835153	15.09643886
H	22.62678275	23.38252233	14.45701554
H	21.82645284	23.21688971	16.02407793
H	19.15192878	21.67811717	13.79464477
H	19.74956141	23.31978799	14.02174652
H	18.25731574	13.20460694	19.94467394
H	17.43855062	13.96347126	21.30697000
H	15.53347833	15.78568778	20.44462326
H	16.98944888	16.54728304	21.11081826
H	16.76099440	14.59359254	18.75244943
H	18.15734397	15.65930477	18.86947464
H	23.39069726	15.15091521	17.73366530
H	25.04252592	14.68101448	17.38683975
H	23.42097199	17.36781359	14.45843084
H	23.46580069	18.02318829	16.08090099
H	25.21555064	16.33077986	15.54073505
H	24.00396414	15.08468223	15.30055878

Figure A54. Optimized coordinates of $Au_{13}(dppp)_4Cl_4^+$.

Coordination of optimized structure for $Au_{13}(AsPh_3)_8Cl_4^+$

Au	19.61197732	21.27598492	18.08530624
Au	20.74000810	18.52090358	17.85463107
Au	20.88831266	20.01451724	20.24881365
Au	22.63049533	20.91389950	18.07070785
Au	18.32976790	19.11567290	19.69122225
Au	20.40524322	17.31469229	20.84693258
Au	23.06464145	18.33551809	19.64791384
Au	21.45387084	22.84688954	19.86107706
Au	21.27225568	21.69882843	22.55201651
Au	23.53865729	20.93280518	20.89595468
Au	18.89595503	21.97906611	20.85893422
Au	19.14386641	19.56997122	22.53355680
Au	22.17198499	18.87752741	22.51408870
Cl	25.72272033	21.37627526	21.66677517
Cl	21.93763447	25.01036531	19.08302516

Cl	23.18436936	17.77892534	24.34871621
Cl	17.34812048	23.77704602	21.06936375
As	24.13719983	22.26359577	16.61588513
As	20.29655620	14.98626738	21.67016162
As	25.13508267	17.07712312	19.18165732
As	17.79544545	19.43640756	24.64714638
As	15.97921286	18.42412195	19.42257978
As	22.08628243	23.16822935	24.33886955
As	20.59802570	17.16735628	15.75838475
As	18.59602424	22.80386082	16.44988993
C	23.45721455	23.81979496	15.61774339
C	23.61929664	25.11177376	16.12602077
H	24.04638815	25.26973249	17.11459787
C	23.23341624	26.20864021	15.35171652
H	23.36603475	27.21567963	15.74867193
C	22.68165251	26.01863709	14.08235700
H	22.38779743	26.87887882	13.47919721
C	22.49611805	24.72419164	13.58897560
H	22.05446342	24.56282124	12.60441220
C	22.88530777	23.62408612	14.35611680
H	22.77037159	22.62144622	13.94993146
C	25.05226031	21.30682812	15.17081453
C	25.69936523	22.00718435	14.14105636
H	25.66861647	23.09639194	14.11013266
C	26.37103160	21.30360026	13.13968351
H	26.87200620	21.84985977	12.33936582
C	26.39861600	19.90614369	13.16631597
H	26.92633395	19.35539350	12.38662410
C	25.75515223	19.21663578	14.19373894
H	25.78289539	18.13086257	14.22617787
C	25.07194588	19.91137552	15.19364656
H	24.56657050	19.36793351	15.99404788
C	25.59377917	23.08620091	17.65301007
C	25.30779693	23.56263437	18.93496249
H	24.31155206	23.44924600	19.35909575
C	26.30828675	24.19703506	19.67619541
H	26.08478756	24.54562773	20.68391002
C	27.58565081	24.35901105	19.13898318
H	28.36570622	24.85072206	19.72140720
C	27.86761833	23.87886302	17.85596366
H	28.86697141	23.99468429	17.43382397
C	26.87533229	23.23820444	17.11052678
H	27.11391390	22.84765707	16.12223219
C	21.85953988	13.89522247	21.20695263
C	23.09381020	14.36307537	21.68131385
H	23.15965671	15.29823746	22.24289765
C	24.24763129	13.61187845	21.45147998
H	25.20540013	13.97561081	21.82184693
C	24.17243398	12.40865384	20.74342027
H	25.07689731	11.82850653	20.55773076
C	22.94250127	11.95410419	20.26419612
H	22.88520858	11.02001405	19.70392072
C	21.77833141	12.69605957	20.49362399
H	20.81948135	12.33265851	20.12446433
C	20.37262095	14.78731746	23.62165002
C	20.22790747	15.90979531	24.43896849

H	20.04725656	16.89157988	23.99949678
C	20.38051458	15.77829997	25.82313037
H	20.32243986	16.66354503	26.45493792
C	20.65378119	14.53255475	26.38627811
H	20.77695666	14.43679093	27.46566929
C	20.80833724	13.41195417	25.56358793
H	21.05264152	12.44124763	25.99629117
C	20.68516917	13.53937555	24.18028336
H	20.87800020	12.67711404	23.54174006
C	18.74470636	13.93856371	21.07780033
C	18.43349036	12.66916651	21.58179920
H	19.04563784	12.21165541	22.35799960
C	17.31954680	11.98293050	21.09070050
H	17.07717949	10.99616347	21.48732022
C	16.51862717	12.55819256	20.09853183
H	15.64879197	12.02005225	19.71984500
C	16.82278539	13.82770149	19.60561567
H	16.19545036	14.29034429	18.84445126
C	17.92852774	14.51985547	20.10303722
H	18.15456474	15.52569891	19.74615843
C	26.11759449	16.64426848	20.82551790
C	25.77908161	17.35336073	21.97841507
H	24.97185782	18.08485739	21.97380541
C	26.47946365	17.12143570	23.16535433
H	26.18753337	17.67142915	24.05946537
C	27.51273001	16.18495486	23.19447010
H	28.05554345	15.99971516	24.12221311
C	27.85312608	15.47859036	22.03421582
H	28.66180350	14.74673107	22.05425236
C	27.15902957	15.70818225	20.84487885
H	27.42957705	15.14799689	19.95100997
C	26.4895182	18.14501575	18.24308345
C	26.83893903	19.34172333	18.88328293
H	26.36539538	19.64931082	19.81731765
C	27.81117847	20.16766843	18.32109848
H	28.06255118	21.10335121	18.81963757
C	28.44151354	19.79769133	17.12945365
H	29.20501758	20.44241587	16.69282446
C	28.08706164	18.60673829	16.49313669
H	28.56642935	18.32431201	15.55503860
C	27.10140281	17.77850606	17.04130238
H	26.81126289	16.86762266	16.51887663
C	24.92358745	15.38703027	18.20685632
C	23.61474138	14.90936740	18.06730282
H	22.78125215	15.48109597	18.47986997
C	23.37536982	13.70241212	17.40686118
H	22.35418604	13.33796078	17.30867480
C	24.44053313	12.97098338	16.87742590
H	24.25223883	12.03078457	16.35770315
C	25.74876595	13.44066605	17.02188948
H	26.58559132	12.86974479	16.61700795
C	25.99548959	14.64553743	17.68674629
H	27.02073000	14.99977449	17.78796620
C	16.57517559	20.95604076	24.90429853
C	16.47836426	21.91862050	23.89950062
H	17.08371319	21.84959564	22.99598393

C	15.59490628	22.99310818	24.04478834
H	15.54555789	23.73654654	23.24956379
C	14.80800770	23.10016662	25.19184098
H	14.12243751	23.94042300	25.30803372
C	14.89622142	22.12634567	26.19385981
H	14.27523544	22.19945689	27.08742853
C	15.77280322	21.05036167	26.05070838
H	15.80915071	20.28557851	26.82476602
C	19.00036131	19.39485546	26.20365598
C	20.37426440	19.36145491	25.95537102
H	20.75974785	19.41180475	24.93630610
C	21.27633544	19.21325597	27.01386755
H	22.33730878	19.12633129	26.78299304
C	20.80640755	19.13723539	28.32493676
H	21.50742238	19.01843971	29.15205885
C	19.43045936	19.19080931	28.57691914
H	19.05707016	19.12477043	29.59958696
C	18.52491166	19.30448047	27.52003257
H	17.45711641	19.29846643	27.73254988
C	16.53412558	17.98550042	25.10222908
C	15.18732453	18.11090701	24.73682606
H	14.84606797	18.97365493	24.16421349
C	14.26851191	17.13531831	25.12896838
H	13.21981937	17.24297492	24.85107476
C	14.69011286	16.02853641	25.87104525
H	13.96860215	15.27203056	26.18144993
C	16.03716175	15.89375265	26.21411314
H	16.37801878	15.03173014	26.78909676
C	16.96054360	16.87047682	25.83132951
H	18.00302134	16.76239086	26.12178237
C	20.31403471	15.22591671	15.97823715
C	19.83029951	14.75017753	17.20093118
H	19.68601532	15.43976944	18.03436672
C	19.55224645	13.38888047	17.35896675
H	19.16742765	13.02502512	18.30948185
C	19.76459295	12.50165289	16.30186705
H	19.54302838	11.44143115	16.42803902
C	20.27345979	12.97238502	15.08815078
H	20.45644874	12.28092244	14.26466968
C	20.55149598	14.33159823	14.92482743
H	20.97258128	14.68297954	13.98329620
C	22.05733460	17.12329220	14.43458638
C	21.94250522	17.79297669	13.21236129
H	21.06119047	18.39558084	12.99717338
C	22.94100052	17.65095419	12.24305942
H	22.84498726	18.17134417	11.28944988
C	24.04210117	16.82797575	12.48540929
H	24.80982908	16.70358994	11.72081833
C	24.16366553	16.17477054	13.71543583
H	25.02404774	15.53544758	13.91865481
C	23.18416018	16.33323719	14.69798185
H	23.28948253	15.81078764	15.64774915
C	19.06952604	17.68827367	14.63284625
C	18.32132389	18.80905739	15.00280844
H	18.57506997	19.35830862	15.91251190
C	17.25208390	19.22588848	14.20415525

H	16.67533497	20.10542855	14.48602707
C	16.92741964	18.51985721	13.04648570
H	16.09302825	18.84824746	12.42560348
C	17.66838972	17.39091944	12.68355710
H	17.41315318	16.83397815	11.78120200
C	18.73911359	16.97250893	13.47448539
H	19.31236709	16.09415059	13.17937387
C	14.66166508	19.85169225	19.67954084
C	15.16822195	21.14605371	19.83101648
H	16.24297654	21.33187622	19.82364766
C	14.29525705	22.22224684	20.00773771
H	14.71724526	23.21902919	20.13513228
C	12.91723202	22.00586784	20.02309938
H	12.23349645	22.84652531	20.14880282
C	12.41019097	20.70784121	19.89058382
H	11.33358146	20.53492425	19.92312769
C	13.27833411	19.62473395	19.72829602
H	12.87158912	18.61543770	19.66081434
C	15.60204251	17.58357416	17.68643972
C	16.58018523	16.69716633	17.21749252
H	17.51845920	16.58629082	17.76304848
C	16.36878333	15.97218743	16.04453034
H	17.13559106	15.28240472	15.69183188
C	15.18736674	16.15200744	15.32014421
H	15.02368355	15.59485003	14.39749239
C	14.22453677	17.05894263	15.76981697
H	13.30719683	17.20921425	15.19914445
C	14.42461570	17.77305953	16.95653334
H	13.66041864	18.46632868	17.30841073
C	15.43546295	16.98085725	20.63620763
C	14.31329001	16.18722240	20.36689416
H	13.70381595	16.36594440	19.48007510
C	13.99649243	15.12866644	21.22053390
H	13.12286621	14.50951566	21.01223137
C	14.81000273	14.85068551	22.32328780
H	14.57175920	14.01375217	22.97961290
C	15.93075963	15.63860201	22.58345100
H	16.57197609	15.41964578	23.43601981
C	16.24013189	16.71212477	21.74646505
H	17.12435918	17.32223363	21.94319799
C	19.14208879	22.45385669	14.59793970
C	20.20557561	21.57639115	14.36991451
H	20.72640842	21.11977346	15.21479898
C	20.60253018	21.29118373	13.06076680
H	21.44616919	20.62263310	12.88849177
C	19.93316895	21.87227326	11.98245733
H	20.24035004	21.64502978	10.96089032
C	18.86817790	22.74933638	12.21313613
H	18.34278151	23.20534234	11.37336660
C	18.46962480	23.04121271	13.51933042
H	17.63201800	23.71759358	13.69310868
C	18.96132940	24.69537951	16.76166666
C	19.62638690	25.49174892	15.82857486
H	20.00437652	25.06943623	14.89871221
C	19.81860618	26.84820366	16.10892942
H	20.33961137	27.47447997	15.38501493

C	19.36262448	27.39313030	17.31099968
H	19.52347790	28.45039458	17.52541977
C	18.72158289	26.57852737	18.24783630
H	18.39347873	26.98457847	19.20476996
C	18.51831699	25.22577775	17.97818716
H	18.03301261	24.60024281	18.72850722
C	16.63421768	22.79594364	16.33200000
C	15.93784970	23.97337729	16.03014666
H	16.47678534	24.91279204	15.90506372
C	14.54601066	23.94518434	15.91384645
H	14.00651726	24.86476884	15.68529635
C	13.85085910	22.74702468	16.09548244
H	12.76376290	22.72870696	16.01061870
C	14.54741779	21.57694160	16.40418158
H	14.00694626	20.64630817	16.56876668
C	15.93806056	21.59942272	16.53354698
H	16.47383747	20.68982394	16.81012912
C	20.81171032	23.52303454	25.77353865
C	19.45244658	23.35457715	25.49019670
H	19.13341347	23.03733592	24.49594354
C	18.50411536	23.59532684	26.48681983
H	17.44636960	23.46342252	26.26391839
C	18.91289634	23.99098818	27.76283496
H	18.17127582	24.16443647	28.54376995
C	20.27200755	24.16608623	28.04088519
H	20.59447707	24.48057411	29.03412233
C	21.22607238	23.93818240	27.04584588
H	22.28547297	24.07330528	27.26639744
C	22.59212831	24.92756457	23.64169057
C	23.24553126	24.98879457	22.40680752
H	23.43819819	24.08027709	21.83479245
C	23.62201328	26.22834562	21.88518449
H	24.09970815	26.27278275	20.90705317
C	23.34353278	27.39868007	22.59384315
H	23.62848396	28.36696988	22.18103646
C	22.68101287	27.33251715	23.82319891
H	22.44860263	28.24629673	24.37188986
C	22.30026223	26.09748801	24.35241551
H	21.76889678	26.05231047	25.30307466
C	23.70088674	22.53445908	25.24782798
C	24.95499075	22.81017481	24.69564894
H	25.04927715	23.41943608	23.79858473
C	26.10129996	22.27569684	25.28806564
H	27.07611499	22.48120850	24.84576414
C	25.99535001	21.46929572	26.42275485
H	26.89166947	21.04745197	26.87857025
C	24.73787658	21.19578356	26.96980163
H	24.64899274	20.56510142	27.85566387
C	23.58763762	21.72342996	26.38233366
H	22.61037669	21.50556052	26.81032364

Figure A55. Optimized coordinates of $Au_{13}(AsPh_3)_8Cl_4^+$.

Coordinates of the optimized structure for $Au_{13}(AsPh_3)_8Cl_4^+$ with different ligand orientation

Au	21.27595771	17.83587528	19.33875530
Au	21.86519876	18.98109244	22.09013500
Au	22.19437548	21.92466328	21.69864541
Au	23.17748595	20.07295123	19.61885231
Au	19.12318635	18.17425223	21.39467737
Au	20.40784124	20.39146997	20.12177745
As	21.94087807	19.72209624	15.04382462
As	21.92948682	15.59060952	18.62629495
As	23.07464091	17.62127317	23.73581993
As	18.99541541	21.35042185	25.16208473
As	17.10733958	22.68765939	16.69654292
As	23.85112466	23.33228144	22.83704241
Au	21.14546843	20.09861209	17.35861829
Au	19.72117775	20.85296180	22.86334103
Au	17.67539912	20.60140410	20.75542934
Au	18.75828548	21.70927574	18.22767838
Au	21.60034053	22.58426249	18.85126215
Au	18.66672553	18.79394789	18.50630976
Au	19.46931294	22.99893780	20.80959873
As	15.32776543	20.57863430	21.42804033
As	22.62771539	24.53491165	17.79159658
Cl	25.54686602	19.77306174	19.32292188
Cl	17.88652257	16.50614403	22.55837926
Cl	17.31211600	17.56392376	16.99253147
Cl	18.84115941	25.26627118	21.26299752
C	22.25951754	21.27533497	13.88690003
C	23.55308831	21.77428027	13.70559640
H	24.40008358	21.31770639	14.21604645
C	23.75980031	22.86409509	12.85526846
H	24.76829302	23.25238270	12.71756599
C	22.68356082	23.44604296	12.18245022
H	22.85073630	24.28972540	11.51208873
C	21.39264274	22.94481030	12.36915466
H	20.54772054	23.38676853	11.84053526
C	21.17377225	21.86912934	13.23172354
H	20.16356203	21.48707739	13.37329003
C	20.79595511	18.60454113	13.90875982
C	20.89453518	18.63115895	12.51069346
H	21.57994326	19.31767168	12.01304786
C	20.07585942	17.79554393	11.74814888
H	20.14599705	17.81852963	10.65974119
C	19.15531192	16.94947168	12.37637022
H	18.50934136	16.30856484	11.77456521
C	19.0521066	16.93937543	13.76863713
H	18.32393293	16.30456101	14.27274069
C	19.87633384	17.76358032	14.53880655
H	19.77120260	17.75779200	15.62353671
C	23.67895265	18.80826815	14.99984635
C	24.39408159	18.69350363	16.19269117
H	23.99903684	19.11020103	17.11881383
C	25.62480832	18.02997182	16.20833856
H	26.16345818	17.94538190	17.15240812

C	26.13341592	17.48369261	15.02851759
H	27.08772605	16.95575319	15.04010191
C	25.41987470	17.61005243	13.83052181
H	25.82102271	17.18773971	12.90818451
C	24.19025394	18.27122655	13.81186367
H	23.63377594	18.35214884	12.87852392
C	21.77296334	15.10869712	16.72980423
C	22.80029386	15.43231150	15.83692151
H	23.69140091	15.95665565	16.18025811
C	22.68990076	15.06030565	14.49475618
H	23.49584599	15.30829761	13.80515340
C	21.55876147	14.37741379	14.04449083
H	21.47695608	14.08601942	12.99693267
C	20.52670605	14.07581876	14.93577080
H	19.63606914	13.55181243	14.58757191
C	20.62700753	14.44292038	16.27948894
H	19.81918190	14.20158267	16.96988221
C	23.79113658	15.16558489	19.05193431
C	24.48326997	16.03337979	19.90192014
H	23.99163420	16.92401705	20.29633506
C	25.81884204	15.77531587	20.22082229
H	26.35145230	16.46488951	20.87497383
C	26.45797118	14.65026823	19.69583224
H	27.50025903	14.44758995	19.94529430
C	25.76670925	13.78969136	18.83649334
H	26.26708299	12.91709301	18.41539020
C	24.43554482	14.04816477	18.50485881
H	23.91564888	13.39286168	17.80533815
C	20.78341827	14.22052286	19.42999348
C	21.17240272	12.87809479	19.49907921
H	22.17081669	12.56804437	19.19268339
C	20.26822552	11.92778421	19.97568850
H	20.56526327	10.87959108	20.02887529
C	18.98618222	12.31464292	20.38193481
H	18.28760250	11.56623530	20.75823735
C	18.60720431	13.65676623	20.31780980
H	17.62297334	13.97942048	20.65668454
C	19.50632516	14.61337340	19.83754728
H	19.20688292	15.66090767	19.79515039
C	22.73950590	15.72089054	23.38370874
C	21.40768378	15.32771477	23.19808335
H	20.59329280	16.05421135	23.20193333
C	21.11303750	13.98374370	22.96481741
H	20.07633046	13.68557061	22.81495376
C	22.14266121	13.04378824	22.88438032
H	21.90793372	11.99867967	22.68179531
C	23.47174225	13.44659470	23.03316210
H	24.28039960	12.71960379	22.94741552
C	23.77606380	14.78721235	23.28559323
H	24.81577132	15.09427765	23.38642776
C	22.63368754	17.80621319	25.64508072
C	21.43830463	17.26850539	26.13667515
H	20.73532715	16.76664369	25.47270369
C	21.14514451	17.36559695	27.49888855
H	20.21036613	16.95199112	27.87585272
C	22.04308551	17.99032698	28.36917476

H	21.81833049	18.04763699	29.43497309
C	23.22160844	18.54929668	27.86893564
H	23.92291889	19.04713868	28.54019410
C	23.51217253	18.47553331	26.50393206
H	24.42471877	18.92989153	26.12091818
C	25.01796623	17.80659566	23.68951828
C	25.56582159	18.59176179	22.67287218
H	24.92086588	19.11009586	21.96313473
C	26.95336946	18.69467520	22.54343418
H	27.36334419	19.29570765	21.73147685
C	27.78826732	18.02165466	23.43671078
H	28.87187702	18.09496281	23.33372882
C	27.23784934	17.24864457	24.46584886
H	27.89039259	16.72553898	25.16600156
C	25.85216769	17.13768764	24.59719760
H	25.42804226	16.53274102	25.39927089
C	18.32643893	19.81074044	26.17352773
C	18.05802971	18.64068651	25.45869572
H	18.20855798	18.59376529	24.37956372
C	17.58837105	17.50972159	26.13098078
H	17.38266682	16.60571081	25.55772260
C	17.38271026	17.55270827	27.51103152
H	17.00838100	16.67270697	28.03602380
C	17.65392826	18.72454812	28.22578458
H	17.49640393	18.75709482	29.30472141
C	18.13289365	19.85571972	27.56146862
H	18.37399579	20.75563461	28.12744887
C	17.56522080	22.69728210	25.17997523
C	17.32056522	23.41791428	24.00859387
H	17.90630749	23.23229752	23.10803203
C	16.31598389	24.39007473	23.98411737
H	16.13857477	24.94399635	23.06327914
C	15.55319712	24.63132829	25.12743824
H	14.75874452	25.37818187	25.10697473
C	15.80809514	23.91566648	26.30334197
H	15.21762131	24.10945324	27.19983604
C	16.81682375	22.95180596	26.33520240
H	17.00153716	22.39537373	27.25331882
C	20.29071566	22.15966491	26.39405616
C	21.05316852	21.35798269	27.24986655
H	20.95038991	20.27361331	27.23643173
C	21.94014555	21.95776320	28.14699871
H	22.50844705	21.33006871	28.83368890
C	22.10010438	23.34585037	28.16081509
H	22.80173622	23.80972070	28.85502647
C	21.36412629	24.14046882	27.27700103
H	21.49381002	25.22248934	27.26800834
C	20.45217657	23.54999196	26.39868041
H	19.86435373	24.17622744	25.72813061
C	14.50742831	22.34820960	21.29478508
C	15.23996825	23.34666222	20.64307463
H	16.23560354	23.13169458	20.25083150
C	14.70825209	24.63223320	20.51851542
H	15.29294141	25.40574351	20.01920173
C	13.44446690	24.91673178	21.04172666
H	13.02647727	25.91995082	20.94790996

C	12.71878934	23.92115830	21.70474999
H	11.73994465	24.14805236	22.12842713
C	13.24952693	22.63637590	21.83961649
H	12.69381799	21.87521171	22.38789250
C	14.91422704	19.94912288	23.24030797
C	14.80748260	18.56782221	23.44807555
H	14.95555425	17.86760043	22.62664260
C	14.51629102	18.08551920	24.72456007
H	14.43199244	17.01029893	24.88463138
C	14.34240129	18.97262599	25.79028361
H	14.11913571	18.58997064	26.78675825
C	14.47030618	20.34675499	25.58059381
H	14.35051332	21.04360472	26.41018890
C	14.76104493	20.84152500	24.30600627
H	14.86072465	21.91546393	24.15365880
C	14.27204601	19.30872974	20.37147103
C	14.96678880	18.25880262	19.76547950
H	16.05584210	18.22101166	19.79990488
C	14.26060271	17.25111917	19.10303809
H	14.81658818	16.44951030	18.61763362
C	12.86621623	17.29556947	19.05358545
H	12.31236959	16.50932119	18.53889271
C	12.17592236	18.35508209	19.65209132
H	11.08728049	18.39789934	19.60092697
C	12.87573833	19.36629994	20.31252576
H	12.32976120	20.19409374	20.76417677
C	16.91475516	24.63250056	16.83282471
C	17.62069366	25.26009399	17.86381463
H	18.30064884	24.69041704	18.49764973
C	17.43895912	26.62385786	18.10772320
H	17.98423705	27.08629115	18.93074091
C	16.56413433	27.36456387	17.31211534
H	16.42052143	28.42974183	17.49973673
C	15.86322551	26.74017471	16.27478542
H	15.17163909	27.31622212	15.65873828
C	16.02810568	25.37336413	16.03486882
H	15.44601829	24.89037171	15.24987513
C	17.40690360	22.21512840	14.80956743
C	17.57507084	20.85524325	14.51009134
H	17.61388321	20.10153177	15.29883229
C	17.70347348	20.45199453	13.17853426
H	17.82418803	19.39315760	12.95216377
C	17.69942019	21.39926709	12.15082698
H	17.81348696	21.07931680	11.11449825
C	17.57048628	22.75634594	12.45718159
H	17.57424477	23.50037941	11.65886284
C	17.42057023	23.16723791	13.78576019
H	17.32115036	24.22717503	14.01457550
C	15.27155980	22.02468692	16.97344508
C	14.23641859	22.89653271	17.32431671
H	14.42890375	23.95456877	17.48932063
C	12.93612879	22.40601700	17.47148643
H	12.13300191	23.09088441	17.74668912
C	12.67071857	21.05151895	17.26673090
H	11.65532129	20.66944900	17.37565360
C	13.71356256	20.17896744	16.94840533

H	13.52276885	19.11340931	16.82802820
C	15.01817273	20.65550499	16.81693720
H	15.81867258	19.94361998	16.61417523
C	23.16037219	26.00153676	18.97661242
C	22.38803426	26.23272515	20.11996607
H	21.56642038	25.56544236	20.38796791
C	22.65320280	27.35404494	20.91204528
H	22.04998296	27.53320047	21.80086045
C	23.68076353	28.23390415	20.56489182
H	23.88062428	29.10983715	21.18334768
C	24.45345197	27.99051578	19.42669698
H	25.25849714	28.67425845	19.15495616
C	24.19746428	26.87259981	18.62960457
H	24.80953791	26.68546075	17.74820304
C	21.45591162	25.47978897	16.53560708
C	20.98380958	26.76464625	16.82567893
H	21.31137606	27.28570000	17.72457484
C	20.07706926	27.38044109	15.95866996
H	19.70280772	28.37788358	16.18988253
C	19.64158630	26.71649708	14.81081579
H	18.92742343	27.19590290	14.14061320
C	20.11929460	25.43499430	14.52559845
H	19.78999948	24.91027124	13.63042345
C	21.02052584	24.80855661	15.38750856
H	21.38111057	23.80530550	15.15924984
C	24.21702759	24.03894262	16.75906929
C	24.76708993	24.86543450	15.77147342
H	24.28423911	25.80586212	15.50266116
C	25.93699005	24.46715695	15.11851260
H	26.37703168	25.11453051	14.35883285
C	26.54051758	23.24426399	15.43198696
H	27.45241048	22.94032861	14.91645933
C	25.96898710	22.40853546	16.39432368
H	26.41486493	21.44410695	16.64049705
C	24.80926516	22.80818277	17.06190391
H	24.37669765	22.15508720	17.82126553
C	23.09499246	24.90521533	23.72086154
C	21.74516190	25.18710810	23.49675021
H	21.14269146	24.54823538	22.84986439
C	21.15778667	26.30521651	24.09435220
H	20.10555023	26.51593462	23.89861337
C	21.92138424	27.13593359	24.91788512
H	21.46675063	28.01253668	25.38193839
C	23.27026304	26.84478999	25.15169479
H	23.86412748	27.48940107	25.80107328
C	23.86213447	25.72657251	24.55833771
H	24.90870563	25.49320175	24.75801995
C	25.22032039	23.96625386	21.59105628
C	25.73619238	23.00959113	20.70997393
H	25.34945041	21.98984290	20.69349349
C	26.75394568	23.36245794	19.82258631
H	27.14830472	22.60846450	19.14220346
C	27.23611115	24.67282523	19.80128572
H	28.01801897	24.95345674	19.09453868
C	26.70530468	25.62760187	20.67266331
H	27.06945507	26.65472512	20.64622126

C	25.69782093	25.27894268	21.57642354
H	25.27783320	26.03344445	22.24007811
C	24.92151598	22.49160915	24.25393935
C	26.20202009	21.99244943	23.99221386
H	26.64492177	22.09054313	23.00169888
C	26.92214711	21.36746982	25.01363004
H	27.91527878	20.96905168	24.80661572
C	26.37031521	21.24809480	26.29102423
H	26.93779020	20.76841328	27.08922896
C	25.08830167	21.74367091	26.54406940
H	24.64659253	21.65206473	27.53542115
C	24.35410336	22.35404224	25.52566002
H	23.35227669	22.73088685	25.73062165

Figure A56. Optimized coordinates of $Au_{13}(AsPh_3)_8Cl_4^+$ with different ligand orientation.

Coordinates of the optimized structure for $Au_{13}(SbPh_3)_8Cl_4^+$

Au	21.25160390	17.82431477	19.35689534
Au	21.87115031	18.96955088	22.04588096
Au	22.17333872	21.88285620	21.71520757
Au	23.21367348	20.06294756	19.60797716
Au	19.09155720	18.15188521	21.36286901
Au	20.41368804	20.37051042	20.11344486
Sb	21.99096339	19.69005607	14.94743673
Sb	21.93830870	15.45735852	18.57704502
Sb	23.15078681	17.55139213	23.79399830
Sb	18.96014000	21.32339445	25.25414310
Sb	17.10003398	22.73997623	16.58383893
Sb	23.93792434	23.36641023	22.90161469
Au	21.18399709	20.06861521	17.39872866
Au	19.69477345	20.79809787	22.81775923
Au	17.69335352	20.62275005	20.67015302
Au	18.86194254	21.74275619	18.20422971
Au	21.64822248	22.54378428	18.89343861
Au	18.65129561	18.80112038	18.48445668
Au	19.47656593	23.00043442	20.82983038
Sb	15.22911193	20.56757818	21.43195472
Sb	22.70202070	24.62571357	17.78869958
Cl	25.58058397	19.78269746	19.30817132
Cl	17.96443636	16.49408227	22.64473069
Cl	17.25000183	17.73559194	16.88830855
Cl	18.90186328	25.28090825	21.27216982
C	22.30668594	21.37856388	13.63675600
C	23.57909913	21.94843328	13.51145236
H	24.43088476	21.54337242	14.05817953
C	23.76090088	23.05791939	12.67943534
H	24.75153890	23.50365022	12.59144426
C	22.67983857	23.59508452	11.97553113
H	22.82585567	24.46053574	11.32853132
C	21.41014270	23.02539515	12.10609198
H	20.56133205	23.43448962	11.55635099

C	21.21710489	21.92259663	12.94253652
H	20.22024930	21.49131017	13.03365865
C	20.74361548	18.44691101	13.70573069
C	20.91122657	18.41502518	12.31483923
H	21.66763138	19.03120785	11.82611245
C	20.07871008	17.60317542	11.53931579
H	20.20556711	17.57674545	10.45610359
C	19.07527465	16.84117411	12.14736903
H	18.42114181	16.21682382	11.53748041
C	18.90576402	16.88573633	13.53311432
H	18.12025817	16.30839243	14.02093534
C	19.74313075	17.68521629	14.31734466
H	19.58425932	17.71612020	15.39534755
C	23.91291553	18.71166628	14.90511765
C	24.58942935	18.54711985	16.11808556
H	24.18098675	18.94065530	17.04932107
C	25.81183867	17.86776391	16.15293893
H	26.32305451	17.75097011	17.10923756
C	26.35157057	17.34883257	14.97400139
H	27.30077654	16.81220025	14.99683209
C	25.67710864	17.52012714	13.75887454
H	26.10129563	17.12062158	12.83620969
C	24.45864076	18.20387687	13.71895858
H	23.94122738	18.32592606	12.76648971
C	21.77641255	14.92770090	16.49230890
C	22.78191475	15.28964993	15.58815405
H	23.68321802	15.80349527	15.92423862
C	22.63045830	14.98675882	14.23202670
H	23.41335064	15.27473146	13.53028421
C	21.48300682	14.33044343	13.78203314
H	21.36375881	14.10728391	12.72155391
C	20.48216369	13.96985634	14.68776762
H	19.58315564	13.46004066	14.33892626
C	20.62343322	14.27029846	16.04460330
H	19.83517882	13.99033280	16.74467102
C	23.98121228	14.99146315	19.06849819
C	24.67771685	15.91613139	19.85630869
H	24.20042610	16.84414465	20.17702308
C	26.00350987	15.66118281	20.21864324
H	26.53934064	16.38636346	20.83126966
C	26.62919813	14.48771166	19.79252808
H	27.66162853	14.28641898	20.08044801
C	25.93922983	13.57565199	18.98695132
H	26.43492047	12.66869014	18.63829693
C	24.61445851	13.82506786	18.61872125
H	24.09227402	13.11591255	17.97433604
C	20.65701182	13.95832989	19.44199932
C	21.00271638	12.60141829	19.45748520
H	21.96549772	12.26261884	19.07320226
C	20.10471944	11.66904489	19.98346218
H	20.37244705	10.61188819	20.00117155
C	18.86901501	12.08890940	20.48755762
H	18.17289202	11.35667434	20.89852018
C	18.52869545	13.44266722	20.47252452
H	17.57940229	13.78828525	20.88258690
C	19.42442319	14.38098704	19.95015229

H	19.15326762	15.43740735	19.96317409
C	22.78962335	15.45810273	23.44203125
C	21.46201685	15.04424851	23.27098287
H	20.62991507	15.75187092	23.28711959
C	21.18847442	13.69412884	23.03900981
H	20.15639714	13.37692653	22.89245009
C	22.23131449	12.76935911	22.95650482
H	22.01147324	11.71981127	22.75886877
C	23.55550987	13.19199109	23.09906845
H	24.37379014	12.47584266	23.01387885
C	23.84000786	14.53895762	23.34326224
H	24.87729950	14.86202890	23.43645563
C	22.70706470	17.76139587	25.90038880
C	21.48126132	17.29409348	26.39093406
H	20.74492274	16.83690690	25.72853301
C	21.19253925	17.40699180	27.75383718
H	20.23185033	17.05402619	28.12830402
C	22.12560503	17.97844498	28.62368405
H	21.90339205	18.05093497	29.68874090
C	23.33788445	18.46346806	28.12734341
H	24.06421821	18.92191721	28.80052873
C	23.62853749	18.36615284	26.76276789
H	24.57277820	18.76038042	26.38600597
C	25.28945873	17.73760033	23.72571707
C	25.84366466	18.50350672	22.69398323
H	25.21328004	19.00987370	21.96170601
C	27.23279865	18.60985571	22.57859344
H	27.65188077	19.19644421	21.75997153
C	28.06352526	17.96365295	23.49698854
H	29.14745170	18.04455108	23.40481451
C	27.50805568	17.20644773	24.53337973
H	28.15543313	16.69804828	25.24915480
C	26.12034035	17.08802988	24.64939896
H	25.69854617	16.48990880	25.45867106
C	18.22408067	19.64732006	26.38729140
C	18.01071064	18.45068561	25.69531918
H	18.19039335	18.37203635	24.62185850
C	17.55238281	17.32411314	26.38410253
H	17.39012732	16.39933039	25.82914658
C	17.30244048	17.39652116	27.75616973
H	16.93990229	16.51836139	28.29218557
C	17.51445633	18.59559197	28.44533206
H	17.32518117	18.65139512	29.51814472
C	17.98153955	19.72349216	27.76552045
H	18.16743434	20.64518442	28.31884067
C	17.41444646	22.83008048	25.27516456
C	17.18583468	23.54526309	24.09447547
H	17.77465746	23.35581785	23.19581825
C	16.19141544	24.52851233	24.05784964
H	16.02141521	25.07751161	23.13193102
C	15.42228139	24.78636647	25.19401011
H	14.63785356	25.54333633	25.16066053
C	15.65735325	24.07531250	26.37675386
H	15.06150010	24.28160680	27.26713753
C	16.65661849	23.09938331	26.42180711
H	16.82682276	22.55037837	27.34880770

C	20.37513590	22.21538585	26.61840145
C	21.10410454	21.42567798	27.51595964
H	20.96742845	20.34459484	27.55452234
C	22.01079331	22.03385369	28.39026966
H	22.56256753	21.41737017	29.10131771
C	22.21202528	23.41620643	28.34825497
H	22.92465929	23.88530692	29.02742072
C	21.50194365	24.19764552	27.43179392
H	21.66874588	25.27377813	27.37767351
C	20.57555931	23.60090914	26.57258377
H	20.01518139	24.22494144	25.87571028
C	14.30402618	22.50681743	21.28761048
C	15.04595099	23.51482305	20.65826008
H	16.04583647	23.30755143	20.27158765
C	14.51653223	24.80307612	20.54266490
H	15.10281826	25.58124177	20.05214375
C	13.24696396	25.08206801	21.05608916
H	12.83001530	26.08576282	20.96496265
C	12.51080385	24.07779379	21.69380813
H	11.52441361	24.29873133	22.10382029
C	13.03756894	22.78805794	21.81492793
H	12.46081073	22.01880364	22.33076541
C	14.79189478	19.91237410	23.43724286
C	14.72591644	18.53451251	23.68953439
H	14.89474526	17.80890155	22.89258939
C	14.44899911	18.08459177	24.98255244
H	14.39692506	17.01312753	25.17892684
C	14.25240626	19.00187226	26.01823340
H	14.04466012	18.64723067	27.02786381
C	14.33593695	20.37253120	25.76428038
H	14.20191685	21.09210826	26.57275388
C	14.60554792	20.83501200	24.47222902
H	14.67078990	21.90838924	24.28987081
C	14.07024327	19.12927881	20.32983847
C	14.77415375	18.14772656	19.62541048
H	15.86302043	18.16223364	19.57499330
C	14.07368889	17.14155576	18.95352151
H	14.63264224	16.38970725	18.39604148
C	12.67814705	17.12608705	18.98023522
H	12.13170940	16.34286881	18.45351056
C	11.97670179	18.11694989	19.67670044
H	10.88609129	18.10774664	19.69018940
C	12.67108139	19.11868956	20.35960972
H	12.11284395	19.88333215	20.90113452
C	16.85809606	24.87135332	16.76692331
C	17.50661152	25.47008312	17.85464419
H	18.15528289	24.89280407	18.51582726
C	17.31153260	26.82868705	18.12149085
H	17.81596954	27.27521296	18.97916289
C	16.47610025	27.58824373	17.29990256
H	16.31893154	28.64727850	17.50863114
C	15.83250771	26.99125640	16.21030762
H	15.17140750	27.58119904	15.57413019
C	16.01618318	25.63161697	15.94222572
H	15.48298098	25.17341914	15.10789062
C	17.37555428	22.22931318	14.50241128

C	17.58293924	20.87510886	14.20168341
H	17.63751745	20.11945835	14.98909265
C	17.72519353	20.47566471	12.86936710
H	17.89385371	19.42351643	12.64048488
C	17.67203971	21.42310699	11.84327489
H	17.79048001	21.10843209	10.80598951
C	17.47653455	22.77358238	12.14655380
H	17.43346616	23.51518416	11.34730757
C	17.32744840	23.18016202	13.47714677
H	17.17968953	24.23661474	13.70279385
C	15.08658266	22.03000916	16.90561215
C	14.06082404	22.92108348	17.23918189
H	14.25950746	23.98525007	17.36558204
C	12.76214954	22.43721245	17.42638118
H	11.96351667	23.13049197	17.69395989
C	12.49333216	21.07515837	17.27973372
H	11.48184924	20.69768731	17.43193357
C	13.52409083	20.18853413	16.95887566
H	13.32564101	19.12059287	16.87469075
C	14.82689108	20.65884366	16.77995500
H	15.62231323	19.94097280	16.57037821
C	23.24805222	26.28292743	19.05189028
C	22.48778091	26.51811179	20.20417777
H	21.66631969	25.85617280	20.48682255
C	22.77242460	27.63167614	21.00163693
H	22.18593290	27.80752605	21.90297247
C	23.80353240	28.50454691	20.64689735
H	24.01795522	29.37491377	21.26817177
C	24.56214502	28.26118929	19.49851447
H	25.37022166	28.93914064	19.22078479
C	24.29013419	27.14710914	18.69982312
H	24.89807020	26.95875901	17.81422108
C	21.40313802	25.62365287	16.38759515
C	20.93606534	26.91368232	16.66509903
H	21.28930067	27.45637167	17.54276263
C	19.99977119	27.50826916	15.81454230
H	19.62694838	28.50848714	16.03626205
C	19.53504945	26.81985065	14.69243150
H	18.79939254	27.28375914	14.03475942
C	20.00638463	25.53324708	14.41806159
H	19.64787564	24.98672771	13.54632288
C	20.93395806	24.92566248	15.26761728
H	21.28239753	23.91642316	15.04326779
C	24.46264084	24.06401473	16.67891216
C	25.07695913	24.89399827	15.73292002
H	24.66611845	25.87725676	15.49821579
C	26.21887158	24.44468235	15.06227417
H	26.70104687	25.08993073	14.32639109
C	26.73693261	23.17123765	15.32290907
H	27.62193182	22.82443850	14.78795983
C	26.11587813	22.34131772	16.26014327
H	26.50118103	21.34289514	16.47072904
C	24.98004633	22.78843831	16.94050958
H	24.50906414	22.12936154	17.67224817
C	23.10133931	25.11054897	23.84173090
C	21.74805829	25.37448603	23.60226173

H	21.14968349	24.72312572	22.96304106
C	21.14634424	26.50158153	24.16916536
H	20.09388369	26.69974280	23.96181925
C	21.89854316	27.36206351	24.97361212
H	21.43289752	28.24524330	25.41278646
C	23.25123176	27.09569341	25.21406681
H	23.83711283	27.76714092	25.84360007
C	23.85752566	25.96693858	24.65286577
H	24.91001887	25.76303790	24.85780395
C	25.46379340	24.06946176	21.55597908
C	25.97573053	23.13717621	20.64454253
H	25.60662610	22.11044285	20.60705707
C	26.96717560	23.52473968	19.73920429
H	27.34776074	22.79542122	19.02459617
C	27.44143104	24.83823850	19.74154166
H	28.20924799	25.14274136	19.02889200
C	26.92134485	25.76642160	20.64821622
H	27.27571674	26.79766501	20.63986182
C	25.92730371	25.38905239	21.55693218
H	25.50478669	26.13301553	22.23296874
C	25.11039195	22.45507182	24.46650622
C	26.38484780	21.94657022	24.18918033
H	26.82594314	22.05706220	23.19782762
C	27.10230295	21.29020855	25.19393347
H	28.08906245	20.88268472	24.97337566
C	26.55163897	21.14649115	26.47028103
H	27.11405990	20.63392599	27.25188137
C	25.27808019	21.65516107	26.74156354
H	24.83659745	21.54245281	27.73161096
C	24.54859467	22.30132623	25.73960891
H	23.55170925	22.68145563	25.96455091

Figure A57. Optimized coordinates of $Au_{13}(SbPh_3)_8Cl_4^+$.

References

1. Logsdon, J. M., John F. Kennedy and the Race to the Moon. In *John F. Kennedy and the Race to the Moon*, Logsdon, J. M., Ed. Palgrave Macmillan US: New York, 2010; pp 223-244.

2. Eigler, D. M.; Schweizer, E. K., Positioning single atoms with a scanning tunnelling microscope. *Nature* **1990,** *344* (6266), 524-526.

3. Feynman, R. P., There's plenty of room at the bottom. In *Feynman and computation*, Anthony, J. G. H., Ed. Perseus Books: 1999; pp 63-76.

4. Rao, R.; Pint, C. L.; Islam, A. E.; Weatherup, R. S.; Hofmann, S.; Meshot, E. R.; Wu, F.; Zhou, C.; Dee, N.; Amama, P. B.; Carpena-Nuñez, J.; Shi, W.; Plata, D. L.; Penev, E. S.; Yakobson, B. I.; Balbuena, P. B.; Bichara, C.; Futaba, D. N.; Noda, S.; Shin, H.; Kim, K. S.; Simard, B.; Mirri, F.; Pasquali, M.; Fornasiero, F.; Kauppinen, E. I.; Arnold, M.; Cola, B. A.; Nikolaev, P.; Arepalli, S.; Cheng, H.-M.; Zakharov, D. N.; Stach, E. A.; Zhang, J.; Wei, F.; Terrones, M.; Geohegan, D. B.; Maruyama, B.; Maruyama, S.; Li, Y.; Adams, W. W.; Hart, A. J., Carbon Nanotubes and Related Nanomaterials: Critical Advances and Challenges for Synthesis toward Mainstream Commercial Applications. *ACS Nano* **2018,** *12* (12), 11756-11784.

5. Salata, O. V., Applications of nanoparticles in biology and medicine. *Journal of nanobiotechnology* **2004,** *2* (1), 3-3.

6. Son, D.; Bao, Z., Nanomaterials in Skin-Inspired Electronics: Toward Soft and Robust Skin-like Electronic Nanosystems. *ACS Nano* **2018,** *12* (12), 11731-11739.

7. Liu, Y.; Tsunoyama, H.; Akita, T.; Xie, S.; Tsukuda, T., Aerobic Oxidation of Cyclohexane Catalyzed by Size-Controlled Au Clusters on Hydroxyapatite: Size Effect in the Sub-2 nm Regime. *ACS Catalysis* **2011,** *1* (1), 2-6.

8. Tsukuda, T.; Tsunoyama, H.; Sakurai, H., Aerobic Oxidations Catalyzed by Colloidal Nanogold. *Chemistry – An Asian Journal* **2011,** *6* (3), 736-748.

9. Daniel, M.-C.; Astruc, D., Gold nanoparticles: assembly, supramolecular chemistry, quantum-size-related properties, and applications toward biology, catalysis, and nanotechnology. *Chemical reviews* **2004,** *104* (1), 293-346.

10. Sharma, P.; Brown, S.; Walter, G.; Santra, S.; Moudgil, B., Nanoparticles for bioimaging. *Advances in colloid and interface science* **2006,** *123*, 471-485.

11. Boisselier, E.; Astruc, D., Gold nanoparticles in nanomedicine: preparations, imaging, diagnostics, therapies and toxicity. *Chemical society reviews* **2009,** *38* (6), 1759-1782.

12. Weare, W. W.; Reed, S. M.; Warner, M. G.; Hutchison, J. E., Improved synthesis of small (d core≈ 1.5 nm) phosphine-stabilized gold nanoparticles. *Journal of the American Chemical Society* **2000,** *122* (51), 12890-12891.

13. Brust, M.; Walker, M.; Bethell, D.; Schiffrin, D. J.; Whyman, R., Synthesis of thiol-derivatised gold nanoparticles in a two-phase liquid–liquid system. *Journal of the Chemical Society, Chemical Communications* **1994,** (7), 801-802.

14. Jadzinsky, P. D.; Calero, G.; Ackerson, C. J.; Bushnell, D. A.; Kornberg, R. D., Structure of a thiol monolayer-protected gold nanoparticle at 1.1 Å resolution. *Science* **2007,** *318* (5849), 430-433.

15. Badia, A.; Singh, S.; Demers, L.; Cuccia, L.; Brown, G. R.; Lennox, R. B., Self-Assembled Monolayers on Gold Nanoparticles. *Chemistry – A European Journal* **1996,** *2* (3), 359-363.

16. Lopez-Acevedo, O.; Akola, J.; Whetten, R. L.; Grönbeck, H.; Häkkinen, H., Structure and bonding in the ubiquitous icosahedral metallic gold cluster Au144 (SR) 60. *The Journal of Physical Chemistry C* **2009,** *113* (13), 5035-5038.

17. Walter, M.; Akola, J.; Lopez-Acevedo, O.; Jadzinsky, P. D.; Calero, G.; Ackerson, C. J.; Whetten, R. L.; Grönbeck, H.; Häkkinen, H., A unified view of ligand-protected gold clusters as superatom complexes. *Proceedings of the National Academy of Sciences* **2008,** *105* (27), 9157-9162.

18. Pyykkö, P., Relativity, Gold, Closed-Shell Interactions, and CsAu· NH3. *Angewandte Chemie International Edition* **2002,** *41* (19), 3573-3578.

19. Pyykkö, P., Theoretical chemistry of gold. *Angewandte Chemie International Edition* **2004,** *43* (34), 4412-4456.

20. Malola, S.; Kaappa, S.; Hakkinen, H., From Molecular to Metallic Gold Nanoparticles: The Role of Nanocrystal Symmetry in the Crossover Region. *arXiv preprint arXiv:1809.04411* **2018**.

21. Lopez, N.; Nørskov, J. K., Catalytic CO oxidation by a gold nanoparticle: A density functional study. *Journal of the American Chemical Society* **2002,** *124* (38), 11262-11263.

22. Anderson, R. M.; Yancey, D. F.; Zhang, L.; Chill, S. T.; Henkelman, G.; Crooks, R. M., A theoretical and experimental approach for correlating nanoparticle structure and electrocatalytic activity. *Accounts of chemical research* **2015,** *48* (5), 1351-1357.

23. DuChene, J. S.; Niu, W.; Abendroth, J. M.; Sun, Q.; Zhao, W.; Huo, F.; Wei, W. D., Halide anions as shape-directing agents for obtaining high-quality anisotropic gold nanostructures. *Chemistry of Materials* **2012,** *25* (8), 1392-1399.

24. Maye, M. M.; Luo, J.; Lim, I.-I. S.; Han, L.; Kariuki, N. N.; Rabinovich, D.; Liu, T.; Zhong, C.-J., Size-controlled assembly of gold nanoparticles induced by a tridentate thioether ligand. *Journal of the American Chemical Society* **2003,** *125* (33), 9906-9907.

25. Sau, T. K.; Murphy, C. J., Room temperature, high-yield synthesis of multiple shapes of gold nanoparticles in aqueous solution. *Journal of the American Chemical Society* **2004,** *126* (28), 8648-8649.

26. Reimers, J. R.; Ford, M. J.; Halder, A.; Ulstrup, J.; Hush, N. S., Gold surfaces and nanoparticles are protected by Au (0)–thiyl species and are destroyed when Au (I)–thiolates form. *Proceedings of the National Academy of Sciences* **2016**, 201600472.

27. Chi, Q.; Ford, M. J.; Halder, A.; Hush, N. S.; Reimers, J. R.; Ulstrup, J., Sulfur ligand mediated electrochemistry of gold surfaces and nanoparticles: What, how, and why. *Current Opinion in Electrochemistry* **2017,** *1* (1), 7-15.

28. Wan, X.-K.; Wang, J.-Q.; Nan, Z.-A.; Wang, Q.-M., Ligand effects in catalysis by atomically precise gold nanoclusters. *Science advances* **2017,** *3* (10), e1701823.

29. Kim, A.; Zeng, C.; Zhou, M.; Jin, R., Surface Engineering of Au36 (SR) 24 Nanoclusters for Photoluminescence Enhancement. *Particle & Particle Systems Characterization* **2017,** *34* (8), 1600388.

30. Crawford, S. E.; Andolina, C. M.; Smith, A. M.; Marbella, L. E.; Johnston, K. A.; Straney, P. J.; Hartmann, M. J.; Millstone, J. E., Ligand-mediated "turn on," high quantum yield near-infrared emission in small gold nanoparticles. *Journal of the American Chemical Society* **2015,** *137* (45), 14423-14429.

31. Konishi, K., Phosphine-coordinated pure-gold clusters: diverse geometrical structures and unique optical properties/responses. In *Gold Clusters, Colloids and Nanoparticles I*, Springer: 2014; pp 49-86.

32. Green, M., A new approach to the formal classification of covalent compounds of the elements. *Journal of Organometallic Chemistry* **1995,** *500* (1-2), 127-148.

33. Green, M. L.; Parkin, G., Application of the covalent bond classification method for the teaching of inorganic chemistry. *Journal of Chemical Education* **2014,** *91* (6), 807-816.

34. Shichibu, Y.; Kamei, Y.; Konishi, K., Unique [core+ two] structure and optical property of a dodeca-ligated undecagold cluster: critical contribution of the exo gold atoms to the electronic structure. *Chemical Communications* **2012,** *48* (61), 7559-7561.

35. Hasan, S., A review on nanoparticles: their synthesis and types. *Research Journal of Recent Sciences* ______________________________ *ISSN* **2015,** *2277*, 2502.

36. Albano, V. G.; Bellon, P. L.; Manassero, M.; Sansoni, M., Intermetallic pattern in metal-atom clusters. Structural studies on Au11X3(PR3)7 species. *Journal of the Chemical Society D: Chemical Communications* **1970,** (18), 1210-1211.

37. Cariati, F.; Naldini, L., Trianionoeptakis(triarylphosphine)undecagold cluster compounds. *Inorganica Chimica Acta* **1971,** *5*, 172-174.

38. McKenzie, L. C.; Zaikova, T. O.; Hutchison, J. E., Structurally similar triphenylphosphine-stabilized undecagolds, Au11 (PPh3) 7Cl3 and [Au11 (PPh3) 8Cl2] Cl, exhibit distinct ligand exchange pathways with glutathione. *Journal of the American Chemical Society* **2014,** *136* (38), 13426-13435.

39. McPartlin, M.; Mason, R.; Malatesta, L., Novel cluster complexes of gold(0)–gold(I). *Journal of the Chemical Society D: Chemical Communications* **1969,** (7), 334-334.

40. Safer, D.; Bolinger, L.; Leigh, J. S., Undecagold clusters for site-specific labeling of biological macromolecules: simplified preparation and model applications. *Journal of Inorganic Biochemistry* **1986,** *26* (2), 77-91.

41. Yang, H.; Reardon, J. E.; Frey, P. A., Synthesis of undecagold cluster molecules as biochemical labeling reagents. 2. Bromoacetyl- and maleimidoundecagold clusters. *Biochemistry* **1984,** *23* (17), 3857-3862.

42. Hainfeld, J. F.; Powell, R. D., New Frontiers in Gold Labeling. *Journal of Histochemistry & Cytochemistry* **2000,** *48* (4), 471-480.

43. Safer, D.; Hainfeld, J.; Wall, J.; Reardon, J., Biospecific labeling with undecagold: visualization of the biotin-binding site on avidin. *Science* **1982,** *218* (4569), 290-291.

44. Wang, L.; Peng, J.; Tang, Z.; Kang, X.; Fu, M.; Chen, S., Styrene oxidation catalyzed by Au11(PPh3)7Cl3 and [Au11(PPh3)8Cl2]Cl nanoclusters: Impacts of capping ligands, particle size and charge state. *Applied Catalysis A: General* **2018,** *557*, 1-6.

45. Woehrle, G. H.; Hutchison, J. E., Thiol-functionalized undecagold clusters by ligand exchange: Synthesis, mechanism, and properties. *Inorganic chemistry* **2005,** *44* (18), 6149-6158.

46. Chrysouli, M. P.; Banti, C. N.; Kourkoumelis, N.; Panayiotou, N.; Markopoulos, G. S.; Tasiopoulos, A. J.; Hadjikakou, S. K., Chloro(triphenylphosphine)gold(I) a forefront reagent in gold chemistry as apoptotic agent for cancer cells. *Journal of Inorganic Biochemistry* **2018,** *179*, 107-120.

47. McAuliffe, C. A.; Parish, R. V.; Randall, P. D., Gold(I) complexes of unidentate and bidentate phosphorus-, arsenic-, antimony-, and sulphur-donor ligands. *Journal of the Chemical Society, Dalton Transactions* **1979,** (11), 1730-1735.

48. Gorin, D. J.; Toste, F. D., Relativistic effects in homogeneous gold catalysis. *Nature* **2007,** *446*, 395.

49. Muñiz, J.; Wang, C.; Pyykkö, P., Aurophilicity: The Effect of the Neutral Ligand L on [{ClAuL}2] Systems. *Chemistry – A European Journal* **2011,** *17* (1), 368-377.

50. Westland, A. D., A study of the complexing of gold(I) with tertiary phosphine, arsine, and stibine. *Canadian Journal of Chemistry* **1969,** *47* (22), 4135-4140.

51. Hutter, J.; Iannuzzi, M.; Schiffmann, F.; VandeVondele, J., CP2K: atomistic simulations of condensed matter systems. *Wiley Interdisciplinary Reviews: Computational Molecular Science* **2014,** *4* (1), 15-25.

52. Hooper, T. N.; Butts, C. P.; Green, M.; Haddow, M. F.; McGrady, J. E.; Russell, C. A., Synthesis, Structure and Reactivity of Stable Homoleptic Gold(I) Alkene Cations. *Chemistry – A European Journal* **2009,** *15* (45), 12196-12200.

53. Ren, X.; Fu, J.; Lin, X.; Fu, X.; Yan, J.; Wu, R. a.; Liu, C.; Huang, J., Cluster-to-cluster transformation among Au6, Au8 and Au11 nanoclusters. *Dalton Transactions* **2018,** *47* (22), 7487-7491.

54. Li, Y.-Z.; Ganguly, R.; Hong, K. Y.; Li, Y.; Tessensohn, M. E.; Webster, R.; Leong, W. K., Stibine-protected Au13 nanoclusters: syntheses, properties and facile conversion to GSH-protected Au25 nanocluster. *Chemical Science* **2018,** *9* (46), 8723-8730.

55. Shichibu, Y.; Suzuki, K.; Konishi, K., Facile synthesis and optical properties of magic-number Au13 clusters. *Nanoscale* **2012,** *4* (14), 4125-4129.

56. Perdew, J.; Burke, K.; Ernzerhof, M., Phys Rev Lett 77: 3865;(b) Perdew P. *Burke K, Ernzerhof M (1997) Phys Rev Lett* **1996,** *78*, 1396.

57. Goedecker, S.; Teter, M.; Hutter, J., Separable dual-space Gaussian pseudopotentials. *Physical Review B* **1996,** *54* (3), 1703-1710.

58. Zhechkov, L.; Heine, T.; Patchkovskii, S.; Seifert, G.; Duarte, H. A., An Efficient a Posteriori Treatment for Dispersion Interaction in Density-Functional-Based Tight Binding. *Journal of Chemical Theory and Computation* **2005,** *1* (5), 841-847.

59. Chassai, T. In *TDDFT approach with Gaussian Augmented Plane Waves*, APS Meeting Abstracts, 2005.

60. Hunter, J. D., Matplotlib: A 2D Graphics Environment. *Computing in Science & Engineering* **2007,** *9* (3), 90-95.

61. Humphrey, W.; Dalke, A.; Schulten, K., VMD: Visual molecular dynamics. *Journal of Molecular Graphics* **1996,** *14* (1), 33-38.

62. Zhang, J.; Badger, P. D.; Geib, S. J.; Petoud, S., Sensitization of Near-Infrared-Emitting Lanthanide Cations in Solution by Tropolonate Ligands. *Angewandte Chemie International Edition* **2005,** *44* (17), 2508-2512.

63. Sugiuchi, M.; Shichibu, Y.; Nakanishi, T.; Hasegawa, Y.; Konishi, K., Cluster–π electronic interaction in a superatomic Au13 cluster bearing σ-bonded acetylide ligands. *Chemical Communications* **2015,** *51* (70), 13519-13522.

64. Zhu, M.; Aikens, C. M.; Hollander, F. J.; Schatz, G. C.; Jin, R., Correlating the Crystal Structure of A Thiol-Protected Au25 Cluster and Optical Properties. *Journal of the American Chemical Society* **2008,** *130* (18), 5883-5885.

65. Kang, X.; Song, Y.; Deng, H.; Zhang, J.; Liu, B.; Pan, C.; Zhu, M., Ligand-induced change of the crystal structure and enhanced stability of the Au11 nanocluster. *RSC Advances* **2015,** *5* (82), 66879-66885.

66. Shichibu, Y.; Negishi, Y.; Watanabe, T.; Chaki, N. K.; Kawaguchi, H.; Tsukuda, T., Biicosahedral Gold Clusters [Au25(PPh3)10(SCnH2n+1)5Cl2]2+ (n = 2−18): A Stepping Stone to Cluster-Assembled Materials. *The Journal of Physical Chemistry C* **2007,** *111* (22), 7845-7847.

67. Borissova, A. O.; Korlyukov, A. A.; Antipin, M. Y.; Lyssenko, K. A., Estimation of Dissociation Energy in Donor−Acceptor Complex AuCl·PPh3 via Topological Analysis of the Experimental Electron Density Distribution Function. *The Journal of Physical Chemistry A* **2008,** *112* (46), 11519-11522.

68. Lumpkin, R. S.; Kober, E. M.; Worl, L. A.; Murtaza, Z.; Meyer, T. J., Metal-to-ligand charge-transfer (MLCT) photochemistry: experimental evidence for the participation of a higher lying MLCT state in polypyridyl complexes of ruthenium (II) and osmium (II). *Journal of Physical Chemistry* **1990,** *94* (1), 239-243.

69. Idrobo, J. C.; Walkosz, W.; Yip, S. F.; Öğüt, S.; Wang, J.; Jellinek, J., Static polarizabilities and optical absorption spectra of gold clusters (Au n, n= 2–14 and 20) from first principles. *Physical Review B* **2007,** *76* (20), 205422.

70. Jablonski, A., Efficiency of Anti-Stokes Fluorescence in Dyes. *Nature* **1933,** *131* (3319), 839-840.

71. Lewis, G. N.; Kasha, M., Phosphorescence and the triplet state. *Journal of the American Chemical Society* **1944,** *66* (12), 2100-2116.

72. Pavlopoulos, T.; El-Sayed, M., Spectroscopic Investigation of the Mechanism of the Intramolecular Heavy Atom Effect on the Phosphorescence Process. I. Naphthalene Emission. *The Journal of Chemical Physics* **1964,** *41* (4), 1082-1092.

73. Eisenthal, K.; El-Sayed, M., Heavy-Atom Effects on Radiative and Radiationless Processes in Charge-Transfer Complexes. *The Journal of Chemical Physics* **1965,** *42* (2), 794-796.

74. Pearson, R. G., Hard and soft acids and bases. *Journal of the American Chemical Society* **1963,** *85* (22), 3533-3539.

75. Libit, L.; Hoffmann, R., Detailed orbital theory of substituent effects. Charge transfer, polarization, and the methyl group. *Journal of the American Chemical Society* **1974,** *96* (5), 1370-1383.

76. Chowdhury, M.; Goodman, L., Polarization of Charge-Transfer Bands. *Journal of the American Chemical Society* **1964,** *86* (14), 2777-2781.

77. Caspar, J. V.; Meyer, T. J., Photochemistry of MLCT excited states. Effect of nonchromophoric ligand variations on photophysical properties in the series cis-Ru (bpy) 2L22+. *Inorganic Chemistry* **1983,** *22* (17), 2444-2453.

78. Colombo, M. G.; Hauser, A.; Guedel, H. U., Evidence for strong mixing between the LC and MLCT excited states in bis (2-phenylpyridinato-C2, N')(2, 2'-bipyridine) iridium (III). *Inorganic chemistry* **1993,** *32* (14), 3088-3092.

79. Harriman, A.; Izzet, G., Direct observation of the fourth MLCT triplet state in ruthenium(ii) tris(2,2′-bipyridine). *Physical Chemistry Chemical Physics* **2007,** *9* (8), 944-948.

80. Hofbeck, T.; Yersin, H., The Triplet State of fac-Ir(ppy)3. *Inorganic Chemistry* **2010,** *49* (20), 9290-9299.

81. Krogstad, D. A.; Young, V. G.; Pignolet, L. H., Synthesis and characterization of a series of diphosphine ligated Pt□Au cluster compounds. *Inorganica Chimica Acta* **1997,** *264* (1), 19-32.